This is to certify that the
thesis entitled

TRIONIC OPTICAL POTENTIALS FOR CHARGE CARRIERS
IN SEMICONDUCTORS

presented by

Martin Johannes Alexander Schütz

has been accepted towards fulfillment
of the requirements for the

M.S. degree in Physics and Astronomy

Major Professor's Signature

7/28/09 7/22/09

Date

TRIONIC OPTICAL POTENTIALS FOR CHARGE CARRIERS IN SEMICONDUCTORS

By

Martin Johannes Alexander Schütz

A THESIS

Submitted to
Michigan State University
in partial fulfillment of the requirements
for the degree of

MASTER OF SCIENCE

Physics and Astronomy

2009

ABSTRACT

TRIONIC OPTICAL POTENTIALS FOR CHARGE CARRIERS IN SEMICONDUCTORS

By

Martin Johannes Alexander Schütz

Optical trapping of neutral particles has led to remarkable advances in precision measurement, quantum information, and addressing fundamental longstanding questions in condensed matter physics. Despite recent advances in the optical and electronic control in semiconductor systems, a similar laser-induced technique to trap and manipulate charged carriers in semiconductor devices has not yet been investigated.

In this thesis, we will propose for the first time analogues optical trapping potentials for charge carriers embedded in a semiconductor quantum well by driving the trion resonance with intense, detuned laser light. A trion is a bound state between an exciton and an excess carrier, that modifies the exciton resonance frequency in the vicinity of a carrier. Accordingly, the Stark energy is modified in proportion to the the light intensity at the carrier location, which serves as a source of mechanical potential energy for the carrier. We show that this novel trion-mediated potential exhibits a non-local character, but can confine carriers at the lengthscale of optical wavelengths. It can be deep compared to the the single electron recoil energy and the carrier's effective temperature which benefits from the omnipresent cooling mechanism of the phonon bath. The model is extended to the new paradigm of a spin-selective carrier lattice in a true Solid State environment which is potentially much simpler to engineer and control than similar lattices in AMO physics. Our results suggest the possibility of integrating ultrafast optics and gate voltages in new single-carrier semiconductor devices with promising applications in quantum information processing, and exploring the physics of interacting electrons in the presence of a periodic potential readily controllable in space and time.

DEDICATION

Dedicated to my mum, my sister, Millhouse and Jaïpur.

ACKNOWLEDGMENT

A few weeks before my year abroad at Michigan State University turns to its end, I am looking back on a year in my life, loaded with experiences. I have grown not only as a physics student, but as a person. Now, it is the right time to express my gratitude to all the people that stood by my side during the past year.

First of all, I would like to thank my advisors, Prof. Michael G. Moore and Prof. Carlo Piermarocchi for the continuous guidance and support they have provided to me. After my undergraduate studies at the University of Karlsruhe, they gave me the opportunity to conduct research for the first time in my life as a physicist. They are great, passionate teachers with an astonishing ability to give precise explanations of complex phenomena and an seemingly inexhaustible patience. Our discussions have never been limited to the scope of this thesis and I have learned much more than I could have ever imagined. Most importantly, their uncomplicated, pleasant and humorous personality made it fun to work with them. Without any exaggeration, I cannot imagine a better team of advisors.

Also, I would like to express my gratitude to Prof. Mark Dykman and Prof. Bhanu Mahanti for their intriguing style of teaching. In their classes I have learnt a lot of new physics, some of which already flowed into this thesis.

Debbie Barratt has always been a very friendly, patient and helpful contact person. Thank you so much!

My stay at MSU would not have been the same without Prof. Wolfgang Bauer and his golf league. I am very thankful that I got the opportunity to join this group. There is nothing better than going out on a warm Tuesday evening to hit some drives. The financial support by the golf league is gratefully acknowledged ;-).

Although a Prussian by birth, Kai was more than a roomate that introduced me to the beauty of Ubuntu and Lyx, he has become a very good friend. We will share many memories and I am looking forward to our trip to the West.

I consider myself very fortunate to have met Kirstie: a friendship that is to be continued in Germany. Martin and Christine have become friends I had a lot of fun with. Then, I will never forget the glorious victories as a member of 'Team Michelle' together with Marshall and Kritsada. Michelle, I have played in your team, but unfortunately I never got to know you. Also, thanks to Philipp for selling a car that doesn't have a radio, but features an on-board swimming pool!

The National German Merit Foundation as well as the Fulbright program supported my exchange year at Michigan State university with a generous scholarship. Also, they organized meetings at Princeton and Denver, where I shared experiences with many young, incredibly talented people that I will never forget.

After a year abroad, far away from my home, I do appreciate even more what great friends I have back in my home territory. We always stayed in contact and I am looking forward to seeing you again! In particular, I would like to mention all of my golf team-mates, Enrico, Erik and Manuel who never gets tired of helping me out.

Vor allem möchte ich aber meiner Mutter, meiner Schwester, meiner Oma und Karl danken. Ohne ihre ständige Unterstützung, ihren Glauben an mich und ihren Zuspruch in persönlich sehr schwierigen Zeiten wäre die Anfertigung dieser Arbeit nicht möglich gewesen. Ich danke Euch von ganzem Herzen!

TABLE OF CONTENTS

LIST OF TABLES

LIST OF FIGURES

Images in this thesis are presented in color

Introduction

Laser induced optical trapping and manipulation of neutral particles have played key roles to the advancement of modern atomic physics and biophysics [1, 2]. The realization of optical traps has enabled numerous fascinating experiments: in biology optical traps, also known as optical tweezers, have led to probing the mechanical properties of DNA [2]. In atomic physics, optical cooling and trapping has become a flourishing technology paving the way to remarkable advances in precision measurement, quantum information and addressing fundamental questions in condensed matter physics. In particular optical lattices, a regular array of microtraps for atoms generated by a standing wave laser field, have made important contributions to a deeper understanding of fundamental Solid State questions and serve as a platform for various promising candidates in quantum information schemes. One exciting outgrowth of this general technique is for example the experimental implementation of a quantum phase transition from a superfluid to a Mott insulator in a gas of ultracold atoms [44] and, very recently, Anderson localization in a disordered optical lattice has been investigated experimentally [3, 4].

A the same time, semiconductor nanostructures continued to attract significant interest due to the technological progress in their fabrication. Some of the most peculiar features of semiconductors become manifest in their optical properties. Despite advances in the optical and electronic control in semiconductors [93, 94], a laser induced method to trap and manipulate charged carriers has not yet been explored.

In this thesis, we will merge for the first time the expertise of these two blossoming fields, semiconductor heterostructure physics and cold atom physics, to propose the laser-induced trapping of a new system: an electron gas confined within a two-dimensional quantum well (QW). In analogy to optical potentials for atoms, an AC Stark shift is generated for the conduction electrons by driving the trion resonance with intense, detuned laser light. Trions are negatively (X^-) or positively charged (X^+) excitons that have been observed as an important spectral signature of QW's in which excess carriers are introduced by modulation doping [16, 17] or optical excitation [19]. In essence, this novel trion-mediated potential for carriers in semiconductors originates from the following mechanism: The trion resonance modifies the exciton resonance frequency in the vicinity of a carrier. Accordingly, the Stark energy of the complete system is modified in proportion to the light intensity at the carrier location. The dependence of the total energy on the carrier's position serves as a source of mechanical potential energy for the carrier.

The thesis is structured as follows: In the first Chapter we will review the core concepts of excitations in semiconductors. We will present a quantum mechanical treatment of excitons, the dominant excitations in undoped semiconductors. Readers familiar with the concept of excitons can skip this introductory part. In the next step, we will obtain a Hyllereaas-type wavefunction based on Ritz's variational technique to accurately describe the trion state. We will verify that trions are stable against dissociation into an exciton and a free excess carrier for every possible electron-hole mass ratio. Our results for the trion binding energies are in a good agreement to experimental values and confirmed by previous theoretical investigations [28, 22]. In addition, we will underline the characteristics of the coupling to light for excitons and trions. While excitons display themselves as a coherent excitation over the whole sample, the trion oscillator strength shows a very different behaviour. In a last step, we will focus on the radiative properties of excitons and trions by calculating their

radiative transition rates and lifetimes, respectively.

The second Chapter gives an introduction to the quantum optical foundation of this thesis. We will review the underlying mechanism of laser-induced dipole potentials for atoms, before we turn to our first theoretical treatment of the trion-mediated optical trapping potential for carriers. Here, we have modelled the QW sample as a collection of two-level systems. The collection consists of exciton-sized cells that can be excited by the photocreation of an exciton or of a trion state if a carrier is in the vicinity of this cell. We will find that the effective polarizibility of the background due to the exciton resonance marks a major distinguishing feature of the trionic potential. It leads to a correction factor to the pure trion contribution and gives a very different scaling behaviour of the potential depth with the detuning, compared to atomic optical potentials.

Chapter 3 is devoted to a derivation of an effective Hamiltonian and the corresponding Schrödinger equation for a single electron that is coupled to virtually excited bound and unbound trion states. The features embodied in the effective Schrödinger equation are discussed in the next chapter.

In Chapter 4 we will report on the results of our investigations. In particular, the trion-mediated potential displays a non-local character that is a consequence of the light effective mass of the electron m_e^* and the 'quivering' of the electron motion once it has virtually mixed with the extended trion state. This non-locality occurs on a lengthscale of the order of the trion size ($\sim 30nm$). We have been able to show that this effect can be neglected in the analysis of the electron trapping at the nodes or antinodes of the intensity pattern, because the trion size is small compared to the periodicity of the potential. In addition, we will show that the extended size of the excited trion level accounts for an effective enhancement factor χ for the potential depth of almost two orders of magnitude with respect to typical excitonic Stark shifts. The quantity χ has been intuitively linked to the integral over all possible bound trion

configurations having one electron and one hole 'on top of each other'. More simply, χ can be viewed as the number of excitons that fit into the trion size without spatial overlap. Also, we will encounter and analyze the correction factor that first appeared in the framework of the previous cell model in Chapter 2. The results of the toy model and the effective Hamiltonian are in a very good agreement, qualitatively and quantitatively: the correction is smaller than one for red detuning and therefore accounts for a decrease in the potential depth. However, for blue detuning, it can give a strong enhancement to the potential depth. We will show that this novel type of potential can be deep compared to the single photon recoil energy E_R and the equilibrium temperature of the electrons. It also benefits from an omnipresent cooling mechanism in the semiconductor environment: the phonon bath.

Chapter 5 is devoted to an analysis of the phonon bath. We will calculate the effective equilibrium temperature of the electrons that arises from the competition of the interaction with the phonons and the heating due to spontaneous emission of photons. According to our results, it even seems feasible to obtain a potential depth that exceeds both the recoil energy and the thermal energy of the carriers by a factor of 10. Therefore, we predict the possibility of confining carriers embedded in a QW system on a lengthscale of optical wavelengths.

In Chapter 6 we will extend our model to the idea of a spin-selective electron lattice which is much simpler to engineer and control than similar lattices for atoms. A possible setup for the experimental investigation of this system is depicted in Fig. (1). The strong Coulombic interactions between the trapped particles give rise to a very strong on-site repulsion and, in contrast to the atomic counterpart, even the interaction between different sites of the lattice is not negligible. The combination of a periodic potential whose properties can be tuned in real time and which is strong enough to trap carriers at a single site, but weak compared to the inter-particle interaction paves the way for intriguing new experiments not feasible in conventional

solid state physics. The level structure of our system allows for a directive mapping of the spin of the localized electron and the optical polarization of the photon that can couple to the trion state. Owing to this scheme, two different potentials for the two possible spin configurations might be created. This property may open up the way to important applications in quantum information processing.

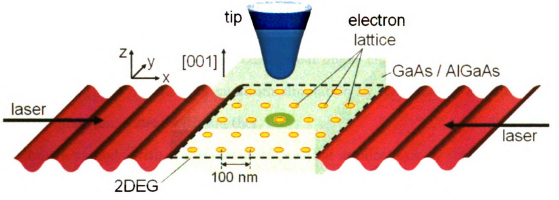

Figure 1: Schematic of optically-confined electron lattice. The 2DEG sample already has electrons confined to an $x-y$ plane below the sample surface. Four incident lasers achieve further confinement using the AC Stark shift effect. For clarity, here the lasers are shown in the x-direction only; an identical pattern of light will be applied in the y-direction, too. The charge modulation can be probed based on a STM technique.

We will focus on small side effects in Chapter 7.

In summary, we will apply recently developed concepts from AMO physics to generate new, interesting ideas for semiconductor systems. Owing to the specific properties of these systems, like the background polarizability, the light particle masses, and the strong inter-particle interactions, semiconductor optical potentials are very different from the conventional optical trapping potentials in AMO systems. The outlook of optically manipulating the motion of electrons seems very promising for at least two purposes: we may expect a deeper understanding of fundamental models like the Hubbard model that are well established in the solid state community. The system proposed in this thesis stimulates further investigations, since this fermionic many-particle quantum state on a regular lattice possibly bridges the gap between current

ultracold atom systems and fundamental concepts in condensed matter physics. A unique dynamic control over all the relevant parameters of the optical lattice allows for experiments not feasible in condensed matter physics. In contrast to ultracold atom systems, strong long range interactions in a true solid state environment can be studied. In addition, the use of the trapped electrons as qubits in quantum information systems may give rise to applications, well beyond the scope of this thesis. Owing to its spin-selectivity, electron spins may be addressed individually and used to create entanglement. In essence, our system might enable the implementation of the pioneering idea of real-time quantum simulation by dynamically simulating one complex quantum system with another.

The thesis ends with a discussion of possible applications of this novel system and identifies possible future directions of research that go beyond the investigations presented in this thesis.

Chapter 1

Excitations in semiconductors

Typically, the optical spectra of undoped semiconductor QWs are dominated by excitons; these are optically excited bound electron-hole pairs that follow the absorption of photons in a semiconductor and result from the binding of the negatively charged electron of the conduction band with the positively charged hole left behind in the valence band. In the case of a small excess density of carriers, an exciton can capture an additional electron to form a charged exciton, which is the bound state of two electrons and a hole or two holes and one electron, depending on the type of doping. The three-body structure of these charged excitons is the origin of its common name in the literature: *trions* [5]. The first theoretical prediction of the existence of trions by Lampert has celebrated its 50th anniversary in 2008 [6]. In best-quality samples, trions exist as free particles and thus carry original properties as mobile charged quasiparticles [7]. Just as excitons, trions can decay radiatively when one electron and one hole recombine emitting a photon. While the exciton problem can be mapped onto the hydrogen problem and is therefore analytically solvable, the analysis of trions from a theoretical point of view bears at least two major difficulties: (i) As trions represent the eigenstates of two electrons and one hole - or viceversa - in the presence of Coulomb interaction, their energies and their wavefunctions are

not analytically known; (ii) since trions are bound objects, they cannot be described using from a (finite) perturbative approach [8].

In this introductory chapter, we will review excitons as the elementary excitations of undoped semiconductors and analytically derive their binding energies and wavefunctions for the two dimensional limit. Based on a variational approach, we will do the same for trions and show that they are stable against dissociation for any possible electron-hole mass ratio. The binding energies we obtain are in a reasonable agreement with experimental values. We will present our numerical results for the two cases of $GaAs/Ga_{1-x}Al_xAs$ and $CdTe/Cd_{1-x}Zn_xTe$ QW systems. The material parameters we used are summarized in Appendix A. Using the so found wavefunctions, we will analyze the coupling of excess electrons to bound and unbound trions, induced by a standing electromagnetic wave. The optical matrix elements are a key ingredient for the work presented in this thesis and will be discussed in section 1.3. In the last section, we will focus on the radiative character of excitons and trions by computing their decay rates and radiative lifetimes.

1.1 Excitons in quantum wells

1.1.1 Wannier-Mott theory

The optical properties of semiconductors are strongly related to interband transitions between valence and conduction bands. Excitons are electronic crystal excitations that have become an indispensable concept in the understanding of these interband transitions. In principle, the term exciton has been coined to signify the modification of the absorption spectrum of photons because of the Coulomb interactions between the conduction band electron and the valence band hole. A very intuitive explanation for the exciton concept can be given based on the schematized configuration in Fig. (1.1). We assume a direct semiconductor, i.e. the conduction band minimum and the

valence band maximum are at the same point in **k**-space. The zero energy is chosen to be at the top of the valence band. Therefore, the bottom of the conduction band lies at the bandgap energy ϵ_c.

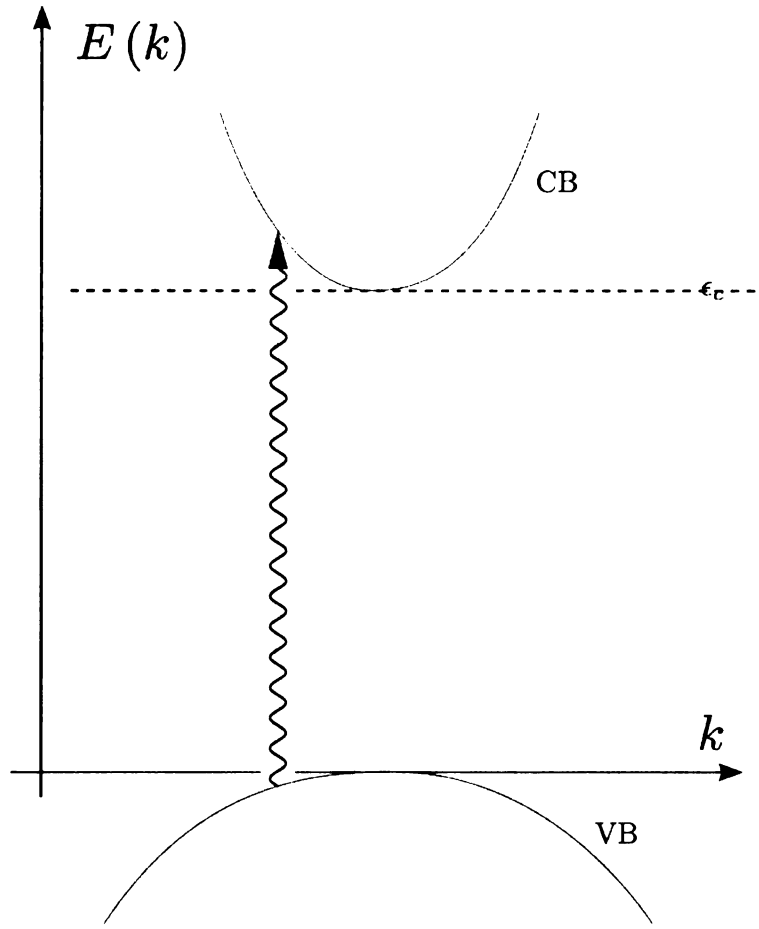

Figure 1.1: Optical transition between the full valence band (VB) and the empty conduction band (CB) for a direct transition.

Initially the system is assumed to be in its ground state, which means that the valence band is filled, and all conduction band states are empty. Optical transitions are induced by photons. For photons in the optical frequency range, the wavevector **Q** is small enough to be neglected, so that the photon is schematized as a vertical arrow. The photon promotes a valence band electron to an unoccupied state in the

conduction band. For simplicity we assume quadratic dispersion relations for both the valence and the conduction band, so that the single electron energies are

$$\epsilon_v(\mathbf{k}) = -\frac{\hbar^2 k^2}{2m_h^*}, \qquad \epsilon_c(\mathbf{k}) = \epsilon_c + \frac{\hbar^2 k^2}{2m_e^*}, \tag{1.1}$$

where m_h^* and m_e^* are the effective masses of the valence and conductions electrons, respectively. In 1937, Wannier was the first to interpret the interband transitions in semiconductors as a two-particle process [9]: as all the valence band states are completely filled, the removal of an electron from this band is accompanied by the creation of an excitation termed a hole. The hole represents the absence of an electron in an otherwise filled band. It can be treated as a particle with an effective mass m_h^*, positive charge e and energy $\epsilon_h(\mathbf{k})$. In the two-particle picture, the absorption of a photon of energy $\hbar\omega$ in the semiconductor entails two excitations: one is the electron in the conduction band of wavevector $\mathbf{k}$ and energy $\epsilon_c(\mathbf{k})$ and the second one is the hole in the valence band of wavevector $-\mathbf{k}$ and energy $\epsilon_h(\mathbf{k}) = \hbar^2 k^2/2m_h^*$. Accordingly, conservation of energy for this process implies

$$\hbar\omega = \epsilon_c + \frac{\hbar^2 k^2}{2m_e^*} + \frac{\hbar^2 k^2}{2m_h^*}. \tag{1.2}$$

In the framework of this two-particle picture additional physics arise that are concealed in a one-particle approach. The essential idea is that the electron and the hole are particles with opposite charges. Therefore, there is a Coulomb attraction $-e^2/\epsilon r$ between them. Here, ϵ is the static dielectric constant due to the effective screening of all not explicitly included charges (electrons and ions). The frequency dependence of ϵ is neglected.

The optical absorption rate for this transition was first calculated by Elliott in 1957 [10]. The final state of the system is described by a two-particle Schrödinger

equation

$$\left[-\frac{\hbar^2\nabla_e^2}{2m_e^*}-\frac{\hbar^2\nabla_h^2}{2m_h^*}-\frac{e^2}{\epsilon\left|\mathbf{r}_e-\mathbf{r}_h\right|}\right]\Phi\left(\mathbf{r}_e,\mathbf{r}_h\right)=E\Phi\left(\mathbf{r}_e,\mathbf{r}_h\right). \tag{1.3}$$

The problem can be transformed into relative $\mathbf{r}=\mathbf{r}_e-\mathbf{r}_h$ and center of mass coordinates $\mathbf{R}$ in the standard way to obtain the *effective mass equation* for excitons in real space representation

$$\left[-\frac{\hbar^2\nabla_{\mathbf{R}}^2}{2M}-\frac{\hbar^2\nabla_{\mathbf{r}}^2}{2\mu_x}-\frac{e^2}{\epsilon r}\right]\Phi\left(\mathbf{R},\mathbf{r}\right)=E\Phi\left(\mathbf{R},\mathbf{r}\right). \tag{1.4}$$

Here, $M=m_e^*+m_h^*$ is the total mass and $\mu_x=m_e^*m_h^*/\left(m_e^*+m_h^*\right)$ is the reduced mass of the electron-hole pair. The center of mass motion is plane-wave like. In optical experiments the corresponding wavevector $\mathbf{K}$ equals the photon wave vector, which is, however, small. The center of mass motion can be separated as

$$\Phi\left(\mathbf{R},\mathbf{r}\right)=\Psi\left(\mathbf{R}\right)\phi\left(\mathbf{r}\right) \tag{1.5}$$

and the Coulomb interaction essentially applies only to the envelope part of the wavefunction

$$\left[-\frac{\hbar^2\nabla_{\mathbf{r}}^2}{2\mu_x}-\frac{e^2}{\epsilon r}\right]\phi\left(\mathbf{r}\right) = E_r\phi\left(\mathbf{r}\right) \tag{1.6}$$

$$E = \epsilon_c+E_r+\frac{\hbar^2K^2}{2M}. \tag{1.7}$$

This is an intriguing and remarkable result: the exciton problem can be mapped in one-to-one correspondence to the well-known hydrogen problem. Excitons appear as quasiparticles in a solid that are the hydrogenic bound state solutions of an excited electron in the conduction band and the remaining hole in the valence band. Eqn. (1.6) is known as the Wannier equation [12].

At this point, we mention that the effective mass equation can be derived from

first principles, taking into account the full electron-electron interaction [11]. Based on a Green's function formalism, Eqn. (1.4) can be obtained in the lowest order approximation to the effective electron-hole interaction.

Moreover, Elliott showed that the optical transition rate $\mathcal{A}(\omega)$ depends on the relative wavefunction, evaluated at $\mathbf{r} = 0$. The transition rate for the absorption of photons is

$$\mathcal{A}(\omega) = \frac{2\pi}{\hbar} |\hat{\epsilon} \cdot \mathbf{p}_{cv}| \sum_j |\phi_j(0)|^2 \delta(\hbar\omega - \epsilon_c - \epsilon_j), \tag{1.8}$$

where the summation over j includes both bound $(\epsilon_j < 0)$ as well as unbound $(\epsilon_j > 0)$ states of the relative motion of the electron-hole pair. The dependence on the relative wavefunction, taken at $\mathbf{r} = 0$, can be understood by very intuitive arguments. Let us consider the situation of an emission process whereby the electron and the hole recombine to emit a photon of energy $\hbar\omega$. Since the relative wavefunction governs the probability to find the electron and the hole at the same spot in the solid, the necessary condition for radiative recombination, it is evident that the emission rate should depend on the relative wavefunction at $\mathbf{r} = 0$. Recombination occurs when the electron and the hole are "on top" of each other, consistent with physical intuition. Since the matrix elements for absorption and emission processes are identical by time reversal, the absorption rate must have the same dependence. Indeed, typical absorption spectra of a direct gap semiconductor show sharp distinct exciton resonances well below the bandgap energy corresponding to the $1s$, $2s$, ... solutions of the Hydrogen problem.

1.1.2 Confined Excitons

Up to now, our review of excitonic excitations in semiconductors has been general. In the following we will focus on confined semiconductor structures, which attract significant interest due to their applications in submicrometer technology. The tech-

nological advances in crystal growth techniques have made possible the fabrication of various types of semiconductor heterostructures whose characteristic dimensions, typically a few nanometers, become comparable to the free carriers DeBroglie wavelength. In this regime the electronic and optical properties can deviate substantially from those of bulk materials, because the effects of spatial confinement become appreciable and restrict the electron and hole mobility to a reduced dimensionality. The energetically low lying electron and hole states are confined in one or more directions within a region of length L_c. Since L_c is still larger than the lattice constant but small enough to cause a quantization of the carriers envelope wave functions, structures of this size are called mesoscopic [12].

The most prominent examples of such mesoscopic semiconductor structures are quantum wells (QW), where confinement along one spatial direction occurs due to the variation of the bandgap energy from one material to another. The translational motion in the plane perpendicular to the confinement direction is still unrestricted. Such a quantum well , e.g. for the III-IV compound semiconductor $GaAs$, can be realized by molecular beam epitaxy to sandwhich several $GaAs$ layers in between layers of a material with a wider band gap, typically $Ga_xAl_{1-x}As$, with $0 < x < 0.4$. For substantially larger Al concentrations, the barrier becomes an indirect-gap semiconductor [12]. The barrier height, i.e. the strength of the confinement, is determined by the difference in the bandgap energies of the two materials involved.

Quantum wells are currently the best studied quantum confined structure and they can serve as a paradigm for others. The system we study is also based on a quantum well structure, so that for the rest of this thesis we will refer to a quasi two dimensional or pure two dimensional system. For completeness, however, we mention the possibility to fabricate quantum wires, where the free electronic motion is confined in two dimensions and even quantum dots, where confinement exists in all three space dimensions.

Our next imminent goal is an accurate description of Wannier excitons, confined in a QW structure. In QW structures, excitons were first observed in an absorption experiment in 1974 [13], where up to eight resolved exciton transitions have been measured.

For simplicity, we consider the pure two-dimensional limit, corresponding to a QW with a very thin QW width. In Appendix B we give a detailed treatment of excitons in two-dimensional structures. The two-dimensional exciton bound state energies are found to be

$$E_n = -E_0 \frac{1}{(n+1/2)^2}, \qquad n = 0, 1, \ldots, \tag{1.9}$$

where E_0 serves as the energy unit

$$E_0 = \frac{\hbar^2}{2\mu_x a_0^2} = \frac{e^2}{2\epsilon a_0} = \frac{e^2 \mu_x}{2\epsilon^2 \hbar^2}. \tag{1.10}$$

and $a_0 = \epsilon\hbar^2/\mu_x e^2$ is the natural lengthscale. In principle, these are the bound state energies for the 2D hydrogen problem. Quite remarkably, the binding energy of the ground state exciton is $4E_0$, which is four times the bulk value. Intuitively, this increase in the binding energy due to the reduced dimensionality can be understood if one considers quantum well structures with decreasing width. Since the admixture of p-wave functions is energetically unfavourable, the wave function tries to conserve its spherical symmetry as much as possible [12]. Therefore, confinement parallel to the quantum wells induces a decrease in the Bohr radius perpendicular to the wells: the oppositely charged electron and hole approach each other, resulting in a higher binding energy. By reducing the dimensionality of the system, the binding energy is considerably increased, which relaxes the requirements for an experimental observation. This is one of the reasons for the remarkable theoretical and experimental interest in systems of reduced dimensionality.

The lowest lying exciton state, the $1s$ exciton wavefunction will be of peculiar

interest, so that we explicitly state its wavefunction

$$\phi_{1s}(\mathbf{r}) = \phi_{0,0}(\mathbf{r}) = \sqrt{\frac{8}{\pi a_0^2}} \exp(-2r/a_0). \tag{1.11}$$

The exciton radius can be deduced from the exponential term of the relative wavefunction. Indeed, in the $1s$ ground state of the two dimensional limit the exciton radius a_x is only half the Bohr radius, i.e. $a_x = a_0/2$, whilst the bulk value for the exciton radius is simply the Bohr radius a_0. The reduction in dimensionality from bulk to a purely two dimensional system causes the exciton radius to shrink to half of its original value.

For a more accurate description of excitons in quantum well structures one has to take into account a finite well width and a subsequent finite extension of the exciton's wavefunction in the direction perpendicular to the well width. The enhancement factor, which is simply four in the 2D limit, for real QWs is then a function of both the well width and the barrier height. At a first glance, one might be led to think that this enhancement factor of four is an upper threshold for excitons that are confined in real quantum well structures. However, accurate theories that have taken into account various effects as valence-band mixing, nonparabolicity of the bulk conduction band, the difference in the dielectric constants between well and barrier materials and the Coulomb coupling between excitons belonging to different subbands, predict very high binding energies, particularly for very narrow quantum wells, that can even exceed the two-dimensional limit of four times the bulk Rydberg [14].

1.2 Trions in quantum wells

In the quantum-mechanical description of excitons, we encountered a striking analogy between the exciton problem and the conventional hydrogen atom. Pushing this

analogy a step further, Lampert envisaged the existence of a class of mobile charged excitons, in analogy to the negative hydrogen ion H^- and the positively charged hydrogen molecule H_2^+ [6] . It can be regarded as a major breakthrough in our understanding of the optical response of doped semiconductor quantum wells. Indeed his theoretical predictions were demonstrated experimentally both in II-VI and III-V semiconductors [15, 16, 17]. Mobile charged excitations had been identified via their optical signature in quantum wells as the negatively X^- and positively charged X^+ exciton, commonly referred to as trions. A trion is a charged bound three-particle complex, consisting of two electrons and one hole (eeh) or two holes and one electron (ehh), interacting via the Coulomb potential. When viewing the trion as a carrier bound to an exciton, it is immediately evident that, as the exciton is neutral, its attraction must be relatively weak which results in a comparatively small binding energy. This is why the unambiguous observation of a spectral line due to the charged excitons did not follow until the advent of high quality lightly doped QW structures where the binding energies are enhanced by approximately an order of magnitude relative to bulk [5].

The possibility of observing trions is tightly linked to the excess density of carriers in the QW. The presence of free excess carriers in the sample is necessary to photocreate trions, whereas excitons can be created just by photoabsorption. This explains why trions appear in the absorption and emission spectra of QWs containing small excess carrier densities only. The most common way to realize an excess carrier density in the QW is by modulation doping. The first observation of trions was also based on this technique [15]. It works as follows: The doping is introduced during the growth process of the sample, but only within a specific region of the barrier material. In order to hold the Fermi energy level constant throughout the doped sample, the donors tend to ionize. As a consequence, the freed carriers will migrate to the lower energy QW. Therefore, the two-dimensional carrier gas exists inside the QW,

spatially separated from the donor layer. In contrast to bulk materials, the ionized donors do not affect the mobility of the electron gas. Subsequently, this technique allows for for high carrier mobilities [20].

The exciton and trion photoluminescence (PL) spectra in QWs have been investigated as a function of the doping [18]: starting from low doping, where the trion line is hardly seen, the excess carrier density has been progressively increased leading to a stronger signal of the trion line. The intensity of the exciton line decreases to the profit of the trion line by increasing the carrier density. The energy between these two lines defines the trion binding energy: it is the energy necessary to dissociate a trion into a neutral exciton and an excess carrier. It should be mentioned, however, that excitonic effects are quenched due to screening and phase space filling for carrier concentrations sufficiently high [21].

1.2.1 Hamiltonian

We explicitly consider a negatively charged trion X^-, consisting of two electrons and one hole, which we assume to be described by their effective isotropic masses m_e^* and m_h^*. We restrict ourselves to the limit of a purely two dimensional semiconductor, therefore omitting the form factors due to the finite extension of the electron's and hole's QW wavefunctions along the QW growth direction[1]. We neglect the electron-hole exchange interaction . Within the envelope-function approximation, the effective-mass Hamiltonian $\mathcal{H}_T$ of the three-particle system reads

$$\mathcal{H}_T = T + V_c + 2\epsilon_c, \tag{1.12}$$

[1]The growth direction is taken to be the $\hat{z}$-direction throughout this thesis.

where ϵ_c is the energy at the bottom of the conduction band, while the top of the valence band was set to zero. T is the kinetic energy operator

$$T = -\frac{\hbar^2}{2m_e^*}\nabla_1^2 - \frac{\hbar^2}{2m_e^*}\nabla_2^2 - \frac{\hbar^2}{2m_h^*}\nabla_h^2. \tag{1.13}$$

The electrons and the hole carry a charge e and therefore the interactions are governed by mutual Coulombic potentials

$$V_c = -\frac{e^2}{\epsilon}\left(\frac{1}{r_{1h}} + \frac{1}{r_{2h}} - \frac{1}{r_{12}}\right), \tag{1.14}$$

where we introduced the mutual distances between the three particles r_{1h}, r_{2h} and r_{12} in a self-explaining notation. To be accurate, $\mathcal{H}_T$ should also include a contribution originating from image charges owing to the discontinuity in the dielectric constant at the interfaces of the well. Usually, however, the dielectric constants of the two materials involved are very similar and this effect can be simply modelized by taking into account an effective dielectric constant ϵ, which is assumed to be the same in the two materials [22].

The total evelope energy is governed by the Hamiltonian

$$H^{tot} = \mathcal{H}_T - 2\epsilon_c. \tag{1.15}$$

We note that the Hamiltonian H^{tot} commutes with both the in-plane momentum operator $\mathbf{P}$ and the projection $\mathcal{L}_z$ of the total angular momentum operator along the $\hat{z}$-axis. Therefore the center of mass motion may be separated

$$H^{tot} = H_T + \frac{\mathbf{P}^2}{2m_t}. \tag{1.16}$$

Here, H_T describes the 'relative' envelope Hamiltonian of the trion complex. Since

this part of $\mathcal{H}_T$ accounts for the binding energy, it is of peculiar interest. The total envelope energy is then given by

$$E^{tot} = E_T^{tot} + \frac{\hbar^2 K^2}{2m_t}, \tag{1.17}$$

with E_T^{tot} being the 'relative' envelope energy and $\mathbf{K}$ being the in-plane wavevector of the center of mass motion; $m_t = 2m_e^* + m_h^*$ is the total effective trion mass. The stability of the trion complex X^- against dissociation into an exciton and a free electron is ensured, if E_T^{tot} is smaller than E_X, the exciton ground state energy: It has to be energetically favourable to bind the second electron to the exciton. Therefore, we can write the stability criterion for the trion as

$$E_T = E_X - E_T^{tot} > 0, \tag{1.18}$$

where E_T is defined as the actual trion binding energy. In this notation it is defined as a positive quantity for a stable bound three particle object.

In what follows, we restrict our considerations to the most stable state, i.e. a symmetric orbital envelope wave function with a zero angular momentum projection along the $\hat{z}$-axis. As a direct consequence of this simplification, the 'relative' envelope wave function φ_b depends solely on the mutual interparticle distance r_{1h}, r_{2h} and r_{12}. In this spirit, the total envelope wave function for the trion factorizes into a center of mass, the relative motion and the spin part

$$\Psi_T = \frac{1}{\sqrt{A}} \exp\left(i\mathbf{KR}\right) \frac{1}{\sqrt{2\pi}} \varphi_b\left(r_{1h}, r_{2h}, r_{12}\right) \chi_{S_e, S_{hz}}\left(s_{1z}, s_{2z}, s_{hz}\right), \tag{1.19}$$

where $\mathbf{R}$ gives the center of mass position, A is the area of the sample and the factor $1/\sqrt{2\pi}$ accounts for the normalization of the overall angle degree of freedom. The fact that we only consider wavefunctions with a zero angular momentum projection

along the $\hat{z}$-axis $m = 0$ gives rise to the simplification $\exp(im\theta) \rightarrow 1$, with θ being the angle that does not affect the mutual distances between the particles.

S_e and S_{hz} describe the spin state; the variables s_{1z}, s_{2z} and s_{hz} represent the spin components along the growth direction $\hat{z}$. We only consider heavy holes which are the the highest confined valence band in typical QW systems with a heavy-hole band angular momentum projection $S_{hz} \in \{\pm 3/2\}$. The spins of the two electrons can either form an antisymmetric nondegenerate singlet state of zero total spin $S_e = 0$ or a symmetric triply degenerate state (triplet) with total spin $S_e = 1$. In total, heavy hole trions have eight spin states. To fulfill the Pauli exclusion principle for a symmetric relative motion wavefunction φ_b, the spin state $\chi_{S_e,S_{hz}}$ has to be an antisymmetric singlet state. Since we are interested in finding the trion ground state, we will only consider singlet trion states which are twofold degenerate because of the additional spin of the heavy hole. Bearing this in mind, the spin part of the trion wavefunction $\chi_{S_e,S_{hz}}$ will be dropped in the following. The specific picture of a negatively charged singlet trion that we have in mind for the rest of this thesis is schematized in Fig. (1.2).

This assumption is well justified since the X^- triplet state is unbound in zero magnetic field and therefore it has been only observed at finite magnetic fields [17].

1.2.2 Variational solution

As stated earlier, the theoretical treatment of trions is difficult. It is a few body problem with strong Coulombic interactions. However, we are interested only in the ground state, and we will use variational techniques. The Ritz procedure that has been successfully applied by Hylleraas to the similar problem of the He ground state in the early days of quantum mechanics [23]. In general, the starting point of this

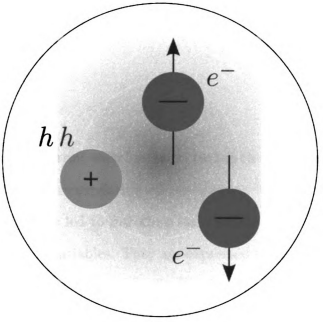

Figure 1.2: A schematic X^- trion singlet.

procedure is the variational principle

$$E[\Psi] = \langle H[\Psi] \rangle = \frac{\langle \Psi | H | \Psi \rangle}{\langle \Psi | \Psi \rangle} \rightarrow min. \tag{1.20}$$

where H as usual denotes the Hamilton operator of the system of interest. One then has to make an "educated" guess for the general form of the eigenfunction Ψ. To begin with, its general form is assumed, but a number of parameters are left arbitrary. In the next step, the necessary integrals are carried out, so that E becomes a function of the parameters which have been introduced previously. By finding the absolute minimum of this function, the parameters, thereby the ground state eigenfunction, and above all, the energy of the system are determined. Subsequently, two major aspects are essential for a successful application and accurate results in this variational method:

first, a choice of the trial wave function suitable for the problem at hand and, second, a number of variational parameters commensurate with a reasonable handling of the calculation and optimization process [24].

Striving for a class of trial wavefunctions to handle two-electron problems that explicitly take into account correlation effects without having to deal with cumbersome angles, Hylleraas was led to introduce only metric distances that have a direct physical interpretation as variables. They are expressed in terms of the three distance coordinates, the two "elliptic coordinates" plus the inter-electron distance which are related to the mutual in-plane distances as

$$s = r_{1h} + r_{2h}, \quad t = r_{1h} - r_{2h}, \quad u = r_{12}. \tag{1.21}$$

The variables s and u are positive by definition, whereas the variable t can take both positive and negative values. Owing to the Pauli exclusion principle, Ψ can either be an even or an odd function of the variable t. Since H is necessarily an even function of t and since the integrals in the variational problem contain two factors, the contributions to the integral from $-t$ has to be the same as that from $+t$. Therefore, it is a legitimate simplification to restrict ourselves to positive values of t in the integrals and multiply the volume element by a factor of 2. The volume element that has to be respected when performing the necessary integrals is derived in detail in Appendix C. The transformation from Cartesian coordinates to the coordinate set $\{\mathbf{R}, \theta, s, t, u\}$ it is given by

$$d^2\mathbf{r}_1\, d^2\mathbf{r}_2\, d^2\mathbf{r}_h \rightarrow \frac{u\left(s^2 - t^2\right)}{2\sqrt{\left(s^2 - u^2\right)\left(u^2 - t^2\right)}}\, d^2\mathbf{R}\, d\theta\, ds\, dt\, du \tag{1.22}$$

with the limits of integration for the Hylleraas coordinates

$$s \geq 0, \quad 0 \leq u \leq s, \quad 0 \leq t \leq u. \tag{1.23}$$

Ever since the introduction of this class of coordinates, their use has proved to be an efficient tool in a number of variational studies [25].

In general, the trial wavefunction used to analyzed the ground-state properties of two-electron problems is assumed to have the form

$$\Psi_H(s,t,u) = Ne^{-ks/2} \sum c_{l,m,n} k^{l+m+n} s^l t^m u^n, \tag{1.24}$$

where k and and the coefficients $c_{l,m,n}$ are to be determined variationally. N is the normalization constant. The exponential decay factor ensures convergence and more accurate results are achieved by a systematic increase of the expansion lengths. This class of Hylleraas type wavefunctions haven proven successful for three body problems as they allow for a diffusive character of the wavefunction but also manage to take into account two-body correlations. Radial and internal angular correlations effects are reasonably modeled by the third Hylleraas coordinate $u = r_{12}$. Therefore, a Hylleraas type wavefunction is expected to lead to an accurate calculation of the ground state of the charged exciton. The next step is a transformation of the "relative" Hamiltonian H_T that governs the trion binding energy by using the Hylleraas coordinates s, t, and u.

The notation can be simplified by switching to effective atomic units: We will use the atomic units $a_D = \epsilon\hbar^2/m_e^* e^2$ as a measure for length and $E_h = m_e^* e^4/\epsilon^2\hbar^2$ as energy unit; a_D is the effective 3D neutral donor Bohr radius and E_h twice the effective 3D neutral donor Rydberg. Moreover we introduce the effective mass ratio $\sigma = m_e^*/m_h^*$ as an important parameter to characterize the specific QW system.

The "relative" Hamiltonian in Hylleraas coordinates is given by

$$\begin{aligned} H_T &= -\frac{\partial^2}{\partial s^2} - \frac{\partial^2}{\partial t^2} - \frac{2}{s^2-t^2}\left(s\partial_s - t\partial_t\right) - \frac{\partial^2}{\partial u^2} - \frac{1}{u}\partial_u \\ &\quad -\frac{2s\left(u^2-t^2\right)}{u\left(s^2-t^2\right)}\partial^2_{su} - \frac{2t\left(s^2-u^2\right)}{u\left(s^2-t^2\right)}\partial^2_{tu} \\ &\quad -2\sigma\left(\frac{s^2-u^2}{s^2-t^2}\frac{\partial^2}{\partial s^2} + \frac{u^2-t^2}{s^2-t^2}\frac{\partial^2}{\partial t^2} + \frac{s}{s^2-t^2}\partial_s - \frac{t}{s^2-t^2}\partial_t\right) \\ &\quad -\frac{1}{\left|\frac{s+t}{2}\right|} - \frac{1}{\left|\frac{s-t}{2}\right|} + \frac{1}{u}, \end{aligned} \tag{1.25}$$

which corresponds to the strictly two dimensional limit of the Hamiltonian given in [22]. The first two lines govern the kinetic energy of the two electrons, the third line stands for the kinetic energy of the hole and the last line represents the Coulombic potential energy.

In order to describe the binding of the trion complex, we use a trial wavefunction which looks strikingly simple in Hylleraas coordinates. It is the so called "Dritte Näherung"

$$\varphi_b\left(s,t,u\right) = \mathcal{N}e^{-\alpha s}\left(1+\beta u+\gamma t^2\right) \tag{1.26}$$

that is equipped with the three variational parameters α, β and γ. Necessarily, $\varphi_b\left(s,t,u\right)$ is an even function of t to describe a trion singlet. Its normalization constant $\mathcal{N}$ is given by

$$\frac{1}{\mathcal{N}^2} = \frac{\pi\left(256\alpha^4 + 240\pi\alpha^3\beta + 405\pi\alpha\beta\gamma + 1152\gamma^2 + 256\alpha^2\left(3\beta^2+2\gamma\right)\right)}{4096\alpha^8}. \tag{1.27}$$

The actual values of the parameters α, β and γ are determined by varying these parameters until the mean value of 'relative' Hamiltonian $\langle H_T\rangle$, which gives the 'relative' ground state energy E_T^{tot}, reaches its minimum. As a consequence, the

variational parameters must satisfy the conditions

$$\frac{\partial \langle H_T \rangle}{\partial \alpha} = \frac{\partial \langle H_T \rangle}{\partial \beta} = \frac{\partial \langle H_T \rangle}{\partial \gamma} = 0. \tag{1.28}$$

However, no matter what the result for the variational parameters, the chosen trial wavefunction $\varphi_b(s,t,u)$ only fulfills its assigned job if it can explain the experimentally confirmed trion binding energy reasonably well. When applying the dissociation criterion stated in Eqn. (1.18), we need to apply our variational found result to the exciton ground state energy E_X. We obtain the ground state energy for the exciton from Eqn. (1.9) in effective atomic units as a simple function of the effective mass ratio σ given by

$$E_X = -4E_0 = -\frac{2}{1+\sigma}. \tag{1.29}$$

Our results are presented in Fig. (1.3). We can confirm that the trion complex is indeed stable against dissociation for any possible effective mass ratio σ. Since E_T is always positive, it is evident that the binding is stable in all cases. Indeed, the binding of an excess electron to a "neutral" exciton appears to be energetically favourable. Moreover we present the trion binding energy E_T measured relative to the exciton ground state binding energy E_x in Fig. (1.4). Intriguingly, this ratio is rather constant over the whole effective mass spectrum and is approximately 10%. Proceeding from this result, we can suggest the following useful rule of thumb: the exciton problem being by far simpler than the trion physics, accurate numbers for the exciton binding energies are very well known for all common QW structures. According to our result, a first valid approximation for the trion binding energy in this QW system can be simply achieved by taking 10% of the exciton binding energy. This result also supports the idea, that the trion originating from the electron-exciton interaction is rather loosely bound compared to the exciton. In this spirit, the trion binding stems from a dipole-charge interaction, whereas the exciton binding energy

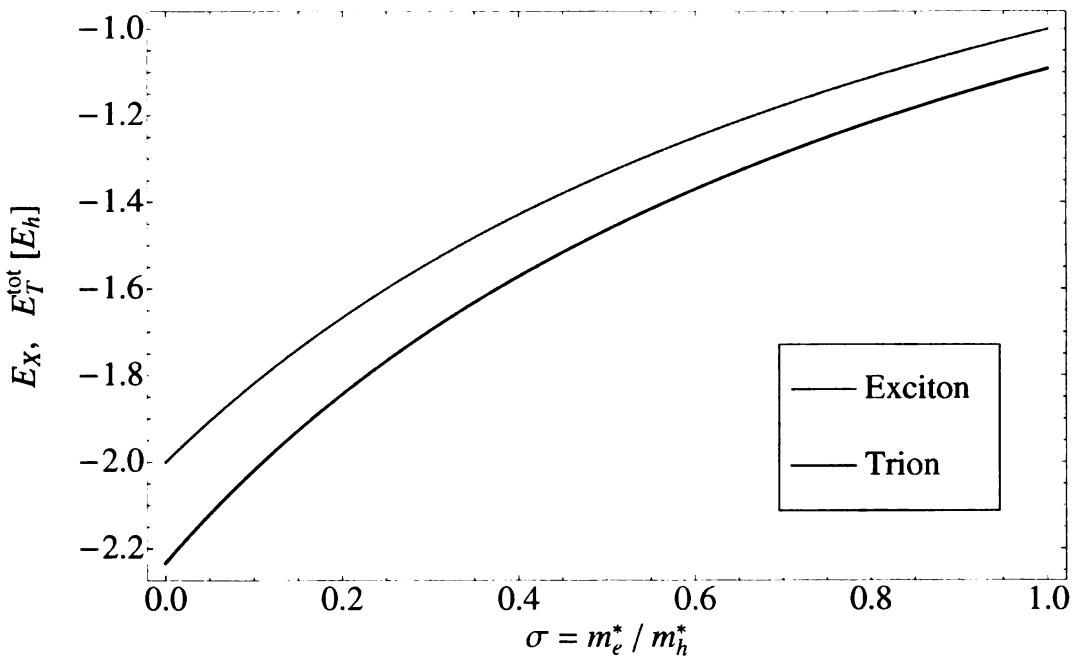

Figure 1.3: Ground state exciton binding energy and variationally optimized "relative" trion energy in Hartree units. The trion is stable against dissociation for any possible massratio σ.

comes from a pure attractive charge-charge interaction, which is essentially stronger than the dipole-charge interaction.

The result shown in Fig. (1.3) proves the stability of the trion with respect to the dissociation to an exciton and a free electron. The binding energy is given in terms of the effective Hartree energy $E_h = m_e^* e^4/\epsilon^2\hbar^2$, which is twice the effective 3D donor Rydberg energy. This quantity, however, strongly depends on the properties of the QW material. A heavier effective electron mass and particularly a smaller dielectric constant lead to a bigger Hartree energy, favouring an increased trion binding energy. Intuitively, it is evident that a smaller dielectric constant ϵ, equivalent to less screening and therefore stronger Coulomb forces, enhances the binding energy. We specify our results for the two typical QW systems $GaAs$ and $CdTe$. They are summarized in Tab. (1.1).

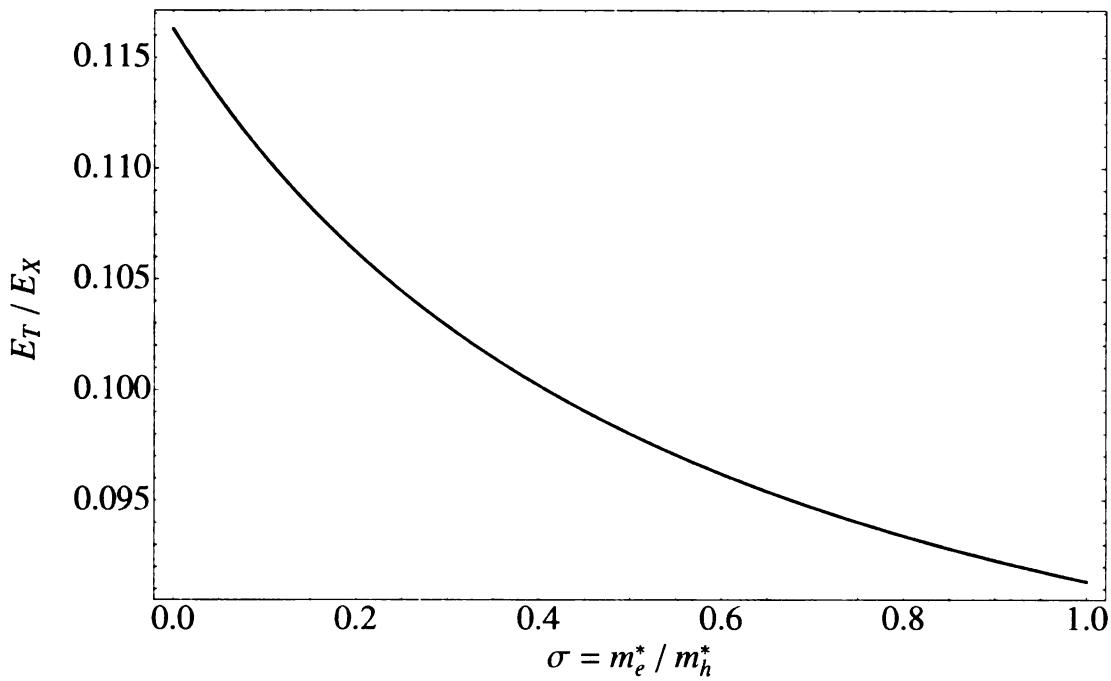

Figure 1.4: Variationally optimized trion binding energy E_T measured relative to the exciton binding energy E_X.

	$GaAs$	$CdTe$
E_T/E_X	0.11	0.10
$E_T\,[meV]$	2.05	3.61

Table 1.1: Calculated trion binding energies for $GaAs$ and $CdTe$.

Although the relative trion binding energy is comparable in both systems, a much stronger absolute trion binding energy can be expected for $CdTe$, evidently owing to the fact that E_h is more than two times bigger in $CdTe$ than in $GaAs$. Our results for the absolute trion binding energies in these two systems are in an excellent agreement to previous theoretical studies and experimentally measured values. In real finite size $GaAs$ QWs the trion binding energy varies with the well width, from$\sim 1\,meV$ in wide $30\,nm$ wells up to $\sim 2\,meV$ in $10\,nm$ QW [5]. Our theoretical value is closer to the latter, which is no suprise at all, as our calculation refers to the purely two dimensional QW. As far as $CdTe$ is concerned, previous theoretical studies have

obtained the value $E_T \approx 3.7\,meV$ and experimentally values of $E_T \approx 3\,meV$ were reported [22, 26]. As a side note, we mention that, by taking the limit $\sigma \to 0$, we recover the two dimensional H^- binding energy [27].

We have obtained an analytic expression for $\langle H_T(\alpha, \beta, \gamma) \rangle$, which is presented in Appendix D along with the results for the variational parameters α, β and γ. We have specified the variationally optimized values for the QW structures $GaAs$ and $CdTe$.

Despite its simple form and the fact that our trial wavefunction depends on three variational parameters only, it obviously captures the essential physics and produces very good results. For our purposes, it represents a very good trade-off between simplicity and accuracy.

Now that we have obtained wavefunctions to describe both ground state excitons and ground state trions, we are in the position to investigate several properties of these two different semiconductor excitations. The first goal will be a comparison of their typical spatial extensions. We have already considered the "size" of the exciton in a purely two dimensional QW; we found that its characteristic size a_x is $a_x = a_0/2 = a_D(1+\sigma)/2$, where a_D is the natural lengthscale that we are using. Naturally, we expect the trion "size" to be more extended compared to the exciton, as its binding energy is about one order of magnitude smaller. To approximate the extension of the three-particle complex of a trion, we calculate the expectation value $\langle s \rangle$ for the Hylleraas coordinate s, based on the variationally found wavefunction $\varphi_b(s,t,u)$, and compare this result to a_x.

Qualitatively, but very intuitively we can also understand the "size" of the trion a_t from the following picture: If we interpret a_t as the characteristic length associated to the weak binding of the trion's second electron, we can express a_t in terms of the

trion binding energy

$$E_T = \hbar^2 \left(m_e^{*-1} + \left(m_e^* + m_h^* \right)^{-1} \right) / 2a_t^2. \tag{1.30}$$

Similarly we define the size of an exciton a_x via

$$E_X = \hbar^2 \left(m_e^{*-1} + m_h^{*-1} \right) / 2a_x^2. \tag{1.31}$$

Both approaches lead to similar results; they are summarized in Tab. 1.2. In the case of $GaAs$ we used $E_X = 20\,meV$, $E_T = 2\,meV$ and for $CdTe$ $E_X = 40\,meV$ and $E_T = 3.6\,meV$, which are the results we obtained for a strictly two dimensional QW with the corresponding material properties. As expected the trion has a more diffusive character compared to an exciton, its typical "size" being about one order of magnitude bigger than the excitons typical spatial extension.

	$GaAs$	$CdTe$
$(\langle s \rangle / a_x)^2$	11.6	12.6
$(a_t/a_x)^2$	9.7	9.9

Table 1.2: Typical trion "size" compared to exciton "size" in $GaAs$ and $CdTe$.

1.3 Light-matter interaction: Optical matrix elements

In this section we focus on the coupling of light with a semiconductor quantum well by calculating the optical matrix elements. These matrix elements express the transition amplitudes between different semiconductor eigenstates. Physically, they are based on the absorption and emission of photons. To be specific, we consider the interaction of the semiconductor QW with a classical monochromatic standing wave

$\mathbf{E}(\mathbf{r},t) = \mathbf{E}_0 \cos(\mathbf{Q}\mathbf{r}) \cos(\omega t)$, where $\mathbf{E}_0$ is the amplitude of the electric field, $\mathbf{Q}$ the in-plane wavevector and ω the frequency of the light. Therefore, the spectrum of photonic modes contains only two contributions, namely photons with the in-plane momenta $\pm\mathbf{Q}$.

Before going into the detailed calculations, let us understand the underlying physics first. Fig. (1.5) draws a scheme of the possible processes that we are about to investigate.

Let us consider the case first where the conduction band is initially empty. This situation refers to the upper half of Fig. (1.5). Under this condition, we can only expect to photoexcite excitons, but not trions. For the creation of excitons the initial state $|i\rangle$ is characterized by a photon of momentum $\mathbf{Q}$, which corresponds to a plane wave. It can either excite a bound exciton X or an unbound electron-hole pair. However, the creation of an exciton is much more likely to happen, because the center of mass of the exciton is a plane wave as well, and therefore the matching between the initial and the final state is larger. The matching is much poorer in the second case, because one initial plane wave photon $\mathbf{Q}$ has to split up into two plane waves, one for the free electron with momentum $\mathbf{k}_e = \mathbf{k} + \alpha_e\mathbf{Q}$ and one for the free hole with momentum with momentum $\mathbf{k}_e = -\mathbf{k} + \alpha_h\mathbf{Q}$. The QW is translationally invariant and therefore the center of mass momentum is always conserved. Hence, in the first case the exciton's center of mass momentum is just the momentum of the incoming photon $\mathbf{Q}$, while in the second case it splits between the two particles according to their masses, $\alpha_e = 1 - \alpha_h = m_e^*/\left(m_e^* + m_h^*\right)$; $\mathbf{k}$ describes the relative motion momentum of the electron hole pair.

Now, let us turn to the situation where the conduction band is not initially empty, i.e. excess electrons are assumed to be already present in the sample. As explained, this can be easily achieved by the method of modulation doping. This situation refers to the lower half of Fig. (1.5). The semiconductor-photon interaction then

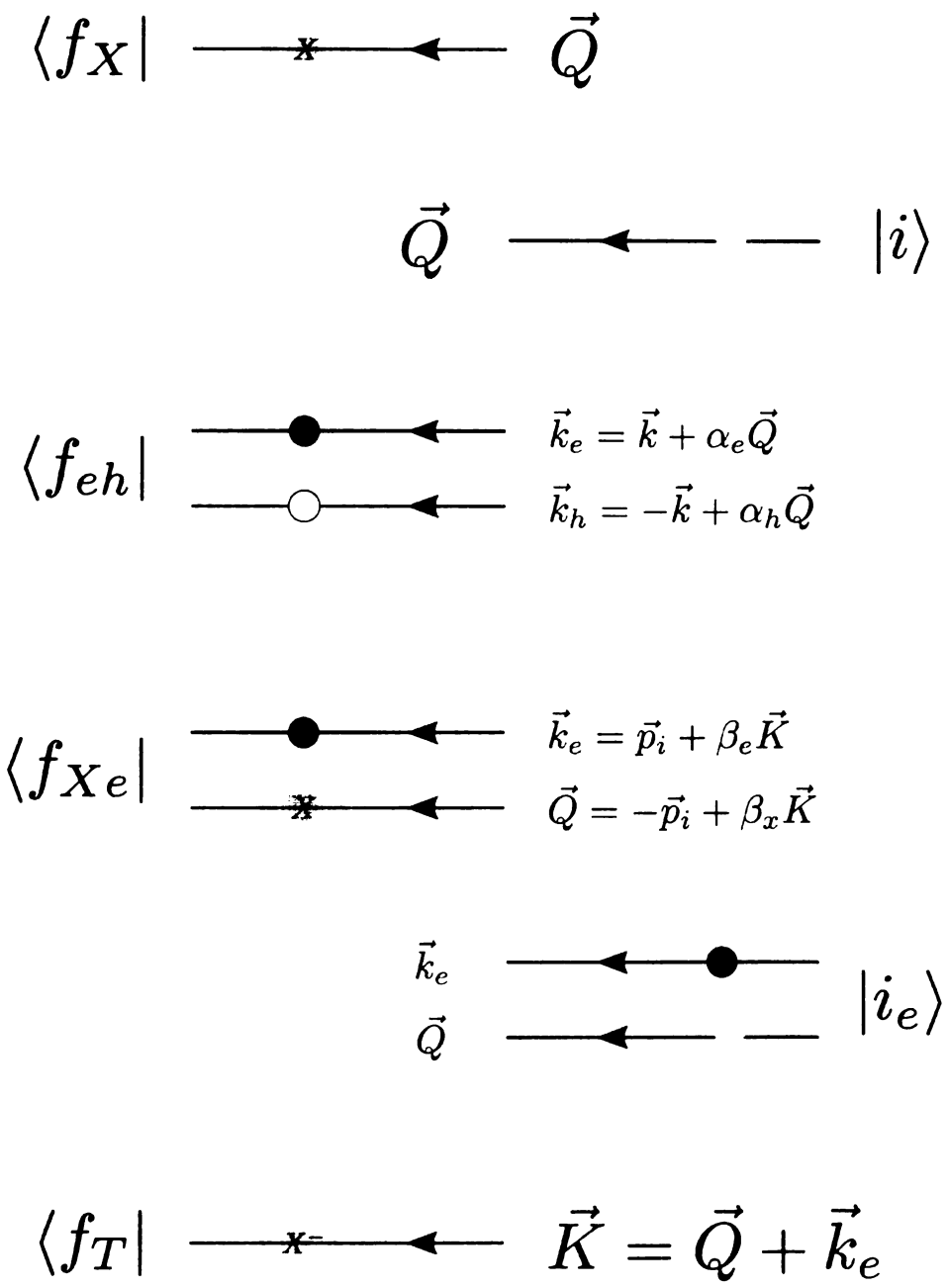

Figure 1.5: Schematic transition processes for a semiconductor QW, coupled to photons with momenta **Q**. Photonic lines, excitonic lines and trionic lines are marked by a red dot, green dot and blue dot respectively; free electrons and holes by black and grey dots, respectively. The upper half displays transitions of photons to excitons or unbound electron-hole pairs. The lower half describes the possible transitions to unbound and bound trions if the initial state contains also an excess electron. See also [32].

couples the excess electrons to bound and unbound trion states. Unbound trion states refer to ionized trions, i.e. to the combination of excitons with free electrons, essentially independent of each other. In contrast to the situation highlighted above the initial state $|i_e\rangle$ contains, besides the photon plane wave, an additional electron with momentum $\mathbf{k}_e$. Two plane waves, one for the free electron and one for the photon, can now either transform into two plane waves, if the final state is an unbound trion, or into one plane wave, if the final state is a bound trion. The bound trion just has one center of mass momentum $\mathbf{K} = \mathbf{Q}+\mathbf{k}_e$, whereas $\mathbf{K}$ splits between the electron-exciton pair according to their masses, namely $\beta_e = 1 - \beta_x = m_e^*/(2m_e^* + m_h^*) = m_e^*/m_t$, for an unbound trion. Accordingly, the total center of mass $\mathbf{K}$ is linked to the momentum of the initial electron $\mathbf{k}_e$ and the exciton momentum $\mathbf{Q}$ as

$$\mathbf{k}_e = \mathbf{p}_i + \beta_e \mathbf{K} \tag{1.32}$$

$$\mathbf{Q} = -\mathbf{p}_i + \beta_x \mathbf{K} \tag{1.33}$$

which shows that

$$\mathbf{p}_i = \beta_x \mathbf{k}_e - \beta_e \mathbf{Q} \tag{1.34}$$

is the relative motion momentum of the initial electron - photocreated exciton pair.

The goal of this section is to derive the transition matrix elements for bound and unbound trions, induced by the light-matter coupling. We will emphasize and discuss their different characteristics. We restrict our analysis to bound singlet trions described by the variationally obtained wavefunction and $1s$ excitons respectively. We can safely neglect the possibility of the photon transforming into an unbound electron-hole pair, because first of all the phase matching is poor for this transition and, moreover, the laser light is assumed to be tuned closer to the trion and $1s$ exciton resonances. To model the interaction Hamiltonian, the first step is to get rid of the fast oscillating time dependence of the electric field by transforming the system into a

"rotating frame" rotating at the detuned laser frequency by a unitary transformation and applying the rotating wave approximation. This widely used procedure will be covered in more detail in the next chapter. We present two models, one modelling the interaction in position space, while the second one models the coupling in momentum space. In position space the light matter coupling is governed by

$$\mathcal{H}_{int} = \mathbf{d}_0 \int d^2\mathbf{r}\, \hat{\Psi}^{\dagger}_{\mp(1/2)}(\mathbf{r})\, \hat{\Psi}^{\dagger}_{\pm(3/2)}(\mathbf{r})\, \mathbf{E}(\mathbf{r}) + h.c., \tag{1.35}$$

where $\hat{\Psi}^{\dagger}_{\mp(1/2)}(\mathbf{r})$ is the field operator to create an electron at position $\mathbf{r}$ with spin $\mp 1/2$. Similarly, $\hat{\Psi}^{\dagger}_{\pm(3/2)}(\mathbf{r})$ is the field operator to create a heavy hole at position $\mathbf{r}$ with spin $\pm 3/2$. An essential ingredient is the interband dipole moment $\mathbf{d}_0$ for a valence-, conduction band transition. Its specific value is material dependent, but can be calculated conveniently from the Kane energy parameter E_P as

$$d_0 = \frac{e\hbar}{\epsilon_c}\sqrt{\frac{E_P}{2m_0}}. \tag{1.36}$$

Here, m_0 is the bare electron mass and ϵ_c the bandgap of the material. The specific values for $GaAs$ and $CdTe$ are listed in Appendix A.

The second approach to model the light matter coupling is formulated in momentum space and reads

$$\mathcal{H}_{int} = \lambda_c \sum_{\pm\mathbf{Q}} \sum_{\mathbf{k}} c^{\dagger}_{\mathbf{Q}+\mathbf{k},\mp(1/2)} d^{\dagger}_{-\mathbf{k},\pm(3/2)} a_{\mathbf{Q},\pm} + h.c., \tag{1.37}$$

where $a_{\mathbf{Q},\pm}$ is the destruction operator of a $(\sigma_{\pm}, \mathbf{Q})$ photon with energy $\hbar\omega$. Note that momentum is conserved only in-plane, which is already included in the above formulation of the coupling $\mathcal{H}_{int}$. The operators $c^{\dagger}_{\mathbf{k},s}$ and $d^{\dagger}_{\mathbf{k},m}$ account for the creation of an electron and a hole respectively. Furtermore, λ_c denotes the light-matter coupling constant. We will show that for $\lambda_c = \mathbf{d}_0\mathbf{E}_0/2 = \Omega_0/2$ the two approaches

yield to the same result; $\mathbf{E}_0$ is the amplitude of the electric field, and Ω_0 has been defined as the bare Rabi frequency

$$\Omega_0 = \mathbf{d}_0 \mathbf{E}_0. \tag{1.38}$$

The Rabi frequency is a key component in the analysis of any transition, as it measures the strength of the coupling between the light and the transition. Note that we will refer to the Rabi frequency expressed in units of energy.

We only consider trion singlets, made with heavy holes. Therefore, for a given electron spin, the polarization of the light that applies to the transition of this electron to a trion singlet state is fixed. Proceeding from a spin down electron, only light with σ_- polarization applies for the transition. For an initial spin up electron, the situation is vice versa and the electron-trion transition can only be induced by σ_+ polarized light. This reasoning is schematized in Fig. (1.6). Based on this argument, we can simplify the notation by considering an initial electron with a given spin, so that only one light polarization applies. Therefore, for a fixed initial spin, we can drop the polarization index of the light and just assume it to be the "right" one.

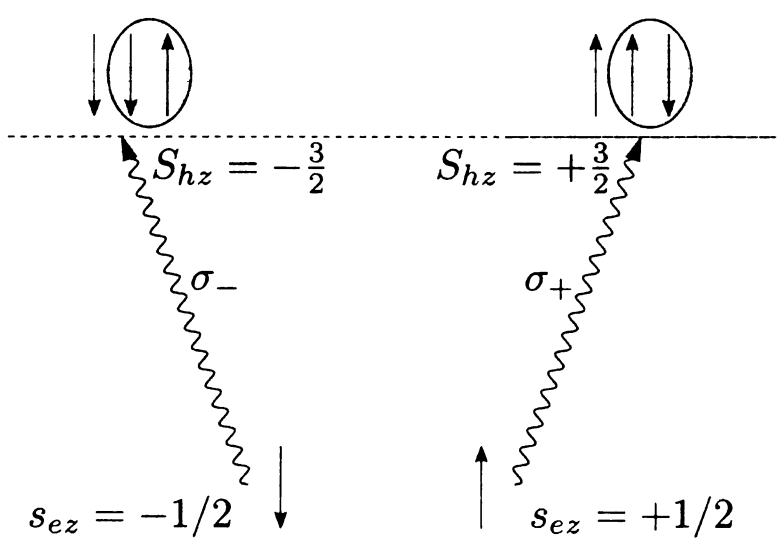

Figure 1.6: Coupling of a free electron to a bound trion singlet state.

1.3.1 Coupling to bound trions

To begin with, let us consider the coupling of a free excess electron to a bound trion state. For the sake of clarity, the initial electron's spin is assumed to be spin down $\downarrow$, as depicted on the left-hand side of Fig. (1.6). Therefore, the transition can only be induced by a σ_- photon. We will cover the problem in position space first. We specify the initial $|i_e\rangle$ and the final state $|f\rangle$ according to

$$|i_e\rangle = \int d^2\mathbf{r}\, \phi_\downarrow(\mathbf{r})\, \hat{\Psi}_\downarrow^\dagger(\mathbf{r})\, |0\rangle \tag{1.39}$$

$$|f\rangle = \int d^2\mathbf{r}_\uparrow d^2\mathbf{r}_\downarrow d^2\mathbf{r}_h \Psi_t(\mathbf{r}_\uparrow, \mathbf{r}_\downarrow, \mathbf{r}_h)\, \hat{\Psi}_\uparrow^\dagger(\mathbf{r}_\uparrow)\, \hat{\Psi}_\downarrow^\dagger(\mathbf{r}_\downarrow)\, \hat{\Psi}_h^\dagger(\mathbf{r}_h)\, |0\rangle . \tag{1.40}$$

Let us just convince ourselves that the final state $|f\rangle$ does represent a singlet trion. By adding and subtracting the same term, we can rewrite the pair of electron creation operators as

$$\begin{aligned}\hat{\Psi}_\uparrow^\dagger(\mathbf{r}_\uparrow)\, \hat{\Psi}_\downarrow^\dagger(\mathbf{r}_\downarrow) = \frac{1}{2}\Big\{ & \hat{\Psi}_\uparrow^\dagger(\mathbf{r}_\uparrow)\, \hat{\Psi}_\downarrow^\dagger(\mathbf{r}_\downarrow) - \hat{\Psi}_\downarrow^\dagger(\mathbf{r}_\uparrow)\, \hat{\Psi}_\uparrow^\dagger(\mathbf{r}_\downarrow) \\ & + \hat{\Psi}_\uparrow^\dagger(\mathbf{r}_\uparrow)\, \hat{\Psi}_\downarrow^\dagger(\mathbf{r}_\downarrow) + \hat{\Psi}_\downarrow^\dagger(\mathbf{r}_\uparrow)\, \hat{\Psi}_\uparrow^\dagger(\mathbf{r}_\downarrow) \Big\} .\end{aligned} \tag{1.41}$$

Obviously, the pair of electron creation operators we are dealing with now displays itself as a superposition of a singlet and a triplet state in the first and the second line, respectively. However, by using the fermion anticommutation relation, the symmetry property of Ψ_t and interchanging the integration dummy variables $\mathbf{r}_\uparrow \leftrightarrow \mathbf{r}_\downarrow$ in the last term, we can see that the triplet part indeed vanishes and we are left with

$$\hat{\Psi}_\uparrow^\dagger(\mathbf{r}_\uparrow)\, \hat{\Psi}_\downarrow^\dagger(\mathbf{r}_\downarrow) = \frac{1}{2}\Big\{ \hat{\Psi}_\uparrow^\dagger(\mathbf{r}_\uparrow)\, \hat{\Psi}_\downarrow^\dagger(\mathbf{r}_\downarrow) - \hat{\Psi}_\downarrow^\dagger(\mathbf{r}_\uparrow)\, \hat{\Psi}_\uparrow^\dagger(\mathbf{r}_\downarrow) \Big\} . \tag{1.42}$$

The initial state $|i_e\rangle$ describes a free excess electron, which is simply taken to be

a plane wave with momentum $\mathbf{k}_e$

$$\phi_{\downarrow}(\mathbf{r}) = \frac{\exp(i\mathbf{k}_e\mathbf{r})}{\sqrt{A}}, \tag{1.43}$$

normalized to the area of the sample A. The final state is a bound trion state with total wavefunction $\Psi_t(\mathbf{r}_{\uparrow}, \mathbf{r}_{\downarrow}, \mathbf{r}_h)$, that separates into three pieces

$$\Psi_t(\mathbf{r}_{\uparrow}, \mathbf{r}_{\downarrow}, \mathbf{r}_h) = \frac{1}{\sqrt{A}} \exp\left[i\mathbf{K}\left(\frac{m_e(\mathbf{r}_{\uparrow} + \mathbf{r}_{\downarrow}) + m_h\mathbf{r}_h}{m_T}\right)\right] \frac{1}{\sqrt{2\pi}}\varphi_b(s,t,u), \tag{1.44}$$

namely a center of mass motion with wavevector $\mathbf{K}$, a rotational part that is simply in its ground state, and the "relative" part $\varphi_b(s,t,u)$ that accounts for the binding of this three particle object and was determined by our variational approach. Electrons and holes being fermions, we can use the anticommutation relations for fermions

$$\left\{\hat{\Psi}_s(\mathbf{r}), \hat{\Psi}^{\dagger}_{s'}(\mathbf{r}')\right\} = \delta_{s,s'}\delta(\mathbf{r} - \mathbf{r}'), \tag{1.45}$$

to write the transition amplitude for this process in the general form

$$\langle f|\mathcal{H}_{int}|i_e\rangle = \mathbf{d}_0 \int d^2\mathbf{r}d^2\mathbf{r}'\, \Psi_t^*(\mathbf{r},\mathbf{r}',\mathbf{r})\, \phi_{\downarrow}(\mathbf{r}')\, \mathbf{E}(\mathbf{r}). \tag{1.46}$$

Although this is not the ultimate result and will be subject to a further evaluation, it already bears some physical insight for the problem at hand. It shows the physically intriguing property that the photoexcited electron-hole pair is created exactly on top of each other at $\mathbf{r}$, exactly at the spot where the photon is destroyed, as the dependence on $\mathbf{E}(\mathbf{r})$ in the integral shows. Owing to this property, we can circumvent a cumbersome evaluation of the remaining integrals due to the relative wavefunction formulated in Hylleraas coordinates: For one electron and one hole at the same spot - the situation we face now - the Hylleraas coordinates boil down to the simple case

where they all take on the same value, namely: $s = t = u = |\mathbf{r} - \mathbf{r}'|$. The evaluation of the remaining integrals essentially becomes a two body problem between an electron of mass m_e^* and an exciton of mass $m_x = m_e^* + m_h^*$, so that it is appropriate for a solution in center of mass $\mathbf{R} = \left(m_x \mathbf{r} + m_e^* \mathbf{r}'\right)/m_t$ and relative coordinates $\mathbf{r} - \mathbf{r}'$. In this fashion, we find that the transition amplitude can be written in the compact form

$$\langle f | \mathcal{H}_{int} | i_e \rangle = \frac{\Omega_0}{2} \left[\delta_{\mathbf{K},\mathbf{k}_e+\mathbf{Q}} I_+ (\mathbf{k}_e) + \delta_{\mathbf{K},\mathbf{k}_e-\mathbf{Q}} I_- (\mathbf{k}_e) \right], \tag{1.47}$$

where we have defined the quantities $I_\pm (\mathbf{k}_e)$ as

$$I_+ (\mathbf{k}_e) = \frac{1}{\sqrt{2\pi}} \int d^2\mathbf{r} \exp\left(i \left(\beta_e \mathbf{Q} - \beta_x \mathbf{k}_e\right) \mathbf{r}\right) \varphi_b (r, r, r) \tag{1.48}$$

$$I_- (\mathbf{k}_e) = \frac{1}{\sqrt{2\pi}} \int d^2\mathbf{r} \exp\left(i \left(-\beta_e \mathbf{Q} - \beta_x \mathbf{k}_e\right) \mathbf{r}\right) \varphi_b (r, r, r). \tag{1.49}$$

The first term in Eqn. (1.47) stands for the interaction with the $+\mathbf{Q}$ mode of the standing wave, whereas the second term stems from the interaction with the $-\mathbf{Q}$ mode. The Kronecker deltas take care of the in-plane momentum conservation: They simply require that the trion center of mass momentum has to match the sum of the photon momentum $\pm\mathbf{Q}$ and the initial momentum of the electron $\mathbf{k}_e$. The essential physics, however, are buried into the expressions $I_\pm (\mathbf{k}_e)$. They cover the intrinsic coupling strength of a single electron to a bound trion. We note that expression (1.48) is identical to the optical matrix element found in previous theoretical studies for the trion-related absorption at $T = 0K$ [30, 31].

Before we we give a detailed analysis of the expressions $I_\pm (\mathbf{k}_e)$, let us first show that we can derive the same expression using a formulation of the problem in $\mathbf{k}$-space, based on the interaction Hamiltonian in Eqn. (1.37). Again, we fix the spin of the initial electron to be in the spin down state $\downarrow$, whereby the polarization of the light has to be σ_-. The initial state we are to consider contains an electron of momentum

$\mathbf{k}_e$ and a photon of in-plane momentum $\mathbf{Q}$. Therefore, we can represent the initial state as

$$|i_e\rangle = \left|\mathbf{k}_e^{\downarrow}, \mathbf{Q}\right\rangle = c^{\dagger}_{\mathbf{k}_e,\downarrow} a^{\dagger}_{\mathbf{Q},-} |0\rangle \,. \tag{1.50}$$

The energy of this state E_i is simply the sum of the energy of the free electron in the conduction band and the photon

$$E_i = \epsilon_c + \frac{\hbar^2 k_e^2}{2m_e^*} + \hbar\omega. \tag{1.51}$$

The final state $|f\rangle$ of the transition is assumed to be a singlet bound ground state trion. By already incorporating momentum conservation into the notation, we express the final state in short as

$$|f\rangle = |\mathbf{k}_e + \mathbf{Q}\rangle_t \,, \tag{1.52}$$

where the subscript denotes a bound trion state. The center of mass momentum of the trion $\mathbf{k}_e + \mathbf{Q}$ appears in the bracket. No further quantum numbers are needed to specify the bound trion state, since we restrict our analysis to singlet trions described by the wavefunction given in (1.44). The energy of the final state E_f contains a bound trion, made of two electrons in the conduction band and one hole in the valence band. The necessary energy has been provided by the initial photon, so that E_f takes on the form

$$E_f = 2\epsilon_c + \frac{\hbar^2 (\mathbf{k}_e + \mathbf{Q})^2}{2m_t} - E_T. \tag{1.53}$$

In $\mathbf{k}$-space the information about the wavefunction enters explicitly via its Fourier transform. In general, a singlet bound trion state is twofold degenerate with respect to the spin of the heavy hole; with a fixed center of mass momentum $\mathbf{q}$ can be

represented in second quantization as

$$|\mathbf{q}\rangle_t = \sum_{\mathbf{k}_1,\mathbf{k}_2} \tilde{\Psi}_t\left(\mathbf{k}_1,\mathbf{k}_2,\mathbf{q}-\mathbf{k}_1-\mathbf{k}_2\right) c^\dagger_{\mathbf{k}_1,\uparrow} c^\dagger_{\mathbf{k}_2,\downarrow} d^\dagger_{\mathbf{q}-\mathbf{k}_1-\mathbf{k}_2,\pm(3/2)} |0\rangle\,, \tag{1.54}$$

where $\tilde{\Psi}_t$ is the Fourier transform of total trion wavefunction Ψ_t, defined by

$$\tilde{\Psi}_t\left(\mathbf{k}_1,\mathbf{k}_2,\mathbf{p}\right) = \frac{1}{A^{3/2}} \int d^2\mathbf{r}_1 d^2\mathbf{r}_2 d^2\mathbf{r}_h e^{-i(\mathbf{k}_1\mathbf{r}_1+\mathbf{k}_2\mathbf{r}_2+\mathbf{p}\mathbf{r}_h)} \Psi_t\left(\mathbf{r}_1,\mathbf{r}_2,\mathbf{r}_h\right), \tag{1.55}$$

where $\mathbf{p} = \mathbf{q}-\mathbf{k}_1-\mathbf{k}_2$. Using the anti-commutation relations for electron creation and annihilation operators

$$\left\{c_{\mathbf{k},s}, c_{\mathbf{k}',s'}\right\} = 0, \qquad \left\{c_{\mathbf{k},s}, c^\dagger_{\mathbf{k}',s'}\right\} = \delta_{s,s'}\delta_{\mathbf{k},\mathbf{k}'} \tag{1.56}$$

and similarly for the hole creation and destruction operators, we obtain that the transition amplitude becomes

$$\left\langle \mathbf{k}_e^\downarrow, \mathbf{Q}\right| \mathcal{H}_{int} |\mathbf{k}_e+\mathbf{Q}\rangle_t = \lambda_c \delta_{\mathbf{K},\mathbf{k}_e+\mathbf{Q}} I_+\left(\mathbf{k}_e\right). \tag{1.57}$$

This reasoning was based on a fixed mode $+\mathbf{Q}$, because we only considered the final state $|\mathbf{k}_e+\mathbf{Q}\rangle_t$. Taking into account the presence of both the $+\mathbf{Q}$ and the $-\mathbf{Q}$ mode of the standing wave, we find

$$\left\langle \mathbf{k}_e^\downarrow\right| \mathcal{H}_{int} |\mathbf{K}\rangle_t = \lambda_c \left[\delta_{\mathbf{K},\mathbf{k}_e+\mathbf{Q}} I_+\left(\mathbf{k}_e\right) + \delta_{\mathbf{K},\mathbf{k}_e-\mathbf{Q}} I_-\left(\mathbf{k}_e\right)\right]. \tag{1.58}$$

Therefore, we have proven the equivalence of the two approaches (see Eqn. (1.47)), if the light matter coupling constant λ_c is chosen to be

$$\lambda_c = \frac{\mathbf{d}_0\mathbf{E}_0}{2} = \frac{\Omega_0}{2}. \tag{1.59}$$

The factor of 1/2 arises from the expansion of the standing wave profile $\cos(\mathbf{Qr})$ into its two mode contributions according to

$$\Omega_0 \cos(\mathbf{Qr}) = \frac{\Omega_0}{2}\left(e^{i\mathbf{Qr}} + e^{-i\mathbf{Qr}}\right). \tag{1.60}$$

We have shown, that both approaches arrive at the same result. After all, the result should be independent of the basis. However, the analysis in terms of both basis provides a better insight on the physics of the process. Let us pause for a moment and give a physical interpretation to the expressions $I_{\pm}(\mathbf{k}_e)$ in Eqn. (1.48) and (1.49). The trion transition amplitude, also called the trion oscillator strength, appears in terms of the Fourier transform $I_{+}(\mathbf{k})$ of the relative motion part of the full trion wave function; the Fourier transform taken for the situation of photocreation - photons create one electron and one hole 'on top' of each other - and $\mathbf{k}$ equal to the relative motion momentum $\mathbf{p}_i$ of the e-X pair made with the initial electron $\mathbf{k}_e$ and the photocreated exciton $\mathbf{Q}$.

On top of this physically intriguing result, we have obtained analytic expressions for the quantities $I_{\pm}(\mathbf{k}_e)$. For the 'relative' trial wavefunction, given in Eqn. (1.26), they read

$$I_{\pm}(\mathbf{k}) = \sqrt{2\pi}\mathcal{N}\frac{C_1\left|\pm\beta_e\mathbf{Q} - \beta_x\mathbf{k}\right|^4 + C_2\left|\pm\beta_e\mathbf{Q} - \beta_x\mathbf{k}\right|^2 + C_3}{\left(\alpha^2 + \left|\pm\beta_e\mathbf{Q} - \beta_x\mathbf{k}\right|^2\right)^{7/2}}. \tag{1.61}$$

Here, C_1, C_2 and C_3 are simply constants, determined by the variational parameters α,β and γ via the expressions

$$C_1 = \alpha - \beta \tag{1.62}$$

$$C_2 = \alpha(\alpha(2\alpha + \beta) - 9\gamma) \tag{1.63}$$

$$C_3 = \alpha^3\left(\alpha^2 + 2\alpha\beta + 6\gamma\right). \tag{1.64}$$

In order to gain a better physical insight, we present plots of the functions $I_{\pm}(\mathbf{k})$ in $\mathbf{k}$-space in Fig. (1.7). To be specific, the parameters for $GaAs$ were taken, but no actual differences occur for $CdTe$. We can see that both are strongly peaked around $\mathbf{k} \approx 0$. The different shifts of the centers are negligible, because the photon wavevector $\mathbf{Q}$ is very small on this scale. While in real space the wavelength λ of the laser is much bigger than the trion size a_t, about one to two orders of magnitude, in momentum space the relation of the associated quantities is reversed: The momentum of the photon $Q = 2\pi/\lambda$ is negligibly small compared to $1/a_t$, which gives the appropriate scaling behaviour of the Fourier transform of the relative trion wavefunction. This is why the functions $I_{\pm}(\mathbf{k})$ rapidly go to zero on a scale of $\sim \alpha \sim 1/a_t$.

The fact that we have analytic expressions for the trion oscillator strength will turn out to be a helpful tool for further calculations.

1.3.2 Coupling to unbound trions

Going back to Fig. (1.5), we see that an electron is not only coupled to the bound trion state, but also unbound trions, meaning free electron - exciton pairs. The bound trion state is energetically more favourable, but the photoexcited exciton can only capture the excess electron if it is created close enough to the electron. A intuitive picture we will refer to later is that the electron and the exciton have to be within the typical trion size $\sim a_t^2$ to be able to generate a bound trion state. Otherwise the exciton and the electron are essentially independent of each other and coexist in the semiconductor QW.

We are going to give a closer look at the transition rate for this process involving unbound electron-exciton pairs. To characterize the unbound trion states, we restrict ourselves to $1s$ excitons, which typically give the strongest peak in absorption measurements and are well separated from the next higher exciton level by about

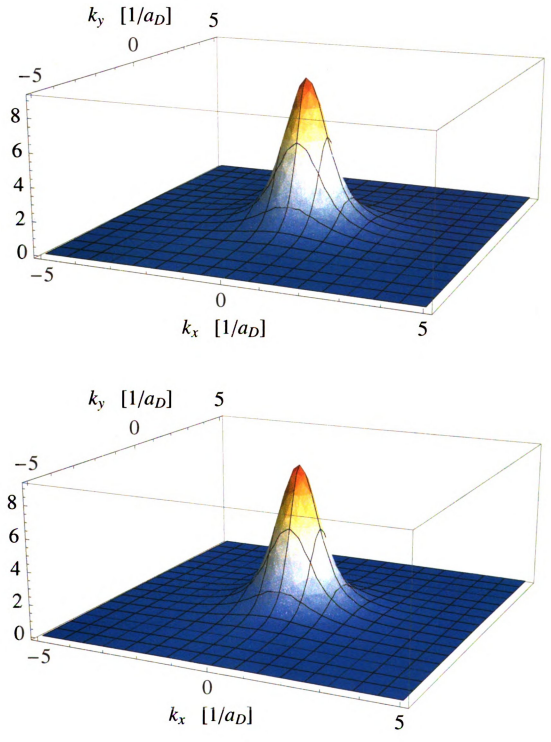

Figure 1.7: Plots of the functions $I_{\pm}(\mathbf{k})$: They govern the trion oscillator strength for the interaction with a $\pm\mathbf{Q}$ mode. The variational parameters for $GaAs$ were used. The value for $\mathbf{Q}$ corresponds to laser light tuned close to the trion resonance at an angle of 30° with respect to the $\hat{z}$-axis.

$\sim 3.5E_0$. We start from a free electron state as our initial state

$$\phi(\mathbf{r}) = \langle \mathbf{r}|i_e\rangle = \frac{\exp(i\mathbf{k}_e\mathbf{r})}{\sqrt{A}}, \tag{1.65}$$

which is a plane wave with momentum $\mathbf{k}_e$. The final state, which shall be described by the wavefunction $\Psi_c(\mathbf{r}_1, \mathbf{r}_2, \mathbf{r}_h)$, contains two plane waves, one for the free electron and one for the $1s$ exciton. The subscript c indicates the exciton states form a continuum. We can write $\Psi_c(\mathbf{r}_1, \mathbf{r}_2, \mathbf{r}_h)$ as a simple product of the electron and the exciton wavefunction

$$\Psi_c(\mathbf{r}_1, \mathbf{r}_2, \mathbf{r}_h) = \langle \mathbf{r}|f\rangle = \frac{\exp(i\mathbf{k}_x(\alpha_e\mathbf{r}_1 + \alpha_h\mathbf{r}_h))}{\sqrt{A}} \frac{\exp(i\mathbf{k}\mathbf{r}_2)}{\sqrt{A}} \phi_{1s}(\mathbf{r}_1 - \mathbf{r}_h), \tag{1.66}$$

where we introduced $\alpha_{e/h} = m^*_{e/h}/m_x$; the electron has an wavevector $\mathbf{k}$, while the exciton's wavevector is $\mathbf{k}_x$. Note that to describe this state we have to assign it the quantum numbers $\mathbf{k}$ and $\mathbf{k}_x$, while for bound trions one wavevector was sufficient to characterize the state. We could equivalently assign it a center of mass momentum, but would still have to define a relative momentum. The nomenclature "exciton continuum" is based on this reasoning. It is important to emphasize that this ansatz to describe the continuum states Ψ_c is not properly symmetrized. However, in Appendix E.1 we show in detail that for a macroscopic sample the exchange effects that arise from a proper symmetrization of the wavefunction are negligible.

To calculate the transition amplitude, we can simply refer to Eqn. (1.46) by replacing Ψ_t with Ψ_c. Expanding the $\cos(\mathbf{Qr})$ into its two modes, we find the transition amplitude to be

$$\langle \mathbf{k}_e|\mathcal{H}_{int}|\mathbf{k}_x, \mathbf{k}\rangle_c = \Omega_x \delta_{\mathbf{k}_e,\mathbf{k}} \left[\delta_{\mathbf{K}-\mathbf{k}_e,\mathbf{Q}} + \delta_{\mathbf{K}-\mathbf{k}_e,-\mathbf{Q}}\right]. \tag{1.67}$$

Here we introduced the effective exciton Rabi frequency Ω_x as

$$\Omega_x = \frac{\Omega_0}{2}\phi_{1s}(0)\sqrt{A}. \tag{1.68}$$

Although the bare coupling Ω_0 being the same, the overall nature of this transition amplitude is strikingly different than from the one we have obtained before for bound trion states. Let us mention the obvious part first: The Kronecker deltas handle the impulse conservation, whereby the photo-excited exciton just takes the photon momentum, while the free electron is unaffected by the transition and simply stays in its initial momentum eigenstate. The fact that the amplitude is proportional to the relative exciton wavefunction taken at $\mathbf{r} = 0$ goes along the line with the result found by Elliott in Eqn. (1.8). In this picture the corresponding expression for bound trions in Eqn. (1.48) can be regarded as a natural generalization of the excitonic transition rate, one relative coordinate being set to zero. The more interesting part is that the exciton oscillator strength appears as an extensive quantity that scales with the area of the sample according to the dependence $\sim \sqrt{A}$. Owing to the normalization constant of the $1s$ wavefunction

$$\phi_{1s}(0) \sim \sqrt{1/(\pi a_x)^2}, \tag{1.69}$$

it can be visualized as proportional to the number of excitons that fit into the sample without spatial overlap. The bigger the sample is, the more excitons can be excited. Every single exciton transition at a particular spot is driven by the bare Rabi frequency Ω_0, but the macroscopic size of the sample accounts for a huge collective enhancement factor for the exciton oscillator strength. This result sheds an interesting light on the nature of excitons: they appear as a coherent elementary excitation over the whole sample, resulting in a macroscopic transition dipole moment and sharp

absorption peaks in ideal cases. Since the presence of the electron effectively does not affect the process studied here, the unbound trion has essentially the same oscillator strength as the exciton.

The oscillator strength decrease from ionized to bound trions is therefore of the order of $\sim a_t^2/A$, which is vanishingly small in the large sample limit. However, this is not suprising, because it considers the somewhat artificial limit of a single electron in a huge macroscopic sample. One single electron cannot have a sizeable effect on the photon absorption. The exciton's oscillator strength is approximately $\sim A/a_x^2$, while the trion oscillator strength scales as $\sim \left(A/a_x^2\right)\left(a_t^2/A\right) \approx a_t^2/a_x^2$, which corresponds to a picture in which the trion oscillator strength is proportional to the number of excitons that fit into a single trion without spatial overlap [32]. We already estimated this ratio to be of the order of 10.

1.4 Radiative lifetimes

In this section we will present the radiative properties of excitons and trions. The intrinsic radiative decay of both free excitons and trions in low-dimensional systems is due to the coupling with a continuum of photon states. We will analyze the different characteristics of these two decay processes. The calculations will be based on the assumption of conservation of the in-plane wavevector, thereby disregarding possible effects of interface roughness and acoustic phonon scattering. The effect of the latter can be minimized in the low temperature regime. Therefore we will consider the $T \rightarrow 0$ limit. The wavevector conservation is likely to be a plausible assumption, whenever the coherence length of the quasiparticles is longer than the wavelength of the light [33]. This condition can be satisfied in good quality samples at low temperatures.

The proper framework to perform the actual calculations is Fermi's Golden Rule:

The decay rate of a state $|\alpha\rangle$ or equivalently the probability to make a transition from the initial state $|\alpha\rangle$ to the final state $|\beta\rangle$ per unit time to first order in perturbation theory is given by

$$\Gamma_{\alpha\to\beta} = \frac{2\pi}{\hbar} \left|\mathcal{M}_{\alpha\beta}\right|^2 \delta\left(E_\beta - E_\alpha\right), \tag{1.70}$$

where $\mathcal{M}_{\alpha\beta}$ is the matrix element which couples the initial and the final states. To find the total decay rate Γ of the initial state $|\alpha\rangle$ we have to sum over all possible final state configurations, the δ-function appearing in Fermi's Golden Rule effectively taking care of energy conservation in this process. We then find the general expression

$$\Gamma = \frac{2\pi}{\hbar} \sum_\beta \left|\mathcal{M}_{\alpha\beta}\right|^2 \delta\left(E_\beta - E_\alpha\right). \tag{1.71}$$

The interaction Hamiltonian $\mathcal{H}_I$ that couples the initial and final states can be expressed in second quantized form as

$$\mathcal{H}_I = g \sum_{\mathbf{Q},\mathbf{k}} c^\dagger_{\mathbf{Q}+\mathbf{k},\mp(1/2)} d^\dagger_{-\mathbf{k},\pm(3/2)} a_{\mathbf{Q},\pm} + h.c. \tag{1.72}$$

Note that in-plane momentum conservation is already included, but the $\hat{z}$-component of the photon is left arbitrary. The coupling constant g is the only difference from Eqn. (1.37), where we considered transitions induced by a classical electromagnetic standing wave. In order to describe the spontaneous decay process, we take g to be

$$g = \mathbf{d}_0 \hat{\epsilon} \mathcal{E}. \tag{1.73}$$

Here, $\mathbf{d}_0$ denotes, as before, the interband transition dipole moment, $\hat{\epsilon}$ is the polarization of the photon and the quantity $\mathcal{E}$

$$\mathcal{E} = \sqrt{\frac{\hbar\omega}{2\epsilon V}}, \tag{1.74}$$

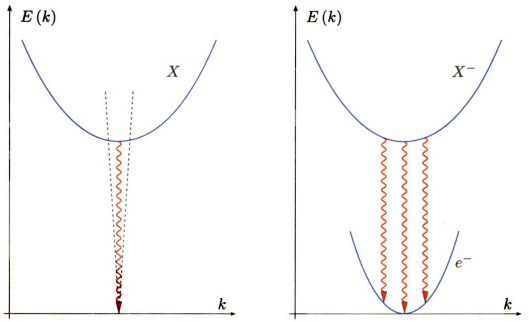

Figure 1.8: Schematic diagrams of the exciton (left) and trion (right) in-plane dispersion relations and the coupling to light. For excitons the radiative zone is restricted by the light cone effect (dashed lines).

can be visualized as the 'electric field per photon' inside the material; ϵ incorporates the refractive index of the material and V is the quantization volume.

Let us first consider the case of an exciton decay. In a bulk crystal, the exciton can interact only with a photon that has the same wavevector in order to obey the translational invariance of the system, resulting in a hybrized exciton - photon mode, a polariton, which is the stationary state of an infinite dielectric medium. The situation is different for a QW system: the exciton with in-plane center of mass wave vector $\mathbf{K}$ interacts with all the photon modes that have the same in-plane wave vector, but no further restriction is imposed on the $\hat{z}$-component of the photon's wavevector. Compared to the bulk case, where radiative recombination occurs only by a leak of the polariton through the surface of the crystal or by (non-)radiative recombination at crystal imperfections, this leads to a large radiative recombination rate in the QW system [34]. In a two-dimensional QW system, an exciton combines the dual

merits of coherent nature on the two-dimensional QW plane and superradiant decay in one direction along the growth direction, owing to its macroscopic transition dipole moment. Therefore, the breakdown in translational symmetry in the growth direction gives rise to profoundly modified coupling of excitons to photons. The radiative zone, however, is restricted by the light cone effect: Radiative recombination can only occur, if the exciton's wavevector $|\mathbf{K}|$ can be matched the photon's wavevector: Consequently, it obeys the constraint $|\mathbf{K}| < n\omega/c$. This is schematized on the left side in Fig. (1.8). Only excitons around $\mathbf{K} \approx 0$ can couple efficiently to light; they are called bright states. States outside the light cone are called dark states and can be thermally populated for sufficiently high temperatures.

We elegantly circumvent these problems by performing the calculation in the exciton's restframe, i.e. we set $\mathbf{K} = 0$, and assume the low temperature limit $T \to 0$. The initial state of the exciton decay process is characterized by the exciton's wavefunction $\Psi_x(\mathbf{r}_e, \mathbf{r}_h)$. We will restrict our analysis to $1s$ excitons and neglect higher states as the interaction with the radiation field is typically dominated by this lowest state, particularly under near resonant excitation. The final state is given by the crystal ground state and the emitted photon. We fix the spin configuration of the initial state as composed of a spin down electron $\sigma = -1/2$ and a heavy hole with spin $\sigma_{hh} = +3/2$. As a consequence, the polarization of the photon is determined to be a σ_+ photon. With this simplification, we will drop the spin indices for the moment and make the replacement $g^2 \to g'^2 = g^2/3$ to correct the dipole moment. We write the initial state $|i\rangle$ for an exciton with center of mass wavevector $\mathbf{K}$ as

$$|i\rangle = \sum_{\mathbf{k}} \tilde{\Psi}_x(\mathbf{k}, \mathbf{K} - \mathbf{k})\, c^\dagger_{\mathbf{k}} d^\dagger_{\mathbf{K}-\mathbf{k}} |0\rangle\,, \tag{1.75}$$

where the Fourier transform of the exciton wavefunction $\Psi_x(\mathbf{r}_e, \mathbf{r}_h)$ is defined via

$$\tilde{\Psi}_x(\mathbf{k}, \mathbf{K}-\mathbf{k}) = \frac{1}{A}\int d^2\mathbf{r}_e d^2\mathbf{r}_h\, \Psi_x(\mathbf{r}_e, \mathbf{r}_h) \exp(-i\mathbf{k}\mathbf{r}_e) \exp(-i(\mathbf{K}-\mathbf{k})\mathbf{r}_h). \quad (1.76)$$

The energy of this initial state E_i is given by

$$E_i = \frac{\hbar^2 K^2}{2m_x} + \epsilon_c - E_X. \quad (1.77)$$

Similarly, we write the final state $|f\rangle$ as

$$|f\rangle = a^\dagger_{\mathbf{Q}} |0\rangle \quad (1.78)$$

with the photon energy

$$E_f = \hbar\omega. \quad (1.79)$$

Using the (anti)-commutation relations for fermions (bosons), we obtain indeed the macroscopic superradiant transition amplitude for a QW exciton

$$\langle f|\mathcal{H}_I|i\rangle = g'\int d^2\mathbf{r} \exp(-i\mathbf{Q}\mathbf{r})\Psi_x(\mathbf{r},\mathbf{r}) = g'\phi_{1s}(0)\sqrt{A}\delta_{\mathbf{K},\mathbf{Q}}. \quad (1.80)$$

We can recognize that the in-plane photon momentum has to fulfill momentum conservation, but no condition is imposed on Q_z. In the subsequent step, the calculation of the radiative decay rate Γ_x, the value of Q_z will be determined by energy conservation. Inserting the transition amplitude into Fermi's Golden rule (1.71), taking the large volume limit to replace the sums by integrals and evaluating the expression for simplicity in the exciton restframe, we find that the exciton's decay rate Γ_x and the exciton's lifetime τ_x can be obtained from

$$\tau_x^{-1} = \Gamma_x = \frac{4d_0^2 n}{3\pi a_0^2 \hbar^2 c\epsilon}(\epsilon_c - E_x). \quad (1.81)$$

Here and in the following, c is the speed of sound in vacuum, n the refractive index of the QW material and a_0 the effective exciton Bohr radius. The values obtained for the specific QW systems $GaAs$ and $CdTe$ are summarized in Tab (1.3). We also state the natural linewidths of the exciton level $\hbar\Gamma_x$, because we will refer to them in the course of the rest of this thesis.

	$GaAs$	$CdTe$
$\tau_x\ [ps]$	15.9	6.9
$\Gamma_x\ [10^{10}s^{-1}]$	6.3	14.5
$\hbar\Gamma_x\ [\mu eV]$	41	95

Table 1.3: Calculated radiative exciton lifetimes, decay rates and level widths for $GaAs$ and $CdTe$.

Indeed, we find very short lifetimes in the range of picoseconds: an evidence for the enhanced radiative recombination rate of excitons, caused by the breakdown of the translational symmetry of the system. Our results are in a good agreement with values from other theoretical and experimental investigations: For $GaAs$ a radiative lifetime of $\tau_x = 10 \pm 4\,ps$ has been measured in the absence of dephasing mechanisms [35]. Due to a smaller dielectric constant ϵ and a bigger effective electron mass m_e^*, the radiative lifetime in a $CdTe$ semiconductor QW is found to be smaller. Esser *et al.* found $\tau_x = 13\,ps$ for $GaAs$ and $\tau_x = 4\,ps$ for $CdTe$ in the $T \to 0$ limit.

Let us turn to the radiative decay of a bound trion. The coupling of delocalized trions to light is very different from that of excitons, since not only a photon, but also an excess electron is involved. In an optical transition, where the photon momentum is negligible, the electron can absorb the trion center of mass momentum $\mathbf{K}$. This fact opens up a radiative decay channel for trions with high $\mathbf{K}$ vectors, that doesn't exist for excitons. In other words, there is no light cone effect for trions. A schematized version of this argument is presented in Fig. (1.8). All trion states can decay radiatively, since the mismatch in the wavevectors between the trion and the photon is absorbed to the excess electron during the optical transition.

The initial state $|i\rangle = |\mathbf{K}\rangle_t$ contains a trion with center of mass momentum $\mathbf{K}$. Again, we fix the spin configuration. The transition amplitude for this process can then be conveniently calculated from an adapted form of (1.47), the optical matrix element, where we replace the coupling constant $\Omega_0/2 \rightarrow g'$ to find

$$\mathcal{M}_{if} = \langle f | \mathcal{H}_I | i \rangle = g' \delta_{\mathbf{K},\mathbf{k}_e+\mathbf{Q}} I_+ (\mathbf{k}_e) . \tag{1.82}$$

We have calculated the trion decay rate Γ_t in the trion restframe, where $\mathbf{K} = 0$, as depicted in Fig. (1.9). In this frame, the in-plane momentum conservation takes on the form $\mathbf{k}_e = -\mathbf{Q}$.

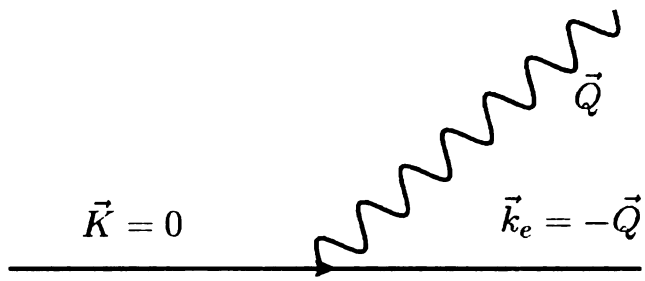

Figure 1.9: A trion in its rest frame decaying into a photon and an electron.

We have obtained an approximative analytic expression for Γ_t, whose derivation is presented in detail in Appendix F. Our numerical results for $GaAs$ and $CdTe$ are summarized in Tab. (1.4).

	$GaAs$	$CdTe$
τ_t $[ps]$	18.9	18.4
Γ_t $[10^{10} s^{-1}]$	5.3	5.4
$\hbar\Gamma_t$ $[\mu eV]$	34	35

Table 1.4: Calculated radiative trion lifetimes, decay rates and level widths for $GaAs$ and $CdTe$.

For both $GaAs$ and $CdTe$ we approximate the trion lifetime to be about $\sim 20\,ps$. Experimentally very similar values have been measured in the range $45 - 60\,ps$ [36]. Our theoretical prediction is in a good agreement to these experimental values, so that

our variational trial wavefunction again proves to be reliable and produces reasonable results.

As a last remark, we want to address the question, why the lifetimes of excitons and trions are in a comparable range, although their oscillator strengths for a light induced transition are very different? While the exciton's oscillator strength f_x is an extensive quantity that scales as $f_x \sim A/A_x$, the trion's oscillator strength f_t is much smaller, since the presence of an excess carrier is required. It has the scaling behaviour of $\sim A_t/A_x$, that can be interpreted as the number of excitons that fit into a trion without spatial overlap. Here, A, A_t and A_x are the sample, the typical trion and the typical exciton size respectively.

In the case of an exciton's radiative decay, the final state is marked by a photon with momentum $\vec{Q} = (\mathbf{Q}, Q_z)$. Since momentum conservation requires that the exciton's momentum equals the photons in-plane momentum, $\mathbf{Q}$ is fixed. Moreover, the value of Q_z is determined by energy conservation, so that in total there is no degree of freedom for the final state of this transition.

The situation is different in the case of trions. When a trion decays radiatively, the final state is not only characterized by a photon, but also by an excess electron that is left in the two-dimensional sample. Consequently, in the case of a radiative decay of a trion the final state is completely determined by five momenta components, three for the photon and two for the free electron. Since momentum and energy conservation again only fix three components, two degrees of freedom are left and need to be summed over to obtain the correct transition rate. This summation dies out for large $\mathbf{k}$ values and has the characteristic size of the trion's relative wavefunction's Fourier transform, namely $\sim 1/A_t$. Thus we can get the scaling behaviour

$$f_t \sum_{k_x,k_y} \frac{1}{A_t} \sim \frac{A_t}{A_x}\frac{A}{A_t} \sim A/A_x \tag{1.83}$$

which is exactly what we expect in the case of excitons. So, the fact that the trion's final state of a radiative decay has two more degrees of freedom than the exciton's exactly cancels the bigger oscillator strength the exciton has due to its macroscopic dipole moment. This gives an explanation for the fact that the radiative lifetimes of trions and excitons are not as different as one maybe expected at a first glance, when considering their very different decay channels and different oscillator strengths.

Chapter 2

Optical Potentials: Atoms vs. semiconductors

The possibility of trapping atoms at the nodes or antinodes of an intense laser standing wave was suggested first by Lethokhov in 1968 [37]. From 1986 on, when the first experimental observation of optically trapped atoms was reported, laser cooling and trapping has become a flourishing new field of modern physics [38]. Laser cooling and trapping rely on the fundamental interaction between laser light and atoms to exert controllable forces on the atoms. Today, the use of lasers to coherently control atoms is a well established technique and many sophisticated schemes have been developed based on special properties of the interaction. For cold atoms, a great variety of potentials can be designed via their interaction with the electromagnetic field, including static magnetic fields (Zeeman shifts), static electric fields (Stark shifts) and optical fields (light shifts).

In this chapter, we will first review the mechanical effects of light on atoms, referring to the concrete example of a two-level atom interacting with a single-frequency light field. Although this marks an idealized model rarely encountered in practice, it is pedagogically very valuable, because it shows many features that will be en-

countered in the rest of this thesis. We will restrict our attention to the problem of trapping atoms in a standing wave. A special property in the study of atoms confined in optical wavelength-size potential wells is that they can simulate many body physics previously accessible only in condensed matter systems. In these systems, the confining force is the so-called dipole force, which is proportional to the laser-intensity gradient, and which is based on a potential $V(\mathbf{r})$ varying in space exactly as the laser intensity pattern. Technically, optical dipole traps rely on the coupling between an induced dipole moment in the atom $\mathbf{d}$ and an external electric field. The atoms then experience a spatially varying AC Stark shift which creates a trapping potential $V(\mathbf{r})$ for the atoms

$$V(\mathbf{r}) = -\mathbf{d} \cdot \mathbf{E}(\mathbf{r}) \propto \alpha(\omega) |\mathbf{E}(\mathbf{r})|^2, \tag{2.1}$$

where $\alpha(\omega)$ gives the frequency-dependent polarizability of an atom and $I(\mathbf{r}) \propto |\mathbf{E}(\mathbf{r})|^2$ describes the intensity of the laser light field; $\mathbf{E}(\mathbf{r})$ is the electric field amplitude at the position $\mathbf{r}$ [39]. The sign of the polarizability $\alpha(\omega)$ is crucial in that it determines if the potential is attractive or repulsive.

It is important to note that the light force is not fully conservative. Since the optical potential derives from optical transitions between two atomic levels, spontaneous emission is inevitable and gives rise to an imaginary part of the polarizability [40]. Therefore, we will discuss below dissipation in optical potentials, an omnipresent, but readily controllable side effect of laser induced potentials.

By reviewing the fundamentals of optical physics of two-level atoms, we will establish notations and conventions and provide reference points we will further use in this thesis. Moreover, in the second part of this chapter, we will introduce our first theoretical approach to model an optical potential for carriers in semiconductors in the second part of this chapter. We will develop a simple picture, which essentially decomposes the quantum well into a collection of single two level systems. Based on

this toy-model, we will be able to deduce similarities between the well established optical dipole trap for atoms and the novel scheme for carriers in a semiconductor QW we propose in this thesis. Besides the similarities, the existence of the extensive, coherent exciton excitations will give rise to striking and physically intriguing new effects that are not present in the case of optical potentials for atoms.

2.1 Optical potentials for atoms

2.1.1 Optical dipole traps for atoms

Based on the dipole interaction between an atom and an electromagnetic standing wave, we will first derive the physics of optical trapping potentials for atoms from first principles. In the course of this derivation we will introduce the rotating reference frame and the rotating wave approximation.

For simplicity, we consider a two-level system atom with an internal ground state $|1\rangle$ and an excited state $|2\rangle$ which is coupled to a monochromatic classical laser field with a detuning $\triangle$. The system, including the chosen sign convention for the detuning $\triangle$, is schematically shown in Fig. (2.1).

The bare Hamiltonian H_0 of the two level system can be written as

$$H_0 = \epsilon_1 |1\rangle \langle 1| + \epsilon_2 |2\rangle \langle 2| , \tag{2.2}$$

with $\epsilon_{1/2}$ being the energy eigenvalues of the eigenstates $|1\rangle$ and $|2\rangle$ for the unperturbed problem. An optical field couples to the the dipole moment of the atom $\mathbf{d}$. Explicitly, we consider the case of a monochromatic standing electromagnetic wave in the dipole approximation, i.e. we neglect the variation of the electromagnetic field $\mathbf{E}(\mathbf{r}, t)$ across the atom and ignore the effects of the magnetic field $\mathbf{B}(\mathbf{r}, t)$. Since a typical wavelength λ used in optics is of the order of $\lambda \sim 400\,nm$, whereas the char-

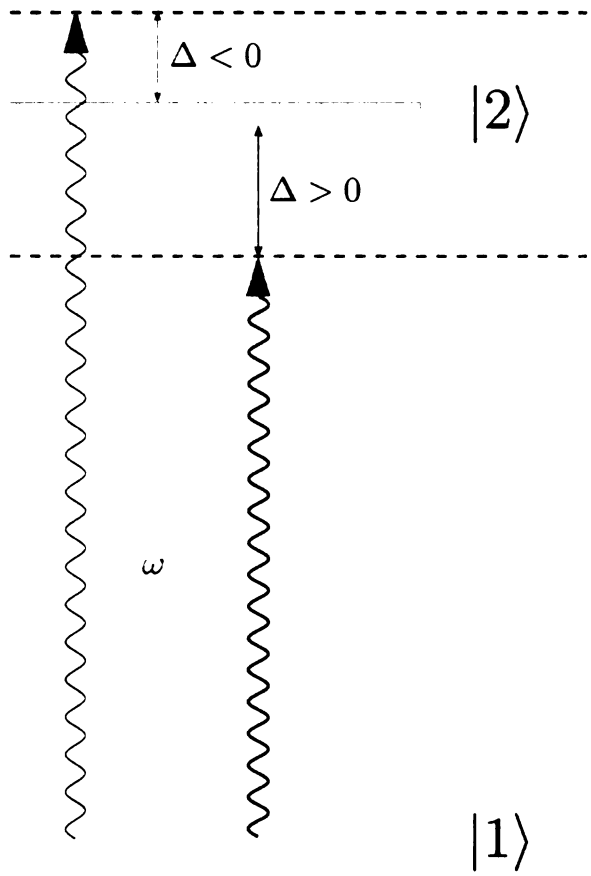

Figure 2.1: Interaction of a laser with a single two-level atom with the chosen sign convention for the detuning $\triangle$.

acteristic size of the atom is about a Bohr radius $a_0 \sim 0.1\,nm$, this approximation is usually very good [41]. The interaction between the atom and the standing wave can be expressed as

$$H_{int} = -\mathbf{d} \cdot \mathbf{E}_0 \cos(\mathbf{Qr}) \cos(\omega t), \tag{2.3}$$

where $\mathbf{E}_0$ is the amplitude of the electric field, $\mathbf{Q}$ the wavevector of the laser and ω the frequency of the light. The laser drives the transition between the two atomic states with a Rabi frequency $\Omega(\mathbf{r})$ which serves as a measure of the interaction strength

$$\Omega(\mathbf{r}) = \langle 1|\,\mathbf{d}\,|2\rangle\, \mathbf{E}_0 \cos(\mathbf{Qr}) = \mathbf{d}_{12}\mathbf{E}_0 \cos(\mathbf{Qr}) = \Omega_0 \cos(\mathbf{Qr}). \tag{2.4}$$

It is proportional to the laser field and the dipole transition matrix element of the atom $\mathbf{d}_{12}$. The amplitude Ω_0 is a constant that depends on the laser intensity as well as the properties of the atom. Without loss of generality, we can choose its phase such that it is a real-valued quantity $\Omega(\mathbf{r}) = \Omega^*(\mathbf{r})$; with this definition, we can express the coupling term of the Hamiltonian as

$$H_{int} = -\Omega(\mathbf{r}) \cos(\omega t) \left[|1\rangle\langle 2| + |2\rangle\langle 1| \right]. \tag{2.5}$$

We now introduce a time-dependent unitary transformation $U(t)$ to a frame rotating at the laser frequency ω

$$U(t) = \exp\left(-i\frac{\omega}{2} t \left(|2\rangle\langle 2| - |1\rangle\langle 1| \right) \right). \tag{2.6}$$

For the remainder of this section, we set $\hbar = 1$. Defining the transformation as $|\Psi(t)\rangle = U(t) \left| \tilde{\Psi}(t) \right\rangle$, the Schrödinger equation in the rotating frame reads

$$i\frac{\partial}{\partial t} \left| \tilde{\Psi}(t) \right\rangle = \tilde{H} \left| \tilde{\Psi}(t) \right\rangle, \qquad \tilde{H} = U^\dagger H U - iU^\dagger \dot{U}. \tag{2.7}$$

To simplify the further analysis, we split up the Hamiltonian in the rotating frame $\tilde{H}$ into two contributions

$$\tilde{H} = \tilde{H}_0 + \tilde{H}_{int} \tag{2.8}$$

$$\tilde{H}_0 = U^\dagger H_0 U - iU^\dagger \dot{U} \tag{2.9}$$

$$\tilde{H}_{int} = U^\dagger H_{int} U \tag{2.10}$$

As far as $\tilde{H}_0$ is concerned, we obtain the expression

$$\tilde{H}_0 = \tilde{\epsilon} \left(|1\rangle\langle 1| + |2\rangle\langle 2| \right) + \frac{\triangle}{2} \left(|2\rangle\langle 2| - |1\rangle\langle 1| \right), \tag{2.11}$$

where we defined the detuning $\triangle$ as the deviation of the laser frequency ω from the transition frequency of the two level system

$$\triangle = (\epsilon_2 - \epsilon_1) - \omega = \omega_{12} - \omega. \tag{2.12}$$

In this definition, $\triangle$ is defined as a positive quantity for red detuning (see Fig. (2.1)). With $\tilde{\epsilon}$ given by $\tilde{\epsilon} = \frac{1}{2}(\epsilon_1 + \epsilon_2)$, the first term in $\tilde{H}_0$ just gives a constant shift in energy, that we can drop in the following. Consequently, we can express $\tilde{H}_0$ in the simplified form

$$\tilde{H}_0 = \frac{\triangle}{2}(|2\rangle\langle 2| - |1\rangle\langle 1|). \tag{2.13}$$

Let's focus on the evaluation of $\tilde{H}_{int} = U^\dagger H_{int} U = -\Omega(\mathbf{r})\cos(\omega t)\hat{h}(t)$, where we defined $\hat{h}(t)$ as

$$\hat{h}(t) = U^\dagger(t)(|1\rangle\langle 2| + |2\rangle\langle 1|)U(t). \tag{2.14}$$

Taking the time derivative twice of $\hat{h}(t)$, we notice that $\hat{h}(t)$ obeys the differential equation of a simple harmonic oscillator with oscillation frequency ω

$$\ddot{\hat{h}}(t) + \omega^2 \hat{h}(t) = 0. \tag{2.15}$$

Using that $U(t=0) = U^\dagger(t=0) = 1$, the complete solution is given by

$$\hat{h}(t) = \hat{h}(0)\cos(\omega t) + \frac{1}{\omega}\dot{\hat{h}}(0)\sin(\omega t) \tag{2.16}$$

$$\hat{h}(0) = |1\rangle\langle 2| + |2\rangle\langle 1| \tag{2.17}$$

$$\dot{\hat{h}}(0) = i\omega(|2\rangle\langle 1| - |1\rangle\langle 2|). \tag{2.18}$$

In this fashion, we find $\tilde{H}_{int}$ to be

$$\tilde{H}_{int} = -\Omega(\mathbf{r})\cos(\omega t)\left[\hat{h}(0)\cos(\omega t) + \frac{1}{\omega}\dot{\hat{h}}(0)\sin(\omega t)\right]. \tag{2.19}$$

Since in optics the frequency ω is typically very high, of the order of $\omega \sim 10^{15}\,Hz$, we will average the Hamiltonian $\tilde{H}$ over one period of oscillation. This approximation is known as the rotating wave approximation, which helps us to get rid of the fast-oscillating terms. It is valid whenever the detuning $\triangle$ is small compared to the light frequency ω. By introducing the time-avergaged Hamiltonian

$$\bar{H} = \frac{\omega}{2\pi} \int_0^{2\pi/\omega} dt\, \tilde{H}(t)\,, \tag{2.20}$$

the Hamiltonian $\bar{H}$ in the rotating frame reads

$$\bar{H} = \frac{\triangle}{2} \left(|2\rangle\langle 2| - |1\rangle\langle 1|\right) - \frac{\Omega(\mathbf{r})}{2} \left(|1\rangle\langle 2| + |2\rangle\langle 1|\right). \tag{2.21}$$

We can see that by applying the rotating wave approximation we are left with a time-independent problem. This is indeed a very valuable simplification of the problem. The eigenvalues of $\bar{H}$ show that the light-shifted energies are given by

$$\epsilon_{\pm} = \pm\frac{1}{2}\Omega' = \pm\frac{1}{2}\sqrt{\triangle^2 + \Omega^2(\mathbf{r})} \tag{2.22}$$

They are illustrated as a function of the detuning $\triangle$ in Fig. (2.2). We see that the coupling $\Omega(\mathbf{r})$ lifts up the degeneracy at $\triangle = 0$. The level crossing is avoided as soon as a perturbation is applied to the system. The eigenstates of the Hamiltonian (2.21) are called dressed states; the light-induced perturbation mixes the states, so that the ground state is mixed with a component of excited state and vice versa. Compared to the unperturbed system, the levels of the dressed states are split farther apart, namely by the amount Ω'. The coherent modification of the atomic spectrum in the electric field of a laser is called optical Stark effect. However, we can recognize another striking feature, namely that an inhomogeneous light field, as in a standing wave, produces a spatially dependent light shift. This is the physical origin of an

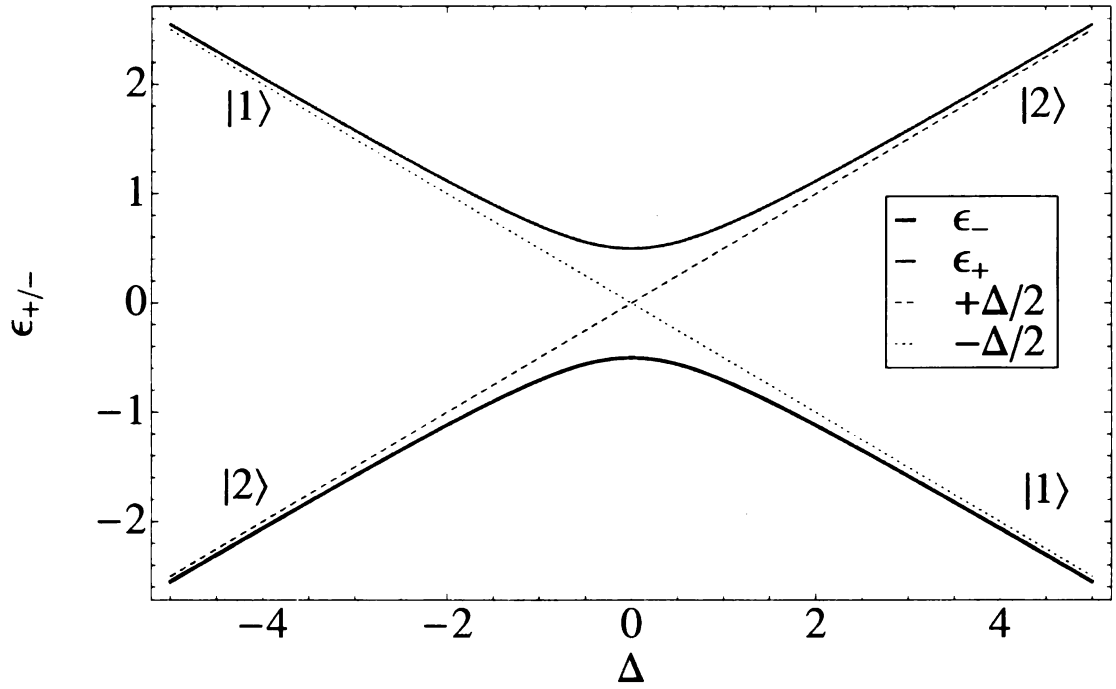

Figure 2.2: Eigenvalues $\epsilon_{\pm}$ of the Hamiltonian $\bar{H}$ in the rotating frame after the rotating wave approximation.

optical dipole trap. The force that stems from this gradient of energy is called the dipole force. It is simply based on the spatial variation of the internal energy of the atom.

Proceeding from the Hamiltonian $\bar{H}$ it is straight forward to explain the presence of an optical potential for atoms. The energy shift to the ground state in second order perturbation theory due to the perturbation $V(\mathbf{r}) = -\frac{\Omega(\mathbf{r})}{2}(|1\rangle\langle 2| + |2\rangle\langle 1|)$ is

$$\triangle E_1^{(2)} = \frac{|\langle 2|V(\mathbf{r})|1\rangle|^2}{E_1^{(0)} - E_2^{(0)}} = -\frac{\Omega^2(\mathbf{r})}{4\triangle} = -\frac{\Omega_0^2}{4\triangle}\cos^2(\mathbf{Qr}), \tag{2.23}$$

which leads to the definition of an optical dipole potential for the specific, but important case of a standing wave as

$$V(\mathbf{r}) = -\frac{\Omega^2(\mathbf{r})}{4\triangle} = -\frac{\Omega_0^2}{4\triangle}\cos^2(\mathbf{Qr}) \tag{2.24}$$

The optical potential due to the optical Stark effect takes on the spatial pattern of the intensity profile with its characteristic spatial dependence $\sim \cos^2(\mathbf{Qr})$. However, the sign of the detuning will decide about the energetically favourable spots for atoms. For red detuning, corresponding to a positive detuning $\triangle > 0$, the potential minima will be at the anti-nodes of the intensity profile, so that the atoms seek the spots of strong field intensities. In the case of blue detuning, where the detuning is negative $\triangle < 0$, the potential minima are at the dark spots of the intensity profile, i.e. the atoms are attracted towards the weak field spots.

Similarly, we can derive the form of the optical potential starting from the eigenvalues $\epsilon_{\pm}(\mathbf{r})$. Expanding them for a small perturbation $\Omega(\mathbf{r})$, small compared to the detuning $\triangle$, we get

$$\epsilon_{\pm}(\mathbf{r}) = \pm\frac{|\triangle|}{2}\sqrt{1+\left(\frac{\Omega(\mathbf{r})}{\triangle}\right)^2} \approx \pm\frac{|\triangle|}{2} \pm \frac{\Omega^2(\mathbf{r})}{4|\triangle|}. \tag{2.25}$$

Dropping the spatially homogeneous term, we obtain

$$\epsilon_{\pm}(\mathbf{r}) \approx \pm\frac{\Omega_0^2}{4|\triangle|}\cos^2(\mathbf{Qr}). \tag{2.26}$$

To show the equivalence to the optical potential $V(\mathbf{r})$ we have to be careful about the choice for the sign in the expression (2.26). In the case of a large positive detuning $\triangle$, we have to pick up the eigenvalue ϵ_- to asymptotically approach the ground state of the unperturbed problem, whereas in the case of a large negative detuning it is vice versa. However, in both cases the spatial dependence of the perturbed ground state is then given by the same expression as derived for $V(\mathbf{r})$ in Eqn. (2.24).

In conclusion of this discussion, we may summarize that optical dipole potentials for atoms are based on the the light-induced Stark shift of the atomic energy levels. The essential findings are schematized in Fig. (2.3), where the different character of

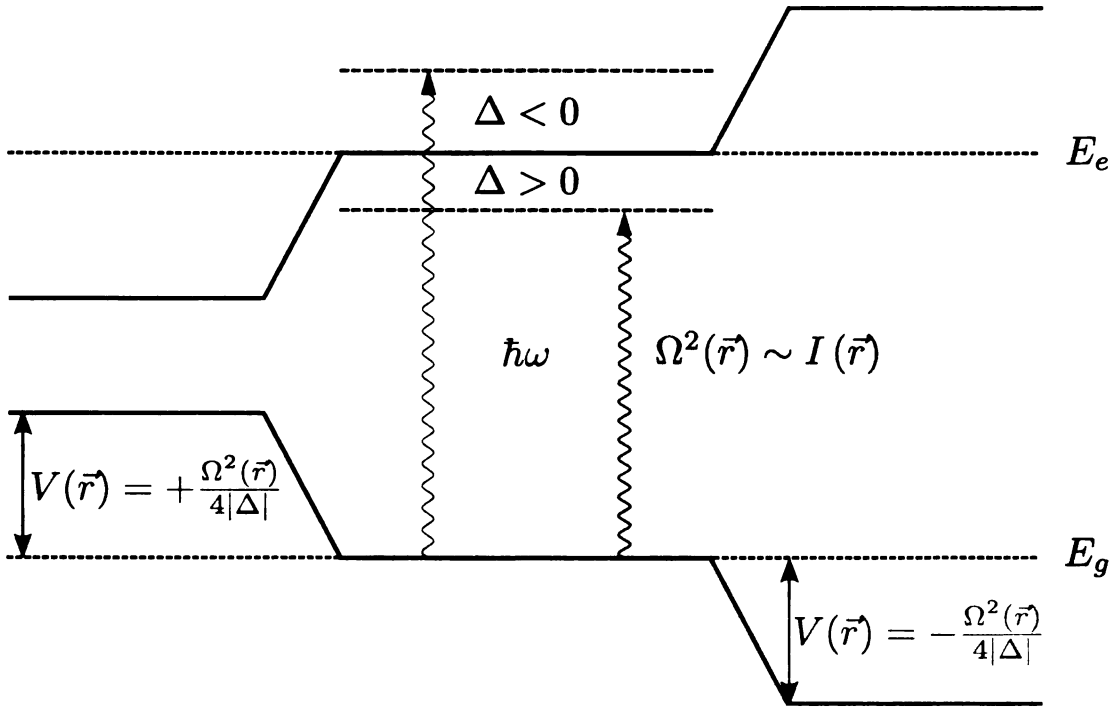

Figure 2.3: The bare two-level system with eigenenergies E_g and E_e are shown in the center. The light shifts for red detuning are displayed on the right, creating an attractive potential. For blue detuning the potential is repulsive, as depicted on the left-hand side.

the potential for blue and red detuning is underlined.

2.1.2 Dissipation in optical potentials

In the course of our introduction to light forces, we have swept one phenomenon under the rug: spontaneous emission. As a direct consequence of momentum conservation, the emission of a photon into the continuum of modes of the electromagnetic field must be accompanied by an atomic recoil. In quantum optics, the recoil aspect of spontaneous emission was ignored until the advent of ultracold atomic samples. The spontaneous emission events lead to random kicks in the atomic momentum, which has the ability to cause an unwanted heating of the atomic sample. We are going to address this dissipative character of the light-atom coupling in the following.

Let us first mention that the decay of the excited state is an irreversible process. In principle, the modes of the spontaneously emitted light also couple to the ground state of the system, but the number of modes is infinite in free space. To find the amplitude for the reverse process, all the contributions from the different modes have to be summed over. Since they add destructively, the total probability for the reverse process becomes zero. However, it is the competition between the excitation by an incident wave and the damping processes due to spontaneous emission that allows the atom to reach a steady state. To handle spontaneous emission, the standard approach is to introduce the density matrix $\hat{\rho}$ of the system and discuss the excitation of the atoms in terms of populations and coherences instead of amplitudes. The *optical Bloch equations* express that the rate of change of the atomic density matrix is a sum of two contributions describing the coupling with the incident wave and the coupling with the empty modes. To describe the effects of spontaneous emission, we add a phenomenological decay term Γ, which is the natural line-width of the excited state, equal to the inverse of the radiative lifetime of the excited state τ.

The *optical Bloch equations* describing the two-level system subject to spontaneous emission read

$$\dot{\rho}_{22} = -\Gamma\rho_{22} - \frac{\Omega}{2i}(\rho_{12} - \rho_{21}) \tag{2.27}$$

$$\dot{\rho}_{11} = +\Gamma\rho_{22} + \frac{\Omega}{2i}(\rho_{12} - \rho_{21}) \tag{2.28}$$

$$\dot{\rho}_{12} = \left(i\triangle - \frac{\Gamma}{2}\right)\rho_{12} + i\frac{\Omega}{2}(\rho_{22} - \rho_{11}) \tag{2.29}$$

$$\dot{\rho}_{21} = -\left(i\triangle + \frac{\Gamma}{2}\right)\rho_{21} - i\frac{\Omega}{2}(\rho_{22} - \rho_{11}), \tag{2.30}$$

where we recognize ρ_{11} and ρ_{22} as the population of the ground state $|1\rangle$ and the excited state $|2\rangle$ respectively as well as the coherence terms ρ_{12}, ρ_{21}. Note that the normalization of $\hat{\rho}$ is conserved: $\dot{\rho}_{22} + \dot{\rho}_{11} = 0$. Throughout this thesis we will be

particularly interested in a weakly driven system, where the detuning is much bigger than the Rabi frequency. Therefore, the probability to be in the excited state ρ_{22} is small, resulting in a small loss rate out of the system and a quasi-closed system. In this regime we approximate the population of the upper state ρ_{22} with the steady state solution for a closed system given by

$$\rho_{22} = \frac{\Omega^2}{4\triangle^2 + 2\Omega^2 + \Gamma^2} = \frac{1}{2}\frac{s_0}{1 + s_0 + (2\triangle/\Gamma)^2}. \tag{2.31}$$

Here, we defined the on-resonance saturation parameter s_0 as

$$s_0 = \frac{2\Omega^2}{\Gamma^2}. \tag{2.32}$$

In the regime where the detuning from the resonance $\triangle$ is much bigger than the driving Ω and the natural linewidth Γ of the excited state, the population of the excited state is approximately

$$\rho_{22} \approx \frac{\Omega^2}{4\triangle^2}. \tag{2.33}$$

Since the population in the excited state decays at a rate Γ, the total scattering rate of light from the laser field, or the effective spontaneous emission rate Γ_{se}, is given by

$$\Gamma_{se} = \rho_{22}\Gamma = \frac{s_0}{1 + s_0}\frac{\Gamma/2}{1 + (2\triangle/\Gamma')^2}. \tag{2.34}$$

For very high intensities, where $s_0 \gg 1$, Γ_{se} saturates at $\Gamma/2$, since an intense excitation equalizes the populations of the two levels. In the last step we defined the power-broadened linewidth of the transition

$$\Gamma' = \Gamma\sqrt{1 + s_0}. \tag{2.35}$$

If the transition is "saturated", the linewidth of the transition is effectively broadened

from its natural linewidth Γ to its power-broadened value Γ'.

The absorption of an incident photon with momentum $\hbar\mathbf{Q}$ leads to a momentum transfer from the optical fields to the atom. The momentum is regained by the incident beam, if the photon is re-emitted by stimulated emission. However, if the atom returns to its ground state by spontaneous emission, the loss of momentum is zero on average, since the recoil associated with the spontaneous fluorescene occurs in a random direction. This picture leads to a dissipative force $\mathbf{F}_{sp}$, often called "radiation pressure force" or "dissipation force", that arises from absorption followed by spontaneous emission

$$\mathbf{F}_{sp} = \Gamma_{se}\hbar\mathbf{Q} = \rho_{22}\Gamma\hbar\mathbf{Q}, \tag{2.36}$$

which is equal to the momentum transfer per photon $\hbar\mathbf{Q}$ times the photons spontaneously emitted per unit time. It relies on the scattering of photons out of the laser beam. The randomness of the spontaneous emission, being itself an irreversible process, gives rise to a heating mechanism, that needs to be taken into account. Illustratively it can be mapped onto a random walk problem in momentum space with step size $\hbar\mathbf{Q}$ and rate Γ_{se}. Fig. (2.4) depicts the situation of an atom starting out from the origin in momentum space at $\mathbf{k} = 0$.

The first kick takes it to a point somewhere on the first circle. The question is where the atom will be after the second kick. Clearly, it will be somewhere on the second circle. The red shaded area accounts for heating, since the energy of the atom has increased with respect to the energy it has gained from the first momentum recoil kick. The blue shaded area depicts an effective cooling process, because the atom's energy has decreased again. However, the red shaded area is bigger than the blue one, so that the probability of a heating kick is bigger than the probability for a cooling kick; eventually, after several kicks, the electron will always have gained energy. We define the corresponding heating rate R_{heat} - the energy the atom absorbs because

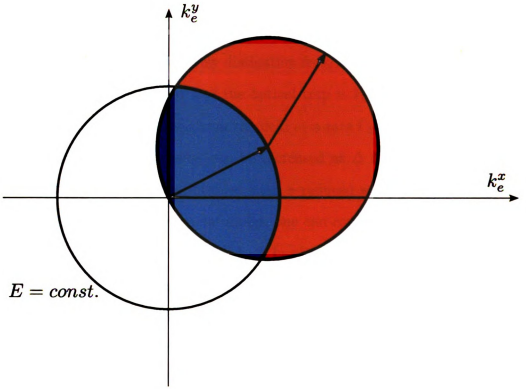

Figure 2.4: Random walk problem in momentum space.

of the dissipative light forces and measured in energy per unit time - as

$$R_{heat} = \Gamma_{se} E_R = \rho_{22} \Gamma E_R \tag{2.37}$$

where we have introduced the single photon recoil energy E_R. It is a figure of merit that sets a natural energy scale for the problem; physically, it is the kinetic energy of an atom of mass m with a momentum whose magnitude $\hbar Q$ equals that of the laser photons

$$E_R = \frac{\hbar^2 Q^2}{2m} \tag{2.38}$$

Also, we have to consider this heating mechanism in the framework of optical dipole traps, since the light fields that form the basis for the traps can induce op-

tical transitions in atoms, which subsequently can result in spontaneous emission and a heating of the atomic sample. There is, however, a easy way to remedy this problem, resulting in an effectively dissipation-free, conservative potential. Assuming $\triangle \gg \Omega, \Gamma$, the potential depth of the optical trap is $V_0 = \Omega^2/4\triangle$, while the atoms spontaneously scatter photons from the field at a rate $\Gamma_{se} = \Gamma\Omega^2/4\triangle^2$. If Ω^2, which is proportional to the intensity, can be increased as $\triangle$ is increased, then the same potential well depth can be obtained with a reduced scattering rate. By choosing high laser intensities and large detunings, one can combine deep potentials with low scattering rates, because the excited level has been eliminated adiabatically. We can conclude that finite dissipation occurs in the optical dipole trap due to spontaneous photon scattering, but it can be sufficiently suppressed to an arbitrary degree in the far-detuned limit, provided that sufficient laser power is available to achieve the desired potential.

2.2 Toy-model optical potentials in semiconductors

Our fundamental review of optical dipole potentials for atoms has taught us that their basic mechanism relies on optical transitions between two internal atomic energy levels driven by intense off-resonant laser light. There, the electromagnetic field couples to to the dipole moment of the atom, inducing a shift in the atom's ground state energy due to the AC Stark effect. For a non-uniform electromagnetic field the atom's energy is spatially modified. Then, the atoms see an optical potential.

Now, we draw an analog picture in a semiconductor host environment: The electron to trion optical transition effectively gives a second internal state to the spin-polarized electron, which is otherwise a pointlike, structureless particle in free space. In a simplified picture, the trion may be viewed as the excited state of an atomic

system, while the electron can be considered as the ground state. However, this comparison has to be handled with care, since, in contrast to a single two-level atom, an optical excitation in a semiconductor material has to be described taking into account its spatially coherent nature in an ideal extended system. To cover this effect in our first theoretical approach, we propose the following idea: We envisage the quantum well as a collection of independent two level systems, each associated with a tiny region whose size is equivalent to exciton size $A_x = \pi a_x^2$. Therefore, the system is discretized into small cells, as depicted in Fig. (2.5), and the total number of cells is $N_x = A/A_x$.

First, let us think about the physics when no conduction electron is present in the sample. Under this assumption, of course, we expect excitations of excitons only. Every single cell is coupled to the laser light; we denote the Rabi frequency for this transition as the bare Rabi frequency $\Omega_0(\mathbf{r})$, since it refers to one specific cell and, as a consequence, has no macroscopicly enhanced dipole moment. The ground state of one specific cell $|g\rangle$ is marked by the absence of an exciton, while the excited state of one cell $|e\rangle$ is described by the presence of a photo-excited exciton. The ground state of the system does not contain a single exciton excitation, all the cells of the system are in the ground state which we express as $|g, g, \ldots, g\rangle$. The elementary excitations of the total system are states in which one of the cells is "filled" with an exciton, such as for example the states $|e, g, \ldots, g\rangle$, $|g, e, \ldots, g\rangle$ or $|g, g, \ldots e, \rangle$. Since excitons are plane waves that are coherent over the whole sample, in the language of the cell-model the creation of an exciton appears as an collective excitation over all the cells

$$\frac{1}{\sqrt{N_x}}\left(|e, g, \ldots, g\rangle + |g, e, \ldots, g\rangle\rangle + \cdots + |g, g, \ldots, e\rangle\right). \tag{2.39}$$

The light-matter interaction creates states that are a linear superposition of all the elementary excitations, whereby every single cell is addressed with the the bare Rabi

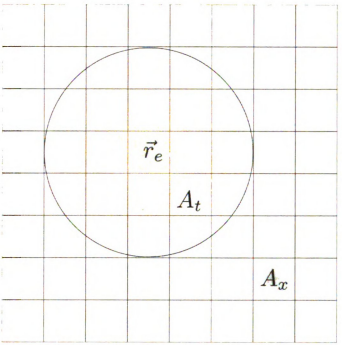

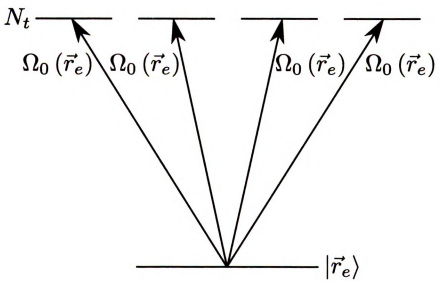

Figure 2.5: An extract from the QW sample: It is discretized into small cells of size A_x, the typical exciton size. If an electron is present, centered at $\mathbf{r}_e$, excitons created within the area A_t, the typical trion size, give rise to the formation of a bound trion. In this model, the electron is coupled effectively to $N_t = A_t/A_x$ trion states.

frequency $\Omega_0(\mathbf{r})$. Compared to the creation of an exciton in one specific cell, the collectivity of the exciton state gives rise to an enhanced, macroscopic dipole moment $\mathbf{d} = \sqrt{N_x}\mathbf{d_0}$.

Now, let us examine the situation where conduction electrons are present in the system. If an exciton is photoexcited in one of the cells close to the electron, assumed to be centered at $\mathbf{r}_e$, it is energetically favourable to form the three particle state of a bound trion; the exciton "captures" the excess electron. The coupling of the electron to the trion resonance is strongly enhanced, since the excited trion level is highly degenerate. Within this toy model the degeneracy factor is $N_t = A_t/A_x$, which is the number of excitons that fit into a trion. Literally, the exciton can be created anywhere within the trion size A_t around the initial electron, with the final result always being the same, namely a bound trion. Thus, the electron is coupled to N_t degenerate trion states, as schematized in Fig. (2.5). It is well known, that the resulting effective Rabi frequency for the electron–trion transition $\Omega_t(\mathbf{r})$ is

$$\Omega_t(\mathbf{r}) = \sqrt{N_t}\Omega_0(\mathbf{r}), \tag{2.40}$$

where we assumed $\Omega_0(\mathbf{r})$ to be constant over A_t. Since the spatial extension of the bound trion is much smaller than the optical wavelength λ, this is the equivalent to the approximation of evaluating the electric field at the atom's center of mass position only. Still, we must not forget the excitation of excitons, even if conduction electrons are present in the system. We assume an unbound trion state whenever an exciton is photoexcited outside the range A_t around the electron, because in this case the exciton is too far away from the single electron to capture it for a subsequent formation of a bound trion.

Let us mention that we have not restricted ourselves to the case of one single electron in the system. To be realistic, we assume a low density electron gas, but

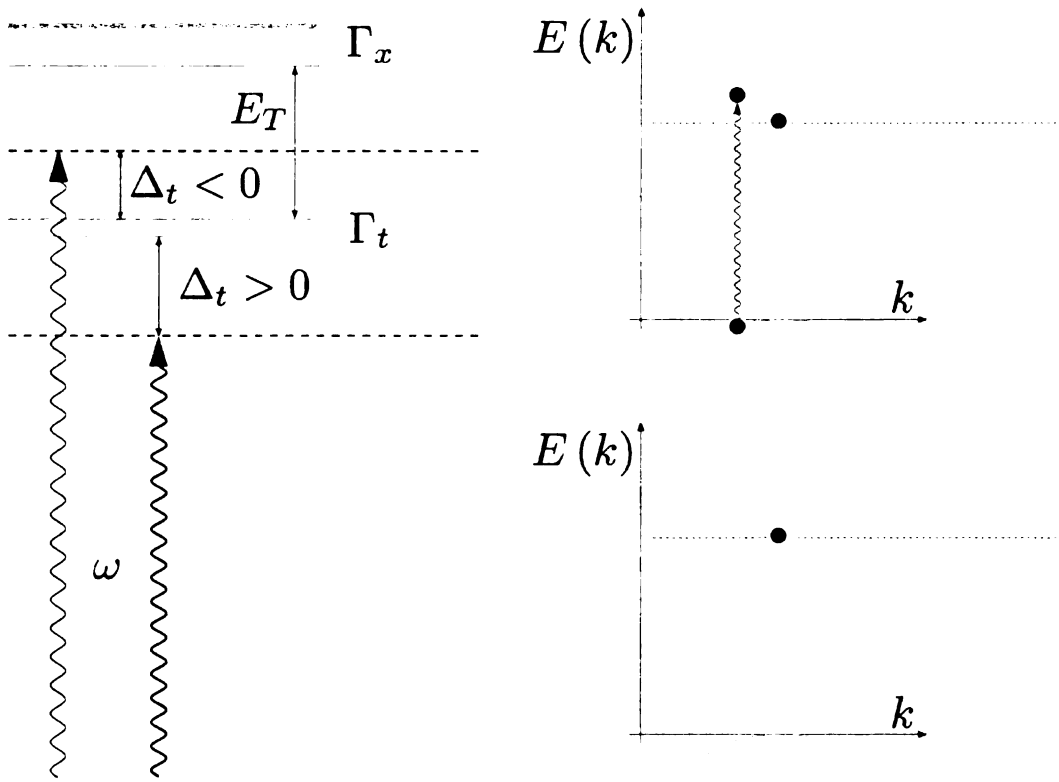

Figure 2.6: Level scheme with trion and exciton resonances and the chosen sign convention for the detuning. The ground state with an electron (blue dot) in the conduction band as well as th excited state after the creation of an electron hole (green dot) pair is depicted on the right.

the essential physics occur near a single electron. Therefore, when contemplating the effects on one electron, we can focus on the cells around that electron solely, disregarding the rest of the macroscopic sample.

In the following we set up a Hamiltonian that takes into account both the trion as well as the exciton resonance. Thus, the system we investigate is drawn in Fig. (2.6). The detunings $\triangle_t$ and $\triangle_x$ from the trion and exciton resonances, respectively, are by definition positive for red detuning. They are separated by the trion binding energy E_T, so that the following relation holds

$$\triangle_x = \triangle_t + E_T. \tag{2.41}$$

Again, we will first analyze the situation in which only excitons may be excited, since initially the conduction band is assumed to be empty. We proceed from the many-body Hamiltonian H, given in the frame rotating at the detuned laser frequency. We express H as

$$H = H_0 + V \tag{2.42}$$

with the excitonic bare Hamiltonian

$$H_0^x = \triangle_x \int d^2\mathbf{r} \; |x, \mathbf{r}\rangle \langle x, \mathbf{r}| \tag{2.43}$$

and the light matter coupling

$$V_x = \int d^2\mathbf{r} \, \rho_x(\mathbf{r}) \left[|0\rangle \langle x, \mathbf{r}| + |x, \mathbf{r}\rangle \langle 0| \right] \tag{2.44}$$

Here $|0\rangle$ denotes the crystal ground state, i.e. a completely filled valence band and an empty conduction band. The light matter coupling creates excitons, where we restrict ourselves to the case of one type of excitons, the $1s$ excitons. The state $|x, \mathbf{r}\rangle$ describes such a $1s$ exciton with its center of mass located at $\mathbf{r}$. The strength of the coupling is governed by the quantity $\rho_x(\mathbf{r})$, which is the spatially dependent Rabi frequency $\Omega_0(\mathbf{r})$ per exciton cell size

$$\rho_x(\mathbf{r}) = \frac{\Omega_0(\mathbf{r})}{\sqrt{A_x}}, \tag{2.45}$$

since the definition of the bare Rabi frequency $\Omega_0(\mathbf{r})$ is related to one cell of size A_x. Even if this definition might seem cumbersome at a first glance, it is evident that the square of it over the detuning $\triangle_x$ gives the energy shift density. This is the quantity we are interested in and which we will encounter below.

The orthonormalization relations are given by

$$\langle 0|0\rangle = 1, \quad \langle 0|x,\mathbf{r}\rangle = 0, \quad \langle x,\mathbf{r}|x,\mathbf{r}'\rangle = \delta\left(\mathbf{r}-\mathbf{r}'\right). \tag{2.46}$$

Along the lines of our analysis for atoms, we use second-order perturbation theory in order to calculate the ground state energy shift E_0 as

$$E_0 = -\int d^2\mathbf{r}\,\frac{|\langle x,\mathbf{r}|\,V_x\,|0\rangle|^2}{\triangle_x} = -\frac{A}{2}\frac{\rho_x^2}{\triangle_x} \tag{2.47}$$

where we have taken the spatial dependence of the bare Rabi frequency as $\Omega_0(\mathbf{r}) = \Omega_0\cos(\mathbf{Qr})$, corresponding to a electromagnetic standing wave. The square of this spatially dependent Rabi frequency is averaged over the area of the sample A, which accounts for the factor of $1/2$. We discover that the coherent excitation of excitons results in a macroscopic background energy shift

$$E_0 = -\frac{N_x}{2}\frac{\Omega_0^2}{\triangle_x} = -N_x\frac{\bar{\Omega}^2}{\triangle_x} \tag{2.48}$$

that is proportional to N_x. For notational convenience, we defined $\bar{\Omega}^2 = \Omega_0^2/2$.

The consecutive step is to include the possibility of an excess electron, whose position we denote as $\mathbf{r}_e$. The essential idea of the toy model is that the presence of the initial electron displaces all exciton states from an area given by the trion area A_t (centered at $\mathbf{r}_e$) and replaces them with less energetic trion states. Furthermore, the assumption that the variation of the field intensity over A_t is negligible will explicitly enter our calculations.

With the initial energy of the electron taken to be zero, the new bare Hamiltonian H_0^t in the rotating frame is

$$H_0^t = \triangle_x\int d^2\mathbf{r}\;|x,\mathbf{r}\rangle\langle x,\mathbf{r}| - \triangle_x\int_{A_t} d^2\mathbf{r}\;|x,\mathbf{r}\rangle\langle x,\mathbf{r}| + \triangle_t\int_{A_t} d^2\mathbf{r}\;|t,\mathbf{r}\rangle\langle t,\mathbf{r}| \tag{2.49}$$

which underlines that within the trion area A_t all exciton states are replaced by energetically more favourable trion states; we denote a bound trion with center of mass position $\mathbf{r}$ as $|t,\mathbf{r}\rangle$. The light matter coupling can be written as

$$\begin{aligned} V_t &= \int d^2\mathbf{r}\,\rho_x(\mathbf{r})\left[|0\rangle\langle x,\mathbf{r}| + |x,\mathbf{r}\rangle\langle 0|\right] \\ &\quad -\rho_x(\mathbf{r}_e)\int_{A_t} d^2\mathbf{r}\,\left[|0\rangle\langle x,\mathbf{r}| + |x,\mathbf{r}\rangle\langle 0|\right] \\ &\quad +\rho_t(\mathbf{r}_e)\int_{A_t} d^2\mathbf{r}\,\left[|0\rangle\langle t,\mathbf{r}| + |t,\mathbf{r}\rangle\langle 0|\right], \end{aligned} \tag{2.50}$$

where the vacuum state $|0\rangle$ is now meant to include the presence of the initial electron, but no excitons or trions. In analogy to $\rho_x(\mathbf{r})$, we introduced $\rho_t(\mathbf{r})$ as the effective trion Rabi frequency related to one trion cell of size A_t

$$\rho_t(\mathbf{r}) = \sqrt{N_t}\frac{\Omega_0(\mathbf{r})}{\sqrt{A_t}}. \tag{2.51}$$

With the presence of the initial electron, the ground state of the system to second order perturbation theory is

$$E_0(\mathbf{r}_e) = -\frac{1}{\triangle_x}\int d^2\mathbf{r}\,|\Omega_x(\mathbf{r}) - \Omega_x(\mathbf{r}_e)\,\theta(\mathbf{r},A_t)|^2 - \frac{1}{\triangle_t}\int_{A_t} d^2\mathbf{r}\,|\Omega_t(\mathbf{r}_e)|^2, \tag{2.52}$$

where $\theta(\mathbf{r},A_t)$ is the two dimensional unit step function, i.e. unity for $\mathbf{r}\in A_t$ and zero else. We can simplify this expression further to find

$$E_0(\mathbf{r}_e) = -\frac{N_x}{2}\frac{\Omega_0^2}{\triangle_x} + N_t\frac{\Omega_0^2(\mathbf{r}_e)}{\triangle_x} - N_t\frac{\Omega_0^2(\mathbf{r}_e)}{\triangle_t}. \tag{2.53}$$

The total second order energy shift at the electron's position $\mathbf{r}_e$ consists of three terms: First of all, we discover again a macroscopic shift due to the coherent excitation of excitons. Moreover, the trion resonance causes a shift that is stimulated by the

degeneracy factor N_t. The exciton shift has to be corrected, since it is not allowed to count the exciton cells that are displaced around the electron. The number of these cells is exactly N_t, with the Stark shift of one single exciton cell inside A_t being $\Omega_0^2(\mathbf{r}_e)/\triangle_x$. The second term accounts for the excitonic shift that is replaced by a trionic shift. Therefore, the first two terms give the total excitonic contribution, while the third term represents the shift due to the bound trion state.

We define the optical potential for the electron $V(\mathbf{r}_e)$ as the total optical Stark shift at $\mathbf{r}_e$, measured with respect to the total optical Stark shift when the electron is placed at a node of the intensity pattern, where the electron sees no light and which therefore simply gives the excitonic background shift. In this way, the optical potential varies with the electron's position as

$$V(\mathbf{r}_e) = N_t \Omega_0^2(\mathbf{r}_e) \left[\frac{1}{\triangle_x} - \frac{1}{\triangle_t}\right] = -N_t \frac{\Omega_0^2(\mathbf{r}_e)}{\triangle_t} f_t(\triangle_t), \tag{2.54}$$

where the factor $f_t(\triangle_t)$ is defined as

$$f_t(\triangle_t) = \frac{E_T}{E_T + \triangle_t} = \begin{cases} < 1 & , \triangle_t > 0 \quad (red) \\ \geq 1 & , \triangle_t \leq 0 \quad (blue) \end{cases} \tag{2.55}$$

This is definitely an intriguing result with no analog in atomic systems. Because of its importance, we will reconstruct it based on Fig. (2.7).

On the left, the macroscopic background shift is depicted. It is constant in space because of the coherent excitations of excitons. It gives the total shift of the system when no conduction electrons are present or, equivalently, when the conduction electron is at the node of the laser light. When on electron is present (right side of Fig. (2.7)), the optical potential starts out from this macroscopic shift and shows a very different behaviour depending on the sign of the detuning from the trion resonance $\triangle_t$. For red detuning the potential is attractive, whereas it is repulsive for blue de-

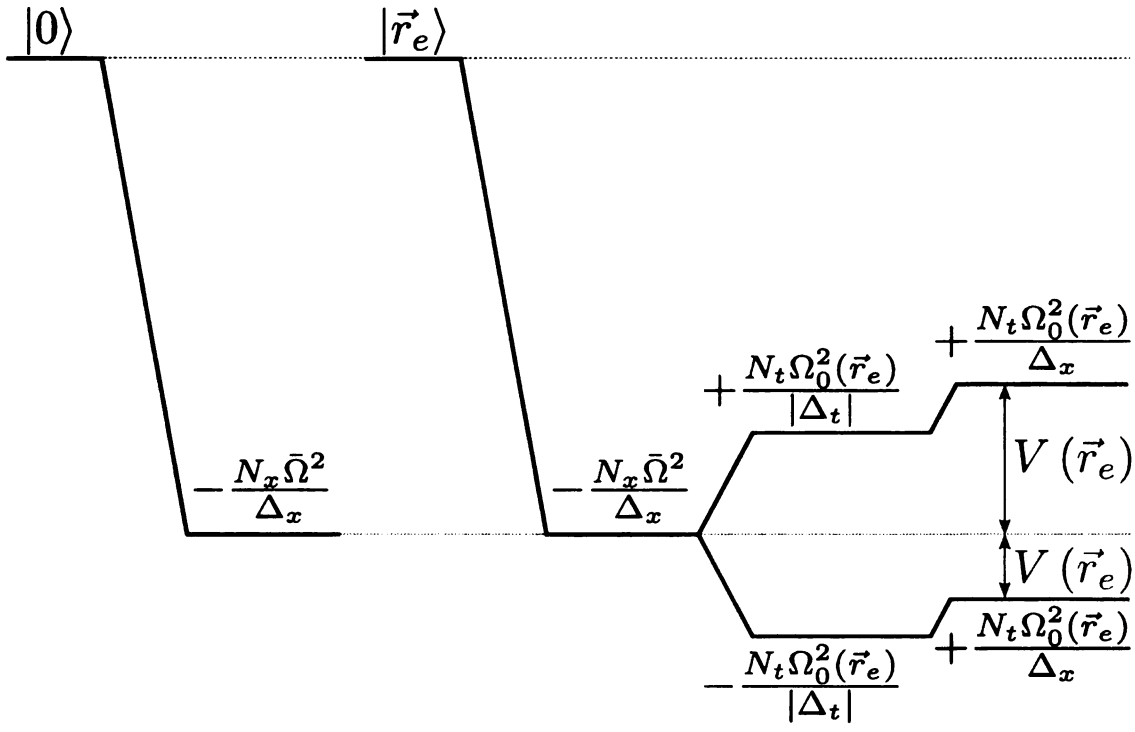

Figure 2.7: Level shifts due to the optical Stark shift. The colouring of the level shifts indicates, if the laser frequency ω is chosen below (red) or above (blue) the trion resonance. The presence of the trion shift causes a lower collective exciton shift, but an additional trion shift.

tuning. The electrons will be attracted either to the antinodes or the nodes of the intensity pattern. The optical trapping potential for electrons we study here shares this property with the optical potentials for atoms we analyzed earlier. However, new physics arises from the factor $f_t(\triangle_t)$. This factor can be smaller than one (red detuning) or bigger than one (blue detuning), and consequently it causes a reduction or an enhancement to the potential depth, respectively. As it can be seen from Eqn. (2.54), the effects of the trion resonance and the exciton correction counteract, if the laser frequency ω is tuned below the trion resonance. If the detuning from the trion resonance is in the blue regime, however, i.e. $\triangle_t < 0$ in our notation, the two effects actually add up in their contribution to the potential depth. Of course, there are subtleties that we have to take into account. As we approach the exciton resonance,

the potential depth increases, but at the same time the probability of creating real excitons in the system goes up, in contrast to virtual excitations of the two level cells. Moreover, we have not addressed the issue of spontaneously emitted light and the subsequent heating processes so far. We will make up for that shortcoming later, when thoroughly discussing the properties of the optical potential in chapter 4. Still, we have introduced here the essential ideas that make this optical potential for carriers feasible, and encountered a novel feature that distinguishes this type of potential from the conventional optical trapping potentials for atoms.

Chapter 3

Effective Hamiltonian from second order perturbation theory

This chapter will be essentially devoted to a derivation of an effective Hamiltonian $\mathcal{H}_{eff}$ for a conduction electron embedded in a semiconductor QW coupled to an electromagnetic standing wave. The interaction with the light field is treated perturbatively to second order, in both the eigenenergies and the eigenstates of the coupled system. This approach is valid as long as the Rabi frequency for a creation of a bound trion is small compared to the detuning from the trion resonance.

The light field induces transitions to bound and unbound trion state with a small probability, according to our perturbative method. Therefore, the basic ingredients for this derivation will be the matrix elements for transitions to the bound trion states, as defined in Eqn. (1.47), and unbound trion states, as given in Eqn. (1.67). As we have observed in the discussion of the toy model, the exciton continuum with its macroscopic dipole moment is crucial to capture the physics of the optical dipole potential for the conduction electron. Since the overlap $\mathcal{O}(\mathbf{K}, \mathbf{k}_e) = \langle \mathbf{K} | \mathbf{K}, \mathbf{k}_e \rangle$ of a bound trion state $|\mathbf{K}\rangle$ with the continuum states $|\mathbf{K}, \mathbf{k}_e\rangle$ is non-zero, we have orthogonalized the continuum states to the bound trion states, so that we can treat these

two different excitations as distinct levels in a three level system. In the next step, we will present Feynman like diagrams that illustrate the basic processes contributing to the second order Hamiltonian. The diagrams are meant to provide an intuitive understanding of the calculations to come that lead to the effective Hamiltonian and to the corresponding Schrödinger equation for a single electron. As it will turn out, this Schrödinger equation features some striking physical properties and will be the focus of the discussion in the subsequent chapters.

In the course of our calculation we will often take the limit $\mathbf{Q} \rightarrow 0$ for the photon's wavevector, since optical wavevectors are in general small compared to the the electron's wavevector $\mathbf{k}$: while Q scales as the inverse of the wavelength $Q = 2\pi/\lambda \approx 10^7 m^{-1}$, the electron wavevector is of the order of the reciprocal lattice constant $k = 2\pi/a \approx 10^{10} m^{-1}$ and thus much bigger than Q. In the two dimensional QW system we study in this thesis the validity of this approximation can be further extended with respect to bulk systems, since translational invariance is given only in the QW. The in-plane wavevector $\mathbf{Q}$ depends on the angle between the laser and the QW, and by tuning this angle, we can easily control $\mathbf{Q}$ without changing the energy of the incident photons. In this spirit, it is easy to find a configuration in which the recoil energies can be neglected with respect to the detuning from the trion resonance.

3.1 Perturbation theory

Let us first explain the general scheme for the upcoming derivation of the effective Hamiltonian $\mathcal{H}_{eff}$ of the coupled semiconductor - laser system. Following the standard procedure of perturbation theory, the full Hamiltonian H of the system we are about to study can be split up into the unperturbed problem H_0, which basically describes the conduction electron in the QW system, whose solutions are known and for simplicity taken to be two dimensional plane waves in the effective mass approxi-

mation, and into the perturbation V, induced by the light field, which gives rise to the formation of bound and unbound trions. Introducing the conventional perturbation parameter λ, the full Hamiltonian H can be expressed as

$$H = H_0 + \lambda V, \tag{3.1}$$

and the corresponding time-independent Schrödinger equation reads

$$H\left|\mathbf{k}\right\rangle = E\left(\mathbf{k}\right)\left|\mathbf{k}\right\rangle. \tag{3.2}$$

In the next step, we expand both the eigenvalues as well as the eigenstates to second order perturbation theory. For the energy eigenvalues we introduce the notation

$$E\left(\mathbf{k}\right) = E^{(0)}\left(\mathbf{k}\right) + \lambda E^{(1)}\left(\mathbf{k}\right) + \lambda^2 E^{(2)}\left(\mathbf{k}\right), \tag{3.3}$$

where the orders of perturbation theory in the energy eigenvalues are given by

$$E^{(0)}\left(\mathbf{k}\right) = \frac{\hbar^2\mathbf{k}^2}{2m_e^*} \tag{3.4}$$

$$E^{(1)}\left(\mathbf{k}\right) = \left\langle \mathbf{k}^{(0)}\right| V \left|\mathbf{k}^{(0)}\right\rangle = 0 \tag{3.5}$$

$$E^{(2)}\left(\mathbf{k}\right) = \sum_{\mathbf{n}\neq\mathbf{k}} \frac{\left|\left\langle \mathbf{n}^{(0)}\right| V \left|\mathbf{k}^{(0)}\right\rangle\right|^2}{E_{\mathbf{k}}^{(0)} - E_{\mathbf{n}}^{(0)}} \tag{3.6}$$

The zeroth order $E^{(0)}\left(\mathbf{k}\right)$ simply represents the dispersion of a free electron of effective mass m_e^*. We have already set the the first order energy correction $E^{(1)}\left(\mathbf{k}\right)$ to zero, since it projects a single electron state $\left|\mathbf{k}^{(0)}\right\rangle$ onto a bound or unbound trion state, which is assumed to be orthogonal to the free electron state $\left|\mathbf{k}^{(0)}\right\rangle$. In the same

fashion, we analyze the new eigenstates of the system to second order

$$|\mathbf{k}\rangle = \left|\mathbf{k}^{(0)}\right\rangle + \lambda \left|\mathbf{k}^{(1)}\right\rangle + \lambda^2 \left|\mathbf{k}^{(2)}\right\rangle . \tag{3.7}$$

For the special case that the first energy correction $E^{(1)}(\mathbf{k})$ vanishes - the case we consider here - the general solutions for the first and second order eigenstate corrections in terms of the zeroth order eigenstates are given by

$$\left|\mathbf{k}^{(1)}\right\rangle = \sum_{\mathbf{n}\neq\mathbf{k}} \frac{V_{nk}}{E_{kn}} \left|\mathbf{n}^{(0)}\right\rangle \tag{3.8}$$

$$\left|\mathbf{k}^{(2)}\right\rangle = \sum_{\mathbf{n}\neq\mathbf{k}} \sum_{\mathbf{l}\neq\mathbf{k}} \frac{V_{nl}V_{lk}}{E_{nk}E_{lk}} \left|\mathbf{n}^{(0)}\right\rangle - \frac{1}{2} \left|\mathbf{k}^{(0)}\right\rangle \sum_{l\neq k} \frac{V_{kl}V_{lk}}{E_{lk}^2}. \tag{3.9}$$

For convenience, we introduced the shorthand notation

$$V_{nk} = \left\langle \mathbf{n}^{(0)} \right| V \left|\mathbf{k}^{(0)}\right\rangle \tag{3.10}$$

and

$$E_{nk} = E_{\mathbf{n}}^{(0)} - E_{\mathbf{k}}^{(0)}. \tag{3.11}$$

Note that in this fashion, we have chosen the state $|\mathbf{k}\rangle$, expanded to second order, to be normalized to one. These equations are the ingredients that allow us to express all the quantities in terms of the well known zeroth order solutions $\left|\mathbf{k}^{(0)}\right\rangle$.

The starting point for the effective Hamiltonian $\mathcal{H}_{eff}$ is

$$\mathcal{H}_{eff} = \sum_{\mathbf{k}} \left(E^{(0)}(\mathbf{k}) + E^{(2)}(\mathbf{k})\right) \left|\mathbf{k}^{(0)}\right\rangle \left\langle \mathbf{k}^{(0)}\right| + \sum_{\mathbf{k}} E^{(0)}(\mathbf{k}) \left[\left|\mathbf{k}^{(0)}\right\rangle \left\langle \mathbf{k}^{(2)}\right| + h.c.\right], \tag{3.12}$$

where all orders higher than second order have been dropped as well as all terms involving the first order corrections to the eigenstates $\left|\mathbf{k}^{(1)}\right\rangle$, whose eventual projection onto electron position eigenstates $|\mathbf{r}\rangle$ give zero because of orthogonality, when

computing the effective Schrödinger equation for the single free conduction electron. In addition, the effective second order theory should also include the first order corrections to the bound and unbound trion states, because these are coupled to zeroth order electron eigenstates. However, in the Appendix I.3 it is shown that these terms are higher order corrections that are proportional to $\sim 1/\triangle_{x,t}^2$. Our model is set up for large detuning values and only respects contributions of the order $\sim 1/\triangle_{x,t}$.

In order to keep track of the various contributions, we split up the effective Hamiltonian $\mathcal{H}_{eff}$ into three terms as follows

$$\mathcal{H}_{eff} = \mathcal{H}_I + \mathcal{H}_{II}^1 + \mathcal{H}_{II}^2. \tag{3.13}$$

Note that in the following we will drop the superscript to indicate the perturbation theory order of the states, since all expressions will be given in terms of the zeroth order solutions, i.e. the free electron states. The first term simply describes the altered dispersion of the electron due to the mixing with the excited trion states

$$\mathcal{H}_I = \sum_{\mathbf{k}} \left(E^{(0)}(\mathbf{k}) + E^{(2)}(\mathbf{k}) \right) |\mathbf{k}\rangle \langle \mathbf{k}| \tag{3.14}$$

This term is diagonal in $\mathbf{k}$-space; therefore, it cannot lead to the optical potential in $\mathbf{r}$-space, because, when sandwiched between electron position eigenstates $|\mathbf{r}\rangle$ and $|\mathbf{r}'\rangle$, it only depends on $\mathbf{r} - \mathbf{r}'$. However, an optical potential requires terms that depend on $\mathbf{r} + \mathbf{r}'$ instead. The next two contributions, $\mathcal{H}_{II}^1$ and $\mathcal{H}_{II}^2$ originate from the second term in Eqn. (3.12), which we have expressed in terms of the zeroth order eigenstates solely and subsequently split up into a diagonal $\mathcal{H}_{II}^1$ and off-diagonal contribution $\mathcal{H}_{II}^2$. They are given by

$$\mathcal{H}_{II}^1 = -\sum_{\mathbf{k}} E^{(0)}(\mathbf{k}) |\mathbf{k}\rangle \langle \mathbf{k}| \sum_{\mathbf{l} \neq \mathbf{k}} \frac{|V_{lk}|^2}{E_{lk}^2} \tag{3.15}$$

and

$$\mathcal{H}_{II}^{2} = \sum_{\mathbf{k}} E^{(0)}(\mathbf{k}) \sum_{\mathbf{q}\neq\mathbf{k}} c_{qk} |\mathbf{q}\rangle \langle \mathbf{k}| + h.c., \tag{3.16}$$

where we have defined the quantity c_{qk} as

$$c_{qk} = \sum_{\mathbf{l}\neq\mathbf{k}} \frac{V_{ql} V_{lk}}{E_{qk} E_{lk}}. \tag{3.17}$$

The term $\mathcal{H}_{II}^{2}$ will be of peculiar interest, because it is the only one that is not diagonal in **k**-space. As it will turn out, the optical trapping potential for the electron originates from the off-diagonal nature of $\mathcal{H}_{II}^{2}$.

3.2 Orthogonalization of the excitonic continuum

The exciton continuum states $|\mathbf{K}, c\rangle$ that we consider in the effective Hamiltonian $\mathcal{H}_{eff}$ have to be orthogonal to the bound trion states which we denote as $|\mathbf{K}\rangle$; therefore,$|\mathbf{K}, c\rangle$ describes an electron - exciton pair with total crystal momentum **K**, properly orthogonalized to the bound trion states $|\mathbf{K}\rangle$ according to

$$\langle \mathbf{K}|\mathbf{K}', c\rangle = 0. \tag{3.18}$$

We can achieve the required orthogonality relation by defining the continuum states $|\mathbf{K}, c\rangle$ in the following way

$$|\mathbf{K}, c\rangle = \mathcal{N}_c \left(|\mathbf{K}, \mathbf{k}_e\rangle - \mathcal{O}(\mathbf{K}, \mathbf{k}_e) |\mathbf{K}\rangle \right), \tag{3.19}$$

where we introduced the overlap integral as

$$\mathcal{O}(\mathbf{K}, \mathbf{k}_e) = \langle \mathbf{K}|\mathbf{K}, \mathbf{k}_e\rangle. \tag{3.20}$$

Since we assume both $|\mathbf{K}\rangle$ and $|\mathbf{K}, \mathbf{k}_e\rangle$ to be normalized to one, the normalization constant $\mathcal{N}_c$ reads

$$\mathcal{N}_c = \frac{1}{\sqrt{1 - |\mathcal{O}(\mathbf{K}, \mathbf{k}_e)|^2}}. \tag{3.21}$$

It is easy to check that this definition for $|\mathbf{K}, c\rangle$ indeed provides us with the desired relation of $\langle \mathbf{K}|\mathbf{K}', c\rangle = 0$. Up to now, this method has been general, without having to specify the actual expression for the overlap integral $\mathcal{O}(\mathbf{K}, \mathbf{k}_e)$.

In order to describe the overlap between the bound and unbound trion states we have derived the following approximate expression

$$\mathcal{O}(\mathbf{K}, \mathbf{k}_e) \cong \sqrt{\frac{\pi a_t^2}{A}} \frac{2\sqrt{2}}{\left(1 + a_t^2 |\beta_e \mathbf{K} - \mathbf{k}_e|^2\right)^{3/2}}. \tag{3.22}$$

where a_t is a parameter which describes the typical size of a bound trion. A detailed derivation is presented in E.2. To obtain this result, exchange effects that vanish in the limit of a macroscopic sample size have been neglected. Moreover, we simplified the result using the fact that bound trions are typically much more spatially extended than $1s$ excitons due to a weaker binding.

Two remarks on this result: first of all, we can recognize that the overlap $\mathcal{O}(\mathbf{K}, \mathbf{k}_e)$ between the bound trion state $|\mathbf{K}\rangle$ and the diffusive electron - exciton pair vanishes in the large sample limit. In fact, the overlap is proportional to the square root of the "trion size" πa_t^2 over the sample size. The center of mass motions are assumed to be ideally coherent plane waves, equally distributed over the whole sample area A, so that the overlap has to decrease as the sample size is increased. Moreover, we notice that $\mathcal{O}(\mathbf{K}, \mathbf{k}_e)$ depends on the relative motion momentum of the initial electron - photocreated exciton pair $\mathbf{p}_i$, just as the optical matrix element for a bound trion, since momentum conservation tells us: $\beta_e \mathbf{K} - \mathbf{k}_e = \beta_e (\mathbf{Q} + \mathbf{k}_e) - \mathbf{k}_e = \beta_e \mathbf{Q} - \beta_x \mathbf{k}_e = -\mathbf{p}_i$. In retrospect, this fact underlines that the optical matrix element for a bound

trion essentially depends on the overlap betwen the bound and diffusive trion states.

3.3 Diagrammatic approach

Now that we have set up the general expression for the effective Hamiltonian $\mathcal{H}_{eff}$ in Eqn. (3.12), and approximatively orthogonalized the bound trion states to the $1s$ exciton continuum in Eqn. (3.19), we are in the position to begin with the actual calculations. Before doing so, however, we will illustrate some of the processes involved in $\mathcal{H}_{eff}$ by drawing the corresponding Feynman-like diagrams.

Let us first consider a "typical" second order process, as known from calculating the second order energy correction $E^{(2)}(\mathbf{k})$. It is schematized in Fig. (3.1). There are only two modes present in the standing wave, $+\mathbf{Q}$ and $-\mathbf{Q}$ respectively, with which the initial electron of momentum $\mathbf{k}$ can interact and possibly form a bound trion state with center of mass momentum $\mathbf{k} \pm \mathbf{Q}$. The coupling strength of this interaction process is proportional to $(\Omega_0/2)\, I_{\pm}(\mathbf{k})$, where $\Omega_0/2$ represents the coupling of the interband transition dipole to the electric field of the laser, and $I_{\pm}(\mathbf{k})$ gives the intrinsic coupling that contains the information about the wavefunctions of the initial and the final state of the process. Second order, of course, implies a second interaction: the virtual trion with crystal momentum $\mathbf{k} \pm \mathbf{Q}$ can interact again with the laser light and decay into the final electron and a photon. A possible configuration for the final state consists of a photon with momentum $\pm\mathbf{Q}$ and a free electron with momentum $\mathbf{k}$, whereby the final state equals the initial state of the process. The coupling strength is the same as for the first vertex, namely $(\Omega_0/2)\, I_{\pm}(\mathbf{k})$; therefore, we expect the overall transition amplitude of this process to be proportional to $(\Omega_0/2)^2\, I_{\pm}^2(\mathbf{k})$.

Very interestingly, the effective Hamiltonian $\mathcal{H}_{eff}$ does not stop here. It also incorporates processes that are off-diagonal in $\mathbf{k}$-space, as schematized in Fig. (3.2). In our system, the final state doesn't have to resemble necessarily the initial state,

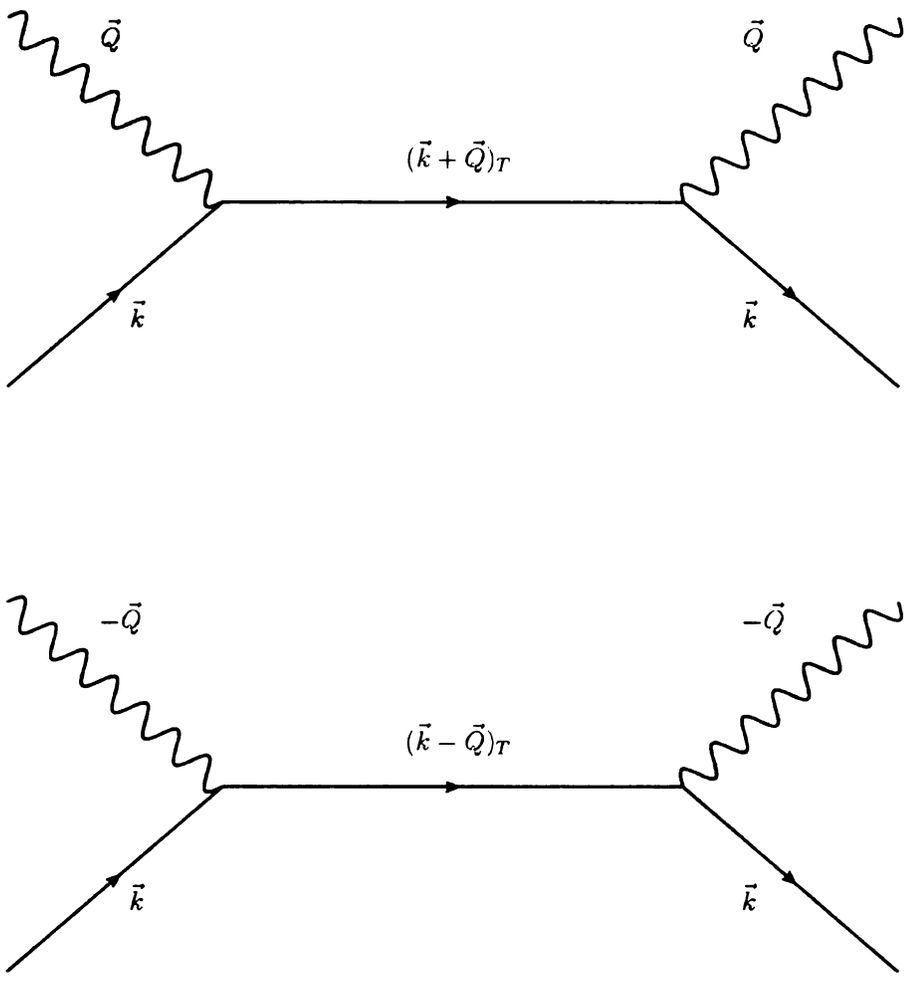

Figure 3.1: Feynman-like diagrams for diagonal contributions.

already in second order: This will occur, if the two vertices are related to different modes. The initial electron with wavevector $\mathbf{k}$ could first interact with the $+\mathbf{Q}$ mode to form a virtual bound trion of center of mass momentum $\mathbf{k}+\mathbf{Q}$. If this trion interacts with the $-\mathbf{Q}$ mode, the final state will consist of a photon with momentum $-\mathbf{Q}$ and, since the in-plane momentum has to be conserved, a free conduction electron with wavevector $\mathbf{k}+2\mathbf{Q}$. Indeed, the final state is not equal to the initial state. Naturally, we expect the coupling strength of this off-diagonal process to be proportional to $(\Omega_0/2)^2 I_+(\mathbf{k}) I_-(\mathbf{k}+2\mathbf{Q})$. If one interchanges the order of the two processes, as depicted in the lower part of Fig. (3.2), the reasoning goes along the lines of the process we explicitly considered here.

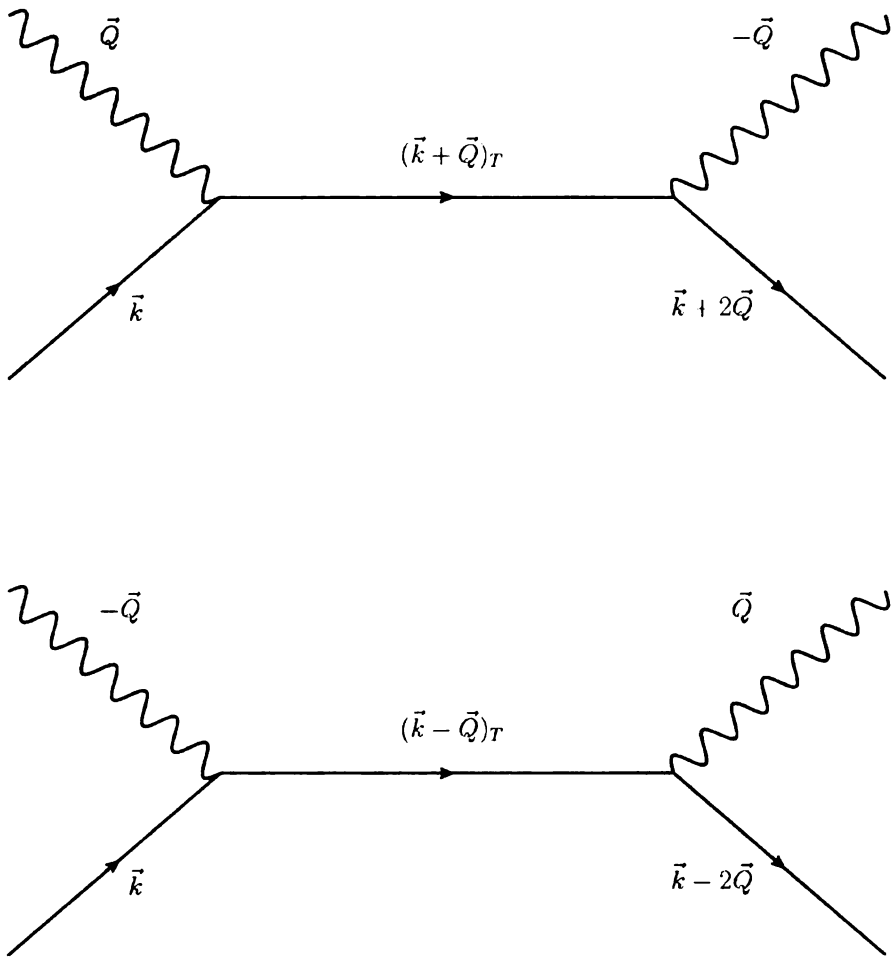

Figure 3.2: Feynman-like diagrams for off-diagonal contributions.

In conclusion, an incident electron with wavevector $\mathbf{k}$ can be coupled to a final electron state with wavevector $\mathbf{k} \pm 2\mathbf{Q}$, already in second order perturbation theory. We will prove that these off-diagonal processes are crucially important in order to derive an optical trapping potential which carries the signature of the intensity profile, namely $\sim \cos^2\left(\mathbf{Q}\frac{\mathbf{r}+\mathbf{r}'}{2}\right)$.

3.4 Second order energy correction

As a first important ingredient of the effective Hamiltonian $\mathcal{H}_{eff}$, we will derive the second order energy shift of the system $E^{(2)}(\mathbf{k})$. For clarity we break it up into

two pieces, the contributions that arise from the presence of the bound trion states $E_t^{(2)}(\mathbf{k})$ and the ones that come from the diffusive continuum states $E_c^{(2)}(\mathbf{k})$,

$$E^{(2)}(\mathbf{k}) = E_t^{(2)}(\mathbf{k}) + E_c^{(2)}(\mathbf{k}) \tag{3.23}$$

Bound trion states: Let us first cover the bound states only, that contribute to $E_t^{(2)}(\mathbf{k})$. The matrix element that couples a free electron of wavevector $\mathbf{k}$ to a bound trion with center of mass momentum $\mathbf{K}$ is expressed as

$$\langle \mathbf{k}| V |\mathbf{K}\rangle = \frac{\Omega_0}{2}\left[\delta_{\mathbf{K},\mathbf{k}+\mathbf{Q}} I_+(\mathbf{k}) + \delta_{\mathbf{K},\mathbf{k}-\mathbf{Q}} I_-(\mathbf{k})\right]$$

When computing $E_t^{(2)}(\mathbf{k})$, the sum over the intermediate states is de facto a sum over $\mathbf{K}$, which, however, is readily simplified due to the in-plane momentum conservation. As a consequence, we obtain right away

$$E_t^{(2)}(\mathbf{k}) = \frac{\Omega_0^2}{4}\left(\frac{|I_+(\mathbf{k})|^2}{\frac{\hbar^2 k^2}{2m_e^*} - \frac{\hbar^2(\mathbf{k}+\mathbf{Q})^2}{2m_t} - \triangle_t} + \frac{|I_-(\mathbf{k})|^2}{\frac{\hbar^2 k^2}{2m_e^*} - \frac{\hbar^2(\mathbf{k}-\mathbf{Q})^2}{2m_t} - \triangle_t}\right). \tag{3.24}$$

This result is what we already expected, based on our discussion of the Feynman-like diagrams. We defined the detuning from the trion resonance $\triangle_t$ as

$$\triangle_t = \epsilon_c - E_T^{tot} - \hbar\omega = \epsilon_c - E_X - E_T - \hbar\omega. \tag{3.25}$$

We can simplify expression (3.24) with the following approximations: as already argued, the limit $\mathbf{Q} \to 0$, is a valid approximation. Moreover, we exploit the fact that the functions $|I_\pm(\mathbf{k})|^2$, physically the squared Fourier transforms of the relative trion wavefunction, are strongly peaked around $\mathbf{k} \approx 0$, as illustrated in Fig. (3.3). Thus, we will keep only the value $\mathbf{k} \approx 0$ in the denominator, meaning that the kinetic energy terms in the denominator can be neglected compared to the detuning $\triangle_t$.

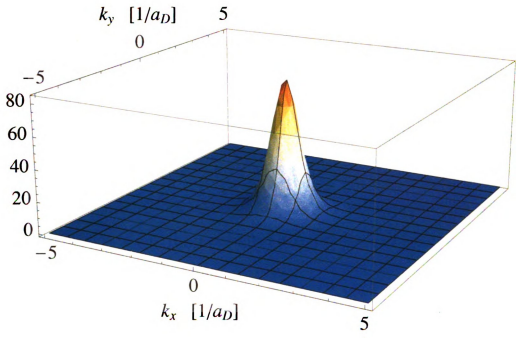

Figure 3.3: Plot of the function $|I_-(\mathbf{k})|^2$: The variational parameters for $GaAs$ were used. The value for $\mathbf{Q}$ corresponds to laser light tuned close to the trion resonance at an angle of 30° with respect to the $\hat{z}$-axis.

Within this approximation, we find

$$E_t^{(2)}(\mathbf{k}) \approx -\frac{\Omega_0^2}{2\triangle_t} |I_+(\mathbf{k})|^2_{\mathbf{Q}=0}, \tag{3.26}$$

where we used the fact, that in the limit $\mathbf{Q} \to 0$ we do not need to distinguish between the two modes. Of course, for $\mathbf{Q} = 0$ the relation $I_+(\mathbf{k}) = I_-(\mathbf{k})$ holds. We already recognize that the strength of the electron's energy shift is enhanced by the fact that the electron effectively couples to many trion states. The position where the additional electron-hole pair is photo-created can be literally anywhere within the trion size. In real space this degeneracy is described by the extension of relative trion wavefunction taken with one hole on top of one electron. In momentum space, this degeneracy is accounted for by the corresponding Fourier transform, namely $I_\pm(\mathbf{k})$.

Unbound trion states: The next step is to find the second order energy shift $E_c^{(2)}(\mathbf{k})$ that arises from the unbound trion states. The total center of mass momentum $\mathbf{K}$ is not sufficient to specify these states; indeed, we can take the electron momentum $\mathbf{k}_e$ as an additional quantum number. Therefore, we aim at calculating

$$E_c^{(2)}(\mathbf{k}) = -\sum_{\mathbf{K}}\sum_{\mathbf{k}_e} \frac{\langle \mathbf{k}| V |\mathbf{K}, c\rangle \langle \mathbf{K}, c| V |\mathbf{k}\rangle}{E_{\mathbf{K},\mathbf{k}_e;\mathbf{k}}} \tag{3.27}$$

Since the evaluation of $E_c^{(2)}(\mathbf{k})$ is rather lengthy and requires some approximations, a detailed derivation of $E_c^{(2)}(\mathbf{k})$ is presented in Appendix H. It is shown that $E_c^{(2)}(\mathbf{k})$ can be written in the following form

$$\begin{aligned} E_c^{(2)}(\mathbf{k}) &= -N_x \frac{\Omega_0^2}{\triangle_x} - \frac{\Omega_0^2}{2\triangle_x} \chi_c(\triangle_x) |I_+(\mathbf{k})|^2_{\mathbf{Q}=0} \\ &\quad + 2\frac{\Omega_0}{\triangle_x}\Omega_x |\mathcal{O}(\mathbf{k}+\mathbf{Q}, \mathbf{k}) I_+(\mathbf{k})|_{\mathbf{Q}=0} \end{aligned} \tag{3.28}$$

where we introduced the quantity

$$N_x = \frac{A}{\pi a_x^2} \tag{3.29}$$

as the number of excitons that fit into the sample without spatial overlap. Therefore, we can recognize that the presence of the exciton resonance accounts for a constant background shift that is simply proportional to N_x, which describes a macroscopic enhancement factor for the intrinsic shift $\Omega_0^2/\triangle_x$. Physically, this macroscopic enhancement factor arises from the fact that the exciton is a coherent excitation over the whole sample and thus carries a macroscopic dipole moment.

Moreover, to shorten the notation, we introduced the quantity

$$\frac{\chi_c(\triangle_x)}{\triangle_x} = \sum_{\mathbf{k}_e} \frac{\mathcal{O}(0, \mathbf{k}_e)^2}{\frac{\hbar^2 k_e^2}{2\mu_t} + \triangle_x} \tag{3.30}$$

where we μ_t is the reduced mass of the trion

$$\mu_t = \frac{m_e^* m_x}{m_e^* + m_x} \tag{3.31}$$

We will discuss the physical meaning of $\chi_c(\triangle_x)$ in more detail later on.

Let us make some remarks on $E_c^{(2)}(\mathbf{k})$. Besides the macroscopic excitonic background shift, it contains competing terms with opposite signs which include information about the relative wavefunction of the bound trion and arise from the orthogonalization of the diffusive electron - exciton pairs to the bound trion states. These physical results would not occur if we had not applied the orthogonalization procedure to obtain two distinct states.

Full second order correction: We can combine the second order energy corrections, obtained for the bound trion states in Eqn. (3.26) and for the excitonic continuum states in Eqn. (3.28), to give the total second order energy shift $E^{(2)}(\mathbf{k})$. In total, we write it as

$$\begin{aligned} E^{(2)}(\mathbf{k}) &= -N_x \frac{\Omega_0^2}{\triangle_x} - \Omega_0^2 \left| I_+(\mathbf{k}) \right|^2_{\mathbf{Q}=0} \frac{1}{2} \left(\frac{1}{\triangle_t} + \frac{\chi_c(\triangle_x)}{\triangle_x} \right) \\ &\quad + 2 \frac{\Omega_0}{\triangle_x} \Omega_x \left| \mathcal{O}(\mathbf{k}+\mathbf{Q}, \mathbf{k}) I_+(\mathbf{k}) \right|_{\mathbf{Q}=0} \end{aligned} \tag{3.32}$$

This result for $E^{(2)}(\mathbf{k})$ represents a major piece of the puzzle in the derivation of the effective Hamiltonian $\mathcal{H}_{eff}$. The next section will be devoted to a discussion of the terms $\mathcal{H}_{II}^1$ and $\mathcal{H}_{II}^2$, as defined in the expressions (3.15) and (3.16), respectively.

3.5 Effective Hamiltonian, Schrödinger equation

In this section we will present an analytic form of the effective Hamiltonian $\mathcal{H}_{eff}$. Before achieving this ultimate goal, we will give the missing pieces, namely the con-

tributions $\mathcal{H}_{II}^{1}$ and $\mathcal{H}_{II}^{2}$, which are by definition diagonal and off-diagonal in $\mathbf{k}$-space, respectively. The intermediate steps that give rise to a more compact form for them are presented in detail in Appendix I.

In the Appendix it is shown, that the diagonal part $\mathcal{H}_{II}^{1}$ can be approximated by

$$\mathcal{H}_{II}^{1} \approx -N_x \frac{\Omega_0^2}{\triangle_x^2} \sum_{\mathbf{k}} E^{(0)}(\mathbf{k}) |\mathbf{k}\rangle \langle \mathbf{k}| \tag{3.33}$$

As this expression is proportional to $\sim 1/\triangle_x^2$, we will drop this term in the further analysis and focus on $\mathcal{H}_I$ and $\mathcal{H}_{II}^{2}$.

Let us summarize the result for $\mathcal{H}_I$ first. It is diagonal and comprises the zeroth order solution as well as the second order energy shift $E_c^{(2)}(\mathbf{k})$. In total, it can be expressed as

$$\begin{aligned} \mathcal{H}_I \;=\; & \sum_{\mathbf{k}} E^{(0)}(\mathbf{k}) |\mathbf{k}\rangle \langle \mathbf{k}| - N_x \frac{\Omega_0^2}{\triangle_x} \sum_{\mathbf{k}} |\mathbf{k}\rangle \langle \mathbf{k}| \\ & -\frac{\Omega_0^2}{2} \left(\frac{1}{\triangle_t} + \frac{\chi_c(\triangle_x)}{\triangle_x} \right) \sum_{\mathbf{k}} |I_+(\mathbf{k})|^2_{\mathbf{Q}=0} |\mathbf{k}\rangle \langle \mathbf{k}| \\ & +2\frac{\Omega_0 \Omega_x}{\triangle_x} \sum_{\mathbf{k}} |\mathcal{O}(\mathbf{k}+\mathbf{Q}, \mathbf{k}) I_+(\mathbf{k})|_{\mathbf{Q}=0} |\mathbf{k}\rangle \langle \mathbf{k}| \end{aligned} \tag{3.34}$$

As far as the off-diagonal part $\mathcal{H}_{II}^{2}$ is concerned, we have derived the following form

$$\begin{aligned} \mathcal{H}_{II}^{2} \;\approx\; & -\frac{\Omega_0^2}{4} \left(\frac{1}{\triangle_t} + \frac{\chi_c(\triangle_x)}{\triangle_x} \right) \sum_{\mathbf{k}} |I_+(\mathbf{k}-\mathbf{Q})|^2_{\mathbf{Q}=0} \left(|\mathbf{k}-\mathbf{Q}\rangle \langle \mathbf{k}+\mathbf{Q}| + h.c. \right) \\ & +\frac{\Omega_0 \Omega_x}{\triangle_x} \sum_{\mathbf{k}} |\mathcal{O}(\mathbf{k}, \mathbf{k}+\mathbf{Q}) I_+(\mathbf{k}-\mathbf{Q})|_{\mathbf{Q}=0} \left(|\mathbf{k}+\mathbf{Q}\rangle \langle \mathbf{k}-\mathbf{Q}| + h.c. \right) \end{aligned} \tag{3.35}$$

These results mark a major result of this research: We have obtained an effective Hamiltonian that approximatively describes our system, an electron in a semiconduc-

tor QW coupled to standing wave that is tuned close to the trion resonance. Since we consider the limit $\mathbf{Q} = 0$, we recognize that the diagonal and off-diagonal part of the effective Hamiltonian $\mathcal{H}_{eff}$ contain similar contributions. As a result, we will be able to combine them; this simplification and a further analysis of the features of the effective Hamiltonian will be done in the framework of the corresponding position space Hamiltonian.

Our ultimate goal is to derive an optical trapping potential in position space. Therefore, we will switch the basis from momentum space to position space. In order to translate our result from $\mathbf{k}$-space to $\mathbf{r}$-space, we sandwhich our expressions in momentum space with electron position eigenstates $|\mathbf{r}\rangle$ and $|\mathbf{r}'\rangle$. Here, we use the relation

$$\langle \mathbf{r}| \left(|\mathbf{k}-\mathbf{Q}\rangle \langle \mathbf{k}+\mathbf{Q}| + |\mathbf{k}+\mathbf{Q}\rangle \langle \mathbf{k}-\mathbf{Q}| \right) |\mathbf{r}'\rangle = \frac{2}{A} e^{i\mathbf{k}\mathbf{x}} \cos\left(2\mathbf{Q}\mathbf{R}\right) \tag{3.36}$$

with $\mathbf{x}$ and $\mathbf{R}$ being defined as

$$\mathbf{x} = \mathbf{r} - \mathbf{r}', \qquad \mathbf{R} = \frac{\mathbf{r}+\mathbf{r}'}{2} \tag{3.37}$$

This relation, being proportional to $\sim \cos\left(2\mathbf{Q}\mathbf{R}\right)$, clearly illustrates that the form of the optical potential will be deduced from the terms that are off-diagonal in momentum space.

Furthermore, we take the usual large volume limit, where $\mathbf{k}$ becomes continuous, as

$$\sum_{\mathbf{k}} \rightarrow \frac{A}{(2\pi)^2} \int d^2\mathbf{k} \tag{3.38}$$

We find that the matrix elements are given by

$$\begin{aligned}\langle \mathbf{r}|\,\mathcal{H}_I\,|\mathbf{r}'\rangle &= -\frac{\hbar^2\nabla^2}{2m_e^*}\delta\left(\mathbf{r}-\mathbf{r}'\right) - N_x\frac{\Omega_0^2}{\triangle_x}\delta\left(\mathbf{r}-\mathbf{r}'\right) \\ &\quad +\frac{\Omega_0^2}{\triangle_x}m_c\left(\mathbf{r}-\mathbf{r}'\right) - \frac{\Omega_0^2}{2}\left(\frac{1}{\triangle_t}+\frac{\chi_c\left(\triangle_x\right)}{\triangle_x}\right)m_t\left(\mathbf{r}-\mathbf{r}'\right) \quad (3.39)\end{aligned}$$

and

$$\begin{aligned}\langle \mathbf{r}|\,\mathcal{H}_{II}^2\,|\mathbf{r}'\rangle &= +\frac{\Omega_0^2}{\triangle_x}m_c\left(\mathbf{x}\right)\cos\left(2\mathbf{QR}\right) \\ &\quad -\frac{\Omega_0^2}{2}\left(\frac{1}{\triangle_t}+\frac{\chi_c\left(\triangle_x\right)}{\triangle_x}\right)m_t\left(\mathbf{x}\right)\cos\left(2\mathbf{QR}\right) \quad (3.40)\end{aligned}$$

where we introduced the functions $m_t\left(\mathbf{x}\right)$ and $m_c\left(\mathbf{x}\right)$ in the following way

$$m_t\left(\mathbf{x}\right) = \int\frac{d^2\mathbf{k}}{\left(2\pi\right)^2}e^{i\mathbf{kx}}\left|I_+\left(\mathbf{k}-\mathbf{Q}\right)\right|^2_{\mathbf{Q}=0} \quad (3.41)$$

and

$$m_c\left(\mathbf{x}\right) = \phi_{1s}\left(0\right)\sqrt{A}\int\frac{d^2\mathbf{k}}{\left(2\pi\right)^2}e^{i\mathbf{kx}}\left|\mathcal{O}\left(\mathbf{k},\mathbf{k}+\mathbf{Q}\right)I_+\left(\mathbf{k}-\mathbf{Q}\right)\right|_{\mathbf{Q}=0} \quad (3.42)$$

They give rise to a nonlocal character of the effective Hamiltonian, as they connect the electron's position coordinates $\mathbf{r}$ and $\mathbf{r}'$ in a way different from the local expression $\delta\left(\mathbf{r}-\mathbf{r}'\right)$. The notation underlines the picture in which we will identify them: They can be interpreted as memory functions. We will address their specific physical meaning in the next chapter.

We have been able to find an analytic form of $m_t\left(\mathbf{x}\right)$, since in the limit $\mathbf{Q}=0$ the problem naturally becomes isotropic. We specifically evaluate $m_t\left(\mathbf{x}\right)$ in the case of the QW systems $GaAs$ and $CdTe$. The results are plotted in Fig. (3.4).

Qualitatively, we see that both systems exhibit a very similar character; for both

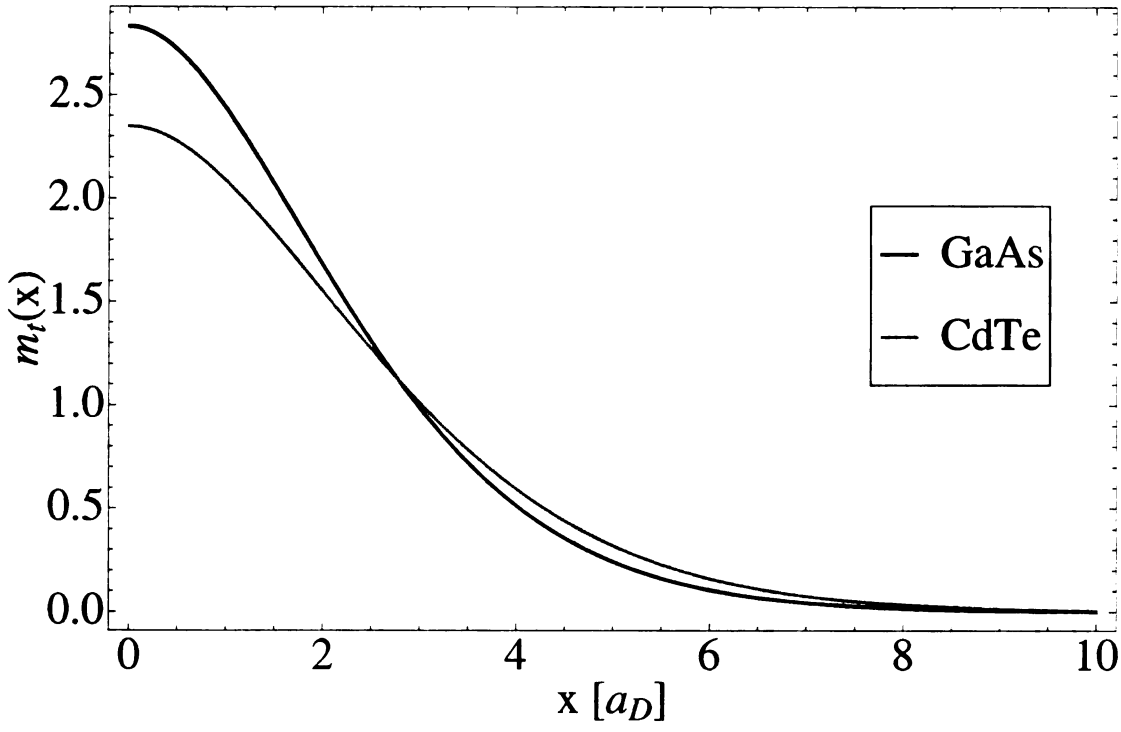

Figure 3.4: Memory functions $m_t(\mathbf{x})$ for $GaAs$ and $CdTe$. Note that the natural length scale, the 3D donor Bohr radius a_D, is slightly different for the two systems.

$GaAs$ and $CdTe$, $m_t(\mathbf{x})$ falls off on a scale of approximately $\sim 3a_D$. We will discuss this behaviour in more detail in the next chapter and give a physically intuitive explanation for this characteristic lengthscale of $\sim 3a_D$.

The second memory function $m_c(\mathbf{x})$ that we encounter arises from the hybrid mixing of the diffusive electron-exciton pairs with the bound trion states, as the overlap function in its definition indicates. The exact value of $m_c(\mathbf{x})$ depends on our choice of the parameter a_t that we introduced when simplifying the calculation of the overlap integral and, in principle, its best value should be obtained from a variational calculation. For consistency we approximate the actual value of a_t by tuning it to a reasonable trion binding energy according to the expression (1.30). Based on this approach, with $E_T = 2.0\,meV$ and $E_T = 3.6\,meV$ for $GaAs$ and $CdTe$ respectively, we estimate the values for a_T as $a_T \approx 1.8\,a_D$ and $a_T \approx 2.3\,a_D$. The corresponding

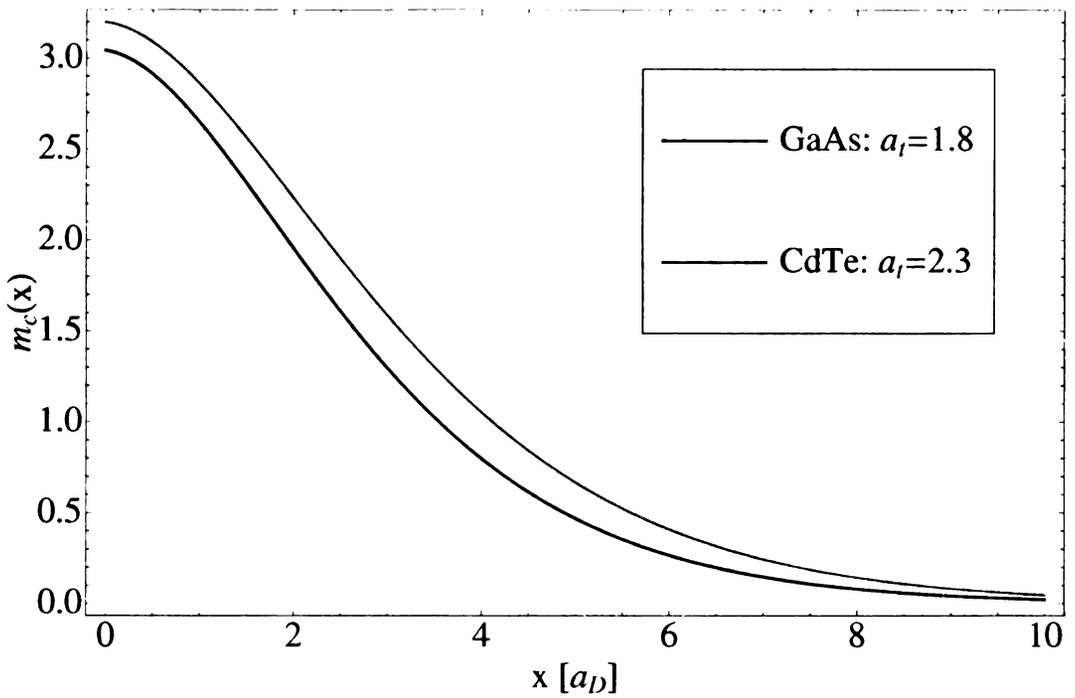

Figure 3.5: Memory functions $m_c(\mathbf{x})$ for *GaAs* and *CdTe*. Note that the natural length scale, the 3D donor Bohr radius a_D, is slightly different for the two systems.

results are shown in Fig. (3.5). We see that the functions $m_c(\mathbf{x})$ are very similar to the memory kernel $m_t(\mathbf{x})$ that arises from the trion resonance. We will exploit this fact for a further simplification by approximating the two types of memory kernels that we encountered in our calculation as equal, i.e. $m_t(\mathbf{x}) \approx m_c(\mathbf{x}) \approx m(\mathbf{x})$.

Proceeding from the matrix elements given in expression (3.39) and (3.40), respectively, we can present the effective Hamiltonian of the system $\mathcal{H}_{eff}$ in the following way

$$\begin{aligned}\mathcal{H}_{eff} &= -N_x\frac{\Omega_0^2}{\triangle_x} + \int d^2\mathbf{r}\,|\mathbf{r}\rangle\left(-\frac{\hbar^2\nabla^2}{2m_e^*}\right)\langle\mathbf{r}| \\ &\quad -\Omega_0^2\left(\frac{1}{\triangle_t}+\frac{\chi_c(\triangle_x)}{\triangle_x}\right)\int d^2\mathbf{r}\,d^2\mathbf{r}'\cos^2\left(\mathbf{Q}\frac{\mathbf{r}+\mathbf{r}'}{2}\right)m_t(\mathbf{r}-\mathbf{r}')\,|\mathbf{r}\rangle\langle\mathbf{r}'| \\ &\quad +2\frac{\Omega_0^2}{\triangle_x}\int d^2\mathbf{r}\,d^2\mathbf{r}'\cos^2\left(\mathbf{Q}\frac{\mathbf{r}+\mathbf{r}'}{2}\right)m_c(\mathbf{r}-\mathbf{r}')\,|\mathbf{r}\rangle\langle\mathbf{r}'| \qquad (3.43)\end{aligned}$$

where we used the trigonometric relation $1+\cos(2x) = 2\cos^2(x)$ to express the result in a more compact form.

The first term represents the constant background shift owing to the coherent excitation of excitons over the whole sample that we previously encountered in the toy model. The last two terms indeed carry the signature of the intensity profile and mark the optical potential for the conduction electron. Compared to the optical trapping potentials for atoms, however, there are important differences: The first one arises from the obvious non-locality of the potential, governed by the memory functions $m_t(\mathbf{x})$ and $m_c(\mathbf{x})$. The second one stems from the presence of detuning dependent correction factors. We will discuss the details and the consequences of this result in the next chapter.

We acknowledge the presence of the macroscopic excitonic background shift, but we will drop it in the following, since it only marks a constant shift in energy and has no influence on the electron's kinetic or potential energy. Moreover, as announced above, we set the two memory functions equal for simplicity, because they show a similar behaviour. In this way, we find an effective Hamiltonian $\mathcal{H}_{eff}$ that contains two terms, a conventional kinetic contribution as well as a term that arises from the interaction with the standing wave

$$\begin{aligned}\mathcal{H}_{eff} &= \int d^2\mathbf{r}\, |\mathbf{r}\rangle \left(-\frac{\hbar^2\nabla^2}{2m_e^*}\right) \langle \mathbf{r}| \\ &\quad -\frac{\Omega_0^2}{\triangle_t} f_c(\triangle_t) \int d^2\mathbf{r}\, d^2\mathbf{r}'\, \cos^2\left(\mathbf{Q}\frac{\mathbf{r}+\mathbf{r}'}{2}\right) m(\mathbf{r}-\mathbf{r}')\, |\mathbf{r}\rangle \langle \mathbf{r}'| \end{aligned} \quad (3.44)$$

Here, we introduced the quantity $f_c(\triangle_t)$. Since the detuning from the exciton resonance $\triangle_x$ is uniquely related to the detuning from the trion resonance $\triangle_t$ via the trion binding energy E_T, we can introduce the correction factor $f_c(\triangle_t)$ as a function

of $\triangle_t$ only

$$f_c\left(\triangle_t\right) = \left(1 + \chi_c\left(\triangle_x\right)\frac{\triangle_t}{\triangle_x} - 2\frac{\triangle_t}{\triangle_x}\right), \qquad \triangle_x = \triangle_t + E_T \tag{3.45}$$

The correction factor $f_c\left(\triangle_t\right)$ pays tribute to the presence of the exciton continuum level in our system and will be subject to a further analysis. In particular, it will be compared to the correction factor $f_t\left(\triangle_t\right)$, Eqn. (2.55), predicted by the toy model.

For completeness, we state the effective Schrödinger equation for an electron with effective mass m_e^* and wavefunction $\Psi\left(\mathbf{r}\right)$ in the system we investigate:

$$-\frac{\hbar^2\nabla^2}{2m_e^*}\Psi\left(\mathbf{r}\right) - \frac{\Omega_0^2}{\triangle_t}f_c\left(\triangle_t\right)\int d^2\mathbf{r}'\,\cos^2\left(\mathbf{Q}\frac{\mathbf{r}+\mathbf{r}'}{2}\right)m\left(\mathbf{r}-\mathbf{r}'\right)\Psi\left(\mathbf{r}'\right) = E\Psi\left(\mathbf{r}\right). \tag{3.46}$$

This equation underlines that a lot of intriguing physics is ahead of us, but, for now, it shall mark the end of this chapter.

Chapter 4

Optical potentials for carriers in semiconductor quantum wells

We have predicted the existence of an optical trion-mediated trapping potential for carriers in a semiconductor QW system following two different approaches. First, based on an analogy to the well-established optical potentials for atoms, we have developed a toy model which stressed the importance of including the exciton level and its coherent character in our analysis. Second, we set up an effective Hamiltonian and extracted the corresponding Schrödinger equation that describes a conduction electron which virtually mixes with the extended bound and unbound trion states and, as a consequence, experiences light shifts.

In this chapter we will cover the key points that feature this novel optical potential for carriers in a QW. Throughout this analysis, we will substantiate the results with simple, but plausible and physically intuitive explanations. In a first step, we will address the origin and the effects of the correction factor $f_c(\triangle_t)$; we will highlight the stunningly comparable behaviour that our two different models predict in this respect. We will then turn to the non-local character of the potential embodied by the kernel $m(\mathbf{x})$ and justify its presence with the properties of the trion wave

function and the light masses of the particles under study. Although the nonlocality is a striking feature of this potential, we will neglect it at first in order to predict the actual potential depth of this optically induced trion-mediated potential. Here, we will stress the key ingredients that support a deep potential with controllable dissipation. In the last section, we will characterize the potential using a harmonic oscillator approximation to show the quantization of the electron motion. Since this approximation is a well-established in the analysis of optical potentials for atoms, we will be able to draw analogies and emphasize the differences to optical dipole potentials for atoms. Finally, the fact that we neglected the non-locality within the harmonic oscillator approximation will be justified by a variational calculation which explicitly incorporates the memory function $m(\mathbf{x})$ in the analysis.

4.1 Influence of exciton level

In both theoretical approaches the toy model as well as the effective Hamiltonian method, we encountered detuning dependent factors which we called $f_t(\triangle_t)$ and $f_c(\triangle_t)$ respectively. They take into account the presence of the coherent, many-body excitation of the exciton level and its competition with the formation of bound trions. The factors strongly affect the actual potential depth. In this section, we will show that the predictions of our two distinct models are in an excellent agreement.

Let us first summarize the expressions we have obtained. It is convenient to present $f_t(\triangle_t)$ and $f_c(\triangle_t)$ in terms of the dimensionless, system-independent quantity

$$\xi = \frac{E_T}{\triangle_x} = \frac{E_T}{E_T + \triangle_t} \tag{4.1}$$

which obeys the conditions

$$\lim_{\triangle_t \to 0} \xi = 1, \qquad \lim_{\triangle_t \to \infty} \xi = 0. \tag{4.2}$$

In terms of the quantity ξ, the toy model yields the compact result

$$f_t(\xi) = \xi, \tag{4.3}$$

while the effective Hamiltonian approach leads to

$$f_c(\xi) = \frac{2\xi^2(\xi - 1 - \ln(\xi))}{(\xi - 1)^2} \tag{4.4}$$

Although these two results might look very different at a first glance, it turns out that they agree not only on a qualitative, but even on a quantitative level. Fig. (4.1) displays the results of our two models in terms of the dimensionless parameter $x = \triangle_t / E_T$, the detuning from the trion resonance $\triangle_t$ in units of the trion binding energy E_T. It is positive for red detuning and negative for blue detuning, and related to ξ via the relation $\xi = 1/(1 + x)$.

For red detuning ($\triangle_t > 0$), both models predict that the correction factors and therefore the potential depth approach zero as the detuning from the trion resonance goes to "infinity". On resonance, i.e. for $\triangle_t = 0$, both correction factors become one: on resonance, the presence of the exciton level has no net effect on the potential for the electrons, so that there is no reduction nor enhancement in the potential depth. When we go to blue detuning ($\triangle_t < 0$), where the potential swaps from attractive to repulsive, the correction factors start to increase non-linearly on the blue side, resulting in a drastic enhancement for the potential depth seen by the conduction electrons. For detunings closer to the exciton resonance than $x = -0.9$, the correction factors even cause an enhancement of more than a factor of 10, which directly maps

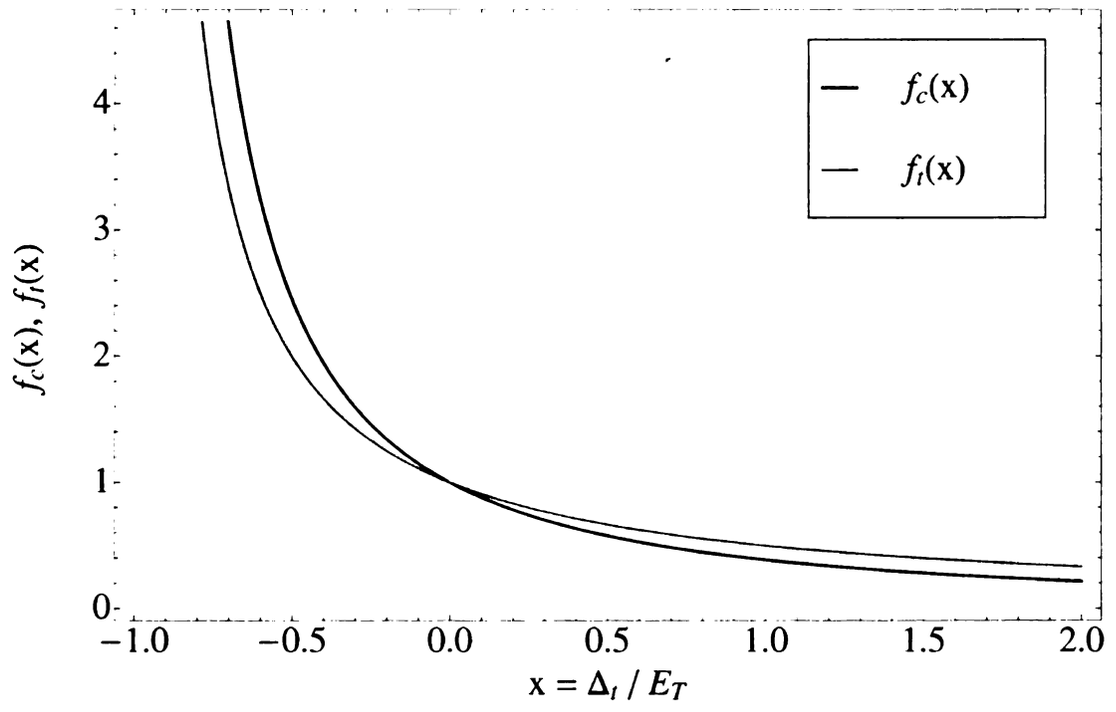

Figure 4.1: Predictions of the toy model and the effective Hamiltonian approach for the detuning dependent correction factors.

onto an increased potential depth by the same factor. As it will turn out later, this rather strong enhancement is crucial to obtain potential depths that dominate over competing effects such as the recoil energy or the thermal energy.

In conclusion, we see that the predictions of our two models concerning the role of the coherent exciton level converge to a beautiful agreement. Therefore, in the following we will use only the correction factor $f_t\,(\xi)$ that we derived in the framework of the cell model in order to specify the potential due to its simpler, convenient algebraic form.

4.2 Memory effect: Non-locality of the potential

Let us turn to another peculiar feature that is included in the effective Schrödinger equation (3.46), its non-locality. It is governed by the kernel $m(\mathbf{x})$, that we identified and labeled as a memory function. According to its definition, it represents the interaction strength per unit area of a second order process in position space: the electron mixes with the extended trion state and "jumps" back gain.

We have two physically intuitive ideas to explain the physics that cause this non-locality with its characteristic length of $\sim 3a_D$, as seen in Fig. (3.4) and (3.5).

The first idea is to associate the non-locality with the momentum kick that the virtual trion obtains from the photon absorption. After this kick, the virtual trion 'travels' for the period of its lifetime. The lifetime of the virtual excitation of the trion level is approximately $\sim 1/\triangle_t$. We work in the electron's restframe, since the off-diagonality is independent of the thermal momentum of the electron $\mathbf{k}_e$. We can estimate the distance d the virtual trion travel as

$$d \approx \frac{\hbar |\mathbf{Q}|}{m_t} \frac{1}{\triangle_t} = \frac{2\pi\hbar}{m_t \lambda_{\shortparallel} \triangle_t} \tag{4.5}$$

where we expressed the magnitude of the in plane momentum $\mathbf{Q}$ in terms of the in plane wavelength $\lambda_{\shortparallel}$. Only close to the trion resonance, i.e. for small $\triangle_t$, d can be comparable to a_D, but for larger detunings it becomes smaller and falls short in explaining the nonlocality of the potential.

However, we can give an even simpler explanation for the potential's non-local character that is essentially independent of the detuning. The optical potential is not diagonal in $\mathbf{r}$-representation because the trion is a rather large object ($\sim 2a_D$) and the effective masses of the particles are relatively small. When the very light electron mixes with the diffusive extended trion state, it wiggles 'inside' the trion complex. Since the characteristic size of the trion matches perfectly with the char-

acteristic length of the kernel $m(\mathbf{x})$, we believe that this simple picture explains the nonlocality of the optical trion-mediated potential. In principle, one can argue that optical potentials for atoms are nonlocal as well, but, due to the large proton mass and the small atomic size, the nonlocal effect is not observable.

Let us mention that the form of the memory function $m(\mathbf{x})$ is well approximated by a Gaussian of the form

$$g(\mathbf{x}) = ae^{-bx^2}. \tag{4.6}$$

We have obtained the numerical values for the fitting parameters a and b based on a least-squares fit; the results are listed in Tab. (4.1). In Fig. (4.2) we present the memory function $m(\mathbf{x})$ and the corresponding fitted Gaussians $g(\mathbf{x})$ for both $GaAs$ and $CdTe$. The very good agreement will allow us to simplify further calculations that explicitly include the kernel $m(\mathbf{x})$ by using the fitted gaussian $g(\mathbf{x})$.

	$GaAs$	$CdTe$
a	2.727	2.262
b	0.109	0.085

Table 4.1: Fitted parameters for $g(\mathbf{x})$ for $GaAs$ and $CdTe$ in effective atomic units.

So far, we have only considered the form of the nonlocal memory effect in the $Q \to 0$ limit. For completeness, we present a numerical solution for a finite value of $\mathbf{Q}$, corresponding to an angle of 70° between the laser and the QW plane. We can see that the $Q \to 0$ limit is perfectly justified. The numerical solution is centered around $\mathbf{k} = 0$ and shows a characteristic size of $\sim 3a_D$, just as the approximative $\mathbf{Q} = 0$ solution. It is displayed in Fig. (4.3).

One might be led to think that the omnipresent quivering motion of the electrons due to their mixing with the excited trion state might impose a serious reduction on the localization effect of the potential. However, the characteristic length of this effect is one to two orders of magnitude smaller than the periodicity of the potential $\lambda_{\parallel}/2$, depending on the chosen angle between the incoming laser and the QW plane.

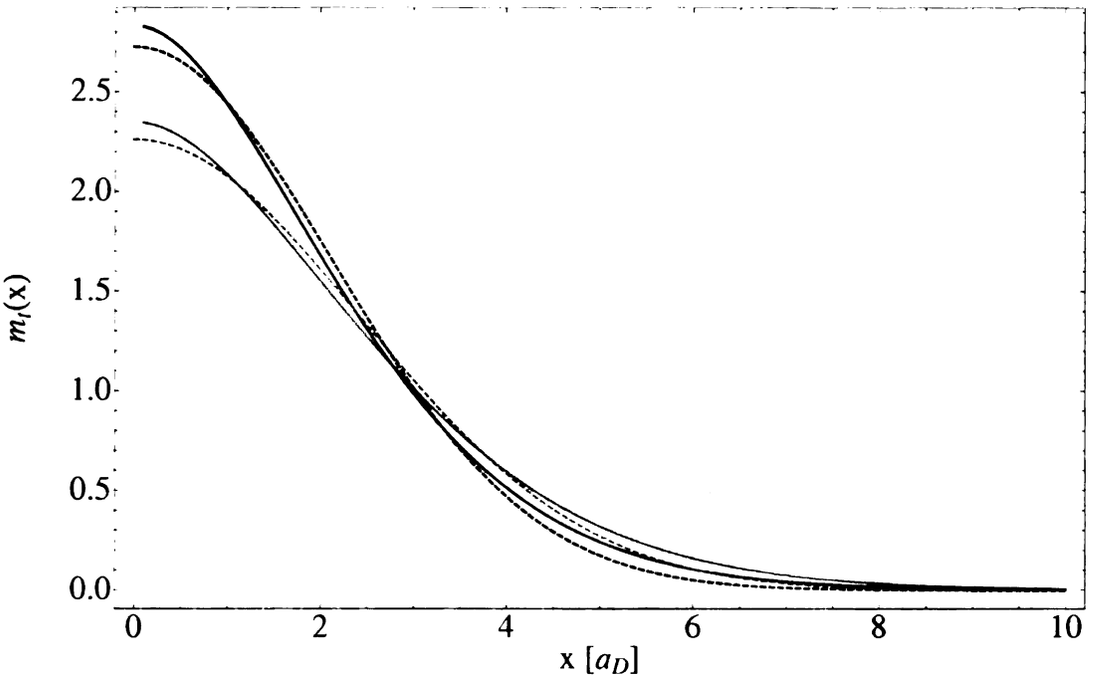

Figure 4.2: Memory function $m_t(\mathbf{x})$ (solid lines) in the $Q = 0$ limit and fitted Gaussians $g(x)$ (dashed lines): $GaAs$ is displayed in blue, $CdTe$ in orange.

Indeed, after this analysis of the nonlocality of the potential, our next step will be to neglect the nonlocality in order to prove the possibility to trap electrons and to estimate the actual strength of the potential.

4.3 Potential depth

Although certainly an intriguing feature, we will neglect the non-locality of the optical trion-mediated potential in this section to present one of the main results of this thesis: the depth of the trapping potential. In order to achieve this goal we make the replacement

$$m(\mathbf{r} - \mathbf{r}') \rightarrow \chi\delta(\mathbf{r} - \mathbf{r}'), \tag{4.7}$$

which enforces a corresponding local potential for the electrons. The dimensionless quantity χ takes into account the presence of the trion resonance and its electron-hole

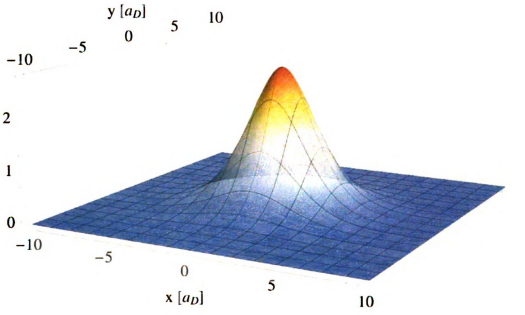

Figure 4.3: Memory function $m_t(\mathbf{x})$ for a finite value of the laser photon momentum $\mathbf{Q}$ projected onto the QW plane. We used the parameters for $GaAs$.

correlation effects. By definition, it is given by

$$\chi = \int d^2\mathbf{x}\, m(\mathbf{x}) = \int d^2\mathbf{x} \int \frac{d^2\mathbf{k}}{(2\pi)^2} e^{i\mathbf{k}\mathbf{x}} |I_+(\mathbf{k})|^2_{\mathbf{Q}=0}. \tag{4.8}$$

The integration is readily done and we obtain the result

$$\chi = \left| \frac{1}{\sqrt{2\pi}} \int d^2\mathbf{r}\, \varphi_b(r,r,r) \right|^2. \tag{4.9}$$

The correlation factor χ appears as the integral over all possible three particle trion configurations corresponding to one electron and the hole on top of each other. This is the natural extension of the two particle exciton picture, where at the moment of photocreation the electron and hole are at the same spot. The coefficient χ takes into account that the exciton needs to be created somewhere inside a reasonable range to possibly bind to an electron and form a bound trion; the range is essentially governed by the relative trion wavefunction $\varphi_b(r,r,r)$: the arguments of φ_b simply

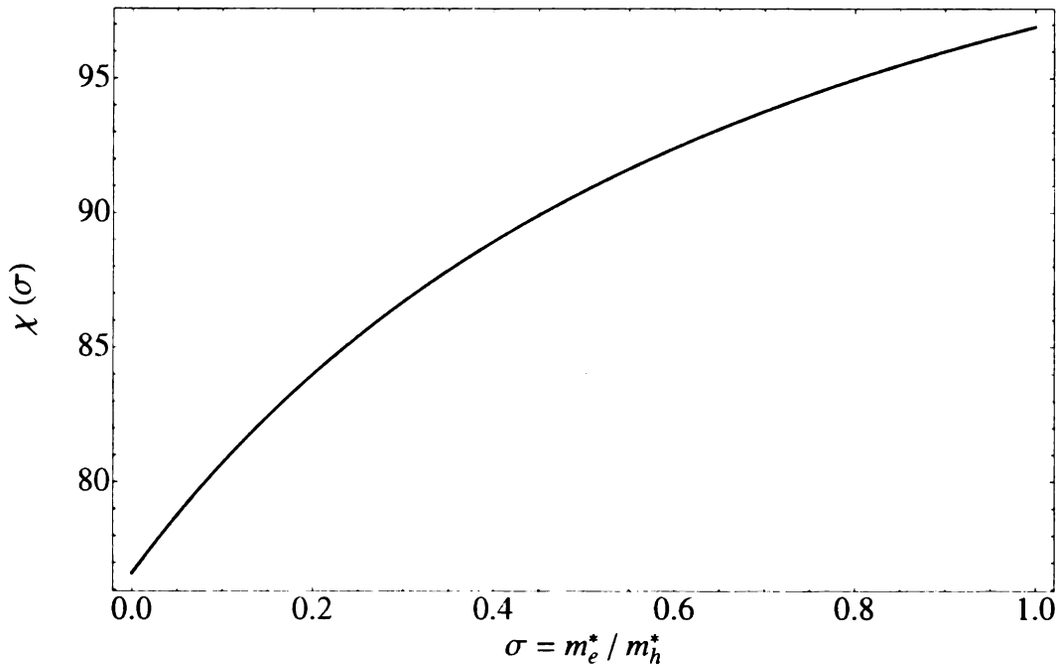

Figure 4.4: Enhancement factor χ as a function of the electron hole massratio σ.

underline that the wavefunction is evaluated with one electron and the hole on top each other, so that the Hylleraas coordinates we used in the formulation of φ_b boil down to $s = t = u = r$. The factor of $1/\sqrt{2\pi}$ arises from the normalization of the overall angular degree of freedom.

Inserting the relative wavefunction given in Eqn. (1.26), we obtain a compact analytic expression for χ

$$\chi = 2\pi\mathcal{N}^2 \left(\frac{\alpha^2 + 2\alpha\beta + 6\gamma}{\alpha^4} \right)^2 \tag{4.10}$$

that depends only on the values of the variational parameters α,β and γ. Consequently, it can be expressed as a function of the electron hole mass ratio $\sigma = m_e^*/m_h^*$ solely. The result for $\chi = \chi(\sigma)$ is presented in Fig. (4.4). We recognize that χ can take on rather large values: we obtain ~ 80 for $GaAs$ and even ~ 90 for $CdTe$.

At this point, we can close the circle between the cell model and the effective

Hamiltonian approach. In the toy model, the effective range around the electron in which the creation of an exciton leads to the formation of a bound trion was simply modelled by a step function around the electron of the trion size A_t. Based on this simplified picture, the fact that one electron is effectively coupled to many trion states gave rise to the definition of $N_t = A_t/A_x$, the number of excitons that fit into the bound trion state without spatial overlap. In principle, the effective Hamiltonian model yields the same result in terms of the relative wavefunction φ_b. Here, the step function is replaced by an integral over all the possible combinations in which the conduction band electron and the photoexcited exciton form a bound trion configuration. Therefore, based on their physical interpretation, the quantities N_t and χ are equivalent. They express the degeneracy factor of the trion levels the free electron is coupled to, since the spot where the additional electron-hole pair is created can be literally anywhere within the trion size. While N_t was found to be ~ 10, the quantity χ is in the range $\sim 80-90$, thus a factor of $8-9$ times bigger than the corresponding prediction of the toy-model. This is far away from being a perfect agreement, but still N_t and χ are within the same order of magnitude. In addition, N_t only serves as an illustrative ingredient in the toy-model, but does not affect our results. For the numerical calculations, we will use the enhancement factor χ, since it contains the actual information about the trion wavefunction.

Based on the local limit in Eqn. (4.7), we recover a simplified Schrödinger equation for the electron with a local potential that obeys the profile of the laser intensity pattern

$$-\frac{\hbar^2\nabla^2}{2m_e^*}\Psi(\mathbf{r}) - \chi\frac{\Omega_0^2}{\triangle_t}f_c(\triangle_t)\cos^2(\mathbf{Qr})\Psi(\mathbf{r}) = E\Psi(\mathbf{r}). \tag{4.11}$$

Consequently, the trapping potential $V(\mathbf{r})$ varies with the electron position as

$$V(\mathbf{r}) = V_0\cos^2(\mathbf{Qr}) = -\epsilon\triangle_t f_c(\triangle_t)\cos^2(\mathbf{Qr}), \tag{4.12}$$

where we introduced the saturation parameter ϵ for the electron trion transition

$$\epsilon = \chi \left(\frac{\Omega_0}{\triangle_t} \right)^2 . \tag{4.13}$$

The parameter ϵ essentially describes two effects: Since the factor $\chi\Omega_0^2$ can be viewed as an effective Rabi frequency for the electron trion transition, in the limit $\triangle_t \gg \Gamma_t$ it gives the probability to be in the excited trion state. By choosing ϵ sufficiently small, the dissipative aspects of the electron dynamics due to spontaneous emission of photons are efficiently suppressed. Photon scattering occurs at the effective spontaneous emission rate $\Gamma_{se} = \epsilon\Gamma_t$, with $\Gamma_t \sim 10^{10} s^{-1}$ being the natural linewidth of the trion level. While Γ_{se} scales as $\sim 1/\triangle_t^2$, the scaling behaviour of the trap depth V_0 is very different for red and blue detuning, owing to the background-polarizability correction factor $f_c(\triangle_t)$. While V_0 scales as $\sim 1/\triangle_t^2$ for red detuning, it scales as $\sim 1/\triangle_t$ only for blue detuning. Therefore, intense blue-detuned light far enough from the trion-resonance provides strong confinement with minimal dissipation with respect to the trion-resonance. However, in this case one has to take into account the presence of the exciton resonance and the subsequent creation of real excitons in the system. We will do so later on by estimating the probability to excite one exciton per cell. Note that the degeneracy factor χ gives rise to a reduction of almost two orders of magnitude in the required intensity to reach a given trap depth. In addition, a small ϵ value prevents power broadening of the trion resonance and subsequent creation of real trions. Thus, we are interested in the large detuning, low saturation limit where the excess conduction band electrons are the only real particles in the system, whereas excitons and trions are excited only virtually.

In the following, we will always associate the potential depth

$$V_0 = -\epsilon \triangle_t f_c(\triangle_t) \tag{4.14}$$

with a fixed value of the saturation parameter ϵ in order to control the dissipative effects. In this representation, the potential depth increases with the detuning from the trion resonance $\triangle_t$, because simultaneously the Rabi frequency Ω_0 is increased. For red detuning the only limitation is set by the maximum laser power available, while for blue detuning we will have to take into account the increasing probability of creating real excitons in the system as we approach the exciton resonance. Below, we will discuss both limitations.

Before outlining the differences with respect to conventional optical dipole potentials for atoms, let us mention the similarities first. The potential $V(\mathbf{r})$ given in (4.12) follows the spatial dependence of the intensity pattern of the laser and its depth is proportional to the applied laser intensity. For red detuning ($\triangle_t > 0$) the potential is attractive, the electrons are attracted towards the bright spots, whereas for blue detuning ($\triangle_t < 0$) the potential is repulsive, so that the electrons tend to accumulate at the nodes of the standing wave pattern, i.e they seek the dark spots of the intensity profile.

Now, let us reiterate the specific properties of the trion-mediated optical potential for electrons embedded in QW system that are distinctive and not present for conventional optical potentials for atoms. The major difference arises from the presence of the factor $f_c(\triangle_t)$. This is substantially underlined in Fig. (4.5), where the potential depth V_0 is given for both red and blue detuning for various values of the control parameter ϵ, which corresponds to a constant rate of spontaneous emission. The detuning $\triangle_t$ as well as the the potential depth V_0 are represented in terms of the trion binding energy E_T, which is of the order of $\sim meV$ for typical semiconductor QW systems.

For red detuning the effects of the exciton level and the trion level on the shift of the electron's ground state energy with respect to the excitonic background shift counteract. As a consequence, the potential depth V_0 shows a saturation behaviour,

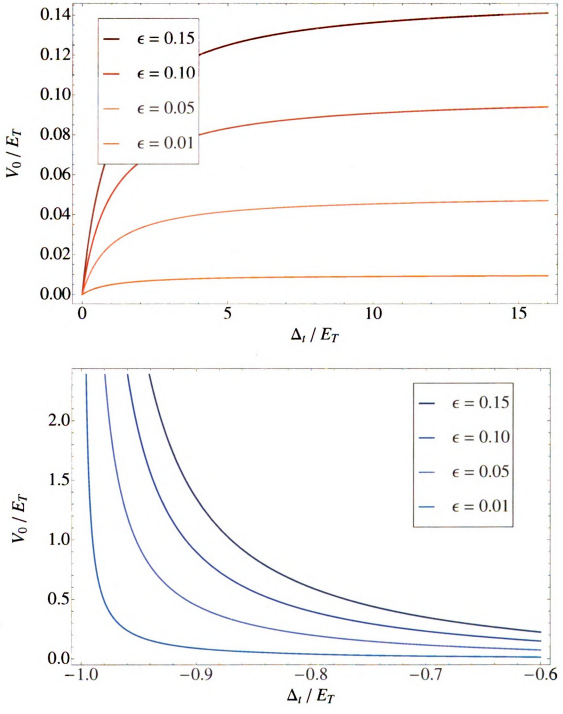

Figure 4.5: Potential depth V_0 for red ($\triangle_t > 0$) and blue ($\triangle_t < 0$) detuning in terms of the trion binding energy E_T for various values of the saturation parameter ϵ.

reaching the value ϵE_T at maximum, if sufficient laser power is provided. To reach the saturative regime we estimate the necessary laser intensity I to be $I \approx 6 \times 10^5 W/cm^2$ for both $GaAs$ and $CdTe$ QW systems.

The physics is different for blue detuning: The effects of the exciton level and the trion level on the shift of the electron's ground state energy with respect to the excitonic background shift add up, resulting in a potential depth that can reach several meV. For blue detuning and ϵ held constant, the potential depth keeps on increasing when increasing the detuning from the trion resonance, thereby showing a highly non-linear behaviour. Of course, in doing so one approaches the exciton resonance whose natural linewidth Γ_x for both $GaAs$ and $CdTe$ is approximately $\Gamma_x/E_T \sim 0.03$. We can estimate the time-averaged probability for the excitation of real excitons $\langle P_x \rangle$ using the two-level Rabi model. Referring to one exciton cell of size A_x, the time-averaged probability that this "two-level" system is in the excited state reads

$$\langle P_x \rangle = \frac{\epsilon/\chi \left(\triangle_t/E_T\right)^2}{4\left(1+\triangle_t/E_T\right)^2 + 2\epsilon/\chi \left(\triangle_t/E_T\right)^2 + \left(\Gamma_x/E_T\right)^2}, \tag{4.15}$$

where we expressed all energies in terms of the trion binding energy E_T and used the relation

$$\Omega_0^2 = \frac{\epsilon}{\chi}\triangle_t^2. \tag{4.16}$$

In this way, $\langle P_x \rangle$ essentially depends only on $\triangle_t$, once the saturation parameter ϵ is fixed. The results for $\langle P_x \rangle$ are presented in (4.6).

At this point, we have built up a powerful scheme which suggests that we can pick a (small) value for the saturation parameter ϵ and tune the detuning from the trion resonance $\triangle_t$. We will find a combination of the potential depth V_0 and the time-averaged probability for exciton creation $\langle P_x \rangle$. Four possible combinations are listed as examples in Tab. (4.2). Let us just describe one specific example explicitly:

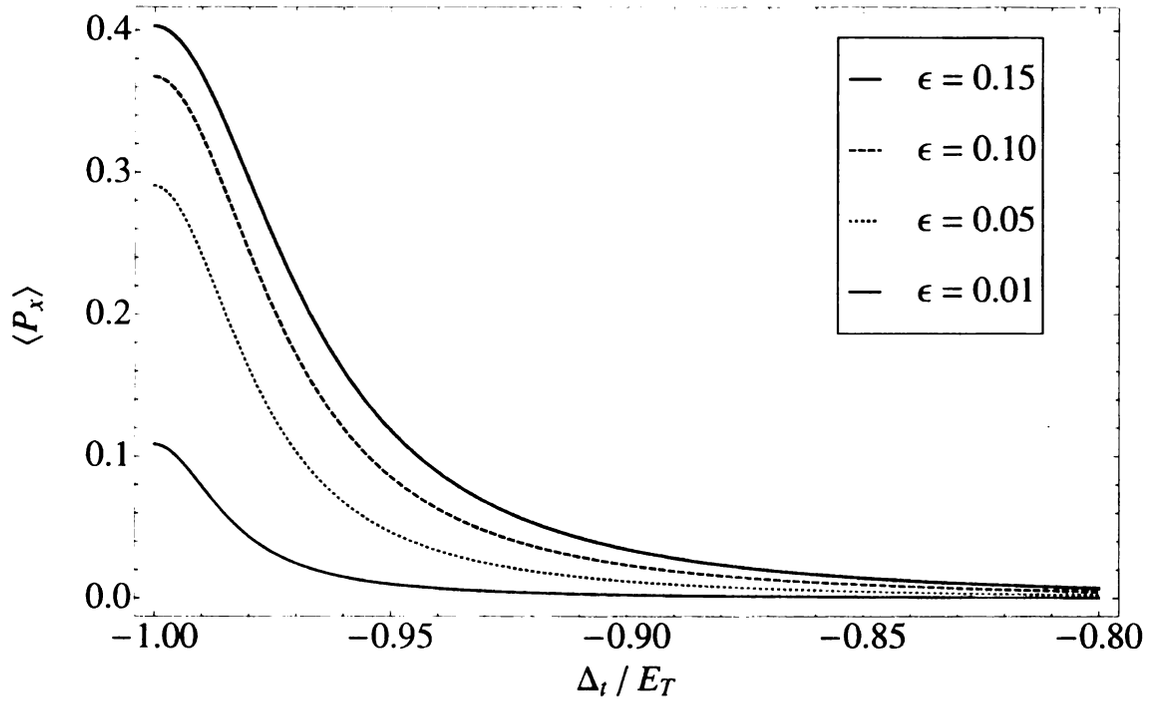

Figure 4.6: Time averaged probability of formation of real excitons per exciton-cell as a function of the detuning from the trion resonance $\triangle_t$ for various values of the saturation parameter ϵ.

for $\epsilon = 0.05$ we find that a potential depth of $V_0 \approx 0.45 E_T$ is feasible, while the probability to excite an exciton per cell is still only about 1.2%. Here, laser intensities of $I \approx 2.5 \times 10^3 W/cm^2$ and $I \approx 7.7 \times 10^3 W/cm^2$ would be required in $GaAs$ and $CdTe$ respectively to achieve potential depths of $V_0 \approx 0.9\, meV$ and $V_0 \approx 1.6\, meV$.

	$\triangle_t = -0.9\, E_T$	$\triangle_t = -0.95\, E_T$
$\epsilon = 0.05$	1.2%, 0.45	4.7%, 0.95
$\epsilon = 0.01$	0.2%, 0.09	1.0%, 0.19

Table 4.2: Combinations of the time averaged probability for exciton creation and potential depth are presented as pairs in the form $\langle P_x \rangle$, V_0 for two values of the saturation parameter ϵ and the detuning from the trion resonance $\triangle_t$.

Lastly, we note that the excitons are created at the bright spots of the intensity pattern, whereas the electrons are located at the dark spots for blue detuning. This combination of a controllable, low excitation probability with significant spatial sep-

aration should strongly suppress the interaction of the electrons with real excitons in the system.

The strength of optical dipole traps for atoms is routinely measured in units of the single photon recoil energy $E_R = \hbar^2 Q^2 / 2m_e^*$. It simply sets a natural energy scale for the problem. Translational invariance along the QW implies conservation of the in-plane momentum only, which reduces the average recoil kick an electron experiences in the process of spontaneous photon emission. By averaging over the solid angle, the average recoil energy is $\langle E_R \rangle = (2/3)\, E_R$. The small effective masses of the electrons, though, give rise to huge recoil energies, compared to atoms. The effective electron masses are about seven orders of magnitude smaller than the masses of rubidium atoms, one of the standard systems for atomic physics and quantum optics so that the recoil energies are correspondingly larger by a factor of $\sim 10^7$. For $GaAs$ and $CdTe$, the average recoil energies amount to $\langle E_R \rangle \approx 0.29meV$ and $\langle E_R \rangle \approx 0.16meV$ respectively. Referring to the specific example just given above, the potential depth V_0 exceeds the recoil energy E_R by a factor of three and even 10 in $GaAs$ and $CdTe$ respectively.

Based on atomic optical potentials, many ground-breaking experiments have been performed. Some examples are the evidence for macroscopic Quantum interference [42], the observation of Bloch oscillations of atoms [43] and the investigation of the quantum phase transition from a superfluid to a Mott insulator [44] to name a few. In principle, they all relied on the power and versatility of optical potentials. The maximum potential depths in these experiments have been $2.1E_R$, $6E_R$ and $22E_R$ respectively. The fact that, despite the huge recoil energies involved in our system, we can still predict potential depths of several E_R substantiates the strength of the trion-mediated trapping potential mechanism we investigate here. So the question that naturally arises in this context is: Why is the trion-mediated potential actually so strong? The bare interband dipole moment d_0 in our system is $\sim 6e$Å, while the dipole

moment for an atom d_{atom} can be approximated based on the Bohr radius in vacuum as $\sim 5 \times 10^{-1} e\text{Å}$. However, the effective dipole moment d for the electron-trion transition is enhanced by the degeneracy factor of the excited trion state. In total, we can estimate that the squared effective dipole moment in our system exceeds its atomic counterpart by three to four orders of magnitude, i.e. $d^2 = \chi d_0^2 \approx 10^3 - 10^4 \times d_{atom}^2$.

Let us briefly summarize the parameters that are in favour of a deep potential depth: In general, a larger value for the saturation parameter yields a deeper potential, but at the same time the dissipative effects due to spontaneous emission of photons become more important. With ϵ held constant, one can deepen the potential depth V_0 by increasing the detuning from the trion resonance $\triangle_t$, provided that sufficient laser power is available. Note, that when following this technique the behaviour is very different for blue and red detuning because of the correction factor $f_c(\triangle_t)$. Finally, host materials with higher trion binding energies allow for considerably stronger potentials.

4.4 Harmonic oscillator approximation

In principle, the Bloch theorem states that the exact solutions to any periodic Schrödinger equation take on the form of non-localized Bloch wavefunctions $\psi_{n,\mathbf{q}}(\mathbf{r})$. They are labeled by a discrete band index n and a quasimomentum $\mathbf{q}$ within the first Brillouine zone of the reciprocal lattice. Upon translation by an arbitrary lattice vector $\mathbf{R}$, Bloch functions are multiplied by a pure phase factor $\exp(i\mathbf{qR})$. As a consequence, they are coherently extended over the whole lattice [40].

From this point of view, the next step we will take seems strikingly contradictive at a first glance and needs some clarification. In the framework of optical lattices of atoms, it has become well-established to approximate the atomic motion near the bottom of the wells by a simple harmonic oscillator that is thermally excited (see

for example [40, 58]). The basic idea is that for deep optical lattice potentials the atoms are tightly confined at a single lattice site which is approximately harmonic. The oscillation frequency ω_{ho} and the trapping frequency $\nu_r = \omega_{ho}/2\pi$ respectively which are easily obtained from this approximation have become figures of merit to characterize the optical potential. However, we note, that it is only meaningful to talk about oscillatory motion if the trapped particle resides at one particular lattice site for a time at least comparable to the oscillation frequency [58]. This is precisely the regime where one has to describe the electron's motion quantum-mechanically.

For atoms, this picture has already been justified experimentally: atoms have been successfully cooled down to the lowest bound state [45, 46, 47] entering a regime where their localized quantum wavepackets could be controlled in real time [48, 49].

As far as our system is concerned, it is easy to imagine mechanisms that lie beyond the scope of our model and do not appear in the Schrödinger equation formulated above: impurities due to defects in the lattice, phonons interactions, just to name a few. These effects can lead to decoherence which makes the picture of a single electron trapped at one lattice site more plausible by suppressing delocalization. Apart from that argument, an appropriate superposition of Bloch states, the energy eigenstates for single electrons, yields a set of Wannier functions which are well localized on the individual trapping sites.

In this spirit, we will derive the essential quantities of the optical potential in the harmonic oscillator approximation to characterize its localization strength and to compare the results to typical values for atomic optical lattices. We will do so first in the limit of a local potential proceeding from Eqn. (4.12); in the second step we will explicitly include the nonlocality governed by the memory function $m(\mathbf{x})$ and show that is is legitimate to neglect the nonlocality when describing the properties of an electron trapped at the bottom of the effective harmonic oscillator potential.

4.4.1 Without memory: Local potential

Our considerations start out from (4.12). Without loss of generality, we align the in-plane photon wavevector along the $\hat{x}$-direction as $\mathbf{Q} = Q\hat{x}$. Expanding the $\cos^2(\mathbf{Qr})$ to second order around the local minimum at $\mathbf{r} = 0$ (for red detuning $\triangle_t > 0$) gives

$$\cos^2(\mathbf{Qr}) \approx 1 - Q^2x^2. \tag{4.17}$$

The potential term in the Schrödinger equation becomes flat in the $\hat{y}$- direction and a simple harmonic oscillator in the $\hat{x}$-direction. In this approximation the Schrödinger equation consequently boils down to

$$-\frac{\hbar^2\nabla^2}{2m_e^*}\Psi(\mathbf{r}) + V_0Q^2\sin^2(\theta)\,x^2\Psi(\mathbf{r}) = E\Psi(\mathbf{r}), \tag{4.18}$$

where we expressed the momentum of the photon projected onto the QW plane in terms of the angle θ between the $\hat{z}$-direction perpendicular to the sample area and $\mathbf{Q}$ according to $Q = Q\sin(\theta)$. By tuning the angle θ, one can easily alter the periodicity of the lattice $a = \lambda_{\shortparallel}/2$, while holding the potential depth of the lattice constant. The smallest periodicity is reached for two counterpropagating laser beams, which corresponds to the specific case where $\mathbf{Q}$ is in the plane of the sample and subsequently θ takes on the value $\pi/2$, by definition the maximum value for θ. By choosing smaller values, one can control the validity of the harmonic approximation: a variation of the angle θ has no impact on the depth of the potential since V_0 is only affected by the total energy of the photons. However, the angle θ does influence the periodicity of the lattice: making the angle θ smaller leads to a bigger periodicity of the lattice, because the in-plane momentum Q decreases; equivalently, the in-plane wavelength increases. If the angle θ is chosen sufficiently small, the harmonic oscillator approximation steadily improves, since the slope of the potential-well flattens out.

The Schrödinger equation describing our system has become the one for a simple harmonic oscillator in the $\hat{x}$-direction and we can readily identify

$$\frac{m_e^*}{2}\omega_{ho}^2 = V_0 Q^2 \sin^2(\theta), \tag{4.19}$$

where ω_{ho} is the oscillation frequency of the harmonic oscillator. Since the two dimensions are decoupled, we proceed by making the product ansatz $\Psi(\mathbf{r}) = \Psi_x(x)\Psi_y(y)$ for the electron's wavefunction and separate the energy eigenvalue $E = E_x + E_y$ to obtain two decoupled one-dimensional Schrödinger equations. The solution to the Schrödinger equation in the $\hat{y}$-direction

$$-\frac{\hbar^2}{2m_e^*}\frac{\partial^2}{\partial y^2}\Psi_y(y) = E_y\Psi_y(y) \tag{4.20}$$

is simply a plane wave with wavevector $\pm\sqrt{2m_e^* E_y}/\hbar$.

Since we are about to study the localization effect of the optical potential, the $\hat{y}$-direction is of no further interest. Owing to the separability of the problem, we have simplified the problem to a one dimensional Schrödinger equation

$$-\frac{\hbar^2}{2m_e^*}\frac{\partial^2}{\partial x^2}\Psi_x(x) + \frac{m_e^*}{2}\omega_{ho}^2 x^2\Psi_x(x) = E_x\Psi_x(x), \tag{4.21}$$

whose solutions are well known. The normalized ground state wavefunction of the one-dimensional harmonic oscillator in the $\hat{x}$-direction is given by

$$\Psi_{x,0}(x) = \left(\frac{m_e^*\omega_{ho}}{\pi\hbar}\right)^{1/4}\exp\left(-\frac{m_e^*\omega_{ho}}{2\hbar}x^2\right). \tag{4.22}$$

The level spacing of the harmonic oscillator is

$$\hbar\omega_{ho} = \hbar\sqrt{\frac{2V_0Q^2\sin^2(\theta)}{m_e^*}} = 2\sqrt{V_0 E_R \sin^2(\theta)}. \tag{4.23}$$

In our context $\hbar\omega_{ho}$ is the energy of local oscillations inside the trapping well. For a deep optical lattice with $V_0 \gg \langle E_R \rangle$, the energy $\hbar\omega_{ho}$ of local oscillations in the well is large compared to the recoil energy and each well supports several quasibound states.

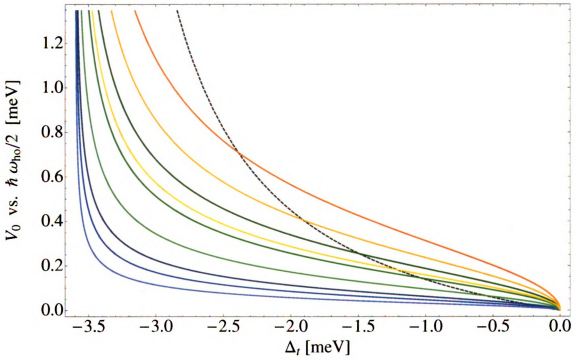

Figure 4.7: The first three levels of the harmonic oscillator are compared to the potential depth (dashed black line) for $CdTe$ and blue detuning: The blue branch shows the ground state level for the angles $\theta = 20°$ (dark blue), $\theta = 15°$ (blue), $\theta = 10°$ (lighter blue). Similarly, the first excited (green) and the second excited level (orange) are depicted.

Fig. (4.7) shows that for blue detuning in a $CdTe$ system and appropriate values for the angle θ, the first three energy levels of the harmonic oscillator can be resolved within the potential depth V_0. As speculated above, the harmonic oscillator approximation is favoured by deeper potentials V_0 and bigger periodicities of the potential.

In the next step, we examine the spatial spread $\triangle X$ of the ground state wave-

function

$$\triangle X = \sqrt{\frac{\hbar}{m_e^* \omega_{ho}}} = \frac{\sqrt{\hbar}}{\left(2 m_e^* V_0 Q^2 \sin^2(\theta)\right)^{1/4}}. \tag{4.24}$$

The result for $CdTe$ and various angels θ is depicted in Fig. 4.8. For red detuning, the spatial spread saturates, simply because the potential depth follows a saturative behaviour. Typical values for the spatial spread $\triangle X$ are $\sim 10 a_D$, which is about five to ten times smaller than the corresponding lattice spacing a.

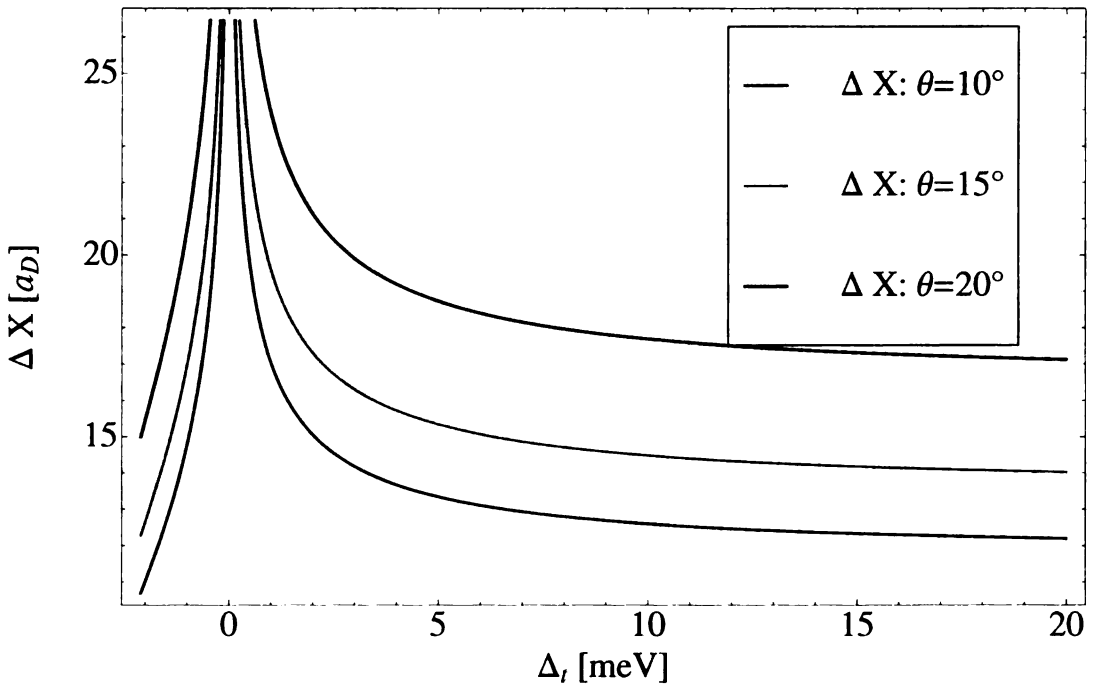

Figure 4.8: Spatial spread $\triangle X$ of the harmonic oscillator ground state as a function of the detuning for a fixed saturation parameter $\epsilon = 0.1$ in $CdTe$ and various values for the angle θ.

For completeness we give the trapping frequency $\nu_r = \omega_{ho}/2\pi$ according to

$$\nu_r = \frac{1}{\pi\hbar}\sqrt{V_0 E_R \sin^2(\theta)}. \tag{4.25}$$

Typical trapping frequencies for atomic optical lattices are in the regime of $\sim 100\,kHz$

[40]. On an absolute scale the potential depths and recoil energies in our system are several orders of magnitudes bigger which yield to trapping frequencies of the order of $\sim 10^{10} - 10^{11} Hz$. As shown in Fig. (4.9), ν_r can easily exceed the comparatively high effective spontaneous emission rate by two orders of magnitude. Accordingly, the vibrational level structure can be highly resolved, as the electron is forced to undergo many oscillations between the inevitable spontaneous emission events where it is randomly scattered due to a recoil kick.

We note that in the limit $E_R \ll \hbar\omega_{ho}$ the localization of the electron by the optical potential strongly suppresses the heating caused by spontaneous emission. This is because the single-photon recoil energy is not large enough to allow the electron to make a 'jump' between the harmonic oscillator levels. In our system, as shown in Fig. (4.10), we have $E_R \sim \hbar\omega_{ho}$, so while heating will not entirely suppressed, it may be significantly reduced.

4.4.2 With memory: Non-local potential

Our next goal is to investigate the case of a single electron trapped at one site of a simple harmonic oscillator, but this time we will explicitly keep the non-local character of the potential in terms of the memory function. For simplicity, we approximate the memory function $m\left(\left|\mathbf{r}-\mathbf{r}'\right|\right)$ with the Gaussian fit presented in Fig. (4.2). We will compute the size of a Gaussian ground state wavepacket based on a variational approach. We will show the procedure for red detuning in detail. The calculation for blue detuning goes along the lines, but one has to expand around a different local minimum as the character of the potential swaps from attractive to repulsive. In this way, we will be able to estimate the effect the nonlocality has on the result obtained above in the local limit of the potential.

Proceeding from the non-local Schrödinger equation, i.e. including the memory

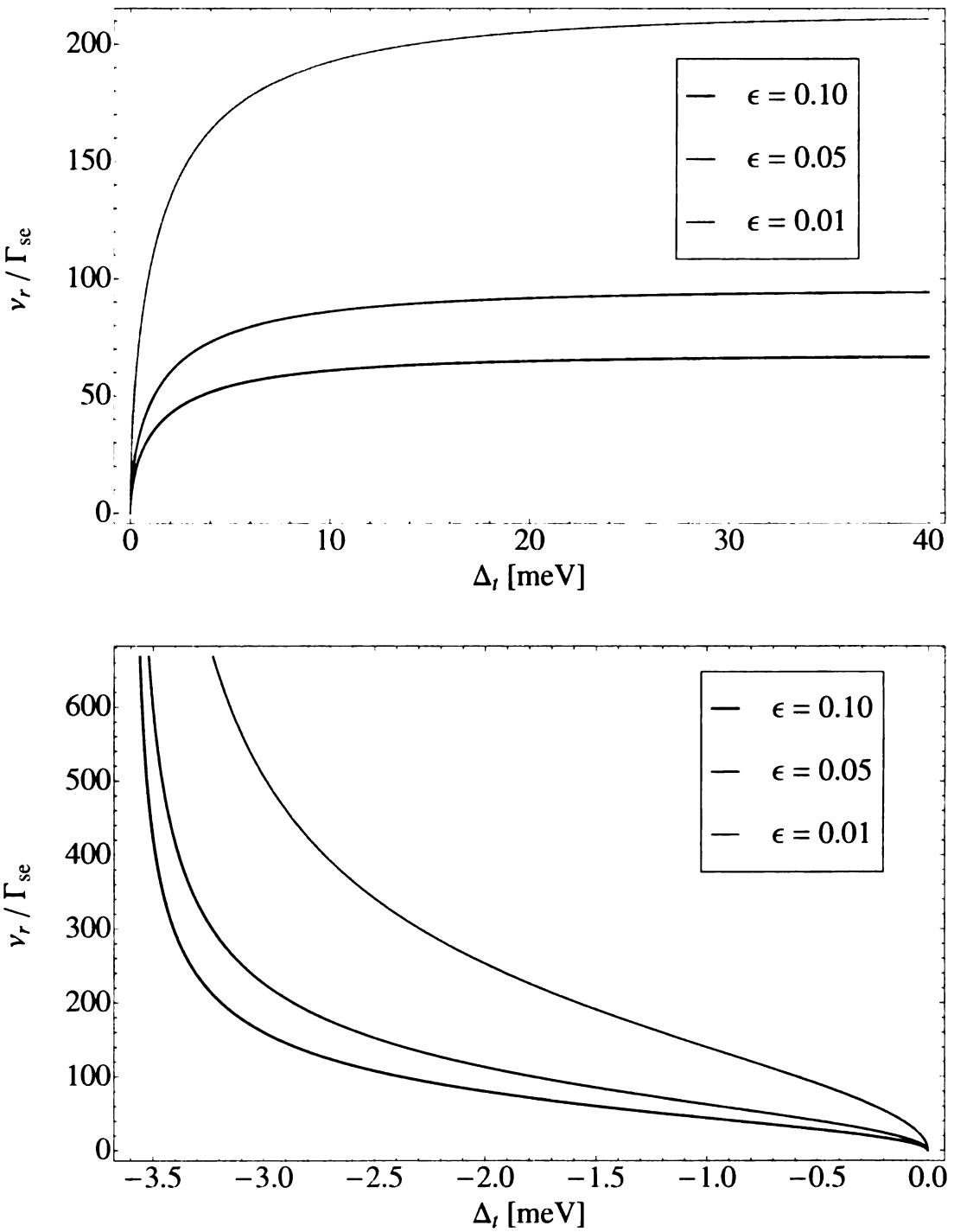

Figure 4.9: Trapping frequencies ν_r compared to the effective spontaneous emission rate for *CdTe*. θ was chosen to be 30°.

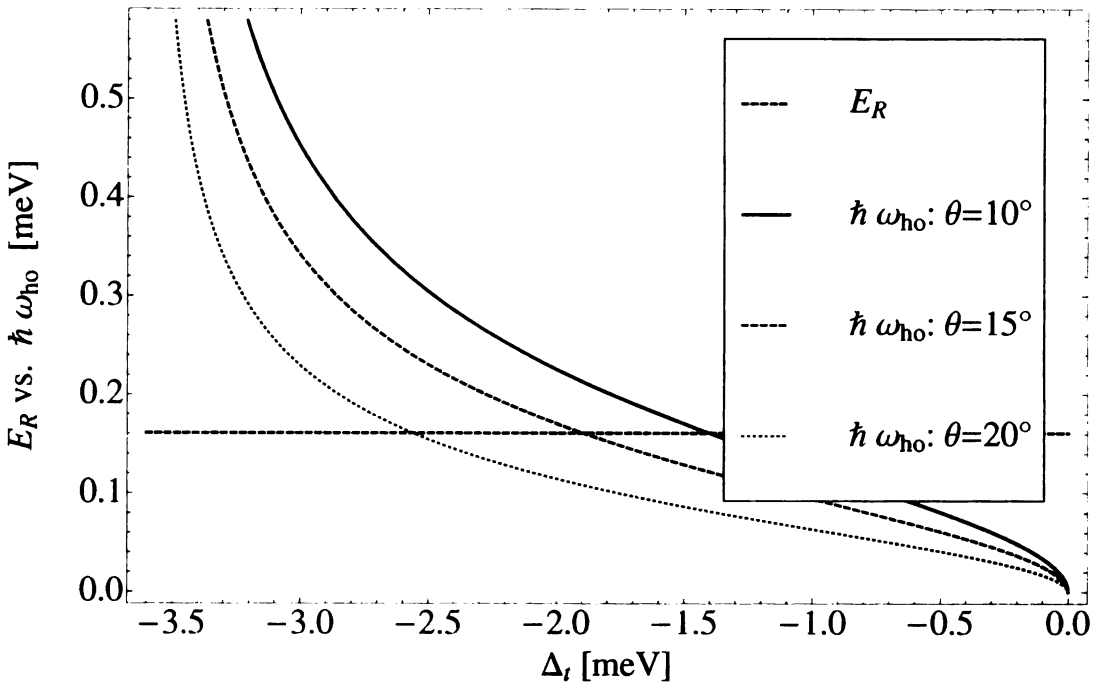

Figure 4.10: Single photon recoil energy E_R compared to the harmonic oscillator level spacing $\hbar\omega_{ho}$ as a function of the detuning for a fixed saturation parameter $\epsilon = 0.1$ in $CdTe$ and various values for the angle θ.

function,

$$-\frac{\hbar^2\nabla^2}{2m_e^*}\Psi(\mathbf{r}) - \frac{\Omega_0^2}{\triangle_t} f_c(\triangle_t) \int d^2\mathbf{r}' \cos^2\left(\mathbf{Q}\frac{\mathbf{r}+\mathbf{r}'}{2}\right) m\left(|\mathbf{r}-\mathbf{r}'|\right)\Psi(\mathbf{r}') = E\Psi(\mathbf{r}), \tag{4.26}$$

we will again expand the $\cos^2\left(\mathbf{Q}\frac{\mathbf{r}+\mathbf{r}'}{2}\right)$ to second order as

$$\cos^2\left(\mathbf{Q}\frac{\mathbf{r}+\mathbf{r}'}{2}\right) = \cos^2\left(Q\frac{x+x'}{2}\right) \approx 1 - \frac{Q^2}{4}\sin^2(\theta)\left(x+x'\right)^2, \tag{4.27}$$

so that the non-kinetic part of the non-local Schrödinger equation explicitly becomes

$$-\frac{\Omega_0^2}{\triangle_t} f_c(\triangle_t) \int d^2\mathbf{r}' \left(1 - \frac{Q^2}{4}\sin^2(\theta)\left(x+x'\right)^2\right) m\left(|\mathbf{r}-\mathbf{r}'|\right)\Psi(\mathbf{r}') \tag{4.28}$$

To find the ground state of this non-local Schrödinger equation, we can use a variational approach with the following ansatz

$$\Psi(\mathbf{r}) = \mathcal{N} e^{-\alpha^* x^2} e^{-\beta^* (y-y_0)^2} \tag{4.29}$$

consisting of two gaussian wave packets. The normalization constant is given

$$\frac{1}{\mathcal{N}^2} = \frac{\pi}{2\sqrt{\alpha^* \beta^*}} \tag{4.30}$$

The expectation value of the kinetic term is

$$\langle E_k \rangle = \frac{\hbar^2}{2m_e^*} (\alpha^* + \beta^*) \tag{4.31}$$

and for the potential term it is given by

$$\begin{aligned} \langle V \rangle &= -2\pi a \frac{\Omega_0^2}{\triangle_t} f_c(\triangle_t) \sqrt{\alpha^* \beta^*} \left\{ \frac{1}{\sqrt{\alpha^* (2b + \alpha^*) \beta^* (2b + \beta^*)}} \right. \\ &\quad \left. - \frac{Q^2 \sin^2(\theta)}{4\sqrt{\alpha^{*3} (2b + \alpha^*) \beta^* (2b + \beta^*)}} \right\} \end{aligned} \tag{4.32}$$

As we can see, both $\langle E_k \rangle$ as well as $\langle V \rangle$ do not depend on the parameter y_0, since for the chosen direction for $\mathbf{Q}$ along the $\hat{x}$-direction the problem is invariant under translations in the $\hat{y}$-direction. By numerically minimizing the total energy $\langle E_k \rangle + \langle V \rangle$, we obtain for example the values shown in Fig. (4.11) as a function of the (red) detuning $\triangle_t$. While α^* which describes the localization in the $\hat{x}$-direction is finite, the variational parameter β^* which is associated with the $\hat{y}$-direction is zero, independent of the chosen angle θ and the detuning $\triangle_t$. Thus, the electron's wave function is flat in the $\hat{y}$-direction and shows no localization. Qualitatively, we obtain the same behaviour for blue detuning.

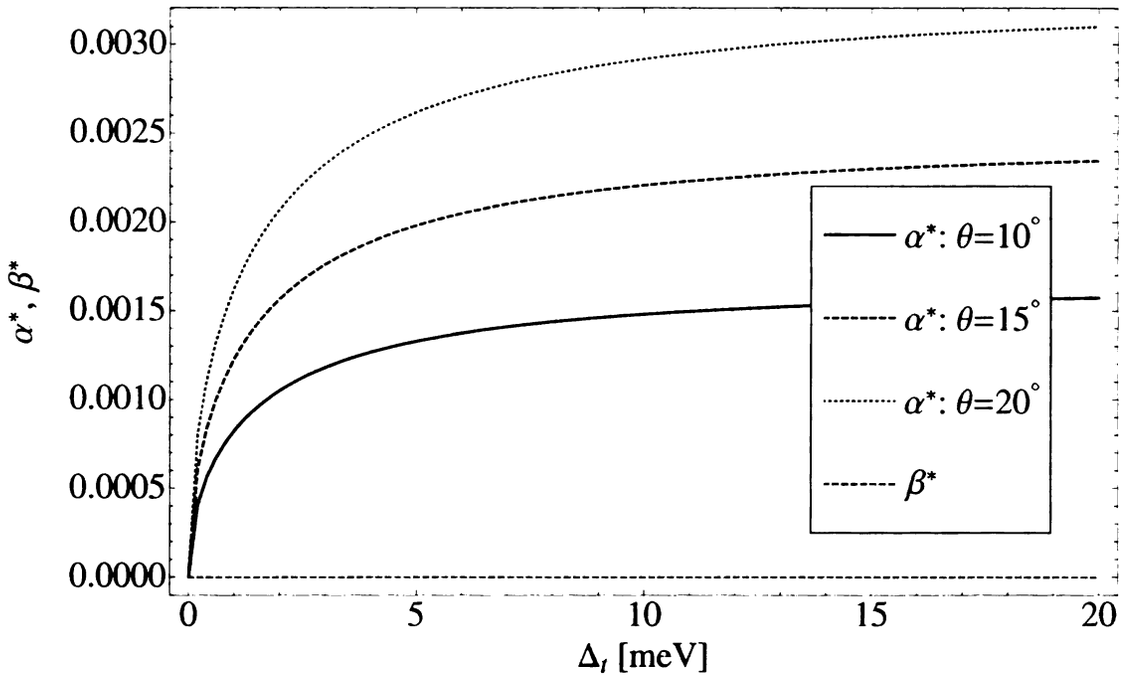

Figure 4.11: Variational parameters α^* and β^* in the harmonic oscillator approximation including the memory effect for $\epsilon = 0.1$ and red detuning. The results for blue detuning (not presented here) are qualitatively the same.

From the values for α^* we can deduce the spread of the gaussian as

$$\sigma_x = \sqrt{\frac{1}{2\alpha^*}}, \tag{4.33}$$

which is depicted in Fig. (4.12).

Compared to the case where we neglected the memory term in the previous section by replacing it with a δ-function (see Fig. (4.8)), we recognize that it is well justified to neglect the nonlocal character of the potential. The spatial spread of the Gaussian wavepacket is effectively not affected by the presence of the non-local memory term $m(\mathbf{x})$, since the additional spread caused by the non-local character of the actual trionic potential is negligibly small compared the spread that we obtained in the approximative local limit of the potential.

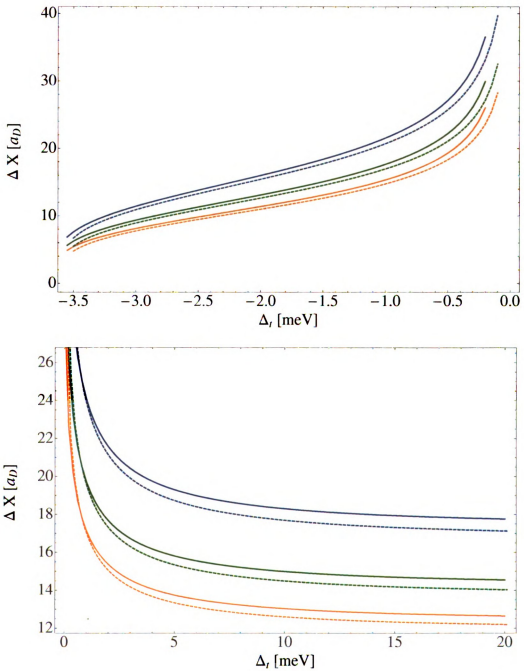

Figure 4.12: σ_x of the gaussian wave packet in the $\hat{x}$-direction as a function of the detuning $\triangle_t$ for $\epsilon = 0.1$ and $CdTe$. The results where the nonlocal effect of the potential was included are shown as solid lines: $\theta = 10°$ (blue), $\theta = 15°$ (green), $\theta = 20°$ (orange). The corresponding values of the local limit where the non-locality was neglected are depicted as dashed lines. The non-locality causes a slight additional spread of the electron wavepacket.

Chapter 5

Effective temperature for the electrons

Up to now, we have focused on a proper description of the coupling of the conduction electrons to laser light, tuned close to the trion resonance. However, we should not forget that these electrons are embedded in a semiconductor host environment at the lattice temperature T_l, which also interacts with the conduction electrons. In this section, we will explore the electron interaction with phonons. More general, we will investigate the electron heating and cooling processes and calculate the strength of the different mechanisms. Due to the host environment, the electrons can emit phonons, whereby the electron energy is lowered; therefore, the emission of phonons serves as a natural cooling mechanism. In other words, the electrons are linked to a macroscopic refrigerator, the semiconductor lattice, and energy is exchanged in terms of its vibrational quanta, the phonons. Here, we will only consider acoustical phonons: Optical phonons will not contribute, because the exchanged energies we consider are always smaller than the characteristic optical phonon energy: In $GaAs$ for example the energy of one optical phonon amounts to $\hbar\omega_{LO} = 36\,meV$. Meanwhile, the electrons also experience effects that tend to increase the electron kinetic energy and

thus heat them up. In addition to cooling, we also need to consider heating effects: While phonons can not only be emitted but also absorbed, and in doing so cause a heating of the electron, such processes need to be activated thermally so that this effect goes to zero as the lattice is cooled down towards a low temperature regime. The primary heating effect that we need to take into account is then the intrinsic omnipresent heating mechanism of any optical potential, namely the spontaneous emission of photons. Once, the electron has entered the excited trion state after the absorption of a laser photon it is subject to spontaneous emission of photons with a rate that is governed by the trion radiative lifetime τ_t and the excitation probability of the trion state. The latter is controllable experimentally by the ratio of the Rabi frequency for the electron-trion transition to the detuning from the trion resonance. The essential goal of this section is a first-principle derivation of a time-dependent equation for the electron energy. Based on this equation, we will find the equilibrium solution at which the heating and cooling mechanisms balance each other. This equilibrium solution will culminate in the definition of an effective electron temperature T^*, which is necessarily higher than the lattice temperature. We will have to compare the associated effective thermal energy $k_B T^*$ to the depth of the optical potential, seen by the electrons, to determine its ability to effectively trap electrons.

5.1 Acoustic phonon scattering rate

In a first approach to the problem, we will calculate the emission rate of acoustic phonons at $T_l = 0$. In this way, we will get a feeling for the typical time scales of intrasubband relaxation processes, comparing our results to values obtained in previous theoretical investigations [51]. Although these results are related to a different energy regime for the electrons and therefore not of interest for the further studies ,

a good agreement will serve as a direct check of the validity of our approach.

We restrict ourselves to the intrasubband contributions arising from the emission of acoustical phonons in order to estimate the relaxation time at which a warm carrier cools down to thermal equilibrium. Usually, it is a very good approximation to assume that intrasubband relaxations are faster than intersubband ones [51]. In the low temperature regime the absorption of phonons can be neglected. Moreover, optical-phonon scattering is negligible at low temperatures ($\lesssim 40\,K$) [50]. Indeed, acoustic phonon scattering is the only way a carrier can relax down to the ground subband edge when its initial excess energy is smaller than the energy of an optical phonon $\hbar\omega_{LO}$. To compute the scattering rate Γ_{ph} of an eigenstate $|\psi_i\rangle$ limited by transitions to all possible final states $|\psi_f\rangle$ induced by the electron-phonon interaction potential $\mathcal{H}_{e-ph}$, we exploit Fermi's Golden Rule

$$\Gamma_{ph} = \frac{2\pi}{\hbar} \sum_{f,\vec{q}} \left| \langle \psi_f | \, \mathcal{H}_{e-ph} \, | \psi_i \rangle \right|^2 \delta \left(\epsilon_f + \hbar\omega_{\vec{q}} - \epsilon_i \right), \tag{5.1}$$

where $\hbar\omega_{\vec{q}}$ is the energy of the emitted phonon and $\epsilon_{i,f}$ give the energies of the initial and final electron's states respectively. The computation of the scattering matrix element requires the knowledge of ψ_i and ψ_f. As usual, we apply the envelope function formalism and restrict our considerations to a parabolic description of the host's bands. This means that for a finite well-width in the $\hat{z}$-direction we write the envelope conduction states in the form

$$\psi_i(\mathbf{r}) = \frac{1}{\sqrt{A}} \exp(i\mathbf{kr}) \, \chi_i(z) \tag{5.2}$$

with the corresponding energy

$$\epsilon_i(\mathbf{k}) = E_i + \frac{\hbar^2 \mathbf{k}^2}{2m_e^*} \tag{5.3}$$

where A is the sample area. Furthermore, $\mathbf{r} = (x, y)$ and $\mathbf{k} = (k_x, k_y)$ give the in-plane components of the electron position vector and wave-vector, respectively, E_i the confinement energy of the i-th subband and $\chi_i(z)$ the associated envelope function. Analogue expressions hold for the final states ψ_f. For simplicity, we assume a very thin quantum well with one relevant mode in the growth direction. We do not take into account the dependence of the envelope function $\chi_{i/f}(z)$ on the energy level and take the form

$$\chi_{i/f}(z) = \frac{1}{\sqrt{L_z}} \tag{5.4}$$

for $0 \leq z \leq L_z$ and zero elsewhere; with L_z being the well width. This approximation is valid for very thin wells that support only a single bound state, so that intersubband relaxations are suppressed.

The main scattering mechanism for electrons interacting with acoustic phonons is provided by the deformation potential interaction, and the assumed electron-phonon interaction Hamiltonian is given by

$$\mathcal{H}_{e-ph} = \sum_{\vec{q}} \left[\alpha(q)\, e^{-i\vec{q}\vec{r}} b^{\dagger}_{\vec{q}} + h.c. \right] \tag{5.5}$$

where $b^{\dagger}_{\vec{q}}$ is the creation operator for a phonon in the mode $\vec{q}$ and

$$|\alpha(q)|^2 = \frac{D^2}{2\rho c_s^2 V} \hbar\omega(q) = \frac{D^2}{2\rho c_s^2 V} \hbar c_s q = \frac{c_0}{V} \hbar c_s q \tag{5.6}$$

is the strength of the electron-acoustical-phonon interaction in the deformation potential approximation. For convenience, we buried most of the constants into the definition of the quantity c_0. The parameters that enter are the deformation potential for electrons D, the density of the host material ρ and the longitudinal speed of sound c_s. We neglect any possible change of the phonon spectra arising from the existence of the heterostructure and thus take isotropic acoustic branches with sound

velocity c_s.

To apply Fermi's Golden Rule, we will first evaluate the transition matrix element for the emission of an acoustic phonon with wavevector $\mathbf{q}$ and we obtain

$$\begin{aligned} \left|\left\langle \psi_f \right| \mathcal{H}_{e-ph} \left|\psi_i\right\rangle\right|^2 &= \left|\alpha\left(q\right)\right|^2 \left|\Xi\left(q_z\right)\right|^2 \delta_{\mathbf{k}_i,\mathbf{k}_f+\mathbf{q}} && (5.7) \\ &= \frac{c_0}{V}\hbar\omega_0 \left|\Xi\left(q_z\right)\right|^2 && (5.8) \end{aligned}$$

where we introduced the function

$$\Xi\left(q_z\right) = \int dz\, e^{-iq_z z} \chi_i\left(z\right) \chi_f^*\left(z\right) = \int dz\, e^{-iq_z z} \left|\chi_{i/f}\left(z\right)\right|^2 \tag{5.9}$$

and the phonons frequency ω_0 that already incorporates the in-plane momentum conservation condition

$$\omega_0 = c_s \sqrt{q_z^2 + \left|\mathbf{k}_i - \mathbf{k}_f\right|^2}. \tag{5.10}$$

Since the system is translationally invariant in the plane, the difference in the electron's in-plane wavevectors has to equal the in-plane component $\mathbf{q}$ of the phonons wavevector $\vec{q} = (\mathbf{q}, q_z)$.

For our particular choice of $\chi_{i/f}\left(z\right)$ being equally distributed on the interval $0 \leq z \leq L_z$ and zero elsewhere, we obtain

$$\left|\Xi\left(q_z\right)\right|^2 = 4\frac{\sin^2\left(q_z L_z/2\right)}{\left(q_z L_z\right)^2} \tag{5.11}$$

Now, that the matrix element is evaluated, we have the necessary ingredients to turn back to our original goal, the calculation of the actual scattering rate Γ_{ph} due to the inelastic interaction with acoustical phonons. We obtain

$$\Gamma_{ph} = \frac{c_0}{\left(2\pi\right)^2} \int_{-\infty}^{\infty} dq_z \left|\Xi\left(q_z\right)\right|^2 \int_0^{2\pi} d\varphi \int_0^{\infty} dk_f\, k_f\, \omega_0 \delta\left(\epsilon_i - \epsilon_f - \hbar\omega_0\right) \tag{5.12}$$

To explore the non-zero temperature limit, this result would have to be multiplied by

$$(1+\bar{n}) = 1 + \frac{1}{e^{\beta\hbar\omega_0} - 1}. \tag{5.13}$$

where $\bar{n}$ is the Bose occupation function that in this context can be viewed as a temperature-dependent stimulation factor.

We have solved the remaining integrals for the computation of Γ_{ph} numerically. In the case of $GaAs$, the calculations have been performed with the material parameters $D = 8.6\,eV$, $\rho = 5.3\,g/cm^3$, and $c_s = 3700\,m/s$ [51]. Here, we give the results for the inverse intrasubband scattering rate $\tau_{1\to 1}$ depending on the well-width L_z that can be directly compared to the results given in Fig. (6) of ref. [51], where the initial electron's energy was chosen to be about $\sim 0.25\,eV$. Our results are about a factor of 2 off from the ones stated in [51], where a more sophisticated approach for the electron's wavefunction in the $\hat{z}$-direction was used. For our purposes the simplified form catches the physics correctly and works fine for very thin well-widths, i.e. the quasi two-dimensional limit. In this limit, the intrasubband relaxation rate due to acoustic phonons $\tau_{1\to 1}$ is very fast, in the range of picoseconds. However, this refers specifically to the chosen electron's energy which is different from the energy range we are to consider. Nevertheless, in this way we have confirmed the validity of our approach.

5.2 Equilibrium temperature

In the next step, we will calculate one of the most important quantities in our analysis: the effective temperature of the conduction electrons T^*. This effective temperature deviates from the temperature of the host environment T_l, because spontaneous emission events render the optical potential dissipative, resulting in an effective heating

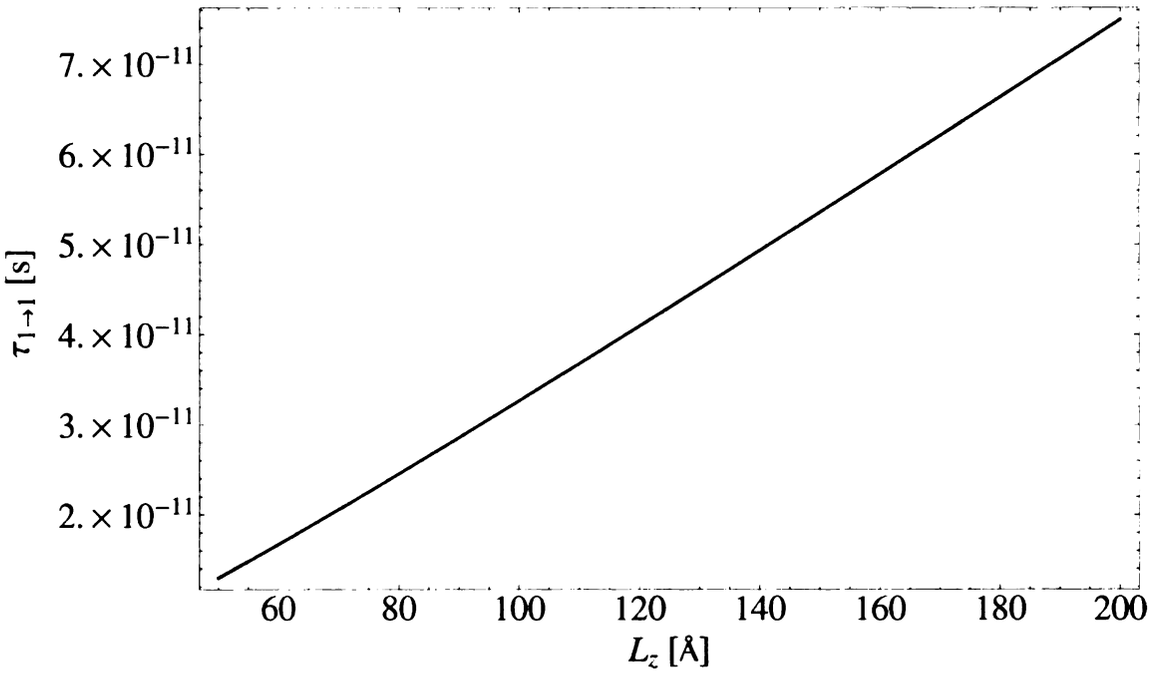

Figure 5.1: Acoustical phonon scattering at a lattice temperature $T_l = 0$: Dependence of the intrasubband relaxation time $\tau_{1\rightarrow 1}$ on the quantum-well thickness L_z.

of the electron. The rate at which the electron experiences the spontaneous scattering events is the effective spontaneous emission rate Γ_{se}, which we estimate as the product of the time-averaged probability to be in the excited trion state times the radiative decay rate, i.e. the natural line-width, of the trion level: $\Gamma_{se} = \langle P_e \rangle \Gamma_t = \epsilon \Gamma_t$; ϵ is the saturation parameter. For our purposes, the associated energy gain rate or heating rate R_{heat}, measured in energy per unit time, is even more important than the scattering rate Γ_{se}, because it carries the actual information about the strength of this mechanism to push the electron effective temperature away from the temperature of the refrigerator T_l. We approximate the corresponding energy gain rate as

$$R_{heat} = \langle P_e \rangle \Gamma_t \langle E_R \rangle = \epsilon \Gamma_t \langle E_R \rangle \tag{5.14}$$

since, on average, every single spontaneous scattering heats the electron up by the average in-plane recoil energy $\langle E_R \rangle$.

Experiments with Bose-Einstein condensates that are loaded into an optical lattice essentially take place in vacuum. The atoms are cooled first, before the lattice is ramped up. Thus, these systems lack a natural cooling mechanism and the heating process due to spontaneous emission of photons sets a boundary on the time-scale on which these experiments can be performed successfully. Once, the atoms have been cooled down to very low temperatures and the interaction with the photons is switched on, the recoil kicks heat the atoms up, which eventually knocks the atoms out of the traps. Therefore very small values for the saturation parameter ϵ have to be chosen in order to control the heating rate. In general, when working with laser-cooled atoms the cooling mechanism stems from the same system as the optical potential, namely the laser, whereas in our system the cooling mechanism is completely independent of the laser-induced potential.

In contrast to these limitations on the optical potentials for atoms, the system we study is equipped with the phonon bath which competes with the heating process described above. In equilibrium, the heating and cooling mechanisms cancel each other. We will derive the associated effective temperature of the electron at this equilibrium point.

As a side note in advance of the later discussion we mention that phonons couple only very weakly to the spin-state of the electrons, so that spin-flip processes due to the phonon bath occur on rather long timescales. This fact has already been used to engineer quantum information systems based for example on quantum dot platforms.

The interaction with the acoustic phonons is essentially a scattering problem. Here, we discuss the validity of Fermi's Golden rule in the specific problem at hand. We will calculate not only a scattering rate, but also energy loss and gain rates because of the emission and absorption of acoustical phonons.

The Hamiltonian $\mathcal{H}$ for the problem of one single electron interacting with a bath of acoustical phonons can be written as

$$\mathcal{H} = \mathcal{H}_0 + \mathcal{H}_{e-ph} \tag{5.15}$$

$$\mathcal{H}_0 = \frac{\hbar^2 \hat{k}^2}{2m_e^*} + V_c + \sum_{\vec{q}} \hbar c_s \left|\vec{q}\right| b_{\vec{q}}^\dagger b_{\vec{q}} \tag{5.16}$$

$$\mathcal{H}_{e-ph} = \sum_{\vec{q}} \alpha\left(q\right) \left[e^{-i\vec{q}\vec{R}} b_{\vec{q}}^\dagger + e^{i\vec{q}\vec{R}} b_{\vec{q}}\right] \tag{5.17}$$

where the unperturbed system contains the electron's kinetic energy in the QW plane, the confinement potential V_c of the QW along the $\hat{z}$-direction and the energy of the phonon bath. Again, $\mathcal{H}_{e-ph}$ is the interaction of the electron with the phonon bath in the deformation potential approximation. Since we are only considering intrasubband scattering, the Hilbert space to describe the problem perpendicular to the QW plane is truncated to one mode only. Subsequently, the identity operator for the electron Hilbert space can be represented as $\mathbf{1} = \left|\chi\right\rangle \left\langle\chi\right| \otimes \mathbf{1}_{\shortparallel}$, where we have decomposed the problem in the in-plane and the out-of-plane part; $\left|\chi\right\rangle$ describes the wavefunction in the $\hat{z}$-direction. After this simplification, we can make the replacement

$$e^{\pm i\vec{q}\vec{R}} \rightarrow \left\langle\chi\right| e^{\pm iq_z z} \left|\chi\right\rangle e^{\pm i\mathbf{qR}} = \Xi_{\pm}\left(q_z\right) e^{\pm i\mathbf{qR}} \tag{5.18}$$

where we introduced the Fourier transform of the squared electron's wavefunction in the $\hat{z}$-direction

$$\Xi_{\pm}\left(q_z\right) = \left\langle\chi\right| e^{\pm iq_z z} \left|\chi\right\rangle = \int dz\, e^{\pm iq_z z} \left|\chi\left(z\right)\right|^2 \tag{5.19}$$

so that in the truncated problem which only allows for one mode in the quantized $\hat{z}$-direction the electron phonon interaction simplifies to

$$\mathcal{H}_{e-ph} = \sum_{\vec{q}} \alpha\left(q\right) \left[\Xi_{-}\left(q_z\right) e^{-i\mathbf{qR}} b_{\vec{q}}^\dagger + \Xi_{+}\left(q_z\right) e^{i\mathbf{qR}} b_{\vec{q}}\right] \tag{5.20}$$

In this way the dependence on the $\hat{z}$-direction is governed as a matrix element in the interaction Hamiltonian which essentially goes to zero for large values of q_z.

Focussing initially on the emission of a single phonon, a convenient set of basis states to tackle the problem is

$$|i\rangle = |\psi_i\rangle \otimes |T\rangle \tag{5.21}$$

$$|\mathbf{q}, +\rangle = \frac{1}{\sqrt{\bar{n}_q + 1}} \left[\hat{T}(-\mathbf{q}) |\psi_i\rangle \otimes b_{\bar{q}}^{\dagger} |T\rangle\right] \tag{5.22}$$

$$|\mathbf{q}, -\rangle = \frac{1}{\sqrt{\bar{n}_q}} \left[\hat{T}(+\mathbf{q}) |\psi_i\rangle \otimes b_{\bar{q}} |T\rangle\right] \tag{5.23}$$

which are tensor products of the electron's state and the state of the bath $|T\rangle$. We assume that the state $|i\rangle$ as well as the states $|\mathbf{q}, \pm\rangle$ are eigenstates of the unperturbed problem with the corresponding eigenvalues

$$\mathcal{H}_0 |i\rangle = E_0 |i\rangle, \qquad \mathcal{H}_0 |\mathbf{q}, \pm\rangle = E_{\pm} |\mathbf{q}, \pm\rangle \tag{5.24}$$

The state $|i\rangle$ describes the initial state of the system. The electron is assumed to be initially in the state

$$|\psi_i\rangle = |\mathbf{k}_i\rangle \otimes |\chi\rangle \tag{5.25}$$

which describes an electron free to move as a plane wave with wavevector $\mathbf{k}_i$ in the QW and confined in the mode $|\chi\rangle$ of the quantized $\hat{z}$-direction. To adequately describe the physics of phonon emission and absorption we have introduced the in-plane momentum-shift operator $\hat{T}(\pm\mathbf{q})$ given by

$$\hat{T}(\pm\mathbf{q}) = e^{\pm i\mathbf{q}\mathbf{R}} \tag{5.26}$$

The phonon bath is initially at thermal equilibrium in the state $|T\rangle$. Thus, we

only require that it obeys the Bose-Einstein distribution

$$\langle T| b_{\vec{q}}^{\dagger} b_{\vec{q}'} |T\rangle = \bar{n}_q \delta_{\vec{q},\vec{q}'} \tag{5.27}$$

which explains the chosen normalization for the states $|\mathbf{q}, \pm\rangle$, assuming $|T\rangle$ to be normalized. This assumption basically states that the phonon modes are uncorrelated. The given basis is sufficient to describe single phonon emission/absorption processes. The system starts out in the state $|i\rangle$ and is then found to be in the state $|\mathbf{q}, +\rangle$, if an acoustic phonon of wavevector $\mathbf{q}$ has been emitted and in the state $|\mathbf{q}, -\rangle$, if an acoustic phonon of wavevector $\mathbf{q}$ has been absorbed by the electron. The momentum shift operator automatically takes care of the inplane momentum conservation.

The orthogonalization conditions read

$$\langle \mathbf{q}, +|\mathbf{q}', -\rangle = \langle \mathbf{q}, \pm|i\rangle = 0 \tag{5.28}$$

$$\langle \mathbf{q}, \pm|\mathbf{q}', \pm\rangle = \delta_{\mathbf{q},\mathbf{q}'} \tag{5.29}$$

In its most general form the state of the system $|\Psi(t)\rangle$ can be written as

$$|\Psi(t)\rangle = c_i(t)|i\rangle + \sum_{\vec{q}} \left[c_+(\vec{q}, t)|\mathbf{q}, +\rangle + c_-(\vec{q}, t)|\mathbf{q}, -\rangle\right] \tag{5.30}$$

where we introduced the time-dependent amplitudes $c_i(t)$ and $c_\pm(\vec{q}, t)$. Normalization of the state $|\Psi(t)\rangle$ requires

$$|c_i(t)|^2 + \sum_{\mathbf{q}} \left[|c_+(\vec{q}, t)|^2 + |c_-(\vec{q}, t)|^2\right] = 1 \tag{5.31}$$

The probability $P_{i\to i}(t)$ to find the system in state $|i\rangle$ at time t is

$$P_{i\to i}(t) = |c_i(\vec{q},t)|^2 = 1 - \sum_{\mathbf{q}} \left[|c_+(\vec{q},t)|^2 + |c_-(\vec{q},t)|^2 \right] \tag{5.32}$$

which is nothing but the condition of the conservation of probability. Hence we see that to calculate the transition probabilities to second order, it is only necessary to compute the corresponding amplitudes to first order.

Later on, we will refer to the completeness relation for the whole system, i.e. the combination of the electron's Hilbert-space and the bath,

$$\sum_{\mathbf{k}} |\mathbf{k}\rangle\langle\mathbf{k}| \otimes |\chi\rangle\langle\chi| \otimes I_{bath} = \mathbf{1} \tag{5.33}$$

The time dependence of the state's system can be buried into the propagator $U(t)$ defined as

$$U(t) = e^{-\frac{i}{\hbar}\mathcal{H}t} \tag{5.34}$$

A similar definition holds for the free propagator $U_0(t)$, where only the Hamiltonian of the unperturbed system $\mathcal{H}_0$ enters. Expanding the full propagator $U(t)$ to first order perturbation theory gives the result

$$U(t) = U_0(t) - \frac{i}{\hbar}\int_0^t dt_1\, U_0(t-t_1)\, V(t_1)\, U_0(t_1) \tag{5.35}$$

which illustratively states that in first order the system can evolve in the time interval $[0,t]$ with either no interaction or one interaction taking place somewhere in this interval. Before and after the interaction, the system evolves essentially as it would in the unperturbed system. In first order perturbation theory, the time-dependent

amplitudes $c_{\pm}(\mathbf{q},t)$ to find the system in the state $|\mathbf{q},\pm\rangle$ are given by

$$c_{\pm}(\vec{q},t) = \langle \mathbf{q},\pm|\Psi(t)\rangle = -\frac{i}{\hbar}\int_0^t dt_1\ \langle \mathbf{q},\pm|\,U_0(t-t_1)\,V(t_1)\,U_0(t_1)\,|i\rangle \qquad (5.36)$$

Now, the interaction term $V(t_1)$ couples the initial state $|i\rangle$ to the states $|\mathbf{q},\pm\rangle$, where one phonon has been emitted or absorbed. Within a first order theory, as proposed here, this is everything that can happen. Multi-phonon processes have been neglected right from the beginning. For the amplitudes $c_{\pm}(\vec{q},t)$ we obtain

$$c_{+}(\vec{q},t) = -\frac{i}{\hbar}\alpha(q)\sqrt{\bar{n}_q+1}\Xi_{-}(q_z)\,e^{-\frac{i}{\hbar}E_{+}t}\int_0^t dt_1\,e^{-\frac{i}{\hbar}(E_i-E_{+})t_1} \qquad (5.37)$$

$$c_{-}(\vec{q},t) = -\frac{i}{\hbar}\alpha(q)\sqrt{\bar{n}_q}\Xi_{+}(q_z)\,e^{-\frac{i}{\hbar}E_{-}t}\int_0^t dt_1\,e^{-\frac{i}{\hbar}(E_i-E_{-})t_1} \qquad (5.38)$$

After the integration in time, we find that the probabilities $|c_{\pm}(\vec{q},t)|^2$ to find the system in the state $|\mathbf{q},+\rangle$ or $|\mathbf{q},-\rangle$ respectively are

$$|c_{+}(\vec{q},t)|^2 = |\alpha(q)|^2\,|\Xi_{-}(q_z)|^2\,(\bar{n}_q+1)\,\frac{4\sin^2\left(\frac{E_i-E_{+}}{\hbar}\frac{t}{2}\right)}{(E_i-E_{+})^2} \qquad (5.39)$$

$$|c_{-}(\vec{q},t)|^2 = |\alpha(q)|^2\,|\Xi_{+}(q_z)|^2\,\bar{n}_q\frac{4\sin^2\left(\frac{E_i-E_{-}}{\hbar}\frac{t}{2}\right)}{(E_i-E_{-})^2} \qquad (5.40)$$

At this stage, we can already recognize that the absorption of acoustical phonons becomes negligible in the limit $T\to 0$, while there can still be spontaneous phonon emission. Only the stimulated processes that are proportional to $\bar{n}_{\mathbf{q}}$ vanish in the low temperature regime. The next step is well known from the general derivation of Fermi's Golden Rule. It is a very crucial approximation that is based on the phenomenon of a separation of time-scales. We are confronted with the function

$$\delta^{(t)}(E_f-E_i) = \frac{1}{\pi}\frac{\sin\left((E_f-E_i)\,t/2\hbar\right)}{(E_f-E_i)} \qquad (5.41)$$

which tends to the delta function $\delta\left(E_f - E_i\right)$ for long times $t \to \infty$. As a matter of fact, it is a diffraction pattern, whose maximal amplitude lies at $t/2\pi\hbar$ for $E_f - E_i = 0$. Its width is on the order of $4\pi\hbar/t$ and its integral yields 1. Thus, it is an approximate delta function that expresses the conservation of energy with an uncertainty $\hbar/t$ because of the finite duration of the interaction [52]. In the Markovian approximation, the scattering events are independent of each other, the system is reset after each interaction: There is no memory. The separation of times scales appears as taking the limit $t \to \infty$, whilst t has to be sufficiently small to justify the perturbative treatment of V, as we allowed for single scattering events only. In this limit, the transition probabilities become

$$|c_+(\vec{q},t)|^2 = \frac{2\pi}{\hbar}|\alpha(q)|^2|\Xi_-(q_z)|^2\left(\bar{n}_q+1\right)\delta\left(E_i-E_+\right)t \tag{5.42}$$

$$|c_-(\vec{q},t)|^2 = \frac{2\pi}{\hbar}|\alpha(q)|^2|\Xi_+(q_z)|^2\bar{n}_q\delta\left(E_i-E_-\right)t \tag{5.43}$$

from which we can readily deduce that the probability to remain in the initial state $|i\rangle$ decays at the rate

$$\begin{aligned}\Gamma_{ph} = \frac{2\pi}{\hbar}\sum_{\vec{q}}|\alpha(q)|^2\Big[&|\Xi_-(q_z)|^2\left(\bar{n}_q+1\right)\delta\left(E_i-E_+\right)\\ &+|\Xi_+(q_z)|^2\bar{n}_q\delta\left(E_i-E_-\right)\Big]\end{aligned} \tag{5.44}$$

The first term accounts for phonon emission, while the second term respects phonon absorption. However, this is not the end of the story. We will make use of the same framework to derive the energy gain and loss rates due to phonon emission and absorption. The strength of these mechanisms as compared to the photon recoil heating R_{heat} will then decide about the electron's equilibrium energy k_BT^*.

In general, the time-dependent expectation value of the electron's energy $\langle E(t)\rangle$,

which is assumed to be purely kinetic, is

$$\langle E(t)\rangle = \sum_{\mathbf{k}} \frac{\hbar^2 k^2}{2m_e^*} \langle \Psi(t)| \left[|\mathbf{k}\rangle\langle\mathbf{k}| \otimes |\chi\rangle\langle\chi| \otimes I_{bath} \right] |\Psi(t)\rangle \tag{5.45}$$

where we inserted the completeness relation (5.33). In the next step, we express the state $|\Psi(t)\rangle$ according to the general expression (5.30) and find that the deviation of the electron's energy from its initial value is given by

$$\begin{aligned} \langle E(t)\rangle - \frac{\hbar^2 k_i^2}{2m_e^*} &= \sum_{\mathbf{q}} \left[\frac{\hbar^2 (\mathbf{k}_i - \mathbf{q})^2}{2m_e^*} - \frac{\hbar^2 k_i^2}{2m_e^*} \right] |c_+(\vec{q},t)|^2 \\ &\quad + \sum_{\mathbf{q}} \left[\frac{\hbar^2 (\mathbf{k}_i + \mathbf{q})^2}{2m_e^*} - \frac{\hbar^2 k_i^2}{2m_e^*} \right] |c_-(\vec{q},t)|^2 \end{aligned} \tag{5.46}$$

The difference in the kinetic energies is exactly the energy $\hbar\omega_q$ of the emitted or absorbed phonon. We define the change in the electron's energy per unit time $R_{ph}(E_i)$ according to

$$\langle E(t)\rangle - \frac{\hbar^2 k_i^2}{2m_e^*} = R_{ph}(E_i)\, t \tag{5.47}$$

When we plug in our results for the transition probabilities and use the energy conservation, we find a very intuitive and simple result

$$\begin{aligned} R_{ph}(E_i) &= -\frac{2\pi}{\hbar} \sum_{\vec{q}} |\alpha(q)|^2 |\Xi_-(q_z)|^2 \hbar\omega_q (\bar{n}_q + 1)\, \delta(E_i - E_f - \hbar\omega_q) \\ &\quad + \frac{2\pi}{\hbar} \sum_{\vec{q}} |\alpha(q)|^2 |\Xi_+(q_z)|^2 \hbar\omega_q \bar{n}_q \delta(E_i - E_f + \hbar\omega_q) \end{aligned} \tag{5.48}$$

The energy loss and gain rates due to acoustical-phonon emission and absorption respectively are obtained by weighting the scattering rates with the energy of the corresponding phonon. Thus, we just have to multiply by $\hbar\omega_q$ before the summations are performed in (5.44).

Now that we have understood the phonon mechanism and its influence on the

electron energy we will find the equilibrium point for the electron effective temperature T^*. To do so, we also have to take into account the recoil heating. Otherwise, without this heating process the result would be trivial: $T^* = T_l$. A thermalized electron would automatically take on the temperature of its lattice environment. We can set up an equation for the electron's energy evolution in time, which respects both the contribution from the recoil heating processes as well as the phonon mechanisms. The electron's energy evolves in time according to

$$\frac{d\langle E(t)\rangle}{dt} = R_{ph}(E) + R_{heat} \tag{5.49}$$

In contrast to $R_{ph}(E)$, the heating rate R_{heat} depends neither on the lattice temperature T_l nor on the the electron's energy. Still, it can be tuned by changing the value of the saturation parameter ϵ. In equilibrium, the time-derivative vanishes and we find $E^* = k_B T^*$ as the point where $R_{ph}(E)$ and R_{heat} cancel each other, i.e. the equilibrium condition reads

$$R_{ph}(E^*) + R_{heat} = 0 \tag{5.50}$$

We specify the results of this procedure in Fig. (5.2) and (5.3) for $GaAs$ and $CdTe$, respectively. The lattice temperature was chosen to be $T_l = 300\,mK$. In this temperature regime the absorption of phonons is negligible and the dominant heating effect is clearly the spontaneous emission of photons. The trion radiative lifetime was taken to be $\tau_t = 100\,ps$ and the corresponding heating rate R_{heat} is plotted for the saturation parameter values $\epsilon = 0.1$, $\epsilon = 0.05$ and $\epsilon = 0.01$, respectively. Of course, a lower value for ϵ results in smaller effective temperatures for the electrons, since the heating rate R_{heat} is linear in the parameter ϵ. We find lower effective temperatures in $CdTe$ than in $GaAs$, because the phonon cooling mechanism shows the same effec-

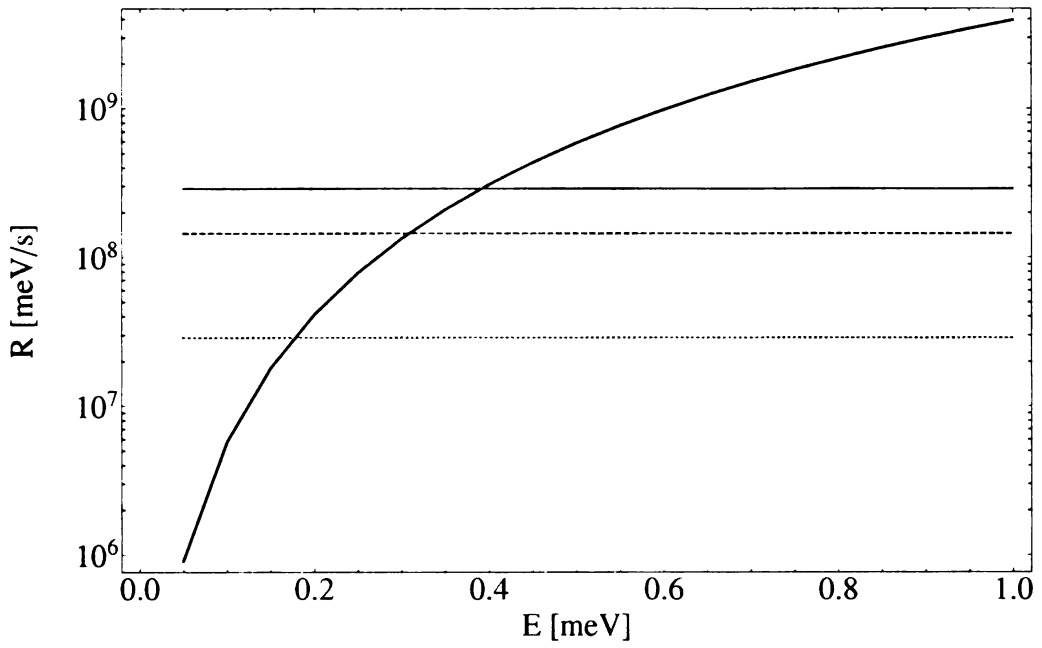

Figure 5.2: *GaAs*: The phonon cooling rate $R_{ph}(E)$ is shown in blue. The heating rate R_{heat} is presented in orange for different values of the saturation parameter ϵ: $\epsilon = 0.1$ (solid line), $\epsilon = 0.05$ (dashed line), $\epsilon = 0.01$ (dotted line). The thermal equilibrium energies can be found where the cooling rate intersects with the heating rate.

tiveness, while the recoil energy $\langle E_R \rangle$ is noticeably smaller for $CdTe$. For saturation parameter values $\epsilon = 0.01 - 0.1$, we obtain equilibrium temperatures $k_B T^*$ in the range $0.2 - 0.4meV$ and $0.1 - 0.3meV$ for $GaAs$ and $CdTe$ respectively. For red detuning, this energy range is of the order of or even bigger than the potential depth V_0, even for laser powers that allow for the saturation regime. For blue detuning, however, we find that the potential depth can exceed $k_B T^*$ considerably. In Tab. (4.2) we have specified for example the potential depth for $\epsilon = 0.05$. Compared to the corresponding electron equilibrium temperatures, the potential depth amounts to $V_0 \approx 3k_B T^*$ and $V_0 \approx 8k_B T^*$ for $GaAs$ and $CdTe$ respectively. Thus, by tuning the laser light above the trion resonance one can reach values for the potential depth V_0 that are considerably larger than the effective thermal energies of the electrons in the system.

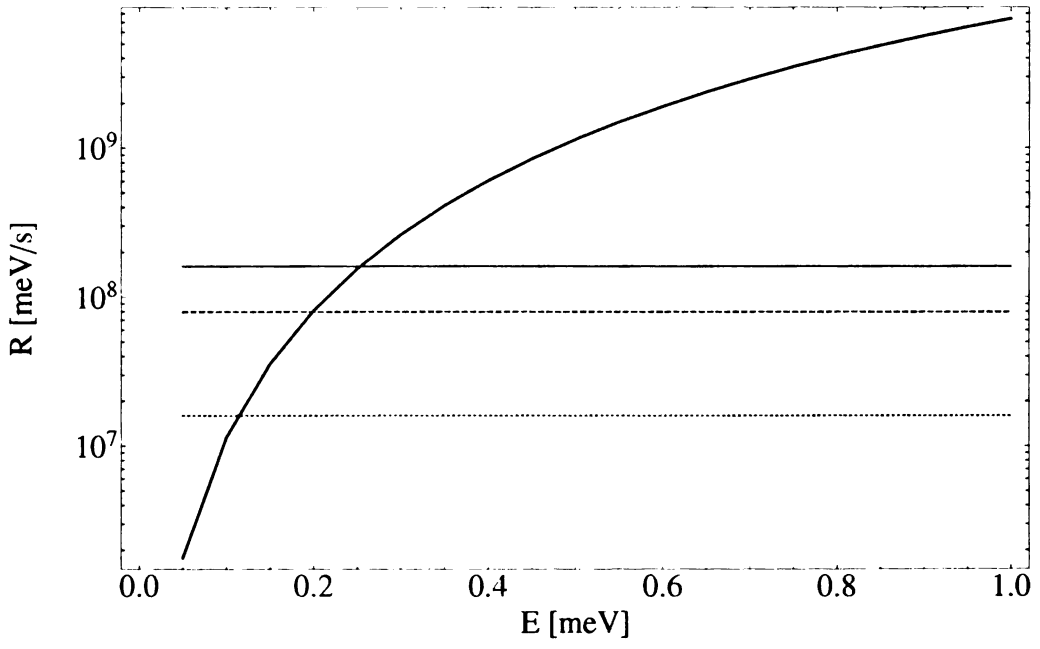

Figure 5.3: *CdTe*: The phonon cooling rate $R_{ph}(E)$ is shown in blue. The heating rate R_{heat} is presented in orange for different values of the saturation parameter ϵ: $\epsilon = 0.1$ (solid line), $\epsilon = 0.05$ (dashed line), $\epsilon = 0.01$ (dotted line). The thermal equilibrium energies can be found where the cooling rate intersects with the heating rate.

Chapter 6

Optical lattices for carriers in semiconductor quantum wells

For the sake of simplicity, so far we have focused on the case of two counter-propagating laser beams, which produces an intensity pattern in the form of periodic stripes along the QW. In this chapter we will extend this model to an intriguing novel phenomenon, namely a two-dimensional optical lattice for the conduction electrons in the QW: periodic arrays of microtraps in one than more dimension are generated by a set of standing wave laser fields. A periodic potential in two dimensions can be easily formed by overlapping two optical standing waves along different, most commonly orthogonal, directions. To eliminate interference terms between the pairs of beams in the different directions, one can either choose orthogonal polarization vectors for the two laser fields [40] or slightly different optical frequencies [53]. In both cases, the resulting optical potential in the center of the trap is simply the sum of a purely sinusoidal potential in both directions. Superimposing two orthogonal standing waves in this way in combination with the confinement in the $\hat{z}$-direction inside the QW results in a two-dimensional array of artificial quantum dots for the electrons.

This step essentially bridges the gap from the concept of a periodic optical po-

tential for electrons to the idea of an optical lattice for electrons. The concept of an lattice as a regular arrangement in space underlines a shift away from a picture of an disordered electron gas towards a possible new physical paradigm of an electron gas whose density is spatially modulated and whose properties can be strongly determined by the periodic optical potential in a time-dependent way. To be precise, we will specify our calculations for a two-dimensional square lattice with lattice periodicity $a = \lambda_{\parallel}/2$; $\lambda_{\parallel}$ is the in-plane wavelength of the laser.

Thanks to recently developed quantum optical tools, a wide range of many body Hamiltonians have been realized with cold atoms in optical lattices. In particular, a whole toolbox to engineer various Hubbard type lattice models for 1D, 2D and 3D Bose- and Fermi systems has been provided whose properties can be controlled by varying external field parameters [54]. The original idea suggesting the possibility of studying non-trivial many-body systems with cold atoms in optical lattices was developed by Jaksch *et al.* [55]. The starting point in their analysis was the so-called Bose-Hubbard model. One of the key parameters that enters any Hubbard model is the on-site interaction energy U due to a repulsive interaction between the particles located at the same site of the lattice. In this chapter we will estimate the parameter U as an integral over a variational on-site wavefunction in a local harmonic oscillator potential. We will cover both spin singlet and triplet states. Compared to optical lattices for ultracold atoms, which interact via short-ranged s-wave interactions [40], we expect this parameter to be very big, because we deal with electrons that carry a charge e and thus interact via the strong, long-ranged Coulomb potential. For the same reason, the interaction between electrons that are located at different sites is not negligible and we will estimate the strength of these interactions as well. It is an interesting feature that the strength of the interaction can be tuned by the laser parameters in real time: For instance it is evident that the repulsion U increases with the potential depth due to a tighter squeezing of the on-site wavefunctions.

Another striking property that comes along with an optical lattice for the electrons is the possibility to engineer a spin-selective lattice: We will show how the underlying level structure of our system can be used to design differing traps for different internal spin states of the electrons.

6.1 Coulomb blocking: On-site repulsion

Before considering into a more accurate approach to determine the on-site repulsion U, let us first get a feeling for the orders of magnitude with rather rough limiting, but simple approximations. First, as a lower limit to the actual value of U, we can easily compute the Coulomb energy between two classical pointlike electrons that are nearest neighbours on a square lattice and therefore separated by the lattice spacing a. The periodicity a depends only very weakly on the detuning from the trion resonance $\triangle_t$, but can be tuned efficiently by altering the angle between the laser beam and the QW within about one order of magnitude. Still, a is typically of the order of $\sim 10^{-7}m$ up to μm for both $GaAs$ and $CdTe$. In this classical picture, we estimate the Coulomb energy V_c as $V_c = e^2/\epsilon a$ and find that the classical repulsive energy between the next neighbours is $\sim 0.2 - 0.6\,meV$ for angles θ in the range $\theta = 10° - 30°$. For red detuning and reasonable values for the saturation parameter ϵ this possibly exceeds the potential depth V_0. In the case of blue detuning, however, potential depths in the range of $1 - 2meV$ are feasible, which is considerably larger than the next-neighbour interaction energy. Still, this reasoning underlines the strength of the Coulomb interaction in our framework and we will come back to these values when discussing the Coulomb energies between the various neighbours on the square lattice.

To obtain a better understanding of the on-site interaction term U that goes beyond the classical approximation, we consider two electrons trapped at one lattice

site, neglecting the possibility of tunneling. As done before, we approximate the lattice potential by a harmonic oscillator of trapping frequency ω_{ho}, this time, though, in two dimensions: we remember that ω_{ho} depends on both the potential depth and the in-plane lattice periodicity. To describe the two electrons which shall both occupy the ground state $|g\rangle$ of the trapping potential, we simply take the product of two Gaussians

$$\langle \mathbf{r}_1, \mathbf{r}_2 | g, g \rangle = \mathcal{N}^2 \exp\left(-\frac{m_e^* \omega_{ho}}{2\hbar} \left(\mathbf{r}_1^2 + \mathbf{r}_2^2 \right) \right), \tag{6.1}$$

where $\mathcal{N}$ is the normalization constant for the single electron solution $\mathcal{N} = \sqrt{\frac{m_e^* \omega_{ho}}{\pi\hbar}}$. This ansatz for the spatial wavefunction is symmetric with respect to particle exchange, so that it only applies to a spin singlet state. Although the two electrons form a singlet state, both are assumed to couple individually to the trion resonance, since the trap size is much bigger than the trion size. Based on this ansatz, we calculate the expectation value for the Coulomb energy and obtain the compact result

$$\langle g, g | V_c | g, g \rangle = \frac{e^2}{\epsilon} \sqrt{\frac{\pi m_e^* \omega_{ho}}{2\hbar}}. \tag{6.2}$$

Of course, this straightforward calculation only sets a upper boundary on the actual value for U, since the wavefunctions were not allowed to change their form as a reaction to the inter-particle Coulomb interaction. With this ansatz we find Coulomb energies that can enter the range of several meV, depending on the combination of potential depth and lattice spacing. In total, we found a lower and a upper limit, from which we deduce that the actual value for U will be more or less around $1 - 3meV$.

After these introductory estimates, let us apply a more sophisticated approach that covers both singlet and triplet states on the same footing. The Hamiltonian for this two particle problem can be decoupled into a center of mass motion $H_{\mathbf{R}}$ and the

relative motion $H_{\mathbf{r}}$

$$H = H_{\mathbf{R}} + H_{\mathbf{r}} = \frac{\mathbf{P}^2}{2M} + \frac{M}{2}\omega_{ho}^2\mathbf{R}^2 + \frac{\mathbf{p}^2}{2\mu} + \frac{\mu}{2}\omega_{ho}^2\mathbf{r}^2 + \frac{e^2}{\epsilon\,|\mathbf{r}|} \tag{6.3}$$

where we introduced the total mass $M = 2m_e^*$ and the reduced mass $\mu = m_e^*/2$. While the center of mass of the system $\mathbf{R}$ moves in a harmonic potential of the trapping frequency ω_{ho}, the potential of the relative coordinate $\mathbf{r}$ is the sum of a harmonic trap of frequency ω_{ho} and the interaction potential. In addition, the Hamiltonian H is spin-independent, so that the total wavefunction can be factorized

$$\Psi(1,2) = \psi(\mathbf{r})\,\xi(\mathbf{R})\,\chi(s_1, s_2) \tag{6.4}$$

The solutions to the center of mass Hamiltonian $H_{\mathbf{R}}$ are well known; therefore, we will focus on $H_{\mathbf{r}}$ in the following. In cylindrical coordinates $\mathbf{r} = (r, \phi)$ the relative Hamiltonian $H_{\mathbf{r}}$ can be written as

$$H_{\mathbf{r}} = -\frac{1}{2}\left[\frac{\partial^2}{\partial r^2} + \frac{1}{r}\frac{\partial}{\partial r} + \frac{1}{r^2}\frac{\partial^2}{\partial \phi^2}\right] + \frac{1}{2}\omega_{ho}^2 r^2 + \frac{1}{r} \tag{6.5}$$

where we switched to a unit system with $\hbar = \mu = e^2/\epsilon = 1$.

Starting from the Schrödinger equation for the relative Hamiltonian

$$H_{\mathbf{r}}\psi(\mathbf{r}) = \epsilon\psi(\mathbf{r}) \tag{6.6}$$

we introduce the replacement

$$\psi(\mathbf{r}) = \frac{\varphi(\mathbf{r})}{\sqrt{r}} \tag{6.7}$$

so that we can express (6.6) in the following way

$$-\frac{1}{2}\left[\frac{\partial^2}{\partial r^2} + \frac{1}{4r^2} + \frac{1}{r^2}\frac{\partial^2}{\partial \phi^2}\right]\varphi(\mathbf{r}) + \left(\frac{1}{2}\omega_{ho}^2 r^2 + \frac{1}{r}\right)\varphi(\mathbf{r}) = \epsilon\varphi(\mathbf{r}) \tag{6.8}$$

Splitting $\varphi(\mathbf{r})$ up into a radial and an angular part

$$\varphi(\mathbf{r}) = R(r)\, e^{im\phi} \tag{6.9}$$

the radial wave equation to solve reads

$$-\frac{1}{2}\frac{\partial^2}{\partial r^2}R(r) + \left(\frac{\left(m^2-\frac{1}{4}\right)}{2r^2} + \frac{1}{2}\omega_{ho}^2 r^2 + \frac{1}{r}\right) R(r) = \epsilon R(r) \tag{6.10}$$

and gives rise to the definition of the effective potential

$$V_{eff}(r) = \frac{\left(m^2-\frac{1}{4}\right)}{2r^2} + \frac{1}{2}\omega_{ho}^2 r^2 + \frac{1}{r} \tag{6.11}$$

If we introduce the scaled coordinate $r = x/\sqrt{\omega}$, this differential equation becomes

$$R''(x) + \left[\frac{2\epsilon}{\omega_{ho}} - x^2 - \frac{\left(m^2-\frac{1}{4}\right)}{x^2} - \frac{2}{\sqrt{\omega_{ho}}x}\right] R(x) \tag{6.12}$$

Let us mention that for the case with no Coulomb interaction, i.e. if we drop the term $2/\sqrt{\omega_{ho}}x$, Eqn. (6.12) can be solved exactly by

$$R(x) = e^{-x^2/2} x^{m+1/2} L_n^{(m)}\left(x^2\right) \tag{6.13}$$

with the quantized energy levels

$$\epsilon = \omega_{ho}(2n + m + 1) \tag{6.14}$$

This short aside justifies our two parameter variational ansatz of the form

$$\psi(\mathbf{r}) = \mathcal{N} e^{-\alpha r^2} r^{\beta} e^{im\phi}, \qquad \mathcal{N}^2 = \frac{2^{2+\beta}\alpha^{1+\beta}}{2\pi\Gamma(\beta+1)} \tag{6.15}$$

to find a reasonable approximate solution to the problem including the Coulomb interaction between the electrons. The factor r^β is crucial in order to handle the divergence in the Coulomb potential.

Under particle exchange the sign of the radial coordinate flips $\mathbf{r} \rightarrow -\mathbf{r}$, which corresponds to $(r, \phi) \rightarrow (r, \phi + \pi)$ in cylindrical coordinates. This gives

$$e^{im(\phi+\pi)} \rightarrow e^{im\pi} e^{im\phi} = \pm e^{im\phi}$$

which shows that for even values of $m = 0, \pm 2, \pm 4, \ldots$ the system is in a spin singlet state, whereas for $m = \pm 1, \pm 3, \ldots$ the system has to be in a triplet state to establish an overall antisymmetric wavefunction. Therefore, our ansatz allows us to investigate singlet and triplet states. After performing the integrals, the expectation value for the "relative energy" is found to be

$$\langle \psi | H_{\mathbf{r}} | \psi \rangle = \frac{\alpha}{\beta} \left(m^2 + \beta \right) + \omega_{ho}^2 \frac{\beta + 1}{4\alpha} + \frac{\sqrt{2\alpha} \Gamma(\beta + 1/2)}{\Gamma(\beta + 1)} \tag{6.16}$$

where $\Gamma(z)$ is the Euler gamma function. To ensure convergence the variational parameters α, β have to be greater than zero; thus, we immediately see that the singlet state with $m = 0$ will always be the state with the lowest energy.

We identify the on-site interaction matrix element U with the difference in energy caused by the Coulomb interaction

$$U = \frac{\alpha}{\beta} \left(m^2 + \beta \right) + \omega_{ho}^2 \frac{\beta + 1}{4\alpha} + \frac{\sqrt{2\alpha} \Gamma(\beta + 1/2)}{\Gamma(\beta + 1)} - \omega_{ho} \tag{6.17}$$

Of course, our results confirm that the strong Coulomb interaction in our system results in a very strong on-site interaction U, as shown in Fig. (6.1). It is typically in the range of meV. We plot U for $CdTe$ and a saturation parameter value $\epsilon = 0.1$. The qualitative behaviour is the same in $GaAs$, but the actual values for $GaAs$ are

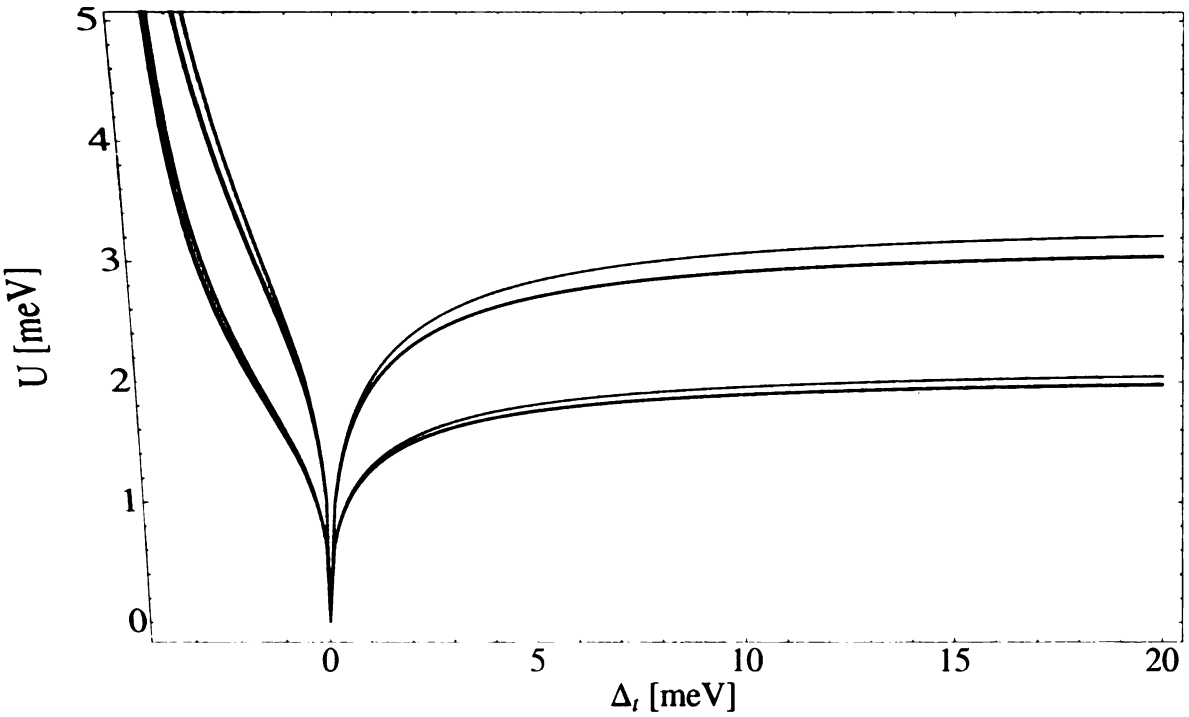

Figure 6.1: On-site repulsion U for $CdTe$ for a square lattice with saturation parameter $\epsilon = 0.1$. Singlet states ($m = 0$) and triplet states ($m = 1$) are shown in blue and orange, respectively, for angles $\theta = 15°$ (lower branch) and $\theta = 30°$ (upper branch).

considerably smaller due to a higher dielectric constant ϵ and smaller potential depths. The intuitive picture that an increase in the lattice depth leads to higher barriers, therefore compressing the two particles and yielding higher values for U, is confirmed. In addition, we see that the singlet states lead to a smaller on-site interaction U than the triplet states. Furthermore, the strength of the interaction crucially depends on the angle θ which essentially tunes the slope of the trap. A bigger angle θ leads to a steeper potential with stronger squeezed wavefunctions and, as a consequence, higher values for the interaction parameter U.

Based on these results, we are led to conclude that the the potential depth is too weak compared to the dominant on-site repulsive interaction U to favour more than one trapped electron per lattice site.

6.2 Filling factor

Dealing with ultracold atoms in optical lattices, one can usually restrict the analysis of the interactions between the atoms to the on-site contribution U. In other words, in the deep optical lattice regime the interaction between Wannier states localized at $\mathbf{R}$ and $\mathbf{R}'$ reduces to a local form $U\delta_{\mathbf{R},\mathbf{R}'}$ [40]. This regime, however, is different from our systems, where the r^{-1} Coulomb behaviour accounts for strong long-range interactions. Therefore, we will give a rough estimate for the interaction energies between electrons that are located at different sites of the square lattice in the next step. The estimate is given by the classical Coulomb energy

$$V_c = \frac{e^2}{\epsilon\,(\zeta a)} \tag{6.18}$$

corresponding to the repulsive Coulomb interaction between two pointlike electrons with charge e, separated by the distance ζa. This approximation is allowed, if the electrons are far enough apart to neglect effects owing to the overlap of the wavefunctions. The parameter ζ counts the separation between the two electrons in terms of the lattice periodicity a. The case $\zeta = 1$ for example corresponds to next neighbours in the lattice. For the first six nearest neighbours in the two-dimensional square lattice, we have

$$\zeta = 1,\ \sqrt{2},\ 2,\ \sqrt{5},\ \sqrt{8},\ 3 \tag{6.19}$$

For laser light tuned close to the trion resonance, the result of this approximation only depends on the angle θ, directly determining the lattice parameter a. Our results for $CdTe$ are shown in Fig. (6.2). The values for $GaAs$ are slightly smaller because of stronger screening effects in $GaAs$. The repulsive interactions between electrons trapped at different sites are still very strong and possibly in the range of the depth of the trapping potential. Only in the regime, where θ is chosen appreciably small,

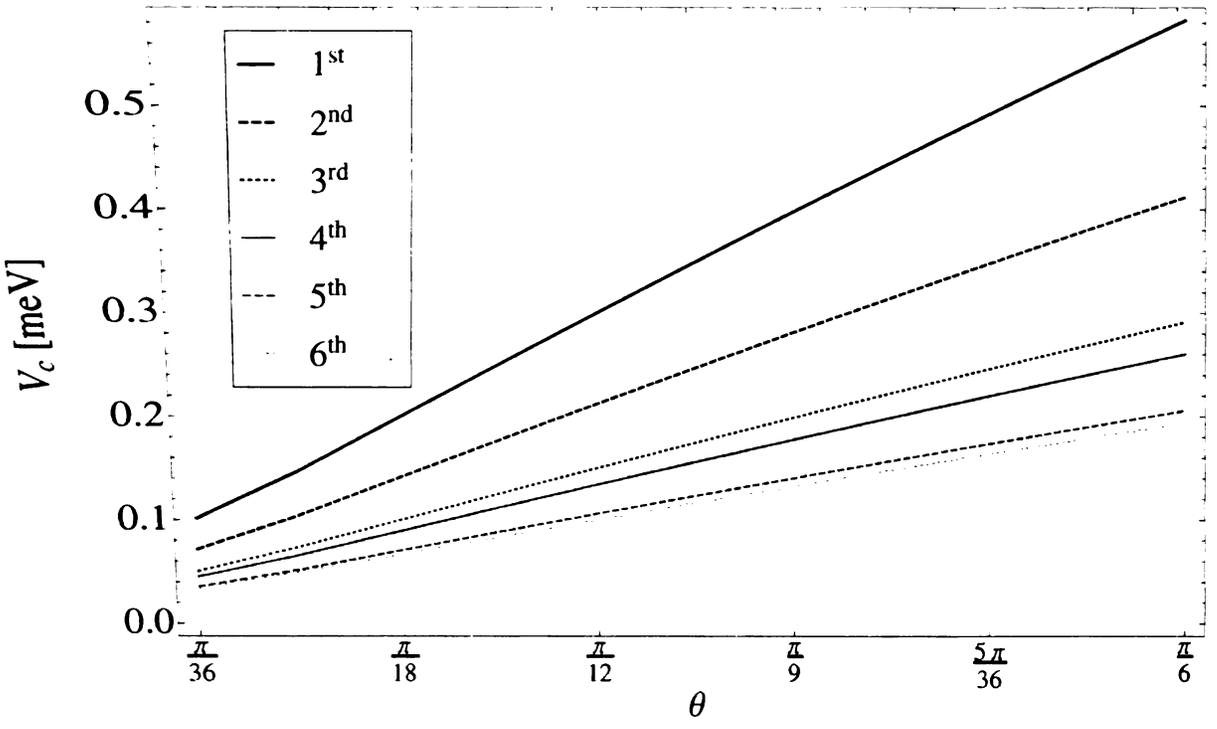

Figure 6.2: Coulomb interaction energies between electrons at different sites of the square lattice for the first six neighbours in $CdTe$. The angle θ ranges from $\pi/36 \equiv 5°$ to $\pi/6 \equiv 30°$. Note that, according to Tab. (4.2), the potential depth V_0 can reach values $\sim 1.6meV$ for blue detuning in $CdTe$, which is considerably larger than V_c.

resulting in larger lattice constans a, the neighbour interactions can become small compared to the potential depth. For both $GaAs$ and $CdTe$ QW systems, the lattice parameter a is $\sim 1.5\,\mu m$ for $\theta = 5°$. This lattice spacing is in the same range as the regime in which optical lattices for atoms are usually operated in the laboratory [56].

Last, but not least we would like to address the following question: What is the maximum electron density n_1 to reach a commensurate filling of one electron per lattice site? With $n_1 = 1/a^2 = 4/\lambda_{||}^2$, we find that n_1 is typically in the range of $\sim 10^9 cm^{-2}$. This is an electron gas in the low density regime.

6.3 Spin-selectivity

The strength of the optical potential crucially depends on the dipole moment between the two electron "internal" states. We can exploit the selection rules for optical transitions to present a remarkable feature of the optical potential we study, namely its spin selectivity: it depends on the spin state of the electron. Configurations are realizable where the two electron spin states are exposed to vastly different optical potentials. This situation is schematized in Fig. (6.3), where, depending on the spin state of the initial electron in the conduction band, two possibly different Rabi-frequencies couple the electron to the trion state, where the two electrons form a singlet state. A spin-down electron only couples to σ^- photons to form a trion singlet state, whereas a spin-up electron is coupled to a trion singlet via σ^+ photons only. Spin-flip Raman transitions are dipole forbidden: Consequently, the trion system at zero magnetic field appears as a double two-level system [57]; a remarkable feature that is not found in cold atom systems.

For instance, spin polarized electron lattices can be created in a standing wave configuration made out of two counterpropagating laser beams with linear polarization vectors enclosing a variable angle ϕ [58]. This configuration is usually called lin-ϕ-lin configuration [59]. The result of this experimental setup is a standing wave light field which can be decomposed into a superposition of a σ^+- and a σ^--polarized standing wave laser field. In this way, two separate lattice potentials $V_+(x,\phi) = V_0 \cos^2(Qx + \phi/2)$ and $V_-(x,\phi) = V_0 \cos^2(Qx - \phi/2)$ have been realized. By changing the polarization angle ϕ, one can control the relative separation between these two potentials $\triangle x = (\phi/\pi)\,\lambda_x/2$. Both potentials can be shifted apart by increasing ϕ, until they overlap again for $\phi = n\pi$, n being an integer. This theoretical scheme has already been applied to atoms: Based on such a configuration, atoms have been moved coherently across several lattice sites [60, 61, 62]. If the trapped par-

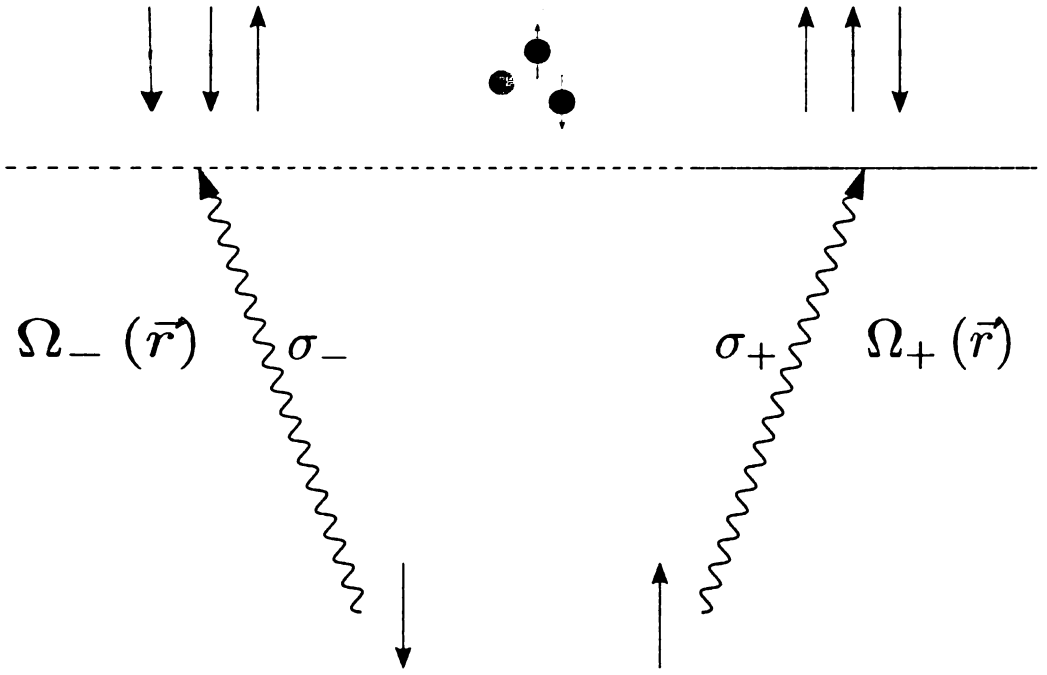

Figure 6.3: Spin selectivity of the optical potential: The trion system appears as a double two-level system. Electron and hole spins are depicted in blue and red, respectively.

ticle is in a superposition of two internal spin states, state selective optical potentials can be used to split the wavefunction and transport the corresponding wavepackets in two opposite directions, as schematized in Fig. (6.4).

This technique could be used to trap two sets of electrons: those in the spin-down state light shifted by the σ_- light, and those in the spin-up state light shifted by the σ_+ light. We refer to these as the $\pm$–species. The ability to dynamically control the angle ϕ allows us to separate and move the electrons of the $\pm$–species relative to each other. In this way, two electrons of different species initially separated by $\triangle x$ can be made to overlap by rotating ϕ by $\phi = 2\pi\triangle x/\lambda_x$.

In this way, a spin-dependent lattice offers the intriguing possibility to tune the interactions between two electrons in different spin states by controlling the spatial separation and possibly the overlap of the on-site spatial wavefunction between zero and its maximum value, just by shifting the spin-dependent lattices to each other.

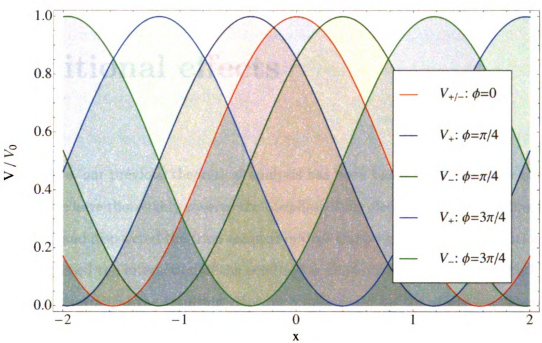

Figure 6.4: Cartoon for the effect of the spin-selective potentials $V_{\pm}$. They overlap for $\phi = 0$. As ϕ is increased adiabatically, the two potentials are pulled in two opposite directions. As a consequence, the two spin states of the electron move into opposite directions, and the electron wavepacket is split apart into its two contributions.

Chapter 7

Additional effects

In principle, our previous theoretical analysis has been based on three major cornerstones: We have thoroughly covered the coupling of the electrons to the standing laser light field and discovered the trion-assisted optical trapping potential. In addition, we have discussed the interaction of the conduction electrons with the phonon bath and we have determined the resulting effective temperature for the electrons. Then, we have extended this single-particle discussion by studying the interparticle Coulomb effects, which coined the picture of a possible electron lattice as a two dimensional regular array of microtraps. In this final chapter of our investigations, we will complete our studies by considering a range of possible side-effects that we have not covered so far. The notation 'side effects' suggests that these effects will be negligible compared to the three cornerstones identified above. To prove this statement will be the actual task of the present chapter. We will highlight the ponderomotive potential, which is an ubiquitous effect whenever an electron is placed in an intense electromagnetic field. Lastly, we will pay tribute to a possible ionization of the conduction electrons above the QW barrier and we will identify the range of electron densities in which an observation of the trapping potential is feasible.

7.1 Ponderomotive potential

With ion traps, charged particles have been trapped in potential wells that are up to several eV deep [63]. In contrast to the trion-mediated potential we propose in this thesis, however, ion traps do not depend on the internal electronic state of the trapped particle. One of the most prominent forms of these traps have been developed by W. Paul [64], in which a spatially varying time-dependent field is used to confine charged particles in space; typically the so-called Paul traps are operated in the radio-frequency (rf) domain. Based on this technique, electrons have been successfully trapped for the first time in 1973 [65].

In this section we study the underlying concept of the "ponderomotive potential" generated by an electromagnetic standing wave. In principle, this is the interaction energy that results from the placement of a charged particle in a rapidly oscillating electric field. The well-known result of this problem states that the average kinetic energy associated with the quivering forced on an electron by a radiation field acts as an effective potential for the averaged motion of the electron [66]. In general, this ponderomotive potential is time dependent. Therefore, the total kinetic energy is not a constant of motion. As a consequence, the ponderomotive potential is, in general, not conservative.

We introduce a time average defined by

$$\langle u(t)\rangle_t \equiv \frac{1}{T}\int_t^{t+T} dt'\, u(t') \tag{7.1}$$

where $u(t)$ is any dynamic variable and T is the period of the wave.

In the following, we wish to analyze the average motion of an electron exposed to an electromagnetic standing wave along the $\hat{x}$-axis, polarized along the $\hat{y}$-axis with wavevector $\mathbf{Q} = Q\hat{x}$ and angular frequency ω. Thus the electric field can be written

in the form

$$\mathbf{E}(x) = E_0 \hat{y} \cos(Qx) \cos(\omega t) \tag{7.2}$$

For convenience, we choose a frame of reference in which near $t = 0$ the electron is, on average, at rest at the origin. The easiest approach to gain insight into the physics of this process is a classical description. With $\mathbf{r}(t) = (x(t), y(t), z(t))$ and $\mathbf{v}(t) = (\dot{x}(t), \dot{y}(t), \dot{z}(t))$ denoting the position vector and the velocity of the electron, the classical equation of motion for the $\hat{y}$-direction reads

$$\ddot{y}(x,t) = -\frac{eE_0}{m_e^*} \cos(Qx) \cos(\omega t) \tag{7.3}$$

which is simply the Newtonian equation for an electron of mass m_e^* subject to the Lorentz force in the $\hat{y}$-direction. Setting the integration constants to zero, the solution is readily found to be

$$y(x,t) = \frac{eE_0}{m_e^* \omega^2} \cos(Qx) \cos(\omega t) \tag{7.4}$$

which shows, that the motion in the $\hat{y}$-direction is a function of the x-position of the electron. The time-averaged kinetic energy E_k associated with this classical motion is then given by

$$\begin{aligned} \langle E_k \rangle_t &= \frac{m_e^*}{2} \left\langle \dot{x}^2 \right\rangle_t + \frac{m_e^*}{2} \left\langle \dot{y}^2 \right\rangle_t \\ &= \frac{m_e^*}{2} \left\langle \dot{x}^2 \right\rangle_t + \frac{e^2 E_0^2}{4 m_e^* \omega^2} \cos^2(Qx) \end{aligned}$$

The average total kinetic energy splits into two parts. The last term acts as an effective potential for the average motion of the electron; it is the ponderomotive potential $U_p(x)$ defined by

$$U_p(x) = \frac{e^2 E_0^2}{4 m_e^* \omega^2} \cos^2(Qx) = U_p^0 \cos^2(Qx) \tag{7.5}$$

Forces arising from this interaction may be directly calculated as a spatial derivative of (7.5). The ponderomotive force simply turns out to be the time-averaged Lorentz force. Its effect is clearly to push the electron away from regions of high laser intensity, and it is completely independent of the light polarization.

In this model, the total energy of the electron is the oscillatory energy $U_p(x)$ plus the directed kinetic energy, the average energy of translation. Once a free electron travels from a region of low intensity to a region of higher intensity, its original translational kinetic energy is converted into oscillatory energy. Thus, the highest intensity region which an electron can enter is one where the oscillatory energy equals the initial kinetic energy outside the beam [67].

Using the relation between the intensity of the laser I and the amplitude of the electric field E_0

$$I = \frac{1}{2} nc\epsilon_0 E_0^2 \tag{7.6}$$

where n gives the refractive index of the material, the potential depth U_p^0 of the ponderomotive potential can be expressed in terms of the laser intensity I as

$$U_p^0 = \frac{e^2 I}{2m_e^* nc\epsilon_0 \omega^2} \tag{7.7}$$

The ponderomotive potential is proportional to the intensity of the laser, but, at the same time, indirectly proportional to the squared frequency ω^2 of the field. Therefore, we can clearly see that the associated Paul traps can possibly represent a strong confinement mechanism for rf frequencies. Using typical values for our system, however, with frequencies in the optical domain, the ponderomotive potential is strongly suppressed: it is of the order of $\sim \mu eV$ at maximum for rather large laser intensities of $I \approx 10^7 W/cm^2$. Despite the small effective masses of the electrons in the semiconductor QW, it is still a negligible effect compared to the strength of the trion-based optical potential; indeed, it is at least three orders of magnitude smaller than the

trion-mediated optical potential which can enter the meV range for blue detuning for relatively small intensities of $I \sim 10^3 W/cm^2$.

7.2 Electron ionization

Up to now, we have analyzed the interaction of the laser photons with the semiconductor QW only in terms of photoexcitations of excitons or, if possible, bound trions. This section will be devoted to the possibility of exciting the conduction band electrons above the barrier of the QW system, which we shall call electron ionization. Of course, the occurrence of this effect is objectable to our goal of trapping electrons that are confined inside the QW.

The ionization process essentially depends on the band structure of the QW system at hand: The incoming photons are tuned close to the trion resonance, a few meV below the conduction band. Since the trion and exciton binding energies are much smaller than the bandgap ϵ_c the photon energies $\hbar\omega$ are approximately $\hbar\omega \approx \epsilon_c$. Both $GaAs$ and $CdTe$ belong to the class of direct semiconductors and their bandgap ϵ_c is shown in Fig. (7.1) between the symmetry points Γ_8 and Γ_6. In principle we also have to consider ionization processes into the barrier material as $Al_xGa_{1-x}As$, but the changes in the bandstructure are negligibly small on the energy scales for this specific process.

The ionization process goes along the following mechanism: In principle, a conduction electron initially close to the Γ_6 point in the conduction band may be excited for example to the Γ_7 point in a higher conduction band. Since photon wavevectors are very small, this process appears as a vertical line in the bandstructure diagram; in (7.1) we can see with the naked eye that the gap E_g that needs to be overcome is much bigger than the bandgap ϵ_c, the photons of the laser are close to in energy. Since we work in the low electron density regime, only this ionization process of con-

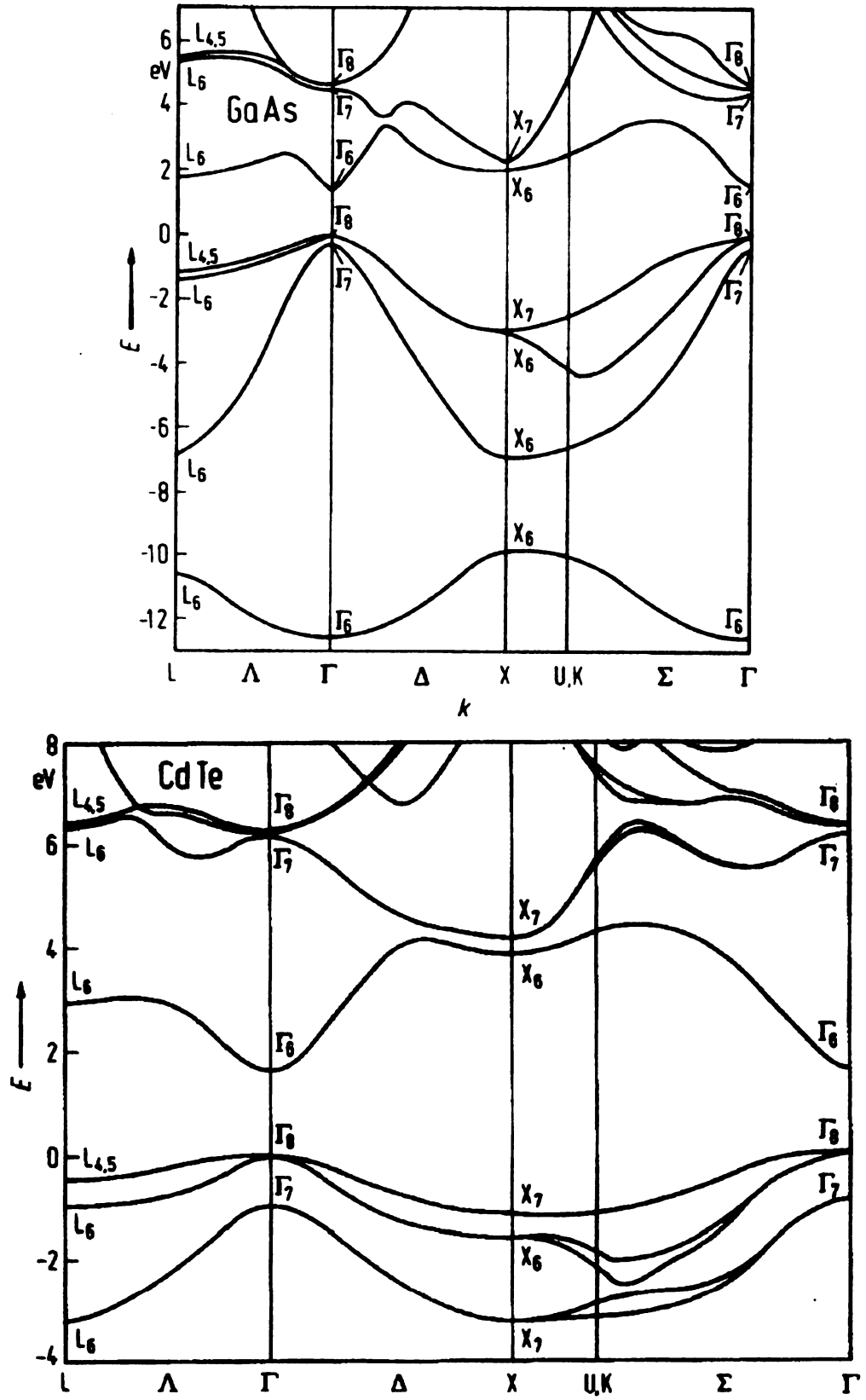

Figure 7.1: Bandstructures of *GaAs* and *CdTe*, taken from [29].

duction electrons needs to be considered. Therefore, as far as the QW systems we have specialized on are concerned, electron ionization can safely be neglected.

For completeness and to keep the discussion as general as possible, though, we underline this reasoning with a calculation based on Fermi's Golden rule, assuming a QW system where the gap E_g for the ionization is comparable to the bandgap ϵ_c. The initial state $|i\rangle = |\mathbf{k}, \mathbf{Q}\rangle$ of the process we are about to consider is characterized by a photon of energy $\hbar\omega$ and momentum $\vec{Q} = (\mathbf{Q}, Q_z)$ and a initial excess electron confined in the QW of width L_z in the growth direction $\hat{z}$. In $\vec{k}$-space, the initial electron is assumed to be in the lowest conduction band close to the Γ_6 point. Assuming a plane wave inside the QW, we write the wavefunction of the initial electron $\Psi_i(\vec{r})$ as

$$\Psi_i(\vec{r}) = \frac{\exp(i\mathbf{kr})}{\sqrt{A}} \phi(z)\, u_c(\mathbf{k}, \mathbf{r}) \tag{7.8}$$

with $\phi(z)$ being the electron's wavefunction along the $\hat{z}$-direction and $u_c(\mathbf{k}, \mathbf{r})$ being the periodic Bloch function in the conduction band. Modelling the confinement as a infinite square well problem in the ground state, $\phi(z)$ is given by

$$\phi(z) = \sqrt{\frac{2}{L_z}} \sin\left(\frac{\pi}{L_z} z\right). \tag{7.9}$$

Consequently, the energy of the initial state E_i is

$$E_i = \hbar\omega + \frac{\hbar^2 \mathbf{k}^2}{2m_e^*} - E_c, \tag{7.10}$$

where the electron energy consists of two contributions: the kinetic energy of a two-dimensional plane wave and the confinement energy E_c due to quantized $\hat{z}$-direction. For an infinite square well E_c amounts to

$$E_c = \frac{\hbar^2}{2m_e^*} \left(\frac{\pi}{L_z}\right)^2. \tag{7.11}$$

The final state $|f\rangle = \left|\vec{k}_f\right\rangle$ consists of an ionized electron which, as a consequence of the photon absorption, is supposed to have left the quantum well. Essentially, it is a free electron which is not subject to the two-dimensional confinement anymore. Consequently, its wavefunction $\Psi_f(\vec{r})$ is modelled as a three-dimensional plane wave

$$\Psi_f(\vec{r}) = \frac{\exp\left(i\vec{k}_f\vec{r}\right)}{\sqrt{V}} u_{c'}\left(\vec{k}_f, \vec{r}\right), \tag{7.12}$$

where V is the quantization volume and $u_{c'}\left(\vec{k}_f, \vec{r}\right)$ is the Bloch function in the higher conduction band which we label as c'. The energy of the final state is

$$E_f = E_g + \frac{\hbar^2 \mathbf{k}_f^2}{2m_e^*} + \frac{\hbar^2 k_{f,z}^2}{2m_e^*} \tag{7.13}$$

where we have separated the z-component explicitly. We calculate the electron's ionization rate Γ_{ion} based on Fermi's Golden rule. The corresponding interaction term $\mathcal{H}_{int}$ is the light-matter coupling for this specific ionization process; we write it in the general form

$$\mathcal{H}_{int} = g_c \sum_{\mathbf{k}} c^\dagger_{c',\mathbf{k}+\mathbf{Q}} c_{c,\mathbf{k}} a_{\mathbf{Q}} + h.c. \tag{7.14}$$

The light-matter coupling constant for this process is called g_c. A photon of in-plane momentum $\mathbf{Q}$ is annihilated, while an electron of in-plane wavevector $\mathbf{k}$ in the conduction band c is promoted to the upper conduction band c'. The strength of the interaction g_c is essentially governed by the overlap between the two wavefunctions of the initial and final state which describe electrons in different bands one being confined in the QW and the other one being free to move in all three directions. Neglecting a mismatch in the Bloch part of the wavefunctions the coupling constant

g_c for this transition is

$$g_c = \tilde{g}_c \int d^3\mathbf{r} \frac{\exp\left(-i\vec{k}_f\vec{r}\right)}{\sqrt{V}} \frac{e^{i\mathbf{kr}}}{\sqrt{A}} \phi(z) = \tilde{g}_c \sqrt{\frac{A}{V}} \tilde{\phi}\left(k_{f,z}\right) \delta_{\mathbf{k}_f,\mathbf{k}+\mathbf{Q}}, \tag{7.15}$$

where $\tilde{g}_c$ governs the bare dipolemoment for this transition, $\tilde{\phi}\left(k_{f,z}\right)$ represents the Fourier transform of $\phi(z)$ and the photon momentum was neglected. For the ionization rate Γ_{ion} we obtain

$$\Gamma_{ion} = \frac{8\tilde{g}_c^2}{\pi\hbar} \frac{1}{\sqrt{\triangle_{c'} E_c}} \frac{1+\cos\left(\pi\sqrt{\triangle_{c'}/E_c}\right)}{\left(1-\triangle_{c'}/E_c\right)^2} \theta\left(\triangle_{c'}\right), \tag{7.16}$$

where $\triangle_{c'} = \hbar\omega - \left(E_g + E_c\right)$ is the detuning of the photon from the energy that has to be overcome: The bandgap energy E_g plus the confinement energy E_c. This result confirms our original expectations: Due to the big energy mismatch for this transition, the ionization rate is zero for the QW systems *GaAs* and *CdTe*.

In principle, the conduction electrons could be ionized by a phonon-assisted process, i.e. a combination of photon plus phonon excitation, as well. Since, this is a second-order process, it is less likely to occur than the first-order photon excitation and can therefore be neglected. In conclusion, we find that the conduction electrons can be assumed to be perfectly confined inside the QW, since ionization processes do not play a great role in our setup.

7.3 Restrictions on the electron density

The density of the excess carriers inside the QW can be easily controlled via modulation doping and, in the course of our studies, we have only touched on the electron density twice: We have determined the density for a commensurate filling of one electron per site n_1 to be $\sim 10^9 cm^{-2}$. We have also mentioned before that exci-

tonic effects are quenched for sufficiently high carrier densities. We will specify this restriction first: We have presented the trion-mediated potential in the framework of a single-particle effect. For this regime to be valid, we need to require that the maximum number of trions that fit into the sample without spatial overlap, given by $N_t^{max} = A/(\pi a_t^2)$, is much smaller than the number of conduction electrons in the sample $N_e = n_e A$; here, n_e denotes the electron density. In a sense, we restrict our considerations to the regime where the trion state can be assigned to one single electron only. Consequently, our results are valid in the regime

$$n_e \ll \frac{1}{\pi a_t^2} \tag{7.17}$$

Based on a typical trion size of approximately $a_t \sim 2 - 3a_D$, the requirement boils down to $n_e \ll 8 \times 10^{10} cm^{-2}$. Since this density is higher than the one-electron-per-site density n_1, the condition, stated in Eqn. (7.17), is a very weak restriction on the electron density n_e.

Let us mention another restriction on the electron density n_e we have to be aware of: Electrons obey the Fermi-Dirac distribution and therefore acquire energy up to the Fermi energy simply by phase-space filling. In a two-dimensional system, the Fermi energy ϵ_F is related linearly to the electron density: $\epsilon_F = \left(\pi\hbar^2/m_e^*\right) n_e$. For an electron density of $n_e = 10^{10} cm^{-2}$, the Fermi energy amounts to $0.25\, meV$ and $0.36\, meV$ for $CdTe$ and $GaAs$ respectively. This energy range is comparable to the the depth of the optical potential for the electrons. If the electron density n_e is modulated to be in the lower $10^9 cm^{-2}$ regime, however, the Fermi energy ϵ_F is appreciably smaller than the depth of the trapping potential.

Conclusion

We have merged concepts from semiconductor physics and cold-atom physics to prove the existence of a novel laser-induced optical dipole potential for electrons in a semiconductor QW. This potential, generated by driving the trion-resonance with intense, detuned laser light is proportional to the light intensity. To properly describe the trion resonance, a bound state between an exciton and a charge carrier, we have obtained a Hylleraas-type wavefunction using Ritz's variational technique. We have investigated the optical potential following two approaches: In Chapter 2.2 we modeled the QW sample as a collection of two-level systems. The trion modifies the exciton resonance frequency in the vicinity of a carrier. Accordingly, the Stark energy is modified in proportion to the light intensity at the carrier location, which serves as a source of mechanical potential energy for the carrier. Chapter 3 was devoted to the derivation of an effective Hamiltonian and the corresponding Schrödinger equation for an electron that is coupled to virtually excited trion and exciton continuum states.

We have found that this trion-mediated potential exhibits several remarkable features. In particular, it displays a non-local character that is a consequence of the light effective masses of the electrons m_e^* and of the "quivering" of the electron motion once it has virtually mixed with the extended diffusive trion state. This non-local effect takes place on a lengthscale of the order of the "trion size", which is approximately $\sim 30nm$. Since this lengthscale is small compared to the periodicity of the potential, we have been able to show that the non-locality can be neglected in the analysis of

the electron trapping at the nodes or anti-nodes of the intensity pattern.

The diffusive character of the excited trion level accounts for an effective enhancement factor χ for the potential depth of almost two orders of magnitude with respect to typical excitonic Stark effects; the quantity χ has been intuitively explained as an integral over all possible bound trion configurations having one electron and one hole "on top of each other". Simply put, χ can be seen as the number of excitons that fit into the trion size without spatial overlap.

The most striking and distinguishing property of this potential relative to its atomic brother, though, stems from the strong effective background polarizability of the semiconductor medium, an effect not present for conventional atomic optical potentials. The coherent exciton resonance gives rise to a very important correction factor $f_c(\triangle_t)$ to the pure trion contribution: for red detuning, this correction is smaller than one and thus leads to a decrease in the potential depth. However, for blue detuning, it can give a strong enhancement to the potential depth.

We have shown that this novel type of potential can be deep compared to the single photon recoil energy E_R and to the effective temperature of the electrons. The latter strongly benefits from an omnipresent natural cooling mechanism in the semiconductor environment, the phonon bath. A regime where the potential depth exceeds both the recoil energy and the effective thermal energy of the carriers by a factor of 10 seems feasible, according to our calculations.

In addition, we have extended our model to the idea of a spin-selective electron lattice which is much simpler to engineer and control than similar lattices in AMO systems. There is a direct mapping of the spin of a localized electron and the optical polarization of the photon that can couple the electron to the trion state. Owing to this level scheme, two different potentials for the two spin configurations can be created.

In summary, we have applied concepts from the AMO community to generate new

ideas for semiconductor systems. Owing to the specific properties of these systems like the background polarizability, the light particle masses, the strong inter-particle interactions, and the electron-phonon cooling, semiconductor optical potentials are very different from the conventional optical potentials in AMO systems.

From a fundamental point of view our results can open up a new paradigm in solid state physics: a gas of charged particles in a periodic potential that is possibly strong enough to trap the carriers at a single site, but weak compared to the inter-particle interactions. This system deserves further investigations, since this fermionic many-particle quantum state on a regular lattice possibly bridges the gap between current ultracold atom systems and fundamental concepts in condensed matter physics. A unique dynamic control over not only all the relevant parameters of the optical lattice allows for experiments not feasible in conventional solid state systems. A wide range of properties can be adjusted through the laser beam geometry, the polarization, the intensity and the frequency of the light. Contributions to a fundamental understanding of the quantum behaviour of a many electron system in a solid might be expected from these systems. In contrast to ultracold atoms in an optical lattice, strong long range interactions occur, as in a true solid. The system we propose might even touch on highly complex questions as high-T_c superconductivity or Mott-insulating phases, since strongly interacting fermionic atoms in optical lattices have previously been suggested for investigations on these ongoing problems [68, 69]. To quote Richard Feynman in 1965: "I think it is safe to say that nobody understands quantum mechanics." Undoubtedly, experiments where the motion of electrons is optically manipulated in real time would continue to push the bizarre features of quantum mechanics to the forefront, realizing the thought experiments once envisaged by the founding fathers of quantum theory.

Today, about 45 years later, with the new language of quantum information emerging we might hope to deepen our understanding of the principles of quantum physics.

But to get there, we need to master one of the great modern scientific challenges: the development of tools to prepare, manipulate and measure the quantum mechanical state of a system. Experimental and theoretical progress has been made based on many different platforms. Examples in which quantum control is sought or has been accomplished include quantum optical systems, such as those utilizing trapped ions [70, 77] or neutral atoms [60, 78, 79], cavity quantum electrodynamics [80, 81, 82] and nuclear magnetic resonance [83, 84], as well as solid state systems, based on nuclear spins [85, 86], quantum dots [87] and Josephson junctions [88]. All this work constitutes important steps towards the realization of a "quantum computer", in which algorithms are implemented as unitary transformations on a many-body quantum state. To come back to Feynman, our model, in essence, might lead one day to the implementation of the pioneering idea due to Feynman of simulating one quantum system with another [89]. Owing to the long spin decoherence times [90] and the potential for scalability of a semiconductor based system, electron spins in semiconductors have been identified as one of the most promising candidates for quantum information science. Cutting-edge technologies for solid state quantum electronics might be merged with those from quantum optics by using light to localize, manipulate and probe the entanglement of electron spins in semiconductors.

Our findings are based on a very general technique so that a wide range of various systems with different applications could be investigated. Obviously, our scheme can be extended for further research including one dimensional systems (quantum wires) with an increased trion binding energy and/or holes as the excess carriers with larger effective masses. More strikingly, though, we can envisage for example a comparable semiconductor based system where the trapped particles interact via shorter-ranged dipole-dipole interactions, instead of the strong long-ranged Coulombic coupling present in the current system. How could we achieve this? Indirect excitons are formed from electrons and holes, that are confined to two different par-

allel QW layers by a potential barrier; they behave as dipoles perpendicular to the plane [93, 94]. The repulsive character of the their interaction has been evidenced in experiments as a positive and monotonic line shift with increasing density [95]. Because of the spatial separation between the electron and hole layers in this coupled QW structure, the intrinsic radiative lifetimes of optically active indirect excitons exceeds that of their direct counterparts by orders of magnitude and can be in the range of several microseconds [94]. The system which we propose as a strikingly promising candidate for interesting future research projects is schematized in Fig. (7.2).

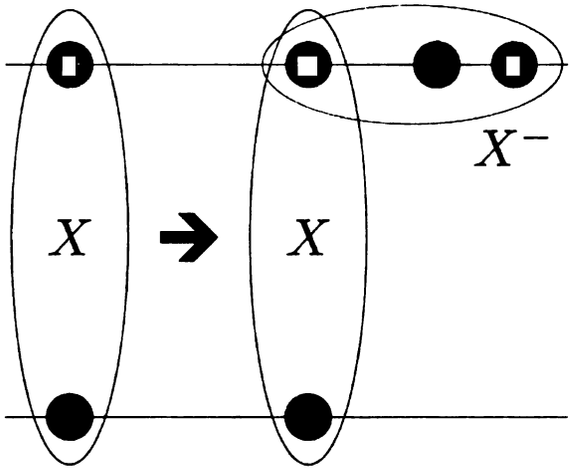

Figure 7.2: Scheme for a bilayer semiconductor QW system where electrons and holes are trapped, but short range dipole-dipole interactions are realized. Electrons are depicted as blue dots, holes as greens dots. Indirect excitons X are composed of electrons and holes from different QW layers.

We start out from an indirect exciton present in the coupled QW system. By coupling the electron or the hole in one of the layers to the trion resonance via a laser standing wave as proposed in this thesis the carrier's position can be controlled; at the same time, its excitonic partner in the other layer will follow due to the strong exciton binding energy. Since the exciton complex is overall neutral, this system has the potential to localize and control carriers which are effectively subject to a short-ranged dipole-dipole interaction because of their excitonic oppositely charged

companion in the second layer. Based on the spin-selectivity of the trion-mediated potential for the qubit carriers, two carriers well separated from each other first can be addressed and subsequently a differential energy shift can be induced due to their dipole-dipole interaction, conditional on the state of the two qubits. Eventually, this could implement a two-qubit phase gate, required for universal quantum computation.

In conclusion, optical trapping and cooling techniques have had a profound impact on the fields of quantum many-body physics and information processing [91, 92]: the flexibility they naturally impart could have a similar impact on solid state physics, vastly beyond the scope of this thesis.

Appendix A

Material parameters

Quantity		Units	$GaAs$	$CdTe$	
Fundamental gap (2 K)	ϵ_c	eV	1.5192	1.6063	[29]
Electron effective mass	m_e^*	m_0	0.0665	0.096	[22]
Heavy hole effective mass	m_h^*	m_0	0.34	0.19	[22]
Effective mass ratio	σ	-	0.2	0.5	[22]
3D donor Bohr radius	a_D	nm	9.95	5.4	[22]
Hartree	E_h	meV	11.58	27.6	[22]
dielectric constant	ϵ_r	-	12.74	9.7	[29]
Kane optical matrix element	E_P	eV	23	21	[29]
Dipole moment	d_0	eÅ	6.2	5.6	

Appendix B

Excitons in quantum wells

In this Appendix we give a quantum-mechanical description of excitons that are confined in QW systems. For simplicity, we consider the pure two-dimensional limit, corresponding to a QW with a very thin QW width. Introducing the scaled radius

$$\rho = \varsigma r, \tag{B.1}$$

we can express the Wannier equation, Eqn. (1.6), as

$$\left[-\nabla_\rho^2 - \frac{\lambda}{\rho}\right]\phi(\rho) = \frac{2\mu_x E_r}{\varsigma^2\hbar^2}\phi(\rho) \tag{B.2}$$

$$\lambda = \frac{2\mu_x e^2}{\varsigma\hbar^2\epsilon} = \frac{2}{\varsigma a_0}, \tag{B.3}$$

where a_0 is given by

$$a_0 = \frac{\epsilon\hbar^2}{\mu_x e^2}. \tag{B.4}$$

In analogy to the hydrogen-problem, the energy E_r is negative for bound states and positive for the ionization continuum. We define

$$a_0^2\varsigma^2 = -\frac{8\mu_x E_r a_0^2}{\hbar^2} = -4\frac{E_r}{E_0}. \tag{B.5}$$

Here, E_0 serves as the energy unit

$$E_0 = \frac{\hbar^2}{2\mu_x a_0^2} = \frac{e^2}{2\epsilon a_0} = \frac{e^2 \mu_x}{2\epsilon^2 \hbar^2}. \tag{B.6}$$

Accordingly, the Wannier equation can be rewritten in the form

$$\left[-\nabla_\rho^2 - \frac{\lambda}{\rho}\right] \phi(\rho) = -\frac{1}{4}\phi(\rho), \tag{B.7}$$

where we introduced λ as

$$\lambda = \frac{e^2}{\hbar\epsilon}\sqrt{-\frac{\mu_x}{2E_r}}. \tag{B.8}$$

With our choice of ς^2, the parameter λ will be real for bound states and imaginary for the ionized continuum. We are interested in a solution for two-dimensional semiconductors. For this purpose, it is convenient to write the Laplace operator in polar coordinates

$$\nabla_\rho^2 = \frac{1}{\rho}\frac{\partial}{\partial\rho}\rho\frac{\partial}{\partial\rho} - \frac{\mathcal{L}_z^2}{\rho^2}, \tag{B.9}$$

where $\mathcal{L}_z$ is the operator for the z component of the total angular momentum

$$\mathcal{L}_z^2 = -\frac{\partial^2}{\partial\varphi^2}. \tag{B.10}$$

It obeys the eigenvalue equation

$$\mathcal{L}_z \frac{1}{\sqrt{2\pi}} e^{im\varphi} = m\frac{1}{\sqrt{2\pi}} e^{im\varphi}, \qquad m = 0, \pm 1, \pm 2, \ldots \tag{B.11}$$

The ansatz

$$\phi(\rho) = f_m(\rho)\frac{1}{\sqrt{2\pi}} e^{im\varphi} \tag{B.12}$$

yields the following equation for the radial part of the wave function

$$\left[\frac{1}{\rho}\frac{\partial}{\partial\rho}\rho\frac{\partial}{\partial\rho}+\frac{\lambda}{\rho}-\frac{1}{4}-\frac{m^2}{\rho^2}\right]f_m(\rho)=0. \tag{B.13}$$

In order to solve this differential equation, we will first examine the asymptotic behaviour of the radial wavefunctions for large radii. In the limit $\rho\to\infty$, the leading order equation reads

$$\left[\frac{d^2}{d\rho^2}-\frac{1}{4}\right]f_\infty(\rho)=0. \tag{B.14}$$

Therefore, the convergent solution takes on the form

$$f_\infty(\rho)=e^{-\rho/2}. \tag{B.15}$$

In the next step we investigate the asymptotic form of the wavefunctions for small ρ. Thus we express $f(\rho)$ as $f(\rho)=f_0(\rho)f_\infty(\rho)$ and see that $f_0(\rho)$ should vary as $\rho^{|m|}$. Factorizing the asymptotic solutions, we make the ansatz for the total radial wave function

$$f_m(\rho)=\rho^{|m|}e^{-\rho/2}R(\rho). \tag{B.16}$$

Inserting this ansatz into Eqn. (B.13) leads to

$$\rho\frac{\partial^2R}{\partial\rho^2}+(2|m|+1-\rho)\frac{\partial R}{\partial\rho}+\left(\lambda-|m|-\frac{1}{2}\right)R=0. \tag{B.17}$$

To shorten the notation we introduce the quantities

$$p=2|m|,\qquad q=\lambda-|m|-\frac{1}{2}. \tag{B.18}$$

We can obtain the solution to Eqn. (B.17) by a power series expansion

$$R(\rho) = \sum_{\nu=0} \beta_\nu \rho^\nu. \tag{B.19}$$

By inserting this expansion into Eqn. (B.17) and comparing the coefficients of the different powers of ρ we get a recursive relation for the coefficients

$$\beta_{\nu+1} = \beta_\nu \frac{\nu - q}{(\nu+1)(\nu+p+1)}. \tag{B.20}$$

Of course, only a result that can be normalized has a physical meaning. Therefore, the series must terminate for some value $\nu = \nu_{max}$, so that all coefficients above this value vanish, i.e. $\beta_{\nu \geq \nu_{max}} = 0$. The condition $\nu_{max} - q = 0$ gives

$$\nu_{max} + |m| + \frac{1}{2} = \lambda \equiv n + \frac{1}{2}, \tag{B.21}$$

where the main quantum number n can assume the values $n = 0, 1, 2, \ldots$, respectively, for $|m| = \nu_{max} = 0$, $|m| = 1$ and $\nu_{max} = 0$ or $|m| = 0$ and $\nu_{max} = 1$, etc. As a matter of fact, we have derived the bound state energies: Combining Eqs. (B.8) and (B.21) yields the two-dimensional exciton bound state energies, as given in Eqn. (1.9).

The solution to the differential Eqn. (B.17) with integer numbers p and q can be expressed in terms of the associate Laguerre polynominals $L_q^p(\rho)$. Using these orthogonal Laguerre polynominals, the properly normalized two dimensional exciton wave functions can be written in general as

$$\phi_{n,m}(\mathbf{r}) = \sqrt{\frac{1}{\pi a_0^2 \left(n+\frac{1}{2}\right)^3} \frac{(n-|m|)!}{[(n+|m|)!]^3}} \rho^{|m|} e^{-\rho/2} L_{n+|m|}^{2|m|}(\rho)\, e^{im\varphi}, \tag{B.22}$$

where $\rho = 2r/[(n+1/2)\, a_0]$.

Appendix C

Derivation of the volume element for Hylleraas coordinates

In this appendix we will give a detailed derivation of the volume element in Hylleraas coordinates for a two dimensional problem. At the expense of mathematical elegance, but for reasons of intuitivity we choose a multi-step derivation. The ultimate goal is to find the volume element when one makes a variable transformation from Cartesian coordinates $\{\mathbf{r}_1, \mathbf{r}_2, \mathbf{r}_h\}$ to a set of coordinates $\{\mathbf{R}, \theta, s, t, u\}$, where $\mathbf{R}$ is the center of mass of the three-body system, θ marks the overall angle degree of freedom that doesn't affect the mutual distance between the particles and s, t, u are the Hylleraas coordinates. They are related to the three mutual in-plane distances between the particles r_{1h}, r_{2h}, r_{12} as

$$s = r_{1h} + r_{2h}, \qquad t = r_{1h} - r_{2h}, \qquad u = r_{12}. \tag{C.1}$$

Our starting point for this derivation is depicted in Fig. C.1.

In the first step we express the positions of the three particles in terms of the coordinates $\{\mathbf{R}, \theta, p, l, \phi\}$, where p is the distance between the hole and the center of

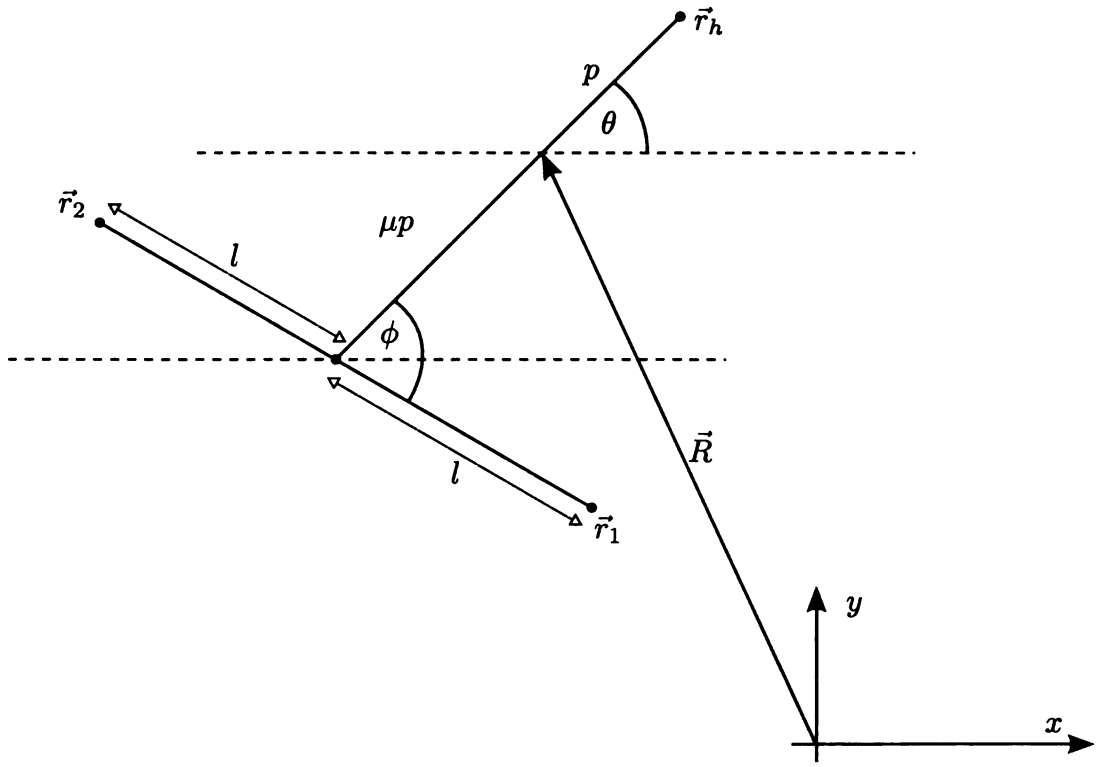

Figure C.1: Possible set of coordinates to describe a three body problem in two dimensions. The factor μ is given by $\mu = m_h^*/2m_e^*$.

mass of the three body system, l is the distance between one electron and the center of mass of the two electron system and ϕ is the angle around the center of mass of the two electrons, measured with respect to the line connecting the center of mass of the two electron and the hole's position. We can express the Cartesian coordinates in terms of this set of coordinates. The hole's position is given by

$$x_h = X + p\cos(\theta) \tag{C.2}$$

$$y_h = Y + p\sin(\theta), \tag{C.3}$$

while the positions of the two electrons are

$$x_1 = X - \frac{m_h^*}{2m_e^*}p\cos(\theta) + l\cos(\phi - \theta) \tag{C.4}$$

$$y_1 = Y - \frac{m_h^*}{2m_e^*}p\sin(\theta) - l\sin(\phi - \theta) \tag{C.5}$$

$$x_2 = X - \frac{m_h^*}{2m_e^*}p\cos(\theta) - l\cos(\phi - \theta) \tag{C.6}$$

$$y_2 = Y - \frac{m_h^*}{2m_e^*}p\sin(\theta) + l\sin(\phi - \theta). \tag{C.7}$$

The Jacobian for this variable transformation

$$d^2\mathbf{r}_1\, d^2\mathbf{r}_2\, d^2\mathbf{r}_h \rightarrow |M(\mathbf{R}, \theta, p, l, \phi)|\, d^2\mathbf{R}\, d\theta\, dp\, dl\, d\phi \tag{C.8}$$

is found to be

$$|M(\mathbf{R}, \theta, p, l, \phi)| = \begin{vmatrix} \frac{\partial x_h}{\partial X} & \frac{\partial x_h}{\partial Y} & \cdots & \frac{\partial x_h}{\partial \phi} \\ \frac{\partial y_h}{\partial X} & \ddots & & \vdots \\ \vdots & & \ddots & \vdots \\ \frac{\partial y_2}{\partial X} & \cdots & \cdots & \frac{\partial y_2}{\partial \phi} \end{vmatrix} = 4\left(1 + \frac{m_h^*}{2m_e^*}\right)^2 pl. \tag{C.9}$$

The next step is rather trivial: We introduce the coordinate $q = \left(1 + \frac{m_h^*}{2m_e^*}\right) p$, so that we obtain

$$d^2\mathbf{r}_1\, d^2\mathbf{r}_2\, d^2\mathbf{r}_h \rightarrow 4ql\, d^2\mathbf{R}\, d\theta\, dq\, dl\, d\phi. \tag{C.10}$$

Now, that we have already separated the center of mass $\mathbf{R}$ and the overall angle θ, we are left with expressing the coordinates $\{q, l, \phi\}$ in terms of the Hylleraas coordinates $\{s, t, u\}$. Before achieving this ultimate goal, we take one more intermediate step by writing $\{q, l, \phi\}$ in terms of the interparticle distances $\{r_{1h}, r_{2h}, u\}$. Using the law of cosines, we find the following relations

$$\begin{aligned} u &= 2l & \text{(C.11)} \\ r_{1h} &= \sqrt{l^2 + q^2 - 2lq\cos(\phi)} & \text{(C.12)} \\ r_{2h} &= \sqrt{l^2 + q^2 + 2lq\cos(\phi)}, & \text{(C.13)} \end{aligned}$$

where the identity $\cos(\pi - \phi) = -\cos(\phi)$ was used in the last line. Inverting these equations to solve for l, q and ϕ gives

$$\begin{aligned} l &= u/2 & \text{(C.14)} \\ q &= \sqrt{\frac{1}{2}\left(r_{1h}^2 + r_{2h}^2\right) - \frac{u^2}{4}} & \text{(C.15)} \\ \phi &= \arccos\left(\frac{r_{2h}^2 - r_{1h}^2}{u\sqrt{2\left(r_{1h}^2 + r_{2h}^2\right) - u^2}}\right). & \text{(C.16)} \end{aligned}$$

Making use of the relations $r_{1h}^2 + r_{2h}^2 = \frac{1}{2}\left(s^2 + t^2\right)$ and $r_{2h}^2 - r_{1h}^2 = -st$, the coordinates $\{q, l, \phi\}$ can be expressed in terms of the Hylleraas coordinates $\{s, t, u\}$ solely

as

$$l = u/2 \tag{C.17}$$

$$q = \frac{1}{2}\sqrt{s^2+t^2-u^2} \tag{C.18}$$

$$\phi = \arccos\left(-\frac{st}{u\sqrt{s^2+t^2-u^2}}\right). \tag{C.19}$$

We are now in a position to take the final step of this derivation

$$d^2\mathbf{r}_1\, d^2\mathbf{r}_2\, d^2\mathbf{r}_h \rightarrow 4J(s,t,u)\, q(s,t,u)\, l(s,t,u)\; d^2\mathbf{R}\, d\theta\, ds\, dt\, du. \tag{C.20}$$

The Jacobian for this transformation is

$$4J(s,t,u) = 4\begin{vmatrix} \frac{\partial l}{\partial s} & \frac{\partial l}{\partial t} & \frac{\partial l}{\partial u} \\ \frac{\partial q}{\partial s} & \frac{\partial q}{\partial t} & \frac{\partial q}{\partial u} \\ \frac{\partial \phi}{\partial s} & \frac{\partial \phi}{\partial t} & \frac{\partial \phi}{\partial u} \end{vmatrix} = \frac{s^2-t^2}{u\left(s^2+t^2-u^2\right)\sqrt{1-\frac{s^2t^2}{u^2\left(s^2+t^2-u^2\right)}}}, \tag{C.21}$$

so that we can readily deduce

$$4J(s,t,u)\, q(s,t,u)\, l(s,t,u) = \frac{1}{4}\frac{u\left(s^2-t^2\right)}{\sqrt{\left(s^2-u^2\right)\left(u^2-t^2\right)}}. \tag{C.22}$$

If the integrand is symmetric in t, as in our case, we can restrict ourselves to positive values of t only, multiplying the volume element by a factor of two. Finally, we state the result

$$d^2\mathbf{r}_1\, d^2\mathbf{r}_2\, d^2\mathbf{r}_h \rightarrow \frac{u\left(s^2-t^2\right)}{2\sqrt{\left(s^2-u^2\right)\left(u^2-t^2\right)}}\, d^2\mathbf{R}\, d\theta\, ds\, dt\, du \tag{C.23}$$

with the limits of integration for the Hylleraas coordinates

$$s \geq 0, \quad 0 \leq u \leq s, \quad 0 \leq t \leq u. \tag{C.24}$$

Our result for the volume element $d\tau$ agrees with the one given in [22], where the specific case of an integrand independent of θ was assumed. In this case, the integration over θ can be performed right away yielding a factor of 2π. We can confirm their result

$$d\tau = \pi \frac{u\left(s^2 - t^2\right)}{\sqrt{\left(s^2 - u^2\right)\left(u^2 - t^2\right)}} ds\, dt\, du. \tag{C.25}$$

Appendix D

Results of variational calculus

In this appendix we give a detailed presentation of our results for the variational calculation of the trion binding energy. Based on the trial wave function, given by Eqn. (1.26), the expectation value for the 'relative' Hamiltonian $\langle H_T(\alpha,\beta,\gamma)\rangle$ has been solved analytically. We have found that it obeys the following analytic expression

$$\begin{aligned}\langle H_T\rangle \;=\; & \Big\{\alpha\Big[9(55\pi-2048)\gamma^2+1024\alpha^5(1+\sigma)+\\ & +1024\Big((2-3\pi)\beta+2\beta^2(1+\sigma)+2\gamma(1+\sigma)\Big)+\\ & +128\alpha\gamma((16-45\pi)\beta+68\gamma(1+\sigma))\\ & +4\alpha^2\Big(8\beta^2(15\pi-256)+4\gamma(21\pi-512)+3\pi\beta\gamma(127+120\sigma)\Big)+\\ & 64\alpha^4(3\pi(2+3\beta+4\beta\sigma)-64)\Big]\Big\}/\\ & \Big(64\alpha^2\Big(16\alpha^2+15\pi\alpha\beta+48\beta^2\Big)+4\alpha\gamma(512\alpha+405\pi\beta)+4608\gamma^2\Big),\end{aligned}$$

where the effective mass ratio σ enters as an external parameter. In a subsequent step we have minimized this function with respect to the variables α, β, γ. The results are presented in Fig. (D.1).

Moreover, let us mention a trick commonly referred to in the literature in the context of this type of trial wavefunction to simplify the minimization process [25, 28].

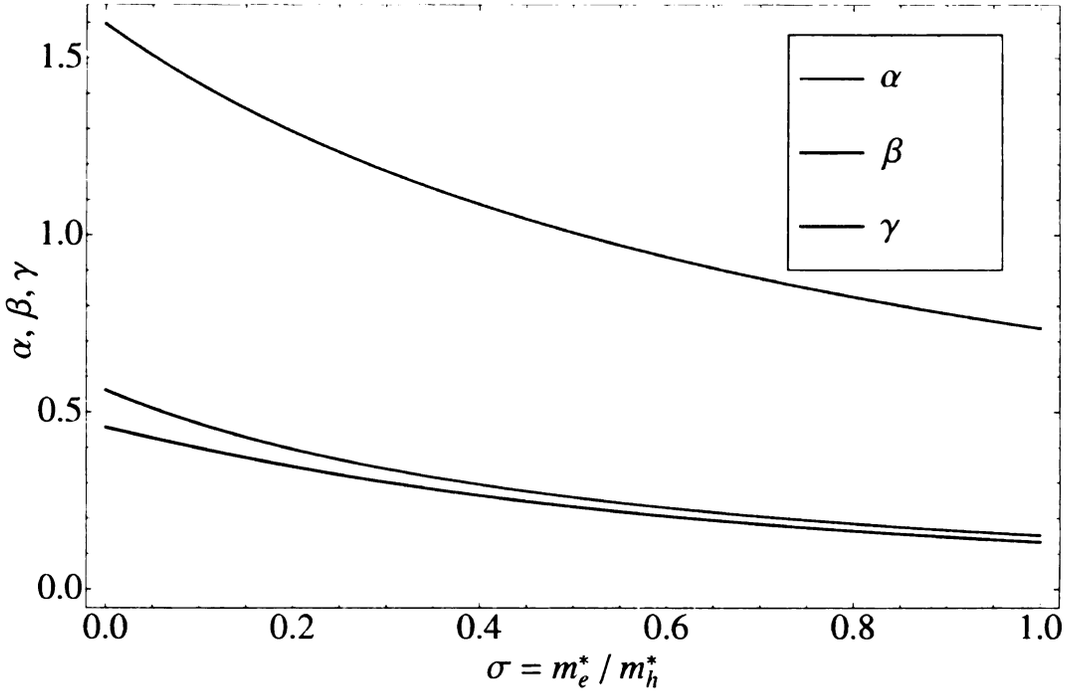

Figure D.1: Numerical results for variational parameters α, β, γ in atomic units.

Omitting the normalization for the moment, one can rescale all the arguments in the general form of $\varphi_b(s,t,u)$ as

$$e^{-\alpha s}\left(1+\beta u+\gamma t^2\right) \rightarrow e^{-s'/2}\left(1+C_1 u'^2+C_2 t'^2\right)=\tilde{\varphi}_b\left(s',t',u'\right) \tag{D.1}$$

with the scaling factor $k=2\alpha$. The parameters C_1 and C_2 are linked to the parameters α, β and γ by the relations

$$C_1=\frac{\beta}{2\alpha}=\frac{\beta}{k}, \qquad C_2=\frac{\gamma}{4\alpha^2}=\frac{\gamma}{k^2} \tag{D.2}$$

i.e. they absorb the scaling factor k. This scaling factor is often referred to as "effective charge". If one substitutes $\tilde{\varphi}_b(s,t,u)$ into the original expectation value

$\langle H_T \rangle$, one obtains the compact form

$$E_T = \frac{k^2 M - kL}{N}, \tag{D.3}$$

with the abbreviations

$$L = \int_0^\infty ds \int_0^s du \int_0^u dt \frac{u\left(s^2-t^2\right)}{2\sqrt{\left(s^2-u^2\right)\left(u^2-t^2\right)}} \left[\frac{4t}{s^2-t^2} - \frac{1}{u}\right] \tilde{\varphi}_b^2 \tag{D.4}$$

$$\begin{aligned} M = \int_0^\infty ds \int_0^s du \int_0^u dt \frac{u\left(s^2-t^2\right)}{2\sqrt{\left(s^2-u^2\right)\left(u^2-t^2\right)}} \tilde{\varphi}_b \Bigg[& -\frac{\partial^2}{\partial s^2} - \frac{\partial^2}{\partial t^2} \\ & -\frac{2}{s^2-t^2}\left(s\partial_s - t\partial_t\right) - \frac{\partial^2}{\partial u^2} - \frac{1}{u}\partial_u \\ & -\frac{2s\left(u^2-t^2\right)}{u\left(s^2-t^2\right)}\partial_{su}^2 - \frac{2t\left(s^2-u^2\right)}{u\left(s^2-t^2\right)}\partial_{tu}^2 \Bigg] \tilde{\varphi}_b \end{aligned} \tag{D.5}$$

$$N = \int_0^\infty ds \int_0^s du \int_0^u dt \frac{u\left(s^2-t^2\right)}{2\sqrt{\left(s^2-u^2\right)\left(u^2-t^2\right)}} \tilde{\varphi}_b^2 \tag{D.6}$$

The expressions L, M and N are quadratic in the coefficients C_1 and C_2 only. Due to Eqn. (D.3), E_T also depends on k. The essential idea is to minimize E_T with respect to k in the first place, which is immediately satisfied by

$$k = \frac{L}{2M}, \tag{D.7}$$

which yields the minimum E_T to solely depend on the parameters C_1 and C_2 as

$$E = -\frac{L^2}{4MN}. \tag{D.8}$$

Our results for the scaled variational parameters C_1 and C_2 are shown in Fig. (D.2). They are in perfect agreement with previous theoretical investigations [28].

The optimized variational parameters for the specific QW systems $GaAs$ and

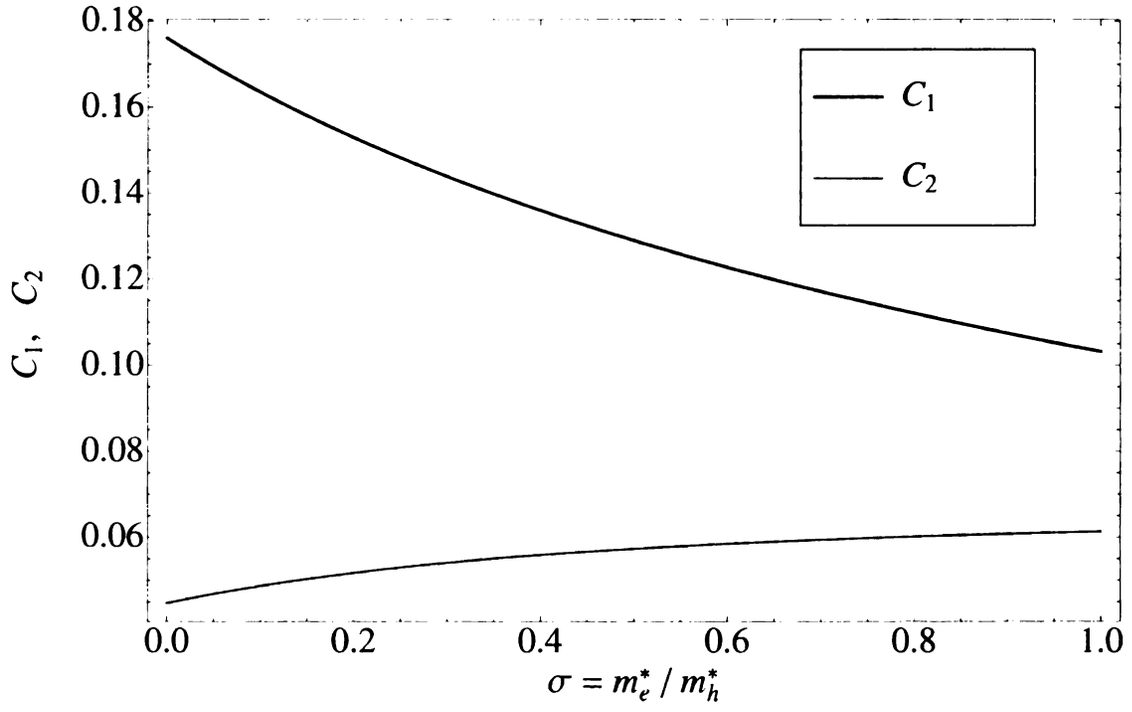

Figure D.2: Numerical results for variational parameters C_1 and C_2 in atomic units.

$CdTe$ are summarized in Tab (D.1).

Variational parameters	$GaAs$	$CdTe$
α	1.293	1.008
β	0.396	0.260
γ	0.347	0.233
C_1	0.153	0.129
C_2	0.052	0.057

Table D.1: Variational parameters for $GaAs$ and $CdTe$ in atomic units.

Appendix E

Exchange effects

In this section we will highlight the exchange effects that arise from a proper symmetrization of the wavefunctions describing the bound and unbound trion states. In the first part, we will show that exchange can be neglected when computing the transition matrix element from a free electron to a the unbound exciton continuum, whenever the sample size A is macroscopic. In the second part, we give a detailed derivation for the overlap between the bound and unbound trion states, which is a key ingredient for the orthonormalization procedure. In the course of the derivation, we present in detail the approximations we made to neglect the exchange effects.

E.1 Exchange effects in the coupling to unbound trions

The properly symmetrized version of the continuum wavefunction for an exciton with momentum $\mathbf{k}_x$ and a free electron with momentum $\mathbf{k}$ is given by

$$\begin{aligned}\Psi_c(\mathbf{r}_1,\mathbf{r}_2,\mathbf{r}_h) &= \frac{\mathfrak{N}}{\sqrt{2}A}\Big[e^{i\mathbf{k}_x(\alpha_e\mathbf{r}_1+\alpha_h\mathbf{r}_h)}e^{i\mathbf{k}\mathbf{r}_2}\phi_{1s}(\mathbf{r}_1-\mathbf{r}_h)\\ &\quad \pm e^{i\mathbf{k}_x(\alpha_e\mathbf{r}_2+\alpha_h\mathbf{r}_h)}e^{i\mathbf{k}\mathbf{r}_1}\phi_{1s}(\mathbf{r}_2-\mathbf{r}_h)\Big] \qquad \text{(E.1)}\end{aligned}$$

where $\alpha_{e/h} = m^*_{e/h}/m_x$ are the mass ratios of the effective mass of the electron / hole to the exciton mass. The upper sign renders an even orbital wavefunction, corresponding to a spin singlet state, while the lower sign represents an odd orbital wavefunction and is therefore only valid in combination with a spin triplet state. Note that, in contrast to the standard textbook examples, this symmetrized ansatz is not built upon a set of separable orthonormal basis wavefunctions. This circumstance leads to the occurrence of the normalization constant $\mathfrak{N}$, which we will discuss below. Proceeding from our ansatz, the wavefunction at the moment of photocreation is

$$\begin{aligned}\Psi_c\left(\mathbf{r},\mathbf{r}',\mathbf{r}\right) &= \frac{\mathfrak{N}}{\sqrt{2}A}\Big[e^{i\mathbf{k}_x(\alpha_e\mathbf{r}+\alpha_h\mathbf{r})}e^{i\mathbf{k}\mathbf{r}'}\phi_{1s}\left(\mathbf{r}-\mathbf{r}\right) \\ &\quad \pm e^{i\mathbf{k}_x\left(\alpha_e\mathbf{r}'+\alpha_h\mathbf{r}\right)}e^{i\mathbf{k}\mathbf{r}}\phi_{1s}\left(\mathbf{r}'-\mathbf{r}\right)\Big] \qquad \text{(E.2)} \\ &= \frac{\mathfrak{N}}{\sqrt{2}A}\left[e^{i\mathbf{k}_x\mathbf{r}}e^{i\mathbf{k}\mathbf{r}'}\phi_{1s}\left(0\right) \pm e^{i(\alpha_h\mathbf{k}_x+\mathbf{k})\mathbf{r}}e^{i\alpha_e\mathbf{k}_x\mathbf{r}'}\phi_{1s}\left(\mathbf{r}'-\mathbf{r}\right)\right] \qquad \text{(E.3)}\end{aligned}$$

Inserting this expression into Eqn. (1.46) gives the transition amplitude

$$\begin{aligned}\left\langle\mathbf{k}_e\right|\mathcal{H}_{int}\left|\mathbf{k}_x,\mathbf{k}\right\rangle_c &= \frac{\Omega_0}{2}\frac{\mathfrak{N}}{\sqrt{2}}\Big\{\phi_{1s}\left(0\right)\sqrt{A}\delta_{\mathbf{k}_e,\mathbf{k}}\left[\delta_{\mathbf{k}_x,\mathbf{Q}}+\delta_{\mathbf{k}_x,-\mathbf{Q}}\right] \\ &\quad \pm\frac{1}{A^{3/2}}\int d^2\mathbf{r}\,d^2\mathbf{r}'\,e^{-i(\alpha_h\mathbf{k}_x+\mathbf{k})\mathbf{r}}e^{-i\alpha_e\mathbf{k}_x\mathbf{r}'}\phi^*_{1s}\left(\mathbf{r}'-\mathbf{r}\right) \\ &\quad \times e^{i\mathbf{k}_e\mathbf{r}'}\left[e^{i\mathbf{Q}\mathbf{r}}+e^{-i\mathbf{Q}\mathbf{r}}\right]\Big\} \qquad \text{(E.4)}\end{aligned}$$

The first line gives the direct term with the exciton wavefunction taken at zero. Note that it scales extensively with the sample size. To calculate the second line, we introduce the variable transformation

$$\mathbf{r}' \rightarrow \boldsymbol{\rho} = \mathbf{r}-\mathbf{r}' \qquad \text{(E.5)}$$

which leads to

$$\frac{1}{A^{3/2}}\int d^2\mathbf{r}\, d^2\boldsymbol{\rho}\, e^{-i(\alpha_h \mathbf{k}_x+\mathbf{k})\mathbf{r}} e^{i(\mathbf{k}_e-\alpha_e\mathbf{k}_x)(\mathbf{r}-\boldsymbol{\rho})}\phi^*_{1s}(\rho)\left[e^{i\mathbf{Q}\mathbf{r}}+e^{-i\mathbf{Q}\mathbf{r}}\right] \tag{E.6}$$

so that the two integrals can be separated

$$\frac{1}{A^{3/2}}\int d^2\mathbf{r}\, e^{i(\mathbf{k}_e-\mathbf{k}_x-\mathbf{k}\pm\mathbf{Q})\mathbf{r}}\int d^2\boldsymbol{\rho}\, e^{i(\alpha_e\mathbf{k}_x-\mathbf{k}_e)\boldsymbol{\rho}}\phi^*_{1s}(\rho) \tag{E.7}$$

The first one simply imposes conservation of total momentum

$$\frac{1}{A^{1/2}}\delta_{\mathbf{k}_e\pm\mathbf{Q},\mathbf{k}_x+\mathbf{k}}\int d^2\boldsymbol{\rho}\, e^{i(\alpha_e\mathbf{k}_x-\mathbf{k}_e)\boldsymbol{\rho}}\phi^*_{1s}(\rho) \tag{E.8}$$

Then, we are left with evaluating the Fourier transform of the relative $1s$ wavefunction. With $\mathbf{q}=\alpha_e\mathbf{k}_x-\mathbf{k}_e$, we obtain

$$\begin{aligned}\int d^2\boldsymbol{\rho}\, e^{i\mathbf{q}\boldsymbol{\rho}}\phi^*_{1s}(\rho) &= \int_0^\infty d\rho\,\rho\phi^*_{1s}(\rho)\int_0^{2\pi} d\varphi\, e^{iq\rho\cos(\varphi)} &\text{(E.9)}\\ &= 2\pi\int_0^\infty d\rho\,\rho\phi^*_{1s}(\rho)\,J_0(q\rho) &\text{(E.10)}\end{aligned}$$

where $J_0(q\rho)$ is the Bessel function of the first kind. Inserting the normalized $1s$ wavefunction

$$\phi^*_{1s}(\rho)=\sqrt{\frac{2}{\pi a_x^2}}e^{-\rho/a_x} \tag{E.11}$$

leads to

$$\int d^2\boldsymbol{\rho}\, e^{i\mathbf{q}\boldsymbol{\rho}}\phi^*_{1s}(\boldsymbol{\rho})=2\sqrt{2\pi}\frac{a_x}{\left[1+a_x^2q^2\right]^{3/2}} \tag{E.12}$$

Therefore, the contribution to the continuum transition amplitude that comes from the exchange term is in total

$$\Omega_0 \mathfrak{N} \delta_{\mathbf{k}_e \pm \mathbf{Q}, \mathbf{k}_x + \mathbf{k}} \frac{a_x}{L} \frac{\sqrt{\pi}}{\left[1 + a_x^2 \left|\alpha_e \mathbf{k}_x - \mathbf{k}_e\right|^2\right]^{3/2}} \tag{E.13}$$

Clearly, it vanishes for a macroscopic sample, where $L = \sqrt{A} \gg a_x$. The importance of exchange is therefore limited to a small, finite range. At the same time, we have seen that the contribution from the direct term in Eqn. (E.4) scales extensively as L/a_x. Consequently, the direct term outnumbers the exchange term by a factor of $\sim A/a_x^2$.

Let us address the proper normalization of $\mathfrak{N}$ of our ansatz in Eqn. (E.1). For convenience, we change variables according to

$$\{\mathbf{r}_1, \mathbf{r}_2, \mathbf{r}_h\} \rightarrow \{\mathbf{r}, \boldsymbol{\rho}, \mathbf{r}_h\} \tag{E.14}$$

$$\mathbf{r} = \mathbf{r}_1 - \mathbf{r}_h \tag{E.15}$$

$$\boldsymbol{\rho} = \mathbf{r}_2 - \mathbf{r}_h \tag{E.16}$$

Note that under exchange of the two indistinguishable electrons the coordinates $\mathbf{r}$ and $\boldsymbol{\rho}$ flip: $\mathbf{r} \leftrightarrow \boldsymbol{\rho}$. Expressed in terms of these new coordinates, the square of $\Psi_c(\mathbf{r}_1, \mathbf{r}_2, \mathbf{r}_h)$ becomes

$$\begin{aligned} \left|\Psi_c(\mathbf{r}, \boldsymbol{\rho}, \mathbf{r}_h)\right|^2 = \frac{\mathfrak{N}^2}{2A^2} \Big\{ & \left|\phi_{1s}(\mathbf{r})\right|^2 + \left|\phi_{1s}(\boldsymbol{\rho})\right|^2 \\ & \pm e^{i(\alpha_e \mathbf{k}_x - \mathbf{k}_e)\mathbf{r}} \phi_{1s}(r)\, e^{-i(\alpha_e \mathbf{k}_x - \mathbf{k}_e)\boldsymbol{\rho}} \phi_{1s}^*(\rho) \\ & \pm e^{-i(\alpha_e \mathbf{k}_x - \mathbf{k}_e)\mathbf{r}} \phi_{1s}^*(r)\, e^{i(\alpha_e \mathbf{k}_x - \mathbf{k}_e)\boldsymbol{\rho}} \phi_{1s}(\rho) \Big\} \end{aligned} \tag{E.17}$$

We examine the normalization condition by integrating over $\{\mathbf{r}, \boldsymbol{\rho}, \mathbf{r}_h\}$. The first two terms inside the bracket give A^2, since they are normalized with respect to one

coordinate $\mathbf{r}$ and $\boldsymbol{\rho}$ respectively. In the last two terms, we can switch the dummy integration variables $\mathbf{r}$ and $\boldsymbol{\rho}$ to combine these two terms. Therefore, we obtain

$$\begin{aligned}\int d^2\mathbf{r}_h d^2\mathbf{r} d^2\boldsymbol{\rho} \left|\Psi_c(\mathbf{r},\boldsymbol{\rho},\mathbf{r}_h)\right|^2 &= \mathfrak{N}^2\left\{1 \pm \frac{1}{A}\int d^2\mathbf{r} e^{i\mathbf{q}\mathbf{r}}\phi_{1s}(r)\int d^2\boldsymbol{\rho} e^{-i\mathbf{q}\boldsymbol{\rho}}\phi_{1s}^*(\rho)\right\} \\ &= \mathfrak{N}^2\left\{1 \pm \frac{1}{A}\left|\int d^2\mathbf{r} e^{i\mathbf{q}\mathbf{r}}\phi_{1s}(r)\right|^2\right\} \qquad \text{(E.18)}\end{aligned}$$

where we again used the foe convenience $\mathbf{q} = \alpha_e\mathbf{k}_x - \mathbf{k}_e$. We recognize an additional term which is basically the Fourier transform of the $1s$ wavefunction. Performing the integral, we find

$$\int d^2\mathbf{r}_h d^2\mathbf{r} d^2\boldsymbol{\rho} \left|\Psi_c(\mathbf{r},\boldsymbol{\rho},\mathbf{r}_h)\right|^2 = \mathfrak{N}^2\left\{1 \pm \frac{\pi a_x^2}{A}\frac{8}{\left(1+a_x^2q_x^2\right)^3}\right\} \qquad \text{(E.19)}$$

so that the result for $\mathfrak{N}$ reads

$$\mathfrak{N} = 1/\sqrt{1 \pm \frac{\pi a_x^2}{A}\frac{8}{\left(1+a_x^2q_x^2\right)^3}} \qquad \text{(E.20)}$$

The exchange contribution is of the order $\mathcal{O}\left(a_x^2/A\right)$ and thus usually very small and can easily be neglected in the large sample limit:

$$A \gg a_x: \quad \mathfrak{N} \approx 1 \qquad \text{(E.21)}$$

In conclusion of this section, we have shown that for the transition amplitude of a single electron to the excitonic continuum exchange effects can be easily neglected in the limit of a macroscopic sample.

E.2 Exchange effects in the overlap

In this section, we are going to present a detailed calculation of the overlap between the symmetrized continuum, consisting of a bound $1s$ exciton and a free electron,

$$\begin{aligned}\Psi_c(\mathbf{r}_1,\mathbf{r}_2,\mathbf{r}_h) &= \frac{\mathfrak{N}}{\sqrt{2}A}\Big\{e^{i\mathbf{k}_x(\alpha_e\mathbf{r}_1+\alpha_h\mathbf{r}_h)}e^{i\mathbf{k}_e\mathbf{r}_2}\phi_{1s}(\mathbf{r}_1-\mathbf{r}_h)\\ &\quad \pm e^{i\mathbf{k}_x(\alpha_e\mathbf{r}_2+\alpha_h\mathbf{r}_h)}e^{i\mathbf{k}_e\mathbf{r}_1}\phi_{1s}(\mathbf{r}_2-\mathbf{r}_h)\Big\} \qquad \text{(E.22)}\end{aligned}$$

and the bound trion states. In order to estimate the overlap in a tractable way, we do not apply the variational Hylleraas relative wavefunction in this context, but model the binding of the trion complex as the combination of one stronger bound electron with the relative wavefunction ϕ_{1s} and a more weakly bound second electron with the relative wavefunction φ; both ϕ_{1s} and φ are taken along the corresponding hole - electron coordinate. Therefore, we describe the bound trions as

$$\begin{aligned}\Psi_t(\mathbf{r}_1,\mathbf{r}_2,\mathbf{r}_h) &= \frac{\mathsf{N}}{\sqrt{2}A}\Big\{e^{i\mathbf{K}(\beta_e\mathbf{r}_1+\beta_e\mathbf{r}_2+\beta_h\mathbf{r}_h)}\phi_{1s}(\mathbf{r}_1-\mathbf{r}_h)\,\varphi(\mathbf{r}_2-\mathbf{r}_h)\\ &\quad \pm e^{i\mathbf{K}(\beta_e\mathbf{r}_2+\beta_e\mathbf{r}_1+\beta_h\mathbf{r}_h)}\phi_{1s}(\mathbf{r}_2-\mathbf{r}_h)\,\varphi(\mathbf{r}_1-\mathbf{r}_h)\Big\} \qquad \text{(E.23)}\end{aligned}$$

The residual factor N takes into account that this symmetrized ansatz is not built upon the slater determinant of a set of orthonormal basis wavefunctions. We will give an explicit expression for N later on. The calculation of the overlap is simplified in the coordinates $\{\mathbf{R},\mathbf{r},\boldsymbol{\rho}\}$ with the three particle center of mass

$$\mathbf{R} = \beta_e\mathbf{r}_1+\beta_e\mathbf{r}_2+\beta_h\mathbf{r}_h \qquad \text{(E.24)}$$

in which the wavefunctions for the continuum and the bound trions respectively read

$$\Psi_c(\mathbf{R},\mathbf{r},\boldsymbol{\rho}) = \frac{\mathfrak{N}}{\sqrt{2}A}e^{i(\mathbf{k}_x+\mathbf{k}_e)\mathbf{R}}\Big\{e^{i\mathbf{p}\mathbf{r}}e^{i\mathbf{q}\boldsymbol{\rho}}\phi_{1s}(r)\pm e^{i\mathbf{q}\mathbf{r}}e^{i\mathbf{p}\boldsymbol{\rho}}\phi_{1s}(\rho)\Big\} \qquad \text{(E.25)}$$

and

$$\Psi_t(\mathbf{R},\mathbf{r},\boldsymbol{\rho}) = \frac{\mathsf{N}}{\sqrt{2A}} e^{i\mathbf{K}\mathbf{R}} \left\{\phi_{1s}(r)\,\varphi(\rho) \pm \phi_{1s}(\rho)\,\varphi(r)\right\} \tag{E.26}$$

Here, for the sake of a more compact notation we introduced the quantities

$$\mathbf{p} = \beta_e(\alpha_e\mathbf{k}_x - \mathbf{k}_e) = \alpha_e(\beta_e\mathbf{K} - \mathbf{k}_e) \tag{E.27}$$

$$\mathbf{q} = \beta_x\mathbf{k}_e - \beta_e\mathbf{k}_x = \mathbf{k}_e - \beta_e\mathbf{K} \tag{E.28}$$

where we already used in the last step that the total momenta of the continuum and bound trion states have to be the same to have a nonzero overlap, i.e. $\mathbf{K} = \mathbf{k}_x + \mathbf{k}_e$.

Now, let us turn to the calculation of the overlap between Ψ_c and Ψ_t. As far as the bound trion states are concerned, we only consider spin singlet states. Consequently, Ψ_t has to be even under particle exchange, i.e. we pick up the upper plus sign. To have a nonzero overlap, the spin functions have to match, so that also for the continuum states Ψ_c we pick up the plus sign, corresponding to a singlet state of the two electrons.

In the first step, the integration over the center of mass coordinate $\mathbf{R}$ gives the condition on the total momentum mentioned above. Assuming $\varphi(\rho)$ to be real valued, we have

$$\begin{aligned}\langle\Psi_t|\Psi_c\rangle &= \frac{\mathfrak{N}\mathsf{N}}{2\sqrt{A}}\delta_{\mathbf{K},\mathbf{k}_x+\mathbf{k}_e}\int d^2\mathbf{r}d^2\boldsymbol{\rho}\,\left[\phi_{1s}(r)\,\varphi(\rho)+\phi_{1s}(\rho)\,\varphi(r)\right] \\ &\quad\times\left[e^{i\mathbf{p}\mathbf{r}}e^{i\mathbf{q}\boldsymbol{\rho}}\phi_{1s}(r)+e^{i\mathbf{q}\mathbf{r}}e^{i\mathbf{p}\boldsymbol{\rho}}\phi_{1s}(\rho)\right]\end{aligned} \tag{E.29}$$

By relabeling the integration variables, we can simplify this expression to one direct

and one exchange term

$$\begin{aligned}\langle\Psi_c|\Psi_t\rangle &= \frac{\mathfrak{N}\mathsf{N}}{\sqrt{A}}\delta_{\mathbf{K},\mathbf{k}_x+\mathbf{k}_e}\left\{\int d^2\mathbf{r}\, e^{i\mathbf{p}\mathbf{r}}\left|\phi_{1s}(r)\right|^2\int d^2\boldsymbol{\rho}e^{i\mathbf{q}\boldsymbol{\rho}}\varphi(\rho)\right.\\ &\left.+\int d^2\mathbf{r}\, e^{i\mathbf{p}\mathbf{r}}\phi_{1s}(r)\,\varphi(r)\int d^2\boldsymbol{\rho}e^{i\mathbf{q}\boldsymbol{\rho}}\phi_{1s}(\rho)\right\}\end{aligned} \tag{E.30}$$

In the following, the momentum conservation is assumed to be fulfilled implicitly and we label the overlap by the total momentum $\mathbf{K}$ and the electron momentum $\mathbf{k}_e$ as $\mathcal{O}(\mathbf{K},\mathbf{k}_e)$. To better distinguish between the direct and the exchange contributions, we split $\mathcal{O}(\mathbf{K},\mathbf{k}_e)$ as

$$\mathcal{O}(\mathbf{K},\mathbf{k}_e)=\mathcal{O}_d(\mathbf{K},\mathbf{k}_e)+\mathcal{O}_{ex}(\mathbf{K},\mathbf{k}_e) \tag{E.31}$$

with

$$\mathcal{O}_d(\mathbf{K},\mathbf{k}_e) = \frac{\mathfrak{N}\mathsf{N}}{\sqrt{A}}\int d^2\mathbf{r}\, e^{i\mathbf{p}\mathbf{r}}\left|\phi_{1s}(r)\right|^2\int d^2\boldsymbol{\rho}e^{i\mathbf{q}\boldsymbol{\rho}}\varphi(\rho) \tag{E.32}$$

$$\mathcal{O}_{ex}(\mathbf{K},\mathbf{k}_e) = \frac{\mathfrak{N}\mathsf{N}}{\sqrt{A}}\int d^2\mathbf{r}\, e^{i\mathbf{p}\mathbf{r}}\phi_{1s}(r)\,\varphi(r)\int d^2\boldsymbol{\rho}e^{i\mathbf{q}\boldsymbol{\rho}}\phi_{1s}(\rho) \tag{E.33}$$

To proceed with our analysis, we have to specify the form of the wavefunction $\varphi(r)$. For the sake of simplicity we assume a $1s$ wavefunction

$$\varphi(r)=\sqrt{\frac{2}{\pi a_t^2}}e^{-r/a_t} \tag{E.34}$$

with a_t characterizing the "trion size"; $\phi_{1s}(r)$ was assumed to be the same for the continuum and the bound trions

$$\phi_{1s}(r)=\sqrt{\frac{2}{\pi a_x^2}}e^{-r/a_x} \tag{E.35}$$

Carrying out the integrals, we find the following analytic expressions for the overlap

$$\mathcal{O}_d\left(\mathbf{K},\mathbf{k}_e\right)=\frac{\mathfrak{N}\mathsf{N}}{\sqrt{A}}\frac{8}{\left(4+a_x^2p^2\right)^{3/2}}\frac{2\sqrt{2\pi a_t^2}}{\left(1+a_t^2q^2\right)^{3/2}} \tag{E.36}$$

and

$$\mathcal{O}_{ex}\left(\mathbf{K},\mathbf{k}_e\right)=\frac{\mathfrak{N}\mathsf{N}}{\sqrt{A}}\frac{8}{\left(1+a_x^2q^2\right)^{3/2}}\frac{\sqrt{2\pi a_x^2}a_xa_t\left(a_x+a_t\right)}{\left(\left(a_x+a_t\right)^2+a_x^2a_t^2p^2\right)^{3/2}} \tag{E.37}$$

Let us compare the overlap $\mathcal{O}_d\left(\mathbf{K},\mathbf{k}_e\right)$ to $\mathcal{O}_{ex}\left(\mathbf{K},\mathbf{k}_e\right)$. Both decrease with increasing momenta $\mathbf{p}$ and $\mathbf{q}$. Very interestingly, the magnitudes of both $\mathbf{p}$ and $\mathbf{q}$ are proportional to $\beta_e\mathbf{K}-\mathbf{k}_e$, which, due to $\mathbf{K}=\mathbf{Q}+\mathbf{k}_e$, can be equivalently expressed as $\beta_e\mathbf{Q}-\beta_x\mathbf{k}_e$. This is exactly the relative motion momentum that determined the momentum dependence of the optical matrix elements (see (1.48) and (1.49)). At maximum, if the relative motion momentum $\mathbf{p}_i=\beta_x\mathbf{k}_e-\beta_e\mathbf{Q}$ is zero, $\mathcal{O}_d\left(\mathbf{K},\mathbf{k}_e\right)$ and $\mathcal{O}_{ex}\left(\mathbf{K},\mathbf{k}_e\right)$ show the following scaling behaviours

$$\mathcal{O}_d\left(\mathbf{p}_i=0\right)\sim\frac{a_t}{L} \tag{E.38}$$

and

$$\mathcal{O}_{ex}\left(\mathbf{p}_i=0\right)\sim\left(\frac{a_x}{L}\right)^2\frac{1}{\left(1+a_x/a_t\right)^2}\frac{a_t}{L} \tag{E.39}$$

which shows that the exchange contribution is considerably smaller, by more than a factor of a_x^2/A: this is nothing but the microscopic exciton size over the macroscopic sample size and therefore a very small number. In the spirit of $a_x/L\rightarrow 0$, we can focus our analysis on the direct term. We have obtained

$$\mathcal{O}_d\left(\mathbf{K},\mathbf{k}_e\right)=\mathfrak{N}\mathsf{N}\sqrt{\frac{\pi a_t^2}{A}}\frac{16\sqrt{2}}{\left(4+a_x^2\alpha_e^2\left|\beta_e\mathbf{K}-\mathbf{k}_e\right|^2\right)^{3/2}\left(1+a_t^2\left|\beta_e\mathbf{K}-\mathbf{k}_e\right|^2\right)^{3/2}} \tag{E.40}$$

We can make further simplification by using the following approximations: First of all, $\alpha_e = m_e^*/m_x$ is relatively small, since the effective masses of the holes are usually much bigger than the effective masses of the electrons. Moreover, we know that the typical trion size a_t is considerably bigger than the exciton size a_x due to the weaker binding. In this limit, we find

$$\mathcal{O}_d\left(\mathbf{K},\mathbf{k}_e\right) \approx \mathfrak{N}\mathsf{N}\sqrt{\frac{\pi a_t^2}{A}}\frac{2\sqrt{2}}{\left(1+a_t^2\left|\beta_e\mathbf{K}-\mathbf{k}_e\right|^2\right)^{3/2}} \tag{E.41}$$

Let us address the normalization constants in front: We have already shown in Eqn. (E.20) that $\mathfrak{N}$ tends to one in the macroscopic limit. However, we have not specified N so far. We are going to make up for that shortcoming now. In analogy to our normalization procedure to find $\mathfrak{N}$, for the bound trion states we obtain

$$\int d^2\mathbf{R}d^2\mathbf{r}d^2\boldsymbol{\rho}\left|\Psi_t\left(\mathbf{R},\mathbf{r},\boldsymbol{\rho}\right)\right|^2 = \mathsf{N}^2\left[1+\left|\int d^2\mathbf{r}\,\phi_{1s}\left(\mathbf{r}\right)\varphi\left(\mathbf{r}\right)\right|^2\right] \tag{E.42}$$

which leads us to

$$\int d^2\mathbf{R}d^2\mathbf{r}d^2\boldsymbol{\rho}\left|\Psi_t\left(\mathbf{R},\mathbf{r},\boldsymbol{\rho}\right)\right|^2 = \mathsf{N}^2\left[1+16\frac{a_x^2a_t^2}{\left(a_x+a_t\right)^4}\right] \tag{E.43}$$

The trion is spatially more diffusive than the exciton and in the limit $a_t \gg a_x$ the correction term is much smaller than one and, subsequently, N is approximately one. Using these simplifications, we find that the overlap between the bound trion states and the continuum states is approximately given by

$$\mathcal{O}_d\left(\mathbf{K},\mathbf{k}_e\right) \approx \sqrt{\frac{\pi a_t^2}{A}}\frac{2\sqrt{2}}{\left(1+a_t^2\left|\beta_e\mathbf{K}-\mathbf{k}_e\right|^2\right)^{3/2}} \tag{E.44}$$

It is intrinsically small and depends on the relative motion momentum $\mathbf{p}_i$.

Appendix F

Trion radiative lifetime

In this appendix we present a calculation that gives an approximative analytical form for the radiative decay rate Γ_t of a bound trion. First of all we fix the spin configuration of the initial trion singlet state. We specifically refer to a trion consisting of a heavy hole with spin $\sigma_{hh} = -3/2$ and an electron singlet. Subsequently, it decays radiatively to a σ_- photon and an free electron with spin down $\downarrow$.

Let us analyze the decay process in the usual lab frame first: The initial state consists of a singlet trion with total momentum $\mathbf{K}$, which we denote as

$$|i\rangle = |\mathbf{K}\rangle_t \,. \tag{F.1}$$

The corresponding initial energy is

$$E_i = \frac{\hbar^2 K^2}{2m_t} + 2\epsilon_c - E_T^{tot}, \tag{F.2}$$

where the 'relative' energy E_T^{tot} is measured w.r.t to the bottom of the conduction band. We can express the initial trion state $|i\rangle = |\mathbf{K}\rangle_t$ with a fixed center of mass $\mathbf{K}$

in terms of its Fourier transform of the trion wavefunction as

$$|i\rangle = \sum_{\mathbf{k}_1,\mathbf{k}_2} \tilde{\Psi}\left(\mathbf{k}_1, \mathbf{k}_2, \mathbf{K} - \mathbf{k}_1 - \mathbf{k}_2\right) c^{\dagger}_{\mathbf{k}_1,\uparrow} c^{\dagger}_{\mathbf{k}_2,\downarrow} d^{\dagger}_{\mathbf{K}-\mathbf{k}_1-\mathbf{k}_2,-(3/2)} |0\rangle , \tag{F.3}$$

where the Fourier transform for a trion of center-of-mass momentum $\mathbf{K}$ is defined in Eqn. (1.55). We write the final state as

$$|f\rangle = \left|\mathbf{k}_e^{\downarrow}, \mathbf{Q}\right\rangle = c^{\dagger}_{\mathbf{k}_e,\downarrow} a^{\dagger}_{\mathbf{Q}} |0\rangle \tag{F.4}$$

with a corresponding final energy of

$$E_f = \frac{\hbar^2 k_e^2}{2m_e^*} + \epsilon_c + \hbar\omega \tag{F.5}$$

which gives us for the energy-conserving δ-function in Fermi's Golden Rule

$$\delta\left(E_f - E_i\right) = \delta\left(\frac{\hbar^2 k_e^2}{2m_e^*} + \hbar\omega - \frac{\hbar^2 K^2}{2m_t} - \tilde{E}\right). \tag{F.6}$$

where the quantity $\tilde{E}$ was introduced as $\tilde{E} = \epsilon_c - E_T^{tot}$; it simply expresses the energy gap between the top of the valence band and the bottom of the bound trion dispersion curve. In Eqn. (1.82), the transition amplitude was given as

$$\langle f | \mathcal{H}_I | i \rangle = g' \delta_{\mathbf{K},\mathbf{k}_e+\mathbf{Q}} I_+\left(\mathbf{k}_e\right)$$

Taking the large volume limit for the photon momentum $(\mathbf{Q}, Q_z)$we write the sum over the final states as

$$\sum_{\beta} \rightarrow \sum_{\mathbf{Q}} \sum_{\mathbf{k}_e} = \frac{V}{(2\pi)^3} \int d^3\mathbf{Q} \sum_{\mathbf{k}_e} \tag{F.7}$$

Consequently the decay rate can be calculated in the trion's resframe, where the trion's center of mass momentum is set to zero, as

$$\Gamma_t = \frac{V}{(2\pi)^2 \hbar} \int d^3\mathbf{Q}\, g'^2\, I_+^2\left(-\mathbf{Q}\right) \delta\left(\frac{\hbar^2 Q^2}{2m_e^*} + \hbar\omega - \tilde{E}\right), \tag{F.8}$$

where $I_+^2\left(-\mathbf{Q}\right)$ is explicitly given by

$$I_+^2\left(-\mathbf{Q}\right) = 2\pi\mathcal{N}^2 \frac{\left(C_1\mathbf{Q}^4 + C_2\mathbf{Q}^2 + C_3\right)^2}{\left(\alpha^2 + \mathbf{Q}^2\right)^7}. \tag{F.9}$$

The approximation we will make is to neglect the recoil energy of the electron $E_{recoil} = \frac{\hbar^2 Q^2}{2m_e^*}$, which drastically simplifies the evaluation of the energy conserving δ-function. This simplification is allowed, since all the values $\mathbf{Q}$ can take on in the integral are effectively restricted to $\sim 1/a_t$ owing to the effect of the function $I_+^2\left(-\mathbf{Q}\right)$. Because of

$$\frac{\hbar^2}{2m_e^* a_t^2} \ll \tilde{E} \tag{F.10}$$

we neglect the recoil term; in other words, the photon energy takes on the gap $\tilde{E}$ and we neglect small changes due to the dispersion relation of the electron. Since we consider a process starting from $\mathbf{K} = 0$ and because of the smallness of the optical photon wavevector $\mathbf{Q}$, the electron will always end up close to to the bottom of its dispersion relation, so that the photon energy is approximated as simply $\hbar\omega \approx \tilde{E}$. In this approximation, we can solve the remaining integrals simply in spherical coordinates

$$\Gamma_t = \frac{d_0^2}{3\epsilon\hbar}\mathcal{N}^2\tilde{Q}^3 \int_0^1 du \frac{\left(C_1\tilde{Q}^4\left(1-u^2\right)^2 + C_2\tilde{Q}^2\left(1-u^2\right) + C_3\right)^2}{\left(\alpha^2 + \tilde{Q}^2\left(1-u^2\right)\right)^7}, \tag{F.11}$$

where in the last step the quantity $\tilde{Q}$ was introduced as $\tilde{Q} = \tilde{E}/(\hbar c/n)$. The remaining

integral over u can be solved analytically.

Appendix G

Three level system in rotating frame

In this appendix, we will derive the general form of a driven three level system Hamiltonian in a frame rotating at the detuned driving frequency ω. We set $\hbar = 1$ and follow the steps taken at the derivation of the optical potential for the two-level atom. Setting the energy of the ground state $|1\rangle$ to zero, the bare Hamiltonian of the three-level system can be written as

$$H_0 = \omega_2 |2\rangle \langle 2| + \omega_3 |3\rangle \langle 3| . \tag{G.1}$$

For the unitary transformation of our system, we define the operator

$$U(t) = e^{-i\omega t(|2\rangle\langle 2|+|3\rangle\langle 3|)} \tag{G.2}$$

which gives the Hamiltonian $\tilde{H}_0$ in the rotating frame

$$\tilde{H}_0 = H_0 - iU^{\dagger}\dot{U} = \triangle_2 |2\rangle \langle 2| + \triangle_3 |3\rangle \langle 3| , \tag{G.3}$$

where we defined the detunings $\triangle_2$ and $\triangle_3$ as positive for red detuning in both cases, i.e.

$$\triangle_2 = \omega_2 - \omega, \qquad \triangle_3 = \omega_3 - \omega. \tag{G.4}$$

The ground state $|1\rangle$ is coupled to the excited states $|2\rangle$ and $|3\rangle$ with the spatially dependent Rabi frequencies $\Omega_2(\mathbf{r})$ and $\Omega_3(\mathbf{r})$, respectively. Assuming a harmonic time dependence, we can then write the interaction Hamiltonian in a semiclassical picture as

$$H_{int} = -\Omega_2(\mathbf{r})\cos(\omega t)\left[|1\rangle\langle 2| + |2\rangle\langle 1|\right] - \Omega_3(\mathbf{r})\cos(\omega t)\left[|1\rangle\langle 3| + |3\rangle\langle 1|\right] \tag{G.5}$$

which becomes in the rotating frame

$$\begin{aligned} \tilde{H}_{int} &= -\Omega_2(\mathbf{r})\cos(\omega t)\left[\hat{h}_2(0)\cos(\omega t) + \frac{\dot{\hat{h}}_2(0)}{\omega}\sin(\omega t)\right] \\ &\quad -\Omega_3(\mathbf{r})\cos(\omega t)\left[\hat{h}_3(0)\cos(\omega t) + \frac{\dot{\hat{h}}_3(0)}{\omega}\sin(\omega t)\right]. \end{aligned} \tag{G.6}$$

Here, we introduced the quantities

$$\begin{aligned} \hat{h}_2(0) &= |1\rangle\langle 2| + |2\rangle\langle 1| \\ \dot{\hat{h}}_2(0) &= i\omega\left[|2\rangle\langle 1| - |1\rangle\langle 2|\right] \end{aligned} \tag{G.7}$$

and similarly for $\hat{h}_3(0)$ and $\dot{\hat{h}}_3(0)$. We now apply the rotating wave approximation by averaging over one period of oscillation $T = 2\pi/\omega$. After the rotating wave approximation, the full Hamiltonian $\bar{H}$ in the rotating frame reads

$$\bar{H} = \triangle_2|2\rangle\langle 2| + \triangle_3|3\rangle\langle 3| - \frac{\Omega_2(\mathbf{r})}{2}\left[|1\rangle\langle 2| + |2\rangle\langle 1|\right] - \frac{\Omega_3(\mathbf{r})}{2}\left[|1\rangle\langle 3| + |3\rangle\langle 1|\right]. \tag{G.8}$$

This is the general form we used extended to the framework of the trion and exciton resonances in a semiconductor system.

Appendix H

Excitonic second order energy shift

In this appendix we give a detailed derivation of the second order energy shift $E_c^{(2)}(\mathbf{k})$ coming from the diffusive unbound trion states. The first approximation we make when calculating

$$E_c^{(2)}(\mathbf{k}) = -\sum_{\mathbf{K}}\sum_{\mathbf{k}_e} \frac{\langle \mathbf{k}| V |\mathbf{K}, c\rangle \langle \mathbf{K}, c| V |\mathbf{k}\rangle}{E_{\mathbf{K},\mathbf{k}_e;\mathbf{k}}} \tag{H.1}$$

is to identify the energies of the orthogonalized states with the corresponding energies of the unorthogonalized states. This approximation is based on the fact that the overlap with the bound trion states $\mathcal{O}(\mathbf{K}, \mathbf{k}_e)$ is rather small; it even vanishes as the sample size A goes to infinity. In this approximation, we express the energy denominators as

$$E_{\mathbf{K},\mathbf{k}_e;\mathbf{k}} \approx \frac{\hbar^2 (\mathbf{K} - \mathbf{k}_e)^2}{2m_x} + \frac{\hbar^2 (k_e^2 - k^2)}{2m_e^*} + \triangle_x, \tag{H.2}$$

where we introduced the detuning from the exciton resonance $\triangle_x$ as

$$\triangle_x = \epsilon_c - E_X - \hbar\omega. \tag{H.3}$$

Next, we write the orthogonalized states $|\mathbf{K}, c\rangle$ in terms of the free continuum $|\mathbf{K}, \mathbf{k}_e\rangle$ and the bound trion states $|\mathbf{K}\rangle$, respectively. Accordingly, we arrive at the equation

$$\begin{aligned} E_c^{(2)}(k) &= -\sum_{\mathbf{K}} \sum_{\mathbf{k}_e} \frac{\mathcal{N}_c^2}{E_{\mathbf{K},\mathbf{k}_e;\mathbf{k}}} \left[\langle \mathbf{k}| V |\mathbf{K}, \mathbf{k}_e\rangle \langle \mathbf{K}, \mathbf{k}_e| V |\mathbf{k}\rangle \right. \\ &\quad + \mathcal{O}(\mathbf{K}, \mathbf{k}_e)^2 \langle \mathbf{k}| V |\mathbf{K}\rangle \langle \mathbf{K}| V |\mathbf{k}\rangle \\ &\quad \left. - 2\mathcal{O}(\mathbf{K}, \mathbf{k}_e) \langle \mathbf{k}| V |\mathbf{K}\rangle \langle \mathbf{K}, \mathbf{k}_e| V |\mathbf{k}\rangle \right]. \end{aligned} \tag{H.4}$$

Here, we used that the matrix elements $\langle \mathbf{k}| V |\mathbf{K}\rangle$ as well as $\langle \mathbf{K}, \mathbf{k}_e| V |\mathbf{k}\rangle$ are real-valued quantities. Clearly, we recognize that the intermediate states can be free continuum states $|\mathbf{K}, \mathbf{k}_e\rangle$, but also bound trion states $|\mathbf{K}\rangle$, which gives rise to a contribution proportional to the squared overlap $\mathcal{O}(\mathbf{K}, \mathbf{k}_e)^2$ or even a hybrid mixture that is proportional to the overlap $\mathcal{O}(\mathbf{K}, \mathbf{k}_e)$.

We will approximate the squared normalization constant, given by

$$\mathcal{N}_c^2 = \frac{1}{1 - \mathcal{O}(\mathbf{K}, \mathbf{k}_e)^2} \approx 1 \tag{H.5}$$

as one, again owing to the fact that the overlap integral $\mathcal{O}(\mathbf{K}, \mathbf{k}_e)$ is assumed to be small, which is always true for a large enough sample. In this fashion, we have simplified the expression for $E_c^{(2)}(k)$ to

$$\begin{aligned} E_c^{(2)}(k) &\approx -\sum_{\mathbf{K}} \sum_{\mathbf{k}_e} \frac{1}{E_{\mathbf{K},\mathbf{k}_e;\mathbf{k}}} \left[\underbrace{\langle \mathbf{k}| V |\mathbf{K}, \mathbf{k}_e\rangle \langle \mathbf{K}, \mathbf{k}_e| V |\mathbf{k}\rangle}_{(i)} \right. \\ &\quad \underbrace{+ \mathcal{O}(\mathbf{K}, \mathbf{k}_e)^2 \langle \mathbf{k}| V |\mathbf{K}\rangle \langle \mathbf{K}| V |\mathbf{k}\rangle}_{(ii)} \\ &\quad \left. \underbrace{- 2\mathcal{O}(\mathbf{K}, \mathbf{k}_e) \langle \mathbf{k}| V |\mathbf{K}\rangle \langle \mathbf{K}, \mathbf{k}_e| V |\mathbf{k}\rangle}_{(iii)} \right] \end{aligned} \tag{H.6}$$

As indicated by the underlying subscripts, we will evaluate the different contributions (i), (ii) and (iii) piece by piece.

In order to evaluate the first term (i), we exploit the fact that

$$\langle \mathbf{k}| V |\mathbf{K}, \mathbf{k}_e\rangle \langle \mathbf{K}, \mathbf{k}_e| V |\mathbf{k}\rangle = \Omega_x^2 \delta_{\mathbf{k},\mathbf{k}_e} \left(\delta_{\mathbf{K}-\mathbf{k}_e,\mathbf{Q}} + \delta_{\mathbf{K}-\mathbf{k}_e,-\mathbf{Q}}\right). \tag{H.7}$$

The presence of the Kronecker deltas eases the evaluation of the first term drastically. We obtain

$$-\sum_{\mathbf{K}}\sum_{\mathbf{k}_e} \frac{1}{E_{\mathbf{K},\mathbf{k}_e;\mathbf{k}}} \langle \mathbf{k}| V |\mathbf{K}, \mathbf{k}_e\rangle \langle \mathbf{K}, \mathbf{k}_e| V |\mathbf{k}\rangle = -\Omega_x^2 \left(\frac{1}{E_{\mathbf{k}+\mathbf{Q},\mathbf{k};\mathbf{k}}} + \frac{1}{E_{\mathbf{k}-\mathbf{Q},\mathbf{k};\mathbf{k}}}\right). \tag{H.8}$$

Neglecting the exciton's recoil energy compared to the detuning from the exciton resonance, i.e.

$$E_{\mathbf{k}\pm\mathbf{Q},\mathbf{k};\mathbf{k}} = \frac{\hbar^2\mathbf{Q}^2}{2m_x} + \triangle_x \approx \triangle_x, \tag{H.9}$$

we obtain

$$-\sum_{\mathbf{K}}\sum_{\mathbf{k}_e} \frac{1}{E_{\mathbf{K},\mathbf{k}_e;\mathbf{k}}} \langle \mathbf{k}| V |\mathbf{K}, \mathbf{k}_e\rangle \langle \mathbf{K}, \mathbf{k}_e| V |\mathbf{k}\rangle = -2\frac{\Omega_x^2}{\triangle_x} \tag{H.10}$$

In order to retrieve a physically very intuitive compact form for the contribution of the term (i), we can rewrite the effective exciton Rabi frequency Ω_x in terms of the number of excitons N_x that fit into the sample without spatial overlap

$$\Omega_x^2 = \frac{\Omega_0^2}{4}\frac{8}{\pi a_0^2}A = \frac{\Omega_0^2}{2}\frac{A}{\pi a_x^2} = N_x\frac{\Omega_0^2}{2}, \tag{H.11}$$

where we used that the exciton radius is half the Bohr radius $a_x = a_0/2$. To sum it up, the term (i) gives the contribution

$$-\sum_{\mathbf{K}}\sum_{\mathbf{k}_e} \frac{1}{E_{\mathbf{K},\mathbf{k}_e;\mathbf{k}}} \langle \mathbf{k}| V |\mathbf{K}, \mathbf{k}_e\rangle \langle \mathbf{K}, \mathbf{k}_e| V |\mathbf{k}\rangle = -N_x\frac{\Omega_0^2}{\triangle_x}. \tag{H.12}$$

The presence of the exciton resonance accounts for a constant background shift that is simply proportional to N_x, which describes a macroscopic enhancement factor for the intrinsic shift $\Omega_0^2/\triangle_x$. Physically, this macroscopic enhancement factor arises from the fact that the exciton is a coherent excitation over the whole sample and thus carries a macroscopic dipole moment.

Next, we evaluate the term (ii). Proceeding from the electron-trion transition matrix element

$$\langle \mathbf{K}| V |\mathbf{k}\rangle = \frac{\Omega_0}{2}\left[\delta_{\mathbf{K},\mathbf{k}+\mathbf{Q}} I_+(\mathbf{k}) + \delta_{\mathbf{K},\mathbf{k}-\mathbf{Q}} I_-(\mathbf{k})\right], \tag{H.13}$$

we find

$$\begin{aligned}\mathcal{O}(\mathbf{K},\mathbf{k}_e)^2 \langle \mathbf{k}| V |\mathbf{K}\rangle \langle \mathbf{K}| V |\mathbf{k}\rangle &= \frac{\Omega_0^2}{4}\Big[\delta_{\mathbf{K},\mathbf{k}+\mathbf{Q}} \mathcal{O}(\mathbf{k}+\mathbf{Q},\mathbf{k}_e)^2 I_+(\mathbf{k})^2 \\ &\quad + \delta_{\mathbf{K},\mathbf{k}-\mathbf{Q}} \mathcal{O}(\mathbf{k}-\mathbf{Q},\mathbf{k}_e)^2 I_-(\mathbf{k})^2\Big]. \end{aligned} \tag{H.14}$$

Consequently, the corresponding contribution in the second order shift $E_c^{(2)}(\mathbf{k})$ reads

$$\begin{aligned}-\sum_{\mathbf{K}}\sum_{\mathbf{k}_e} \frac{\mathcal{O}(\mathbf{K},\mathbf{k}_e)^2}{E_{\mathbf{K},\mathbf{k}_e;\mathbf{k}}} \langle \mathbf{k}| V |\mathbf{K}\rangle \langle \mathbf{K}| V |\mathbf{k}\rangle &= -\frac{\Omega_0^2}{4}\sum_{\mathbf{k}_e}\Bigg[\frac{\mathcal{O}(\mathbf{k}+\mathbf{Q},\mathbf{k}_e)^2}{E_{\mathbf{k}+\mathbf{Q},\mathbf{k}_e;\mathbf{k}}} I_+(\mathbf{k})^2 \\ &\quad + \frac{\mathcal{O}(\mathbf{k}-\mathbf{Q},\mathbf{k}_e)^2}{E_{\mathbf{k}-\mathbf{Q},\mathbf{k}_e;\mathbf{k}}} I_-(\mathbf{k})^2\Bigg]. \end{aligned} \tag{H.15}$$

Again, we will approximate this expression by taking the limit $\mathbf{Q} \to 0$, but also $\mathbf{k} \to 0$, because big values for $\mathbf{k}$ are effectively suppressed by the functions $I_\pm(\mathbf{k})^2$. However, there is no restriction on $\mathbf{k}_e$, so that we keep this dependence. In this way,

the denominators simplify to

$$E_{\mathbf{k}\pm\mathbf{Q},\mathbf{k}_e;\mathbf{k}} = \frac{\hbar^2 (\mathbf{k} \pm \mathbf{Q} - \mathbf{k}_e)^2}{2m_x} + \frac{\hbar^2 (k_e^2 - k^2)}{2m_e} + \triangle_x$$
$$\approx \frac{\hbar^2 k_e^2}{2\mu_t} + \triangle_x, \tag{H.16}$$

where we introduced the reduced mass of the trion μ_t as

$$\mu_t = \frac{m_e^* m_x}{m_e^* + m_x} \tag{H.17}$$

Within the approximation of both $\mathbf{Q} \to 0$ and $\mathbf{k} \to 0$, we find $\mathcal{O}(\mathbf{k}+\mathbf{Q}, \mathbf{k}_e) = \mathcal{O}(\mathbf{k}-\mathbf{Q}, \mathbf{k}_e)$ and $I_+(\mathbf{k}) = I_-(\mathbf{k})$. Finally, we write the term (ii) in a rather compact form as

$$-\sum_{\mathbf{K}} \sum_{\mathbf{k}_e} \frac{\mathcal{O}(\mathbf{K}, \mathbf{k}_e)^2}{E_{\mathbf{K},\mathbf{k}_e;\mathbf{k}}} \langle \mathbf{k}| V |\mathbf{K}\rangle \langle \mathbf{K}| V |\mathbf{k}\rangle \approx -\frac{\Omega_0^2}{2} |I_+(\mathbf{k})|^2_{\mathbf{Q}=0} \frac{\chi_c(\triangle_x)}{\triangle_x}, \tag{H.18}$$

where we introduced the quantity $\chi_c(\triangle_x)$ as

$$\frac{\chi_c(\triangle_x)}{\triangle_x} = \sum_{\mathbf{k}_e} \frac{\mathcal{O}(0, \mathbf{k}_e)^2}{\frac{\hbar^2 k_e^2}{2\mu_t} + \triangle_x}. \tag{H.19}$$

Since the squared overlap $\mathcal{O}(0, \mathbf{k}_e)^2$ boils down to

$$\mathcal{O}(0, \mathbf{k}_e)^2 = \frac{\pi a_t^2}{A} \frac{8}{\left(1 + a_t^2 k_e^2\right)^3} \tag{H.20}$$

we can give an explicit solution to find $\chi_c(\triangle_x)$. Taking the large sample limit in order to replace the sum by an integral and expressing the integral in polar coordinates, we

obtain

$$\begin{aligned}\frac{\chi_c(\triangle_x)}{\triangle_x} &= 4a_t^2\int_0^\infty dk_e \frac{k_e}{\left(\frac{\hbar^2k_e^2}{2\mu_t}+\triangle_x\right)\left(1+a_t^2k_e^2\right)^3} \\ &= 4\int_0^\infty dk \frac{k}{\left(E_Tk^2+\triangle_x\right)\left(1+k^2\right)^3}, \end{aligned} \tag{H.21}$$

where we identified in the last step the trion binding energy

$$E_T = \frac{\hbar^2}{2\mu_t a_t^2}. \tag{H.22}$$

This is certainly an approximation; a_t has not been specified so far, but was left as a free parameter in the approximative ansatz for the trion wavefunction in (??). Appreciating this ansatz as an educated guess, we should be in the right order of magnitude with this approximation for the trion binding energy. Based on this approximation, we have obtained an analytic expression for $\chi_c(\triangle_x)$, namely

$$\chi_c(\xi) = \frac{2\xi^2\ln(\xi)+(4-3\xi)\xi-1}{(\xi-1)^3} \tag{H.23}$$

which is expressed in terms of the quantity $\xi = E_T/\triangle_x$, the trion binding energy over the detuning from the exciton resonance.

As far as the evaluation of the (ii) term is concerned, we shall halt here.

Therefore, we are left with an evaluation of the (iii) term, which has an hybrid character as it contains as an intermediate state the bound trion part as well as the unbound diffusive continuum states; this mixed character is governed by the overlap $\mathcal{O}(\mathbf{K},\mathbf{k}_e)$. The product of matrix elements that occur here are given by

$$\langle\mathbf{k}|V|\mathbf{K}\rangle\langle\mathbf{K},\mathbf{k}_e|V|\mathbf{k}\rangle = \frac{\Omega_0}{2}\Omega_x\delta_{\mathbf{k},\mathbf{k}_e}\left[\delta_{\mathbf{K},\mathbf{k}+\mathbf{Q}}I_+(\mathbf{k})+\delta_{\mathbf{K},\mathbf{k}-\mathbf{Q}}I_-(\mathbf{k})\right]. \tag{H.24}$$

Again, neglecting the optical wavevector $\mathbf{Q}$, we find

$$2\sum_{\mathbf{K}}\sum_{\mathbf{k}_e}\frac{\mathcal{O}(\mathbf{K},\mathbf{k}_e)}{E_{\mathbf{K},\mathbf{k}_e;\mathbf{k}}}\langle\mathbf{k}|V|\mathbf{K}\rangle\langle\mathbf{K},\mathbf{k}_e|V|\mathbf{k}\rangle \approx 2\frac{\Omega_0}{\triangle_x}\Omega_x|\mathcal{O}(\mathbf{k}+\mathbf{Q},\mathbf{k})I_+(\mathbf{k})|_{\mathbf{Q}=0}\,. \tag{H.25}$$

In conclusion of this appendix, we have shown that the second order energy shift $E_c^{(2)}(\mathbf{k})$ due to the orthogonalized continuum states can be approximately expressed as

$$\begin{aligned} E_c^{(2)}(\mathbf{k}) &= -N_x\frac{\Omega_0^2}{\triangle_x}-\frac{\Omega_0^2}{2\triangle_x}\chi_c(\triangle_x)|I_+(\mathbf{k})|^2_{\mathbf{Q}=0} \\ &\quad +2\frac{\Omega_0}{\triangle_x}\Omega_x|\mathcal{O}(\mathbf{k}+\mathbf{Q},\mathbf{k})I_+(\mathbf{k})|_{\mathbf{Q}=0}\,. \end{aligned} \tag{H.26}$$

Appendix I

Derivation of effective Hamiltonian

In this appendix we close the gap in our analysis of the effective Hamiltonian $\mathcal{H}_{eff}$ by deriving compact expressions for $\mathcal{H}^1_{II}$ and $\mathcal{H}^2_{II}$. We will put emphasis on the off-diagonal term $\mathcal{H}^2_{II}$, which is of a much greater importance for the understanding of the optical trapping potential for the electron. Therefore we will first cover the derivation of $\mathcal{H}^2_{II}$, before turning to the diagonal part $\mathcal{H}^1_{II}$.

I.1 Off-diagonal contribution $\mathcal{H}^2_{II}$

The starting point for an analysis of the off-diagonal term $\mathcal{H}^2_{II}$ is the quantity c_{qk}, as defined in Eqn. (3.17). The intermediate states can be bound trion states $|\mathbf{K}\rangle$ or continuum states $|\mathbf{K}, c\rangle$, properly orthogonalized to the bound states. Separating c_{qk} into these two pieces we have

$$c_{qk} = \sum_{\mathbf{K}} \left[\frac{\langle \mathbf{q}| V |\mathbf{K}\rangle \langle \mathbf{K}| V |\mathbf{k}\rangle}{E_{\mathbf{qk}} E_{\mathbf{K};\mathbf{k}}} + \sum_{\mathbf{k}_e} \frac{\langle \mathbf{q}| V |\mathbf{K}, c\rangle \langle \mathbf{K}, c| V |\mathbf{k}\rangle}{E_{\mathbf{qk}} E_{\mathbf{K}\mathbf{k}_e;\mathbf{k}}} \right]. \tag{I.1}$$

We emphasize, that, according to the general definition in Eqn. (3.16), the case $\mathbf{q} = \mathbf{k}$ is ruled out right away. The energies $E_{\mathbf{K}\mathbf{k}_e;\mathbf{k}}$ are approximately given by the

expression (H.2).

In the first step we express the orthogonalized continuum states in terms of the bound trion states $|\mathbf{K}\rangle$ and the free diffusive continuum states $|\mathbf{K}, \mathbf{k}_e\rangle$ to obtain

$$\begin{aligned} c_{qk} \;=\; \sum_{\mathbf{K}} \Bigg[& \frac{\langle \mathbf{q}| V |\mathbf{K}\rangle \langle \mathbf{K}| V |\mathbf{k}\rangle}{E_{\mathbf{qk}} E_{\mathbf{K};\mathbf{k}}} \\ & + \sum_{\mathbf{k}_e} \mathcal{N}_c^2 \frac{\langle \mathbf{q}| V |\mathbf{K}, \mathbf{k}_e\rangle \langle \mathbf{K}, \mathbf{k}_e| V |\mathbf{k}\rangle}{E_{\mathbf{qk}} E_{\mathbf{K}\mathbf{k}_e;\mathbf{k}}} \\ & + \sum_{\mathbf{k}_e} \mathcal{N}_c^2 \mathcal{O}(\mathbf{K}, \mathbf{k}_e)^2 \frac{\langle \mathbf{q}| V |\mathbf{K}\rangle \langle \mathbf{K}| V |\mathbf{k}\rangle}{E_{\mathbf{qk}} E_{\mathbf{K}\mathbf{k}_e;\mathbf{k}}} \\ & - \sum_{\mathbf{k}_e} \mathcal{N}_c^2 \mathcal{O}(\mathbf{K}, \mathbf{k}_e) \frac{\langle \mathbf{q}| V |\mathbf{K}\rangle \langle \mathbf{K}, \mathbf{k}_e| V |\mathbf{k}\rangle}{E_{\mathbf{qk}} E_{\mathbf{K}\mathbf{k}_e;\mathbf{k}}} \\ & - \sum_{\mathbf{k}_e} \mathcal{N}_c^2 \mathcal{O}(\mathbf{K}, \mathbf{k}_e) \frac{\langle \mathbf{q}| V |\mathbf{K}, \mathbf{k}_e\rangle \langle \mathbf{K}| V |\mathbf{k}\rangle}{E_{\mathbf{qk}} E_{\mathbf{K}\mathbf{k}_e;\mathbf{k}}} \Bigg] . \end{aligned} \tag{I.2}$$

We can drop the second line right away, because it imposes the conditions $\delta_{\mathbf{k},\mathbf{k}_e}$ as well as $\delta_{\mathbf{q},\mathbf{k}_e}$ which results in $\delta_{\mathbf{k},\mathbf{q}}$ and is therefore not allowed. In the consecutive step, we use that the overlap $\mathcal{O}(\mathbf{K}, \mathbf{k}_e)$ is a small quantity to approximate

$$\mathcal{N}_c^2 \mathcal{O}(\mathbf{K}, \mathbf{k}_e)^2 \;=\; \frac{\mathcal{O}(\mathbf{K}, \mathbf{k}_e)^2}{1 - \mathcal{O}(\mathbf{K}, \mathbf{k}_e)^2} \approx \mathcal{O}(\mathbf{K}, \mathbf{k}_e)^2 \tag{I.3}$$

$$\mathcal{N}_c^2 \mathcal{O}(\mathbf{K}, \mathbf{k}_e) \;=\; \frac{\mathcal{O}(\mathbf{K}, \mathbf{k}_e)}{1 - \mathcal{O}(\mathbf{K}, \mathbf{k}_e)^2} \approx \mathcal{O}(\mathbf{K}, \mathbf{k}_e) . \tag{I.4}$$

Based on the approximations $\mathbf{Q} \to 0$ and $\mathbf{k} \to 0$, that we have already made before, we find

$$E_{\mathbf{K};\mathbf{k}} = \frac{\hbar^2 K^2}{2m_t} - \frac{\hbar^2 k^2}{2m_e^*} + \triangle_t \approx \triangle_t, \tag{I.5}$$

where we used that, owing to in-plane momentum conservation, $\mathbf{K}$ has to be a combination of $\mathbf{k}$ and $\mathbf{Q}$, which we both neglect. Proceeding from these approximations,

we express c_{qk} in the following way

$$c_{qk} = c_{qk}^{(a)} + c_{qk}^{(b)}, \tag{I.6}$$

where $c_{qk}^{(a)}$ and $c_{qk}^{(b)}$ have been defined as

$$c_{qk}^{(a)} = \sum_{\mathbf{K}} \frac{\langle \mathbf{q}| V |\mathbf{K}\rangle \langle \mathbf{K}| V |\mathbf{k}\rangle}{E_{\mathbf{qk}}} \left[\frac{1}{\triangle_t} + \sum_{\mathbf{k}_e} \frac{\mathcal{O}(\mathbf{K}, \mathbf{k}_e)^2}{E_{\mathbf{K}\mathbf{k}_e;\mathbf{k}}} \right] \tag{I.7}$$

and

$$c_{qk}^{(b)} = -\sum_{\mathbf{K}} \sum_{\mathbf{k}_e} \frac{\mathcal{O}(\mathbf{K}, \mathbf{k}_e)}{E_{\mathbf{qk}} E_{\mathbf{K}\mathbf{k}_e;\mathbf{k}}} \left[\langle \mathbf{q}| V |\mathbf{K}\rangle \langle \mathbf{K}, \mathbf{k}_e| V |\mathbf{k}\rangle + \langle \mathbf{q}| V |\mathbf{K}, \mathbf{k}_e\rangle \langle \mathbf{K}| V |\mathbf{k}\rangle \right], \tag{I.8}$$

where the quantity $c_{qk}^{(a)}$ includes bound trion states only as intermediate states, while $c_{qk}^{(b)}$ comprises mixed terms because of the appearance of one single overlap $\mathcal{O}(\mathbf{K}, \mathbf{k}_e)$.

Using Eqn. (1.47) for the transition matrix element, we can express $c_{qk}^{(a)}$ as

$$\begin{aligned} c_{qk}^{(a)} = \frac{\Omega_0^2}{4} \Bigg[& \frac{I_+(\mathbf{q}) I_-(\mathbf{k})}{E_{\mathbf{qk}}} \delta_{\mathbf{q},\mathbf{k}-2\mathbf{Q}} \left(\frac{1}{\triangle_t} + \sum_{\mathbf{k}_e} \frac{\mathcal{O}(\mathbf{k}-\mathbf{Q}, \mathbf{k}_e)^2}{E_{(\mathbf{k}-\mathbf{Q})\mathbf{k}_e;\mathbf{k}}} \right) \\ & + \frac{I_+(\mathbf{k}) I_-(\mathbf{q})}{E_{\mathbf{qk}}} \delta_{\mathbf{q},\mathbf{k}+2\mathbf{Q}} \left(\frac{1}{\triangle_t} + \sum_{\mathbf{k}_e} \frac{\mathcal{O}(\mathbf{k}+\mathbf{Q}, \mathbf{k}_e)^2}{E_{(\mathbf{k}+\mathbf{Q})\mathbf{k}_e;\mathbf{k}}} \right) \Bigg]. \end{aligned} \tag{I.9}$$

Let us examine the corresponding part of the Hamiltonian which we define as

$$\mathcal{H}_{II}^{2(a/b)} = \sum_{\mathbf{k}} E^{(0)}(\mathbf{k}) \sum_{\mathbf{q}\neq\mathbf{k}} c_{qk}^{(a/b)} |\mathbf{q}\rangle \langle \mathbf{k}| + h.c. \tag{I.10}$$

If we plug in $c_{qk}^{(a)}$ from expression (I.9) into $\mathcal{H}_{II}^{2(a)}$ and let $\mathbf{k} \rightarrow \mathbf{k} + \mathbf{Q}$ in the first line

and $\mathbf{k} \rightarrow \mathbf{k} - \mathbf{Q}$ in the second line, we arrive at

$$\begin{aligned}
\mathcal{H}_{II}^{2(a)} &= \frac{\Omega_0^2}{4} \sum_{\mathbf{k}} \Bigg\{ E^{(0)}(\mathbf{k}-\mathbf{Q}) \frac{I_+(\mathbf{k}-\mathbf{Q}) I_-(\mathbf{k}+\mathbf{Q})}{E_{\mathbf{k}+\mathbf{Q},\mathbf{k}-\mathbf{Q}}} \\
&\times \left(\frac{1}{\triangle_t} + \sum_{\mathbf{k}_e} \frac{\mathcal{O}(\mathbf{k},\mathbf{k}_e)^2}{E_{\mathbf{k}\mathbf{k}_e;\mathbf{k}-\mathbf{Q}}} \right) (|\mathbf{k}-\mathbf{Q}\rangle \langle \mathbf{k}+\mathbf{Q}| + h.c.) \\
&+ E^{(0)}(\mathbf{k}+\mathbf{Q}) \frac{I_+(\mathbf{k}-\mathbf{Q}) I_-(\mathbf{k}+\mathbf{Q})}{E_{\mathbf{k}-\mathbf{Q},\mathbf{k}+\mathbf{Q}}} \\
&\times \left(\frac{1}{\triangle_t} + \sum_{\mathbf{k}_e} \frac{\mathcal{O}(\mathbf{k},\mathbf{k}_e)^2}{E_{\mathbf{k}\mathbf{k}_e;\mathbf{k}+\mathbf{Q}}} \right) (|\mathbf{k}-\mathbf{Q}\rangle \langle \mathbf{k}+\mathbf{Q}| + h.c.) \Bigg\}. \qquad \text{(I.11)}
\end{aligned}$$

Again, in the expressions $E_{\mathbf{k}\mathbf{k}_e;\mathbf{k}\pm\mathbf{Q}}$ we only keep the detuning from the exciton resonance $\triangle_x$ and the dependence on $\mathbf{k}_e$ as

$$E_{\mathbf{k}\mathbf{k}_e;\mathbf{k}\pm\mathbf{Q}} \approx \frac{\hbar^2 k_e^2}{2\mu_t} + \triangle_x \qquad \text{(I.12)}$$

Using the fact that $I_+(\mathbf{k}-\mathbf{Q}) I_-(\mathbf{k}+\mathbf{Q})$ are strongly peaked around $\mathbf{k} \approx 0$, taking the limit $\mathbf{Q} \rightarrow 0$, and exploiting the relation

$$\frac{E^{(0)}(\mathbf{k}-\mathbf{Q})}{E_{\mathbf{k}+\mathbf{Q},\mathbf{k}-\mathbf{Q}}} + \frac{E^{(0)}(\mathbf{k}+\mathbf{Q})}{E_{\mathbf{k}-\mathbf{Q},\mathbf{k}+\mathbf{Q}}} = \frac{E^{(0)}(\mathbf{k}-\mathbf{Q})}{E_{\mathbf{k}+\mathbf{Q},\mathbf{k}-\mathbf{Q}}} - \frac{E^{(0)}(\mathbf{k}+\mathbf{Q})}{E_{\mathbf{k}+\mathbf{Q},\mathbf{k}-\mathbf{Q}}} = -1 \qquad \text{(I.13)}$$

the simplified version of $\mathcal{H}_{II}^{2(a)}$ is given by

$$\mathcal{H}_{II}^{2(a)} \approx -\frac{\Omega_0^2}{4} \sum_{\mathbf{k}} |I_+(\mathbf{k}-\mathbf{Q})|^2_{\mathbf{Q}=0} \left(\frac{1}{\triangle_t} + \frac{\chi_c(\triangle_x)}{\triangle_x} \right) (|\mathbf{k}-\mathbf{Q}\rangle \langle \mathbf{k}+\mathbf{Q}| + h.c.). \qquad \text{(I.14)}$$

Now, let us turn to $c_{qk}^{(b)}$ and its contribution to the effective Hamiltonian $\mathcal{H}_{II}^{2(b)}$.

It implies products of mixed matrix elements which we can write as

$$\begin{aligned}\langle \mathbf{q}| V |\mathbf{K}, \mathbf{k}_e\rangle \langle \mathbf{K}| V |\mathbf{k}\rangle &= \frac{\Omega_0}{2}\Omega_x \delta_{\mathbf{q},\mathbf{k}_e} \left(\delta_{\mathbf{q},\mathbf{k}+2\mathbf{Q}}\delta_{\mathbf{K},\mathbf{k}+\mathbf{Q}} I_+(\mathbf{k})\right. \\ &\left. + \delta_{\mathbf{q},\mathbf{k}-2\mathbf{Q}}\delta_{\mathbf{K},\mathbf{k}-\mathbf{Q}} I_-(\mathbf{k})\right) \qquad \text{(I.15)}\end{aligned}$$

and similarly

$$\begin{aligned}\langle \mathbf{q}| V |\mathbf{K}\rangle \langle \mathbf{K}, \mathbf{k}_e| V |\mathbf{k}\rangle &= \frac{\Omega_0}{2}\Omega_x \delta_{\mathbf{k},\mathbf{k}_e} \left(\delta_{\mathbf{q},\mathbf{k}+2\mathbf{Q}}\delta_{\mathbf{K},\mathbf{k}+\mathbf{Q}} I_-(\mathbf{q})\right. \\ &\left. + \delta_{\mathbf{q},\mathbf{k}-2\mathbf{Q}}\delta_{\mathbf{K},\mathbf{k}-\mathbf{Q}} I_+(\mathbf{q})\right). \qquad \text{(I.16)}\end{aligned}$$

The sums appearing in the definition of $c_{qk}^{(b)}$ are readily taken care of, and we find

$$\begin{aligned}c_{qk}^{(b)} &= -\frac{\Omega_0}{2}\Omega_x \left\{ \frac{\mathcal{O}(\mathbf{k}+\mathbf{Q},\mathbf{q})}{E_{\mathbf{qk}} E_{(\mathbf{k}+\mathbf{Q})\mathbf{q};\mathbf{k}}} I_+(\mathbf{k})\,\delta_{\mathbf{q},\mathbf{k}+2\mathbf{Q}} + \frac{\mathcal{O}(\mathbf{k}-\mathbf{Q},\mathbf{q})}{E_{\mathbf{qk}} E_{(\mathbf{k}-\mathbf{Q})\mathbf{q};\mathbf{k}}} I_-(\mathbf{k})\,\delta_{\mathbf{q},\mathbf{k}-2\mathbf{Q}} \right. \\ &\left. + \frac{\mathcal{O}(\mathbf{k}-\mathbf{Q},\mathbf{k})}{E_{\mathbf{qk}} E_{(\mathbf{k}-\mathbf{Q})\mathbf{k};\mathbf{k}}} I_+(\mathbf{q})\,\delta_{\mathbf{q},\mathbf{k}-2\mathbf{Q}} + \frac{\mathcal{O}(\mathbf{k}+\mathbf{Q},\mathbf{k})}{E_{\mathbf{qk}} E_{(\mathbf{k}+\mathbf{Q})\mathbf{k};\mathbf{k}}} I_-(\mathbf{q})\,\delta_{\mathbf{q},\mathbf{k}+2\mathbf{Q}} \right\} \qquad \text{(I.17)}\end{aligned}$$

which gives rise to the following contribution to the Hamiltonian

$$\begin{aligned}\mathcal{H}_{II}^{2(b)} &= -\frac{\Omega_0}{2}\Omega_x \sum_{\mathbf{k}} \left\{ E^{(0)}(\mathbf{k}-\mathbf{Q}) \frac{\mathcal{O}(\mathbf{k},\mathbf{k}+\mathbf{Q})\, I_+(\mathbf{k}-\mathbf{Q})}{E_{\mathbf{k}+\mathbf{Q},\mathbf{k}-\mathbf{Q}} E_{\mathbf{k}(\mathbf{k}+\mathbf{Q});\mathbf{k}-\mathbf{Q}}} \times \right. \\ &\quad \times \left(|\mathbf{k}+\mathbf{Q}\rangle \langle \mathbf{k}-\mathbf{Q}| + h.c.\right) \\ &\quad + E^{(0)}(\mathbf{k}+\mathbf{Q}) \frac{\mathcal{O}(\mathbf{k},\mathbf{k}-\mathbf{Q})\, I_-(\mathbf{k}+\mathbf{Q})}{E_{\mathbf{k}-\mathbf{Q},\mathbf{k}+\mathbf{Q}} E_{\mathbf{k}(\mathbf{k}-\mathbf{Q});\mathbf{k}+\mathbf{Q}}} \left(|\mathbf{k}+\mathbf{Q}\rangle \langle \mathbf{k}-\mathbf{Q}| + h.c.\right) \\ &\quad + E^{(0)}(\mathbf{k}+\mathbf{Q}) \frac{\mathcal{O}(\mathbf{k},\mathbf{k}+\mathbf{Q})\, I_+(\mathbf{k}-\mathbf{Q})}{E_{\mathbf{k}-\mathbf{Q},\mathbf{k}+\mathbf{Q}} E_{\mathbf{k}(\mathbf{k}+\mathbf{Q});\mathbf{k}+\mathbf{Q}}} \left(|\mathbf{k}+\mathbf{Q}\rangle \langle \mathbf{k}-\mathbf{Q}| + h.c.\right) \\ &\quad \left. + E^{(0)}(\mathbf{k}-\mathbf{Q}) \frac{\mathcal{O}(\mathbf{k},\mathbf{k}-\mathbf{Q})\, I_-(\mathbf{k}+\mathbf{Q})}{E_{\mathbf{k}+\mathbf{Q},\mathbf{k}-\mathbf{Q}} E_{\mathbf{k}(\mathbf{k}-\mathbf{Q});\mathbf{k}-\mathbf{Q}}} \left(|\mathbf{k}+\mathbf{Q}\rangle \langle \mathbf{k}-\mathbf{Q}| + h.c.\right) \right\}.\end{aligned}$$

Here, we make the familiar approximations

$$E_{\mathbf{k}(\mathbf{k}\pm\mathbf{Q});\mathbf{k}\mp\mathbf{Q}} = \frac{\hbar^2\mathbf{Q}^2}{2m_x} \pm \frac{2\hbar^2}{m_e^*}\mathbf{k}\mathbf{Q} + \triangle_x \approx \triangle_x \tag{I.18}$$

$$E_{\mathbf{k}(\mathbf{k}\pm\mathbf{Q});\mathbf{k}\pm\mathbf{Q}} = \frac{\hbar^2\mathbf{Q}^2}{2m_x} + \triangle_x \approx \triangle_x \tag{I.19}$$

and obtain the simplified expression

$$\begin{aligned}\mathcal{H}_{II}^{2(b)} = \frac{\Omega_0\Omega_x}{2\triangle_x}\sum_{\mathbf{k}} \{&\mathcal{O}(\mathbf{k},\mathbf{k}+\mathbf{Q})\, I_+(\mathbf{k}-\mathbf{Q})\,(|\mathbf{k}+\mathbf{Q}\rangle\langle\mathbf{k}-\mathbf{Q}| + h.c.) \\ &\mathcal{O}(\mathbf{k},\mathbf{k}-\mathbf{Q})\, I_-(\mathbf{k}+\mathbf{Q})\,(|\mathbf{k}+\mathbf{Q}\rangle\langle\mathbf{k}-\mathbf{Q}| + h.c.)\}\end{aligned} \tag{I.20}$$

Taking the limit $\mathbf{Q} \to 0$, we get

$$\mathcal{H}_{II}^{2(b)} \approx \frac{\Omega_0\Omega_x}{\triangle_x}\sum_{\mathbf{k}} |\mathcal{O}(\mathbf{k},\mathbf{k}+\mathbf{Q})\, I_+(\mathbf{k}-\mathbf{Q})|_{\mathbf{Q}=0}\,(|\mathbf{k}+\mathbf{Q}\rangle\langle\mathbf{k}-\mathbf{Q}| + h.c.)\,. \tag{I.21}$$

In conclusion, we have shown that the off-diagonal part $\mathcal{H}_{II}^2 = \mathcal{H}_{II}^{2(a)} + \mathcal{H}_{II}^{2(b)}$ takes on the form

$$\begin{aligned}\mathcal{H}_{II}^2 \approx &-\frac{\Omega_0^2}{4}\sum_{\mathbf{k}} |I_+(\mathbf{k}-\mathbf{Q})|^2_{\mathbf{Q}=0}\left(\frac{1}{\triangle_t} + \frac{\chi_c(\triangle_x)}{\triangle_x}\right)(|\mathbf{k}-\mathbf{Q}\rangle\langle\mathbf{k}+\mathbf{Q}| + h.c.) \\ &+\frac{\Omega_0\Omega_x}{\triangle_x}\sum_{\mathbf{k}} |\mathcal{O}(\mathbf{k},\mathbf{k}+\mathbf{Q})\, I_+(\mathbf{k}-\mathbf{Q})|_{\mathbf{Q}=0}\,(|\mathbf{k}+\mathbf{Q}\rangle\langle\mathbf{k}-\mathbf{Q}| + h.c.)\end{aligned} \tag{I.22}$$

I.2 Diagonal contribution $\mathcal{H}_{II}^1$

From the general analysis of the Hamiltonian in second order perturbation theory, we are left with evaluating the contribution

$$\mathcal{H}_{II}^1 = -\sum_{\mathbf{k}} E^{(0)}(\mathbf{k})\, d_{\mathbf{k}}\, |\mathbf{k}\rangle\langle\mathbf{k}|\,, \tag{I.23}$$

where $d_{\mathbf{k}}$ is given by

$$d_{\mathbf{k}} = \sum_{\mathbf{l}\neq\mathbf{k}} \frac{|V_{lk}|^2}{E_{lk}^2} = \sum_{\mathbf{K}} \frac{\langle \mathbf{q}| V |\mathbf{K}\rangle \langle \mathbf{K}| V |\mathbf{k}\rangle}{E_{\mathbf{K};\mathbf{k}}^2} + \sum_{\mathbf{K}} \sum_{\mathbf{k}_e} \frac{\langle \mathbf{q}| V |\mathbf{K}, c\rangle \langle \mathbf{K}, c| V |\mathbf{k}\rangle}{E_{\mathbf{K}\mathbf{k}_e;\mathbf{k}}^2}. \quad \text{(I.24)}$$

Plugging in the results for the transition matrix elements, for the contribution from the bound trion states we obtain

$$\sum_{\mathbf{K}} \frac{\langle \mathbf{q}| V |\mathbf{K}\rangle \langle \mathbf{K}| V |\mathbf{k}\rangle}{E_{\mathbf{K};\mathbf{k}}^2} \approx \frac{\Omega_0^2}{4\triangle_t^2} \left[I_+ (\mathbf{k})^2 + I_- (\mathbf{k})^2 \right], \quad \text{(I.25)}$$

where we neglected the $\mathbf{k}$ dependence in the denominator, since the functions $I_\pm (\mathbf{k})^2$ are strongly peaked at small values $\mathbf{k} \approx 0$, and dropped the trion recoil energy versus the detuning from the trion resonance. In the limit $\mathbf{Q} \to 0$, we can further simplify the expression above to

$$\sum_{\mathbf{K}} \frac{\langle \mathbf{q}| V |\mathbf{K}\rangle \langle \mathbf{K}| V |\mathbf{k}\rangle}{E_{\mathbf{K};\mathbf{k}}^2} \approx \frac{\Omega_0^2}{2\triangle_t^2} |I_+ (\mathbf{k})|_{\mathbf{Q}=0}^2 . \quad \text{(I.26)}$$

Following the same analysis and approximations as in the derivation of the second order energy shift $E_c^{(2)} (\mathbf{k})$, we obtain for $\mathcal{H}_{II}^1$ only terms that are proportional to $1/\triangle_t^2$ or $1/\triangle_x^2$; this arises from the squared denominator in the general equation for $\mathcal{H}_{II}^1$. We then find

$$\begin{aligned} \mathcal{H}_{II}^1 \;=\; & -\sum_{\mathbf{k}} E^{(0)} (\mathbf{k}) |\mathbf{k}\rangle \langle \mathbf{k}| \left\{ N_x \frac{\Omega_0^2}{\triangle_x^2} + \frac{\Omega_0^2}{2\triangle_x^2} |I_+ (\mathbf{k})|_{\mathbf{Q}=0}^2 \right. \\ & + \frac{\Omega_0^2}{2} |I_+ (\mathbf{k})|_{\mathbf{Q}=0}^2 \sum_{\mathbf{k}_e} \frac{\mathcal{O} (0, \mathbf{k}_e)^2}{\left(\frac{\hbar^2 k_e^2}{2\mu_t} + \triangle_x \right)^2} \\ & \left. - \frac{\Omega_0 \Omega_x}{2\triangle_x^2} |\mathcal{O} (\mathbf{k}+\mathbf{Q}, \mathbf{k}) I_+ (\mathbf{k})|_{\mathbf{Q}=0}^2 \right\}. \end{aligned} \quad \text{(I.27)}$$

Since all the terms but the first one involve the functions $I_\pm (\mathbf{k})$ that suppress big

k values, these terms have to be small due to the smooth function $E^{(0)}(k) \propto k^2$ in front. Therefore, we drop all the terms besides the first one and find

$$\mathcal{H}_{II}^{1} \approx -N_x \frac{\Omega_0^2}{\triangle_x^2} \sum_{\mathbf{k}} E^{(0)}(\mathbf{k}) |\mathbf{k}\rangle \langle \mathbf{k}| . \tag{I.28}$$

I.3 Trionic contributions in the effective Hamiltonian

In principle, the effective second order Hamiltonian also contains terms of the form

$$\mathcal{H}_{eff}^{T} = \sum_{\mathbf{K}} E_{\mathbf{K}}^{(0)} \left|\mathbf{K}^{(1)}\right\rangle \left\langle \mathbf{K}^{(1)}\right|, \tag{I.29}$$

where $\left|\mathbf{K}^{(1)}\right\rangle$ is the first-order correction of the bound or unbound trion states and $E_{\mathbf{K}}^{(0)}$ is the corresponding zeroth-order energy eigenvalue. The states $\left|\mathbf{K}^{(1)}\right\rangle$ are coupled to the zeroth-order electron eigenstates $\left|\mathbf{k}^{(0)}\right\rangle$ via the relation

$$\left|\mathbf{K}^{(1)}\right\rangle = \sum_{\mathbf{k}} \frac{V_{\mathbf{kK}}}{E_{\mathbf{Kk}}} \left|\mathbf{k}^{(0)}\right\rangle, \tag{I.30}$$

so that $\mathcal{H}_{eff}^{T}$ can be rewritten as

$$\mathcal{H}_{eff}^{T} = \sum_{\mathbf{K}} E_{\mathbf{K}}^{(0)} \sum_{\mathbf{k},\mathbf{q}} \frac{V_{\mathbf{kK}}}{E_{\mathbf{Kk}}} \frac{V_{\mathbf{qK}}^{*}}{E_{\mathbf{Kq}}} \left|\mathbf{k}^{(0)}\right\rangle \left\langle \mathbf{q}^{(0)}\right|. \tag{I.31}$$

When keeping the detuning in the denominators only, we immediately see that this effect is a higher order correction that is proportional to $\sim 1/\triangle_t^2$. The reasoning for unbound trions goes along the lines. To be consistent, we will neglect this higher order correction.

BIBLIOGRAPHY

[1] Phillips, W. D. Nobel lecture: Laser cooling and trapping of neutral atoms. *Rev. Mod. Phys.* **70**, 721 (1998)

[2] Ashkin, A. History of optical trapping and manipulation of small-neutral particle, atoms, and molecules. *IEEE J. Sel. Top. Quantum Electron.* **6**, 841-856 (2000)

[3] White, M. *et al.* Strongly interacting bosons in a disordered optical lattice. *Phys. Rev. Lett.* **102**, 055301 (2009)

[4] Chen, Y. P. *et al.* Phase coherence and superfluid-insulator transition in a disordered Bose-Einstein condensate. *Phys. Rev. A* **77**, 033632 (2008)

[5] Bar-Joseph, I. Trions in GaAs quantum wells. *Semicond. Sci. Technol.* **20**, R29-R39 (2005)

[6] Lampert, M.A. Mobile and immobile effective-mass-particle complexes in nonmetallic solids. *Phys. Rev. Lett.* **1**, 450 (1958)

[7] Savitto, D. *et al.* Observation of charge transport by negatively charged excitons. *Science* **294**, 26 (2001)

[8] Combescot, M., Betbeder-Matibet, O. & Dubin, F. The trion: two electrons plus one hole versus one electron plus one exciton. *Eur. Phys. J. B.* **42**, 63-83 (2004)

[9] Wannier, G.H. The structure of electronic excitations levels in insulating crystals. *Phys. Rev.* **52**, 191 (1937)

[10] Elliott, R. J. Intensity of optical absorption by excitons. *Phys. Rev.* **108**, 1384 (1957)

[11] Sham, L. J. & Rice, T. M. Many-particle derivation of the effective-mass equation for the Wannier exciton. *Phys. Rev.* **144 (2)**, 708 (1966)

[12] Haug, H. & Koch, S. W. *Quantum theory of the optical and electronic properties of semiconductors.* World Scientific Publishing Company (2005)

[13] Dingle, R., Wiegmann, W. & Henry, C. H. Quantum states of confined carriers in very thin $Al_xGa_{1-x}As - GaAs - Al_xGa_{1-x}As$ heterostructures. *Phys. Rev. Lett.* **33**, 827 (1974)

[14] Andreani, L. C. & Pasquaerello, A. Accurate theory of excitons in $GaAs - Ga_{1-x}Al_xAs$ quantum wells. *Phys. Rev. B.* **42**, 8928 (1990)

[15] Kheng, K. *et al.* Observation of negatively charged excitons X^- in semiconductor quantum wells. *Phys. Rev. Lett.* **71**, 1752 (1993)

[16] Finkelstein, G., Shtrikman, H. & Bar-Joseph, I. Optical spectroscopy of a two-dimensional electron gas near the metal-insulator transition. *Phys. Rev. Lett.* **74**, 976 (1995)

[17] Shields, A. J., Pepper, M., Ritchie, D. A., Simmons, M. Y. & Jones, G. A. C. Quenching of excitonic optical transitions by excess electrons in *GaAs* quantum wells. *Phys. Rev. B.* **51**, R18049 (1995)

[18] Huard, V., Cox, R. T., Saminadayar, K., Arnoult, A., Tatarenko, S. Bound states in optical absorption of semiconductor quantum wells containing a two-dimensional electron gas. *Phys. Rev. Lett.* **84**, 187 (2000)

[19] Manassen, A. *et al.* Exciton and trion spectral line shape in the presence of an electron gas in *GaAs/AlAs* quantum wells. *Phys. Rev. B* **54**, 10609 (1996)

[20] Dingle, R., Störmer, H. L., Gossard, A. C. & Wiegmann, W. Electron mobilities in modulation-doped semiconductor heterojunction superlattices. *Appl. Phys. Lett.* **33**, 665 (1978)

[21] Ciulin, V. *Picosecond dynamics of neutral and charged excitons in semiconductor quantum wells.* Thesis 2410, EPFL (2001)

[22] Stébé, B., Munschy, G., Stauffer, L, Dujardin, F. & Murat, J. Excitonic trion X^- in semiconductor quantum wells. *Phys. Rev. B.* **56**, 12454 (1997)

[23] Hylleraas, E. A. Neue Berechnung der Energie des Heliums im Grundzustande, sowie des tiefsten Terms von Ortho-Helium. *Z. Physik* **54**, 347 (1929)

[24] Flores-Riveros, A. Generalized Hylleraas-Gaussian basis sets applied to the variational treatment of the two-electron atoms. *Int. J. Quant. Chem.* **66**, 287-300 (1998)

[25] Bethe, H. A. & Salpeter, E. E. *Quantum Mechanics of One- and Two-Electron Atoms Ch. 2* (Dover Publications Inc., Mineola, New York, 2008).

[26] Portella-Oberli, M. T. Trions and excitons in *CdTe* quantum wells: Lifetimes, coherence, diffusion and localization. *Phys. Stat. Sol. (b)* **234**, 294-303 (2002)

[27] Phelps, D. E. & Bajaj, K. K. Ground-state energy of a D^- ion in two-dimensional semiconductors. *Phys. Rev. B.* **27**, 4883 (1983)

[28] Bobrysheva, A. I., Grodetskii, M. V. & Zyukov, V. T. Binding energy for the surface biexcitonic positive ion. *J. Phys. C: solid State Phys.* **16**, 5723-5728 (1983)

[29] Landolt Börnstein. *Semiconductors: Intrinsic properties of Group IV elements and III-V, II-VI and I-VII compounds.* New Series III/22a (1987)

[30] Esser, A., Runge, E., Zimmermann, R. & Langbein, W. Photoluminescene and radiative lifetime of trions in *GaAs* quantum wells. *Phys. Rev. B.* **62**, 8232 (2000)

[31] Stébé, B., Feddi, E., Aiane, A. & Dujardin, F. Optical and magneto-optical absorption of negatively charged excitons in three- and two-dimensional semiconductors. *Phys. Rev. B.* **58**, 9926 (1998)

[32] Combescot, M. & Tribollet, J. Trion oscillator strength. *Solid State Commun.* **128**, 273-277 (2003)

[33] Adreani, L. C. Optical transitions, excitons, and polaritons in bulk and low-dimensional semiconductor structures. Eds. Burstein, E. & Weisbuch, C. '*Confined electrons and photons: new physics and devices*'. Plenum Press (1994)

[34] Hanamura, E. Rapid radiative decay and enhanced optical nonlinearity of excitons in a quantum well. *Phys. Rev. B.* **38**, 1228 (1988)

[35] Deveaud, B. *et al.* Enhanced radiative recombination of free excitons in *GaAs* quantum wells. *Phys. Rev. Lett.* **67**, 2335 (1991)

[36] Ciulin, V. *et al.* Radiative lifetime of negative trions in *GaAs* and *CdTe* quantum wells. *Phys. Stat. Sol. (a)* **178**, 495 (2000)

[37] Lethokov, V. S. Narrowing of the Doppler width in a standing light wave. *JETP Lett.* **7**, 272 (1968)

[38] Chu, S., Bjorkholm, J. E., Ashkin, A. & Cable, A. Experimental observation of optically trapped atoms. *Phys. Rev. Lett.* **57**, 314 (1986)

[39] Bloch, I. Ultracold quantum gases in optical lattices. *Nature* **1**, 23-30 (2005)

[40] Bloch, I., Dalibard, J. & Zwerger, W. Many-body physics with ultracold gases. *Rev. Mod. Phys.* **80**, 885-964 (2008)

[41] Vedral, V. *Modern foundations of quantum optics.* World Scientific (2005)

[42] Anderson, B. P. & Kasevich, M. A. Macroscopic quantum interference from atomic tunnel arrays. *Science* **282**, 1686 (1998)

[43] Dahan, M. B., Peik, E., Reichel, J., Castin, Y. & Salomon, C. Bloch oscillations of atoms in an optical potential. *Phys. Rev. Lett.* **76**, 4508 (1996)

[44] Greiner, M., Mandel, O., Esslinger, T., Hänsch, T. W. & Bloch, I. Quantum phase transition from a superfluid to a Mott insulator in a gas of ultracold atoms. *Nature* **415**, 39 (2002)

[45] Hamann, S. *et al.* Resolved-sideband Raman cooling to the ground state of an optical lattice. *Phys. Rev. Lett.* **80**, 4149-4152 (1998)

[46] Vuletic, V., Chin, C., Kerman, A. J. & Chu, S. Raman sideband cooling of trapped cesium atoms at very high densities. *Phys. Rev. Lett.* **81**, 5768-5771 (1998)

[47] Perrin, H., Kuhn, A., Bouchoule, I. & Salomon, C. Sideband cooling of neutral atoms in a far-detuned optical lattice. *Europhys. Lett.* **42**, 395-400 (1998)

[48] Raithel, G., Phillips, W. D. & Rolston, S. L. Coherence decay of wave-packets in optical lattices. *Phys. Rev. Lett.* **81**, 3615 (1998)

[49] Haycock, D. L., Alsing, P. M., Grondalski, J., Deutsch, I. H. & Jessen, P. S. Mesoscopic quantum coherence in in an optical lattice. *Phys. Rev. Lett.* **85**, 3615 (2000)

[50] Okuyama, Y. & Tokuda, N. Electron-phonon interactions in modulation-doped $Al_xGa_{1-x}As/GaAs$ heterojunctions. *Phys. Rev. B.* **40**, 14 (1989)

[51] Ferreira, R. & Bastard, G. Evaluation of some scattering times for electrons in unbiased and biased single- and multiple-quantum-well-structures. *Phys. Rev. B.* **40**, 2 (1989)

[52] Cohen-Tannoudji, C., Dupont-Roc, J. & Grynberg, G. *Atom-Photon interactions. Basic processes and applications.* Wiley & Sons (2004)

[53] Deutsch, I. H., Brennen, G. K. & Jessen, P. Quantum computing with neutral atoms in an optical lattice. *Fortsch. Phys.* **48**, (2008)

[54] Jaksch, D. & Zoller, P. The cold atom Hubbard toolbox. *Ann. Phys.* **315**, 52-79 (2005)

[55] Jaksch, D., Bruder, C., Cirac, J. I., Gardiner, C. W. & Zoller, P. Cold bosonic atoms in optical lattices. *Phys. Rev. Lett.* **81**, 3108 (1998)

[56] Zwerger, W. Mott-Hubbard transition of cold atoms in optical lattices. *J. Opt. B: Semiclass. Opt.* **5**, S9-S16 (2003)

[57] Xu *et al.* Coherent population trapping of an electron spin in a single negatively chaged quantum dot. *Nature* **4**, 692-695 (2008)

[58] Jessen, P. & Deutsch, I. H. Optical lattices. *Adv. At., Mol., Opt. Phys.* **37**, 95 (1996)

[59] Marksteiner, S., Walser, R., Marte, P. & Zoller, P. Localization of atoms in light fields: Optical molasses, adiabatic compression and squezzing. *Appl. Phys. B.* **60**, 145 (1995)

[60] Jaksch, D., Briegel, H.-J., Cirac, J.I., Gardiner, C.W. & Zoller, P. Entanglement of atoms via cold controlled collisions. *Phys. Rev. Lett.* **82**, 9 (1999)

[61] Mandel, O., Greiner, M., Widera, A., Rom, T., Haensch, T.W. & Bloch, I. Coherent transport of neutral atoms in spin-dependent optical lattice potentials. *Phys. Rev. Lett.* **91**, 1 (2003)

[62] Mandel, O., Greiner, M., Widera, A., Rom, T., Haensch, T.W. & Bloch, I. Controlled collisions for multiparticle entanglement of optically trapped atoms. *Nature* **425**, 937 (2003)

[63] Leibfried, D., Blatt, R., Monroe, C. & Wineland, D. Quantum dynamics of single trapped ions. *Rev. Mod. Phys.* **75**, 281 (2003)

[64] Paul, W. Electromagnetic traps for charged and neutral particles. *Rev. Mod. Phys.* **62**, 531-540 (1990)

[65] Dehmelt, H. G. Proposed 1014δ nu less than nu laser fluorescene spectroscopy on $TL+$ mono-ion oscillator. *Bull. Am. Phys. Soc.* **18**, 1521 (1973)

[66] Joensson, L. Energy shifts due to the ponderomotive potential. *J. Opt. Soc. Am. B.* **4**, 9 (1987)

[67] Freeman, R. R., Bucksbaum, P. H. & McIlrath, T. J. The ponderomotive potential of high intensity light and its role in the multiphoton ionization of atoms. *IEEE Journal of Quantum Electronics* **24**, 7 (1988)

[68] Hofstetter, W., Cirac, J.I., Zoller, P., Demler, E. & Lukin, M . D. High-Temperature superfluidity of fermionic atoms in optical lattices. *Phys. Rev. Lett.* **89**, 220407 (2002)

[69] Rigol, M., Muramatsu, A., Batrouni, G. G. & Scalettar, R. T. Local quantum criticality in confined fermions on optical lattices. *Phys. Rev. Lett.* **91**, 130403 (2003)

[70] Cirac, J. I. & Zoller, P. Quantum computation with cold trapped ions. *Phys. Rev. Lett.* **74**, 4091-4094 (1995)

[71] Cirac, J. I. & Zoller, P. A scalable quantum computer with ions in an array of microtraps. *Nature* **404**, 579-581 (2000)

[72] Monroe, C., Meekhof, D. M., King, B. E., Itano, W. M. & Wineland, D. J. Demonstration of a fundamental quantum logic gate. *Phys. Rev. Lett.* **75**, 4714-4717 (1995)

[73] Poyatos, J. F., Cirac, J. I., & Zoller, P. Quantum gates with hot trapped ions. *Phys. Rev. Lett.* **81**, 1322-1325 (1998)

[74] Stean, A. The ion trap quantum information processor. *Appl. Phys. B* **64**, 623-642 (1997)

[75] Turchette, Q. A. *et al.* Deterministic entanglement of trapped ions. *Phys. Rev. Lett.* **81**, 3631-3634 (1998)

[76] Sorensen, A. & Molmer, K. Quantum computation with ions in thermal motion. *Phys. Rev. Lett.* **82**, 1971-1974 (1999)

[77] Wineland, D. J. *et al.* Experimental issues in coherent quantum-state manipulation of trapped atomic ions. *J. Res. Natl Inst. Stand. Technol.* **103**, 259 (1998)

[78] Brennen, G. K., Caves, C. M., Jessen, P. S. & Deutsch, I. H. Quantum logic gates in optical lattices. *Phys. Rev. Lett.* **82**, 1060-1063 (1999)

[79] Calcaro, T. *et al.* Quantum gates with neutral atoms: Controlling collisional interactions in time dependent traps. *Phys. Rev. A* **61**, 022304-11 (1999)

[80] Pellizzari, T., Gardiner, S. A., Cirac, J. I. & Zoller, P. Decoherence, continous observation, and quantum computing: a cavity QED model. *Phys. Rev. Lett.* **75**, 3788-3791 (1995)

[81] Turchette, Q. A., Hood, C. J., Lange, W., Mabuchi, H. & Kimble, H. J. Measurement of conditional phase shifts for quantum logic. *Phys. Rev. Lett.* **75**, 4710-4713 (1995)

[82] Maître, X. *et al.* Quantum memory with a single photon in a cavity. *Phys. Rev. Lett.* **79**, 769-772 (1997)

[83] Cory, D. G., Fahmy, A. F. & Havel, T. F. Ensemble quantum computing by NMR spectroscopy. *Proc. Natl Acad. Sci. USA* **94**, 1634-1639 (1997)

[84] Gershenfeld, N. A. & Chuang, I. L. Bulk spin-resonance quantum computation. *Science* **275**, 350-356 (1997)

[85] DiVincenzo, D. P. Two-bit gates are universal for quantum computation. *Phys. Rev. A* **51**, 1015-1022 (1995)

[86] Kane, B. E. A silicon-based nuclear spin quantum computer. *Nature* **393**, 133-137 (1998)

[87] Loss, D. & DiVincenzo, D. P. Quantum computation with quantum dots. *Phys. Rev. A* **57**, 120-126 (1998)

[88] Mahklin, Y. & Schön, G. Josephson-junction qubits with controlled couplings. *Nature* **398**, 305-307 (1999)

[89] Feynman, R. Simulatin Physics with computers. *Int. J. Theor. Phys.* **21**, 467 (1982)

[90] Peta, J. R. *et al.* Coherent manipulation of coupled electron spins in semiconductor quantum dots. *Science* **309**, 2180 (2005)

[91] Bloch, I. Exploring quantum matter with ultracold atoms in optical lattices. *J. Phys. B: At. Mol. Opt. Phys.* **38**, S629-S643 (2005)

[92] Monroe, C. Quantum information processing with atoms and photons. *Nature* **416**, 238-246 (2002)

[93] Hammack, A. T. *et al.* Trapping of cold excitons in quantum well structues with laser light. *Phys. Rev. Lett.* **96**, 227402 (2006)

[94] Hammack, A. T. *et al.* Kinetics of indirect excitons in an optically induced trap in *GaAs* quantum wells. *Phys. Rev. B* **76**, 193308 (2007)

[95] Butov, L. V. *et al.* Condensation and pattern formation in cold exciton gases in coupled quantum wells. *J. Phys. Condens. Matter* **16**, R1577 (2004)